UNIVERSIDADE DE LISBOA

INSTITUTO SUPERIOR TÉCNICO

Deciphering the Bone Marrow Microenvironment in Idiopathic Acquired Aplastic Anemia

Isabel Filipa Bogalho Henriques Martins

Supervisor: Doctor Cláudia Alexandra Martins Lobato da Silva

Co-Supervisor: Doctor Domingos Manuel Pinto Henrique

Thesis approved in public session to obtain the PhD Degree in

Biotechnology and Biosciences

Jury Final Classification: **Pass with Distinction**

2025

TÉCNICO LISBOA

UNIVERSIDADE DE LISBOA

INSTITUTO SUPERIOR TÉCNICO

Deciphering the Bone Marrow Microenvironment in Idiopathic Acquired Aplastic Anemia

Isabel Filipa Bogalho Henriques Martins

Supervisor: Doctor Cláudia Alexandra Martins Lobato da Silva

Co-Supervisor: Doctor Domingos Manuel Pinto Henrique

Thesis approved in public session to obtain the PhD Degree in

Biotechnology and Biosciences

Jury Final Classification: **Pass with Distinction**

Jury

Chairperson: Doctor Arsénio do Carmo Sales Mendes Fialho, Instituto Superior Técnico, Universidade de Lisboa.

Members of the Committee:

Doctor Arsénio do Carmo Sales Mendes Fialho, Instituto Superior Técnico, Universidade de Lisboa;

Doctor Luís Miguel Nabais Borrego, Faculdade de Ciências Médicas | Nova Medical School, Universidade Nova de Lisboa;

Doctor Cláudia Alexandra Martins Lobato da Silva, Instituto Superior Técnico, Universidade de Lisboa;

Doctor Raquel Madeira Gonçalves, Instituto de Ciências Biomédicas Abel Salazar, Universidade do Porto;

Doctor Ana Margarida Pires Fernandes-Platzgummer, Instituto Superior Técnico, Universidade de Lisboa;

Doctor Elsa Margarida Cavaco Abranches, ViSync Technologies SA.

Funding Institution – FCT: Fundação para a Ciência e a Tecnologia

2025

Resumo

A anemia aplásica idiopática adquirida (AA) é uma doença rara, caracterizada por insuficiência da medula óssea (MO), redução significativa do número de células hematopoiéticas estaminais e progenitoras (HSPC) e alteração do microambiente medular (ex., adipogénese). Além do ataque imunológico mediado por células T citotóxicas, têm sido descritas alterações do nicho hematopoiético com possível implicação na fisiopatologia da doença. Publicações prévias demonstraram a presença de alterações funcionais nas células estromais mesenquimais da MO (BM-MSCs), contudo os dados são escassos e heterogéneos. Neste projeto, foi realizado o estudo comparativo de BM-MSCs de utentes com AA em comparação a controlos saudáveis. Foram analisados: o perfil imunofenotípico, diferenciação tri-linhagem e capacidade proliferativa (Secção III); a capacidade de suporte hematopoiético (Secção IV); o perfil de expressão génica (Secção V). Para melhor recriar o microambiente natural da MO, foi estabelecido um protocolo de descelularização de osso femoral humano como plataforma para co-cultura de BM-MSCs (Secção VI). No âmbito do projecto, foi desenvolvido um biobanco de amostras de MO de dadores com AA e saudáveis. No presente estudo concluiu-se que: o perfil imunofenotípico e proliferativo *in vitro* das BM-MSCs de AA foi semelhante aos controlos saudáveis; as BM-MSCs de AA exibiram uma maior tendência para a diferenciação adipogénica; globalmente, a taxa de proliferação de HSPC saudáveis em co-cultura com BM-MSCs de AA foi menor comparativamente à co-cultura com BM-MSCs saudáveis ou sem células de suporte; as BM-MSCs de AA mostraram padrões moleculares distintos, relacionados com mecanismos de resposta imunitária, adipogénese, metabolismo lipídico, diferenciação e atividade osteoblástica e osteoclástica, remodelação da matriz extracelular (ECM), suporte hematopoiético, angiogénese, reparação de DNA, resposta ao stress e sinalização celular. O modelo de osso humano descelularizado demonstrou ser eficaz, o que suporta a sua aplicação como plataforma de co-cultura celular com o objectivo de melhor representar o microambiente natural da MO.

Palavras-chave: anemia aplásica idiopática adquirida; células estromais mesenquimais de medula óssea; células hematopoiéticas estaminais e progenitoras; matriz óssea descelularizada; medicina regenerativa.

Abstract

Acquired idiopathic aplastic anemia (AA) is a rare disorder, characterized by bone marrow (BM) failure with severe reduction in the number of hematopoietic stem and progenitor cells (HSPC) and BM microenvironment disturbances (e.g., BM replacement by fat cells). Besides cytotoxic T-cell–mediated attack to CD34+ HSPC, stem cell niche modulation has been implicated in pathophysiology of AA. Several reports have demonstrated an abnormal function of key BM elements, namely dysfunctional mesenchymal stromal cells (MSCs), however with scarce and heterogeneous data.

In this project, AA-derived BM-MSCs were studied in comparison to control-derived BM-MSCs, in what regards: immunophenotypic profile, trilineage differentiation and proliferative capacity (Section III); supportive capacity of HSPC expansion (Section IV); and transcriptional profile by bulk RNA-Seq and RT-qPCR (Section V). To better recreate the natural BM microenvironment, a human femoral bone decellularization protocol was established as a platform for BM-MSCs co-culture (Section VI). Throughout the project, a cell biobank of BM samples from AA and healthy donors was established.

It was concluded that: immunophenotypic profile and *in vitro* proliferative capacity of AA-derived BM-MSCs was similar to healthy controls; AA-derived BM-MSCs exhibited a tendency for higher adipogenic differentiation in comparison to controls; globally, the proliferative rate of healthy HSPC co-cultured with AA-derived BM-MSCs feeder layer was lower in comparison to control-derived BM-MSCs feeder layer or without feeder layer; AA-derived BM-MSCs showed distinct molecular patterns associated to immune response, adipogenesis, lipid metabolism, osteoblast and osteoclast differentiation and activity, cell-ECM/ECM remodeling, hematopoietic support, angiogenesis, DNA repair/DNA damage response, stress response and cell signaling. The human decellularized bone model showed to be effective, which supports its application in the setting of a co-culture platform to better represent the natural BM microenvironment.

Keywords: Idiopathic acquired aplastic anemia; bone marrow-derived mesenchymal stromal cells; hematopoietic stem and progenitor cells; decellularized bone matrix; regenerative medicine.

Acknowledgements

"As palavras são o muro de pedra e cal a fechar o horizonte infinito das grandes ideias claras."

(Florbela Espanca)

Several years ago, during my medical residency and after specializing in Clinical Hematology, while following patients diagnosed with bone marrow failure and acute hematological malignancies, I felt that we were far from understanding such disorders. Even when an initial remission was attained, patients usually experienced both progress and setbacks, which limited their quality of life and, unfortunately, survival. As a junior professional, I was often challenged by personal doubts and questioned the meaning of clinical practice, at least in that form. It was especially difficult to maintain an enthusiastic perspective knowing that the therapeutic outcomes would probably be limited. At some point, almost solely the perspective of ameliorating symptoms felt real and encouraging.

Fortunately, when something goes wrong, something from within reminds us of things that bring joy and fresh air to continue the journey. Science and research were always a passion for me, but due to academic and professional duties, time passed, and choices focused primarily on clinics were made. However, after some years working in the clinics, the moment to jump into the laboratory had arrived.

Admission to the PhD program at IST-iBB was a crucial step toward the so-desired scientific path. At that time, I was as excited as I was afraid because everything was different from the work I had been used to doing. The first months were challenging, but I had the opportunity to meet excellent colleagues and assistants who helped me to feel included and part of the group. This was really important for successfully completing the first-year curricular units. Special thanks are directed to Professor Miguel Teixeira, who helped me find a research group to develop my thesis project and introduced me to Cláudia Lobato da Silva, my supervisor.

All the work developed in the context of the PhD was performed with the support and help of several people, to whom I would like to express my huge acknowledgment.

To Cláudia Lobato da Silva, my supervisor, who from the very beginning trusted in the project and in me as a student, even though I came from a completely different area. I will always remember the day we met at the Taguspark *campus* and the feeling of hope and optimism after the meeting. In addition to her scientific career, Cláudia is also a fantastic person and human being, inspiring her students in both ways, which was a true privilege.

To Domingos Henrique, my co-supervisor, who, at the very beginning of my laboratory incursions, long before this PhD, was always ready to help me and teach me how to think and how to do science. I know that I am still far from possessing such knowledge, however, I know that Domingos will always be there to provide me with useful insights and constructive criticism.

To Ana Fernandes-Platzgummer, who helped me plan and organize the laboratory tasks, always grounding me in reality. Ana is also a good friend whom I will cherish for life. In the most difficult moments, she was there to talk and listen, and I will never be able to sufficiently repay her kindness and (she will deny it) patience.

To Jaqueline Garcia, our Lab Manager at the Stem Cell Engineering and Regenerative Medicine Research Group (SCERG, IST-iBB), who was always available for any doubt or trouble in the laboratory, and always with a gentle and friendly smile. I feel truly lucky to have had the opportunity to work with Jaqueline.

Regarding SCERG's laboratory researchers and students, I especially thank Raquel Cunha, who taught me everything from the beginning, from good laboratory practices to cell culture and so on. She is a person of character and integrity, and I truly appreciate these attributes. Fortunately, I had the opportunity to work with her. I also thank Mariana Branco, João Silva, Marta Carvalho, and André Branco, from whom I learned a lot of laboratory methodologies. Without their help, I would not have been able to adequately proceed with the experiments.

Regarding external collaborations, I hereby thank Gabriela Rodrigues (Assistant Professor at the Faculty of Sciences, University of Lisbon) and Pedro Santos (PhD student at FCUL), Ana Rita Pires and Ana Margarida Pinto (Histopathology, Gulbenkian Institute of Molecular Medicine), and Isabel Nogueira (MicroLab, IST), whose expertise was fundamental in the final section of this project.

All the work would not have been possible without samples. The last few years have been challenging in terms of clinical practice, and that was not just a matter of pandemics, as one could see from the news regarding our health services. Besides that, during the PhD, there was always someone reminding me that, despite all hurdles, we must always continue. That person is Paula Kjöllerström, and no words can express how much I am thankful to her. Also in the clinical context, a huge thank you goes to João Sarmento Esteves and Joana Santos, as well as to Margarida Coucelo and Ana Teresa Simões (Functional Unit of Molecular Hematology, ULS de Coimbra), who collaborated on this project in an interested and altruistic way. I would also like to acknowledge all patients (and tutor, in case of pediatric donors), as well as the units and institutions that agreed to collaborate on this work, including all the participating staff, namely: Pediatrics Hematology Unit, Hospital Dona Estefânia, ULS de São José (represented by Paula Kjöllerström, MD); Orthopedics and Traumatology Unit, Hospital CUF Tejo/Hospital CUF Sintra (represented by João Sarmento Esteves, MD); Hematology Unit, Hospital CUF Tejo (Manuela Bernardo, MD)/Hospital CUF Descobertas (João Paulo Fernandes, MD; Cátia Gaspar, MD)/Hospital CUF Sintra; and Hematology Unit, Hospital de São Bernardo, ULS da Arrábida (Joana Santos, MD; Anabela Neves, MD).

Finally, but always foremost, I warmly thank my family (father, mother, sister) for their support and understanding (I know it is not easy), my dog soulmates (Bogas and Lira), who never (and never) leave my side (probably the ones who most enjoyed the thesis writing period), my longtime friend Florinda Duarte, and Ana Ribeiro Moreira, who has been helping me deal with life's challenges.

Since this PhD journey began, many things have happened. Some important people have left, while others have entered my life. It was a truly pleasant and enriching path that changed my life and career perspectives. Aware that the best is yet to come, I hope to continue this research journey toward the "limitless horizon" of science. At least, all efforts will be focused on that.

Table of Contents

List of Figures

Figure 4: Summary of the project outline and future directions (AA - aplastic anemia; HSPC - human hematopoietic stem and progenitor cells; MSCs - mesenchymal stromal cells; ME – microenvironment; BMFS – bone marrow failure syndromes).

Figure 5: Fibroblastic, spindle-shape morphology of AA and healthy control-derived BM-MSCs cultured under expansion conditions. Representative image of cell morphology of both disease and healthy samples imaged at 4x magnification on bright-field microscope (Olympus IX51 Inverted Microscope equipped with an attached digital camera). P = cell passage number; D = day number of cell culture (the day of BM-MSCs seeding was considered D0).

Figure 6: AA-derived and control-derived BM-MSCs immunophenotypic profile - % of cells expressing cell surface positive markers for MSCs identification (CD73, CD90, CD44) (±SE mean); % of live cells (±SE mean). All samples were negative for CD34, CD14, CD19, HLA-DR (data not shown). Data acquisition performed with FACSCalibur™ flow cytometer (BD Biosciences). P = cell passage number.

Figure 7: AA-derived and control-derived BM-MSCs immunophenotypic profile - % of cells expressing cell surface positive markers for MSCs identification (CD73, CD90, CD44) (±SE mean); % of live cells (±SE mean). All samples were negative for CD34, CD14, CD19, HLA-DR (data not shown). Data acquisition performed with FACSCanto™ II (BD Biosciences). P = cell passage number.

Figure 8: AA-derived BM-MSCs trilineage differentiation assay - osteogenic, adipogenic and chondrogenic differentiation. Samples imaged on bright-field microscope (Olympus IX51 Inverted Microscope equipped with an attached digital camera). Representative images of cells are shown.

Figure 9: Healthy control-derived BM-MSCs trilineage differentiation assay - osteogenic, adipogenic and chondrogenic differentiation. Samples imaged on bright-field microscope (Olympus IX51 Inverted Microscope equipped with an attached digital camera). Representative images of cells are shown.

Figure 10: AA-derived and control-derived adipogenic differentiation assay after AdipoRed™ Assay Reagent (Lonza) staining. Samples imaged at 4x magnification on fluorescence microscope (Olympus IX51 Inverted Microscope equipped with an attached digital camera). Representative images of cells are shown.

Figure 11: Proliferation performance (defined by the number of days to reach 70% of cell confluency) of AA-derived and control-derived BM-MSCs upon isolation from BM-derived MNC (±SE mean). Samples M78, M11 and M08 were seeded on uncoated cell culture plates. The remaining samples were seeded on gelatin 0.1% coating.

Figure 12: Proliferative rate, defined by Fold Increase (FI) at 70% confluency of AA-derived and control-derived BM-MSCs after thawing and expansion on T-25 flasks (±SE mean). No significant differences between AA and Controls (p = 0.80). P = cell passage number.

Figure 13: Proliferative rate, defined by Fold Increase (FI) at 70% confluency of AA-derived and control-derived BM-MSCs after thawing and expansion on T-75 flasks (±SE mean). No significant differences between AA and Controls (p = 0.70). P = cell passage number.

Figure 14: Proliferative rate, defined by Fold Increase (FI) at 70% confluency of AA-derived and control-derived BM-MSCs after one passage post-thawing and expansion on T-75 flasks (±SE mean). No significant differences between AA and Controls (p = 0.48). P = cell passage number.

Figure 15: Representative image of proliferative BM-MSCs kinetics (±SE mean). No significant differences between AA-derived and control-derived BM-MSCs (D1, p = 0.35; D2, p = 0.92, D3, p = 0.79, D4, p = 0.99, D5, p = 0.81, D6, p = 0.70, D7, p = 0.68).

Figure 16: Proliferative rate (defined by confluence (%) and fold increase (FI) at day 10) of AA-derived and control-derived BM-MSCs (±SE mean), cultured on LN521 (Biolaminin 521 LN, BioLamina) coated versus uncoated 12-well plates. At right side, representative morphological image of BM-MSCs cultured on LN521 coated 12-well plates, imaged on bright-field microscope (Olympus IX51 Inverted Microscope equipped with an attached digital camera).

Figure 17: Absolute telomere length for AA-derived and control-derived BM-MSCs. Data is presented as the average of telomere length on each chromosome in kilobase (±SE mean). No significant difference of average telomere length on each chromosome between groups. Donor-age and passage number effect for both groups, with shorter telomere length for older donors and higher cell passage number. kb/92 = average of telomere length on each chromosome in kilobase; a = AA-derived BM-MSCs; c = control-derived BM-MSCs; BC = buffy-coat; P = cell passage number.

Figure 18: Absolute telomere length of BMF patients-derived MNC compared to controls. For each BMF patient with pathogenic variants, average telomere length on each chromosome (kb/92) was under the lower percentile determined for healthy controls. In addition, four patients with VUS in telomeropathies-related genes were identified to be under the lower percentile, demonstrating that RT-qPCR absolute telomere assay is a useful complementary assay for this subset of patients, supporting diagnosis. kb/92 = average of telomere length on each chromosome in kilobase; VUS = variants of uncertain significance.

Figure 19: Representative image of AA-derived and control-derived BM-MSCs feeder layers. For both sampling groups it was possible to establish confluent feeder layers for co-culture with HSPC. Samples imaged at 10x magnification on bright-field (Olympus IX51 Inverted Microscope equipped with an attached digital camera). AA = aplastic anemia; HSPC = hematopoietic stem and progenitor cells; BM-MSCs = bone marrow-derived mesenchymal stromal cells.

Figure 20: HSPC expansion (co-)cultured with AA-derived and control-derived BM-MSCs feeder layers, or without feeder layer, in the context of: HSPC single donor experiment; Pool#2 experiment. Representative images captured on Day 7 of HSPC expansion. Samples were imaged at 10x magnification on bright-field (Olympus IX51 Inverted Microscope equipped with an attached digital camera). AA = aplastic anemia; HSPC = hematopoietic stem and progenitor cells; BM-MSCs = bone marrow-derived mesenchymal stromal cells.

Figure 21: HSPC single donor experiment - HSPC expansion after 7-day (co-)culture with AA-derived (red bar) and control-derived BM-MSCs (blue bar) feeder layers, or without

feeder layer (grey bar). * p = 0.006; ** p = 0.04; ns = not significant. Fold increase (FI) represents the fraction of CD34+ cells at Day 7 divided by the number of CD34+ cells enriched sample from single donor (M66) (±SE mean). AA-MSCs = aplastic anemia-derived bone marrow mesenchymal stromal cells; Control-MSCs = control-derived derived bone marrow mesenchymal stromal cells; HSPC = hematopoietic stem and progenitor cells.

Figure 22: HSPC Pool#2 experiment - HSPC expansion after 7-day (co-)culture with AA-derived (red bars) and control-derived BM-MSCs (blue bars) feeder layers, or without feeder layer (grey bars). * p = 0.003; ** p = 0.03; ns = not significant. Fold increase (FI) represents the fraction of CD34+ cells at Day 7 divided by the number of CD34+ cells enriched Pool#2 (±SE mean). AA-MSCs = aplastic anemia-derived bone marrow mesenchymal stromal cells; Control-MSCs = control-derived derived bone marrow mesenchymal stromal cells; HSPC = hematopoietic stem and progenitor cells.

Figure 23: HSPC expansion (co-)cultured with AA-derived and control-derived BM-MSCs feeder layers, or without feeder layer, in the context of: Pool#1 experiment; Pool#3 experiment. Representative images captured on Day 7 of HSPC expansion. Samples were imaged at 10x and magnification, respectively, on bright-field (Olympus IX51 Inverted Microscope equipped with an attached digital camera). AA = aplastic anemia; HSPC = hematopoietic stem and progenitor cells; BM-MSCs = bone marrow-derived mesenchymal stromal cells.

Figure 24: HSPC Pool#1 experiment - HSPC expansion after 7-day (co-)culture with AA-derived (red bars) and control-derived (blue bars) BM-MSCs feeder layers, or without feeder layer (grey bars). * p = 0.02; ** p = 0.02; *** p = 0.01; ns = not significant. Fold increase (FI) represents the fraction of CD34+ cells at Day 7 divided by the number of CD34+ cells enriched Pool#1 (±SE mean). AA-MSCs = aplastic anemia-derived bone marrow mesenchymal stromal cells; Control-MSCs = control-derived derived bone marrow mesenchymal stromal cells; HSPC = hematopoietic stem and progenitor cells.

Figure 25: HSPC Pool#3 experiment - HSPC expansion after 7-day (co-)culture with AA-derived (red bars) and control-derived (blue bars) BM-MSCs feeder layers, or without feeder layer (grey bars). * p = 0.02; ** p = 0.03; *** p = 0.02. Fold increase (FI) represents the fraction of CD34+ cells at Day 7 divided by the number of CD34+ cells enriched Pool#3 (±SE mean). AA-MSCs = aplastic anemia-derived bone marrow mesenchymal stromal cells; Control-MSCs = control-derived derived bone marrow mesenchymal stromal cells; HSPC = hematopoietic stem and progenitor cells.

Figure 26: Clonogenic potential of HSPC (co-)cultured with AA-derived and control-derived BM-MSCs feeder layers, or without feeder layer. CFU number was normalized by the number of MethoCult™ seeded cells and multiplied by the total number of CD34+ cells harvested on Day 7 of HSPC expansion. Plotted results correspond to the mean value of total CFU number of Pool#2 experiment, performed in technical triplicates (±SE mean).

Figure 27: Heatmap and dendrogram designed from scaled (z-score) VST-transformed counts matrix of the 500 most variable genes. Clustering of samples by gene expression. Gene identification (GENCODE ID) shown along the right axis. Aplastic anemia (AA) samples: AM10, AM15, AM08, and AM87 (dendrogram orange

bars). Control samples: CF18, CM11, CF10, CM78 (dendrogram blue bars). Heatmap Color key: Blue indicates increased expression; red indicates decreased expression.

Figure 28: Heatmap and dendrogram designed from scaled (z-score) VST-transformed counts matrix of the 500 most variable genes. Clustering of samples by gene expression. CF10 sample removed. Gene identification (GENCODE ID) shown along the right axis. Aplastic anemia (AA) samples: AM10, AM15, AM08, and AM87 (dendrogram orange bar). Control samples: CF18, CM11, CM78 (dendrogram blue bar). Heatmap Color key: Blue indicates increased expression; red indicates decreased expression.

Figure 29: Principal component analysis (PCA) - Principal component analysis (PCA) revealed that PC1 and PC2 segregated AA and control samples, explaining 63.5% of the variance (42% [PC1], 21.5% [PC2]).

Figure 30: Volcano plot representing differently expressed genes between AA versus control samples (padj < 0.05; L2FC cutoff of <-1.5 and >1.5). n=966 refers to the total number of differently expressed genes (padj < 0.05) before filtering for L2FC threshold of <-1.5 and >1.5, for down and upregulated genes, respectively.

Figure 31: GO enrichment analysis (GSEA) representing downregulated and upregulated genes accordingly to biological function (AA versus control samples). Genes related to DNA repair and immunoregulation seem to play a role in disease.

Figure 32: Heatmap of differently expressed genes (AA versus controls) by biological function - immune response-related genes (pro-inflammatory pattern): AA-derived BM-MSCs showing up-regulation of pro-inflammatory genes and down-regulation of anti-inflammatory genes in comparison to controls [detailed references Appendix G, Table – G.1.]. Gene symbols shown along the right axis. Aplastic anemia (AA) samples: AM10, AM15, AM08, and AM87 (dendrogram orange bar). Control samples: CF18, CM11, CM78 (dendrogram blue bar). Heatmap Color key: Blue indicates increased expression; red indicates decreased expression.

Figure 33: Heatmap of differently expressed genes (AA versus controls) by biological function - immune response-related genes (immunomodulatory pattern): AA-derived BM-MSCs showing down-regulation of pro-inflammatory genes and up-regulation of anti-inflammatory genes in comparison to controls [detailed references in Appendix G, Table – G.2.]. Gene symbols shown along the right axis. Aplastic anemia (AA) samples: AM10, AM15, AM08, and AM87 (dendrogram orange bar). Control samples: CF18, CM11, CM78 (dendrogram blue bar). Heatmap Color key: Blue indicates increased expression; red indicates decreased expression.

Figure 34: Heatmap of differently expressed genes (AA versus controls) by biological function - adipogenesis-related genes: AA-derived BM-MSCs showing down-regulation of both adipogenesis promotion and adipogenesis inhibition genes, in comparison to controls [detailed references in Appendix G, Table G.3. and Table G.4.]. Gene symbols shown along the right axis. Aplastic anemia (AA) samples: AM10, AM15, AM08, and AM87 (dendrogram orange bar). Control samples: CF18, CM11, CM78 (dendrogram blue bar). Heatmap Color key: Blue indicates increased expression; red indicates decreased expression.

Figure 35: Heatmap of differently expressed genes (AA versus controls) by biological function - lipid metabolism-related genes. AA-derived BM-MSCs showing downregulation of genes that could functionally translate into increase of lipolysis and lipoprotein lipase (LPL) activity, decrease in triglyceride synthesis, decrease in uptake and storage of fatty-acids, decrease in lipogenesis, decrease in biosynthesis of very long chain fatty acids (VLCFA) and increase in lipid transport proteins. AA-derived BM-MSCs upregulated genes related to cell membrane phospholipid composition and organization [detailed references in Appendix G, Table G.5.]. Gene symbols shown along the right axis. Aplastic anemia (AA) samples: AM10, AM15, AM08, and AM87 (dendrogram orange bar). Control samples: CF18, CM11, CM78 (dendrogram blue bar). Heatmap Color key: Blue indicates increased expression; red indicates decreased expression.

Figure 36: Heatmap of differently expressed genes (AA versus controls) by biological function. 36a. Osteoblast differentiation and activity - AA-derived BM-MSCs downregulation of genes involved in promotion of osteoblast differentiation and activity and upregulation of genes involved in inhibition of osteoblast differentiation and activity. 36b. Osteoclast differentiation and activity - AA-derived BM-MSCs downregulation of genes involved in inhibition of osteoclast differentiation and activity and upregulation of genes involved in osteoclast activation [detailed references in Appendix G, Table G.6. and Table G.7.]. Gene symbols shown along the right axis. Aplastic anemia (AA) samples: AM10, AM15, AM08, and AM87 (dendrogram orange bar). Control samples: CF18, CM11, CM78 (dendrogram blue bar). Heatmap Color key: Blue indicates increased expression; red indicates decreased expression.

Figure 37: Heatmap of differently expressed genes (AA versus controls) by biological function - hematopoietic support-related genes. AA-derived BM-MSCs showing downregulated and upregulated genes that could phenotypically translate into impairment of BM niche support of HSPC and/or be involved in HSPC lineage differentiation bias [detailed references in Appendix G, Table G.8.]. Gene symbols shown along the right axis. Aplastic anemia (AA) samples: AM10, AM15, AM08, and AM87 (dendrogram orange bar). Control samples: CF18, CM11, CM78 (dendrogram blue bar). Heatmap Color key: Blue indicates increased expression; red indicates decreased expression.

Figure 38: Heatmap of differently expressed genes (AA versus controls) by biological function - ECM remodeling and cell-ECM interactions. AA-derived BM-MSCs downregulation of genes related to cell-ECM interactions and ECM remodeling, suggesting a BM niche unbalance and, consequently, a less supportive environment for hematopoiesis and immune regulation in AA [detailed references in Appendix G, Table G.9.]. Gene symbols shown along the right axis. Aplastic anemia (AA) samples: AM10, AM15, AM08, and AM87 (dendrogram orange bar). Control samples: CF18, CM11, CM78 (dendrogram blue bar). Heatmap Color key: Blue indicates increased expression; red indicates decreased expression.

Figure 39: Heatmap of differently expressed genes (AA versus controls) by biological function - DNA repair and DNA damage response. AA-derived BM-MSCs showing upregulation and downregulation of genes functionally associated with DNA damage response, cell cycle checkpoint control and apoptosis [detailed in references Appendix G, Table G.10.]. Gene symbols shown along the right axis. Aplastic anemia (AA) samples: AM10, AM15, AM08, and AM87 (dendrogram orange bar). Control samples: CF18,

CM11, CM78 (dendrogram blue bar). Heatmap Color key: Blue indicates increased expression; red indicates decreased expression.

Figure 40: Heatmap of differently expressed genes (AA versus controls) by biological function - Stress response. AA-derived BM-MSCs showing downregulation of genes involved in response to oxidative stress, hypoxia and nutrient deprivation [detailed references in Appendix G, Table G.11.]. Gene symbols shown along the right axis. Aplastic anemia (AA) samples: AM10, AM15, AM08, and AM87 (dendrogram orange bar). Control samples: CF18, CM11, CM78 (dendrogram blue bar). Heatmap Color key: Blue indicates increased expression; red indicates decreased expression.

Figure 41: Heatmap of differently expressed genes (AA versus controls) by biological function - Angiogenesis. AA-derived BM-MSCs showing either up or downregulation of pro-angiogenic genes [detailed references Appendix G, Table G.12.]. Gene symbols shown along the right axis. Aplastic anemia (AA) samples: AM10, AM15, AM08, and AM87 (dendrogram orange bar). Control samples: CF18, CM11, CM78 (dendrogram blue bar). Heatmap Color key: Blue indicates increased expression; red indicates decreased expression.

Figure 42: Heatmap of differently expressed genes (AA versus controls) by biological function - Cell signaling. AA-derived BM-MSCs showing - downregulation of genes related to MAPK inhibition, JAK-STAT inhibition, Wnt/ß-catenin inhibition or activation; upregulation of genes related to MAPK, PI3K/Akt and NF-kB activation, Wnt/ß-catenin inhibition or activation, Wnt (noncanonical) activation. As shown, the simultaneous up- and downregulation of genes within the same signaling pathway highlights the intricate nature of cellular signaling interactions. This complexity underscores the challenges in interpreting transcriptomic results and their biological significance [detailed references in Appendix G, Table G.13.]. Gene symbols shown along the right axis. Aplastic anemia (AA) samples: AM10, AM15, AM08, and AM87 (dendrogram orange bar). Control samples: CF18, CM11, CM78 (dendrogram blue bar). Heatmap Color key: Blue indicates increased expression; red indicates decreased expression.

Figure 43: Uniform Manifold Approximation and Projection (UMAP) of differently expressed genes (AA versus controls) by biological function. Two distinct molecular patterns were observed in AA-derived BM-MSCs: downregulation of genes related to MAPK inhibition, JAK-STAT inhibition, Wnt/ß-catenin inhibition or activation; upregulation of genes related to MAPK, PI3K/Akt or NF-kB activation, Wnt/ß-catenin inhibition or activation, Wnt (noncanonical) activation. Symbols: (-) indicates pathway inhibition; (+) indicates pathway activation.

Figure 44: Summary of bulk transcriptomic analysis comparing AA-derived BM-MSCs to healthy controls. Solid blue line: activation; solid red line: inhibition; dashed red line: functional disruption; cell signaling (+): activation; cell signaling (-): inhibition; cell signaling (+/-): either activation or inhibition. AA-BM-MSCs: bone marrow-derived mesenchymal stromal cells from aplastic anemia patients; ECM: extracellular matrix; HSPC: hematopoietic stem and progenitor cells. Created with BioRender.com. Lira, K. (2024) BioRender.com/g26e388.

Figure 45: RT-qPCR results for genes selected according to functional properties, transcriptomics analysis and AA biology. Results determined by delta-delta Ct (ΔΔCt)

method and plotted as Log2 fold change (L2FC; FC = $2^{-\Delta\Delta Ct}$) between AA and control-derived BM-MSCs (±SE mean). AA - aplastic anemia.

Figure 46: RT-qPCR results for selected genes after 6-day exposure of AA and control-derived BM-MSCs to isotretinoin (10μM). Results determined by delta-delta Ct (ΔΔCt) method and plotted as Log2 fold change (L2FC; FC = $2^{-\Delta\Delta Ct}$) between treated and untreated samples (±SE mean). AA - aplastic anemia.

Figure 47: RT-qPCR results for selected genes after 6-day exposure of AA and control-derived BM-MSCs to isotretinoin (10μM). Results determined by delta-delta Ct (ΔΔCt) method and plotted as Log2 fold change (L2FC; FC = $2^{-\Delta\Delta Ct}$) between treated and untreated samples contrasting by disease status – AA versus controls (±SE mean). AA - aplastic anemia.

Figure 48: Cellular metabolic activity at 24 hours after *in vitro* AA and control-derived BM-MSCs drug-modulation with isotretinoin (0.1 μM, 1 μM, 10 μM). Viability/metabolic assay performed with PrestoBlue™. Results expressed as mean fold increase of relative fluorescence units (RFU), normalized for negative control (cell medium) (±SE mean). AA - aplastic anemia.

Figure 49: Proliferative rate by day 6 of *in vitro* AA and control-derived BM-MSCs drug-modulation with isotretinoin (no drug, 1 μM, 10 μM). Significance attained for 10 μM isotretinoin concentration (p = 0.15, for 1 μM versus no drug; p = 0.03 for 10 μM versus no drug; p = 0.42 for 1 μM versus 10 μM). Results expressed by mean fold increase (FI) of cell number by day 6 (±SE mean). AA - aplastic anemia.

Figure 50: Bone marrow microenvironment. The bone marrow (BM) hosts two crucial hematopoietic stem cell (HSC) microenvironments: the endosteal and vascular niches. The endosteal niche, located at the bone surface, is recognized as the "osteoblastic niche" due to the significant role of osteoblasts in promoting HSC quiescence and self-renewal. In parallel, the vascular niche, positioned alongside blood vessels, serves to stimulate HSC proliferation and differentiation through its rich supply of nutrients and signaling factors. This latter niche comprises endothelial cells, pericytes, and smooth muscle cells. Collectively, these distinct niches are fundamental to regulating HSC maintenance and activity within the BM. HSC: hematopoietic stem cells; CAR cell: CXCL12-abundant reticular stromal cells; LepR+: leptin receptor positive perivascular stromal cells; NG2+: neuroglial antigen 2 stromal pericytes. OPN: Osteopontin. ANG1: Angiopoietin-1, SCF: Stem cell factor (from [129]).

Figure 51: Human femoral bone samples – **a)** after surgical collection (upper row), after PBS (1x) washing of the surgical piece, before bone separation in smaller fragments and decellularization (middle row), and after decellularization (lower row); **b)** schematic representation of bone sample collection area (between the dashed red lines) **c)** representative image of decellularized femoral bone scaffolds placed in ultra-low attachment 24-well plate - empty scaffolds (upper row); BM-MSCs seeded scaffolds embed in 10% FBS MSCs-qualified supplemented medium (lower row).

Figure 52: Representative H&E stainings of decellularized human bone (femoral head/neck) scaffolds. Eosin staining (pink-red color) representing preservation of extracellular matrix (ECM) components and bone trabeculae (T) after decellularization. Absence of blue-purple staining representative of cell nuclei (as

would be revealed by hematoxylin). Histological samples imaged at 4x and 20x magnification on bright-field microscope (Olympus IX51 Inverted Microscope equipped with an attached digital camera).

Figure 53: Representative immunohistochemical stainings of collagen type I (COL1A1), fibronectin (FN) and stromal cell–derived factor 1 (SDF-1), on human decellularized bone (femoral head/neck) extracellular matrix scaffolds (dECM). Positive staining for collagen type I (strong) and fibronectin (weak). Minimal staining/negativity for SDF-1. T = bone trabeculae; ECM = extracellular matrix. Histological samples imaged at 20x and 40x magnification on bright-field microscope (Olympus IX51 Inverted Microscope equipped with an attached digital camera).

Figure 54: Representative SEM images of decellularized human bone (femoral head/neck) scaffolds – a) interface between compact bone (CB) and spongy bone (SB), showing preserved structural integrity; b) and d) decellularized bone trabecula with remaining ECM fibers/fibrils (*); c) bone structural disruption at the limits of bone cutting area (dashed box). Samples visualized on Hitachi scanning electron microscope (SEM), model S2400, with digital image acquisition by Bruker, software Quantax Esprit 1.9.

Figure 55: Cellular metabolic activity of control-derived BM-MSCs co-cultured in human bone (femoral head/neck) decellularized scaffolds of 5 mm, 10 mm or 15 mm of diameter, at different timepoints. Viability/metabolic assay performed with PrestoBlue™. Results expressed as mean relative fluorescence units (RFU) (±SE mean).

Figure 56: H&E stainings of decellularized human bone (femoral head/neck) scaffolds (upper row) in head-to-head comparison to BM-MSCs + dECM sets after 17-day co-culture. In contrast to dECM scaffolds, co-culture sets showed increased ECM deposition (pink-red color from eosin staining) and cellularity (dark-blue dots revealed by hematoxylin), in a heterogeneous pattern. T = bone trabeculae; * = ECM/cell lower-density areas; ** = ECM/cell higher-density areas. Histological samples imaged at 4x, 10x, 20x and 40x magnification on bright-field microscope (Olympus IX51 Inverted Microscope equipped with an attached digital camera).

Figure 57: Representative immunohistochemical stainings of collagen type I (COL1A1), fibronectin (FN) and stromal cell–derived factor 1 (SDF-1), on BM-MSCs + dECM sets after 17-day co-culture. Positive staining for collagen type I (strong), fibronectin (strong) and SDF-1 (strong). ** = ECM/cell higher-density areas; dashed box = SDF-1 staining in blood vessel. T = bone trabeculae. Histological samples imaged at 20x and 40x magnification on bright-field microscope (Olympus IX51 Inverted Microscope equipped with an attached digital camera).

Figure 58: Representative SEM images of decellularized human bone (femoral head/neck) matrix (dECM) scaffold [a) and b)], compared to BM-MSCs + dECM scaffold set after 17-day co-culture [c) and d)]. Images c) and d) denoting rougher bone surface (**) in comparison to a) and b) (*), corresponding to active ECM deposition secondary to BM-MSCs activity. Mesenchymal stromal cell depicted in d) (dashed box). Samples visualized on Hitachi scanning electron microscope (SEM), model S2400, with digital image acquisition by Bruker, software Quantax Esprit 1.9.

List of Tables

List of Abbreviations and Acronyms

A/A - antibiotic antimycotic solution (A/A)

AA - aplastic anemia

AA-derived BM-MSCs - mesenchymal stromal cells derived from aplastic anemia patients

AA-HSPC - hematopoietic stem and progenitor cells derived from aplastic anemia patients

ACD - ACD shelterin complex subunit and telomerase recruitment factor

ACTB - beta-actin

ADIPOQ - adiponectin

AGM - aorta-gonad-mesonephros

AHNAK2 - AHNAK Nucleoprotein 2

AL - acute leukemia

Allo-HCT - allogeneic hematopoietic cell transplantation

ALP - alkaline phosphatase

AML - acute myeloid leukemia

ANGPT1 - Angiopoietin 1

ANKRD1 - Ankyrin Repeat Domain 1

APC -allophycocyanin

APLN - apelin

APOL4 - apolipoprotein 4

ARID5A - AT-rich interaction domain 5A

AT-MSCs - adipose tissue-derived MSCs

ATG - anti-thymocyte globulin

ATG - Anti-thymocyte globulin

ATO - arsenic trioxide

Au/Pd - gold/palladium

Auto-HCT - autologous hematopoietic cell transplantation

bFGF - basic fibroblast growth factor

BFU-E - erythroid burst-forming unit

BGLAP - osteocalcin

BHLHE41 - basic helix-loop-helix family member e41

BM - bone marrow

BM-AT - bone marrow adipose tissue

BM-MSCs - bone marrow-derived mesenchymal stromal cells

BMA - bone marrow adipocytes

BMF - bone marrow failure

BMME -bone marrow microenvironment

C/EBPα - CCAAT/enhancer-binding protein alpha

CCL2 also known as MCP-1 - monocyte chemoattractant protein-1

CD - cluster of differentiation

CD105 - ENDOGLIN

CD11b - integrin primarily expressed on monocytes, macrophages, granulocytes and natural killer cells, and also a marker for microglia

CD34 - transmembrane glycoprotein highly expressed on HSPC

CD44 - cell-surface-based glycoprotein

CD45RA - protein tyrosine phosphatase primarily expressed on naïve B and T cells

CD73 - ecto-5'-nucleotidase

CD74 - HLA class II histocompatibility antigen gamma chain

CD80 - B7-1 primarily expressed on the surface of antigen presenting cells as dendritic cells, macrophages and B cells

CD90 - Thy-1 cell surface glycoprotein

cDNA - complementary deoxyribonucleic acid

CFU - colony-forming unit assay

CFU-GEMM - colony-forming unit-granulocyte, erythrocyte, monocyte, megakaryocyte

CFU-GM - colony forming unit granulocyte-monocyte

COL1A1 - collagen type I alpha 1 chain

CsA - cyclosporin A

Ct - Ct value (number of cycles it takes for the fluorescence signal to cross a certain threshold; threshold is set above the background fluorescence level)

CTC 1 - CTC1 stands for "CST Telomere Replication Complex Component 1

CTNNB1 - beta-catenin

DAPI - 4’,6-diamidino-2-phenylindole

DBA - Diamond-Blackfan anemia

DDX4 - DEAD-box helicase 4

DGE - differential gene expression analysis

DK1 - Dyskerin Pseudouridine Synthase 1

DMEM - Dulbecco's Modified Eagle Medium

DMSO - dimethyl sulfoxide

DNA - deoxyribonucleic acid

DNAse - deoxyribonuclease

dNTPs - deoxyribonucleotide triphosphate

DOCK5 - Dedicator of Cytokinesis protein 5

EBMT - European Group for Blood and Marrow Transplantation

ECM - extracellular matrix

EDTA - ethylenediaminetetraacetic acid

ERCCL2 - ERCC Excision Repair 6 Like 2

FABP4 - fatty acid-binding protein 4

FBS - fetal bovine Serum

10% FBS-DMEM (1% A/A) - 10% fetal bovine Serum + Dulbecco's Modified Eagle Medium + 1% Antibiotic Antimycotic

FGF2 - Fibroblast Growth Factor 2

FI - fold increase

FITC - fluorescein isothiocyanate

FLG-AS1 - Filaggrin Antisense RNA 1

Flt-3L - FMS-like tyrosine kinase 3 ligand

FN - fibronectin

FN1 – fibronectin (gene)

FRZB also known as SFRP3 - Frizzled-Related Protein (known as Secreted Frizzled-Related Protein 3)

FW - forward

G-CSF - granulocyte colony-stimulating factor

GAPDH - glyceraldehyde-3-phosphate dehydrogenase

GATA 2 - GATA-binding factor 2

GIMM - Gulbenkian Institute of Molecular Medicine

GO - gene ontology

GSEA - gene set enrichment analysis

GVHD - graft-versus-host-disease

H&E - hematoxylin and eosin stain

HCT - hematopoietic cell transplantation

HCV - hepatitis C virus

HGF - Hepatocyte Growth Factor

HIV 1/2 - human immunodeficiency virus type 1 and type 2

HLA-DR - Human Leukocyte Antigen – DR isotype primarily expressed on the surface of antigen presenting cells as dendritic cells, macrophages and B cells

HLA-G5 - Human Leukocyte Antigen G5

HOTAIR - HOX transcript antisense RNA

HSC - hematopoietic stem cell

HSPC - hematopoietic stem and progenitor cells

ID - identification

IDO - indoleamine 2,3-dioxygenase

IFN-γ - interferon-gamma

IGC - Instituto Gulbenkian Ciência

IL- interleukin

INESC MN - Instituto de Engenharia de Sistemas e Computadores Microsistemas e Nanotecnologias

ISCT - International Society of Cellular Therapy

IST - immunosuppressive therapy/therapies

IST-iBB - Institute for Bioengineering and Biosciences of Instituto Superior Técnico

JMML - Juvenile Myelomonocytic Leukemia

kb - kilobase

KCTD9 - potassium channel tetramerization domain containing 9

L/D - live/dead cell viability assay

L2FC - log2 fold change

LEP - leptin

LEP-R - leptin receptor

LEPR - leptin receptor (gene)

LIG4 - DNA Ligase 4

LN-521 - Biolaminin 521 LN

MACS - magnetic-activated cell sorting

MAMDC2 - MAM Domain Containing 2

Mb - megabase

MDS - myelodysplastic syndrome

ME - microenvironment

MNC - mononuclear cells

MPL - MPL Proto-Oncogene, Thrombopoietin Receptor

MSCs - mesenchymal stromal cells

MYBL1 - MYB proto-oncogene like 1

NAF1 - Nuclear Assembly Factor 1

NAMPT - visfastin

NF1 - Neurofibromatosis type 1

NGS - next-generation sequencing

NHP2 - NHP2 Ribonucleoprotein

NK – natural killer cells

NOP10 - NOP10 Ribonucleoprotein

ns - not statistically significant

NSAA - non-severe AA

OB - osteoblast(s)

OBFC1 - oligonucleotide/oligosaccharide binding fold containing 1

ORA - over representation analysis

P - cell passage number

PARN - Poly(A)-Specific Ribonuclease

PB - peripheral blood

PBS - filtered phosphate-buffered saline

PBSC - peripheral blood stem cells

PCA - principal component analysis

PCR - polymerase chain reaction

PDGFA - Platelet-Derived Growth Factor Subunit A

PDGFB - Platelet-Derived Growth Factor Subunit B

PE- phycoerythrin

PerCP-Cy5.5 - peridinin chlorophyll-protein-cyanine tandem fluorophore

PFA - paraformaldehyde

PGE2 - Prostaglandin E2

PMSF - phenylmethanesulphonylfluoride

PNH - paroxysmal nocturnal hemoglobinuria

PODXL - podocalyxin

POT1 - Protection of Telomeres 1

PPARγ - peroxisome proliferator-activated receptor gamma

PRXL2A - Peroxiredoxin Like 2A

PSIS - posterior superior iliac spine

QC - quality control

RAB27A - Ras-related protein Rab-27A

RARA - retinoic acid receptor alfa

RARA - retinoic acid receptor alpha

RARs - retinoic acid receptors

RBC - red blood cells

RBP1 - retinol binding protein 1

RETN - resistin

RFU - relative fluorescence units

RMRP - RNA component of mitochondrial RNA processing endoribonuclease

RNA-Seq - ribonucleic acid sequencing

RNAses - ribonucleases

ROS - reactive oxygen species

RPA - Replication Protein A1

RPL35 - Ribosomal Protein L35

RPL5 - Ribosomal Protein L5

RPS19 - Ribosomal Protein S19

RT - room temperature

RT-qPCR - reverse transcription quantitative polymerase chain reaction

RTEL1 - Regulator of Telomere Elongation Helicase 1

RUNX1 - Runt-related transcription factor 1

RUNX2 – Runt-related transcription factor 2

RV - reverse

RXRs - retinoid X receptors (RXRs).

SAA - severe aplastic anemia

SALL4 - Spalt Like Transcription Factor 4

SAMD9L - Sterile Alpha Motif Domain Containing 9 Like

SBDS - Shwachman-Bodian-Diamond syndrome

SCERG - Stem Cell Laboratory of Stem Cell Engineering Research Group

SCF - stem cell factor

SD - standard deviation

SDF1 - stromal cell-derived factor 1

SE mean - standard error of the mean

SELENOP - selenoprotein P

SEM - scanning electron microscopy

SOCS - Suppressor of Cytokine Signaling

SOCS2 - suppressor of cytokine signaling 2

SOCS3 - suppressor of cytokine signaling 3

SPARC - Secreted Protein Acidic and Rich in Cysteine

SPP1 - osteopontin

SRP54 - Signal Recognition Particle 54

STATs - Signal Transducer and Activator of Transcription

STK4 - Serine/Threonine Kinase 4

TEL - telomere

TERC - telomerase RNA component

TERT - telomerase reverse transcriptase

TGF-beta 1 - transforming growth factor-beta

TGFB1 - Transforming Growth Factor Beta 1

TINF2 - TERF1-Interacting Nuclear Factor 2

TNC - total nucleated cell number

TNFRSF11B - osteoprotegerin

TNFSF9 - Tumor Necrosis Factor Superfamily Member 9 (also known as 4-IBB or CD137)

TNFSF9 - tumor necrosis factor superfamily member 9

TP53 - tumor protein p53

TPO - thrombopoietin

TPP1 - Tripeptidyl Peptidase 1

UC-MSCs - human umbilical cord-derived MSCs

UMAP - Uniform Manifold Approximation and Projection

USB1 - U6 snRNA biogenesis phosphodiesterase 1

UV - ultraviolet

VEGFA - Vascular Endothelial Growth Factor A

VLCFA - very long chain fatty acids

VSAA - very Severe AA

VST - variance stabilizing transformation

VUS - variants of uncertain significance

WAS – Wiskott-Aldrich syndrome

WRAP53 - WD Repeat Containing Antisense to TP53

ΔΔCt - delta-delta Ct method

I. Introduction and Thesis outline

I.1. Summary

Aplastic anemia (AA) is a rare disease characterized by bone marrow (BM) hypocellularity, in which hematopoietic cells are replaced by fat cells, resulting in severe reductions in the numbers of hematopoietic stem and progenitor cells (HSPC). AA patients display not only reduced HSPC numbers, but also an altered BM microenvironment, although the mechanisms contributing to the modulation of the stem cell niche are poorly known. Several reports have demonstrated an abnormal function of key BM elements, namely the existence of dysfunctional mesenchymal stromal cells (MSCs). However, when comparing MSCs derived from healthy controls with AA-derived MSCs, published data are controversial, probably due to sample heterogeneity, as well as to technical discrepancies. The therapeutic backbone of AA consists in allogeneic hematopoietic cell transplantation (HCT), considered first line for eligible patients with a matched, preferable related, donor, or in immunosuppressive therapy (IST), for those patients without a matched donor or ineligible (e.g., older age; low performance status) for allogeneic HCT, limiting treatment options in this group. Incomplete understanding of AA pathogenesis has hampered the development of therapeutic strategies to efficiently circumvent those limitations.

Autologous HCT has been hypothesized as a useful strategy for AA treatment, especially for patients without an available allogeneic HCT donor. This therapeutic approach is in the halfway between allogeneic HCT and IST solely, benefiting from reduced intensity, less toxic, autologous HCT conditioning regimens, independently of the availability of a matched donor. This strategy could be a significant therapeutic achievement, especially for those patients in which allogeneic HCT is unfeasible (e.g., minorities lacking a suitable HLA-matched donor) and/or who do not respond effectively to IST. Despite feasible, autologous HCT in AA has been hampered by the limiting numbers of HSPC that are possible to collect from AA patients. Based on that theoretical framework, this doctoral project was outlined to better understand the role of BM microenvironment (ME), namely of BM-MSCs, on the pathophysiology of AA, and to contribute to the development of an *ex vivo* cell culture model for disease study and autologous HSPC expansion, towards the development of regenerative medicine-based therapeutic strategies for AA.

I.2. Introduction

I.2.1. The Disease – Aplastic Anemia

Aplastic anemia (AA) is a life-threatening hematologic syndrome (if untreated, it has a one-year mortality of over 70%) characterized by pancytopenia (peripheral blood deficiency of red cells, neutrophils, monocytes, platelets, and reticulocytes) and bone marrow hypoplasia/aplasia associated with fatty replacement of the bone marrow and near absence of hematopoietic precursor cells (Figure 1). The AA-BM aspirate typically contains numerous spicules with empty, fat-filled spaces, and relatively few hematopoietic cells. Lymphocytes, plasma cells, macrophages, and mast cells may be present. Occasional spicules are found to be cellular or even hypercellular (so called hot spots), but megakaryocytes are usually reduced. In fact, the term “aplastic anemia” is a misnomer since pancytopenia and not anemia alone is present [1,2,3].

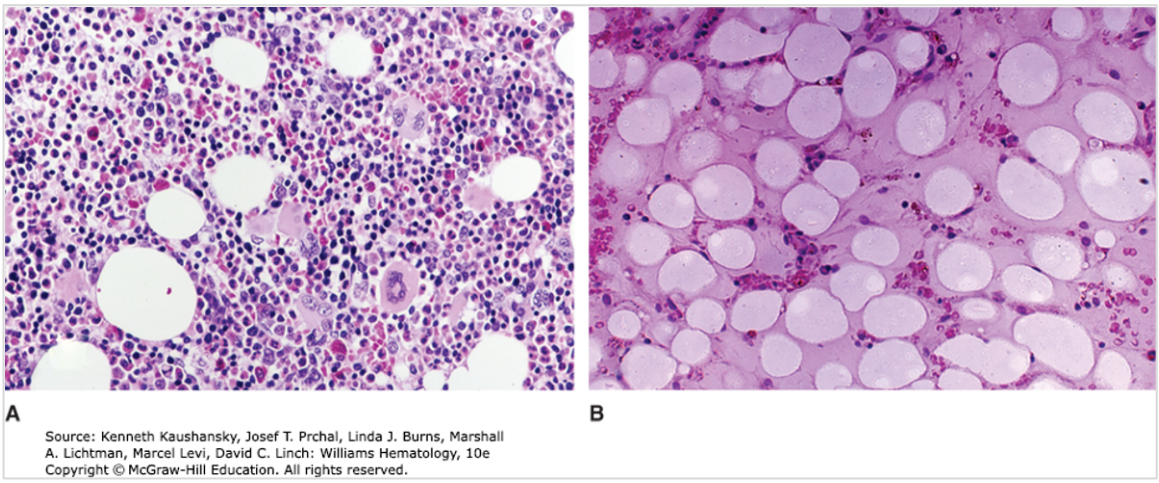

Figure 1: Marrow biopsy in aplastic anemia. A) A normal marrow biopsy section of a young adult. B) The marrow biopsy section of a young adult with very severe aplastic anemia. The specimen is devoid of hematopoietic cells and contains only scattered lymphocytes and stromal cells. The hematopoietic space is replaced by reticular cells converted to adipocytes (from [115]).

Aplastic anemia is a rare disorder, with an incidence of approximately 2 per 1,000,000 persons per year in western countries and with an estimated two- to threefold higher incidence in Asia [1,5,6]. Half of the cases occur in the first three

decades of life (between 15 to 25 years of age) and a second peak occurs between the ages of 65 and 69 years. The sex ratio of AA is close to 1:1 [4,5,6,7,8,9].

Aplastic anemia is classified according to both severity (severe AA (SAA): marrow cellularity <25% [or 25–50% with <30% residual hematopoietic cells], plus at least 2 of (i) neutrophils <0.5 x10^9/L, (ii) platelets <20 x 10^9/L (iii) reticulocyte count <20 x 10^9/L; Very Severe AA (VSAA): as for SAA but neutrophils <0.2 x 10^9/L; non-severe AA (NSAA): not fulfilling the criteria for SAA or VSAA) and etiology (acquired [most of the cases] or inherited [fewer cases, occurring in the context of an inherited BM failure syndrome, such as Fanconi anemia, Schwachman-Diamond syndrome, Dyskeratosis congenita, or others]) [10].

Most cases of aplastic anemia are acquired and idiopathic, with no established etiology. In most cases of acquired AA, either if it is idiopathic or secondary (e.g., to viral infection, autoimmune disease, etc.), reduced hematopoiesis seems to result from cytotoxic T-cell–mediated attack to CD34+ hematopoietic stem and progenitor cells (HSPC), hence the successful treatment with immunosuppressive agents, alone or in combination with a stem cell stimulating agent (e.g., eltrombopag, a thrombopoietin (TPO) nonpeptide agonist which increases platelet counts by binding to and activating the human TPO receptor) [11].

The treatment of SAA differs according to patient's age and performance status. In young patients (< 40 years of age) with a matched sibling donor, allogeneic hematopoietic cell transplantation (allo-HCT) should be considered first-line therapy. In older patients (> 40-50 years of age), and for patients without a matched sibling donor, immunosuppressive therapy (IST) (e.g., Anti-thymocyte globulin (ATG) + Cyclosporin A (CsA)) is recommended as first-line [12,13,14].

In older patients allo-HCT is associated with a higher incidence of graft failure and graft-versus-host disease (GVHD). Despite IST is recommended as first-line therapy in this population, there is a significant age effect over IST treatment outcome, with survival of 82% and 58% for patients younger than 20 years or older than 40 years, respectively (A.B., The European Group for Blood and Marrow Transplantation's (EBMT) database, unpublished data) [12].

I.2.2. Bone Marrow Microenvironment in AA

I.2.2.1. Role of Bone Marrow Mesenchymal Stromal Cells in AA

Alongside with the (auto)immune pathophysiology of AA, it has been hypothesized that the bone marrow microenvironment (ME) could also contribute to AA's defective hematopoiesis through diverse mechanisms (e.g., impairment in osteoblastic, vascular and HSPC niches) [15,16,17].

Bone marrow mesenchymal stromal cells (BM-MSCs) are found as a normal component of stromal BM cellular environment. MSCs are also found in umbilical cord-derived Wharton's jelly, in adipose tissue, in dental pulp tissue, and in amniotic fluid and other fetal and postnatal tissues. According to the International Society of Cellular Therapy (ISCT), MSCs are cells that: must be plastic-adherent when maintained in standard culture conditions; are characterized by expression of cell surface antigens CD105, CD73, and CD90, and lack of expression of CD34, CD45, CD14 or CD11b, CD79a, and HLA-DR surface molecules; show the capacity to differentiate *in vitro* into adipocytes, osteoblasts, and chondroblasts [18,19].

BM-MSCs provide cellular and structural elements required to support hematopoiesis. They have been shown to support hematopoiesis by paracrine mechanisms, such as secretion of bioactive molecules that support proliferation and long-term growth of HSPC. In addition, MSCs also demonstrate immunomodulatory activity, which supports their use as a cellular therapy in multiple conditions (e.g., minimization or treatment of graft-versus-host-disease (GVHD) after hematopoietic stem cell transplantation (HCT); enhancement of HSPC engraftment; and treatment of auto-immune diseases, such as Crohn's disease). Figure 2 represents some of the mechanisms by which MSCs could mediate immunomodulation. As illustrated, MSCs exert their effect on innate and adaptive immune systems via cell-cell interactions and immunomodulatory or regenerative factors. It appears to be a redundant system, and none of the molecules has an exclusive role [20].

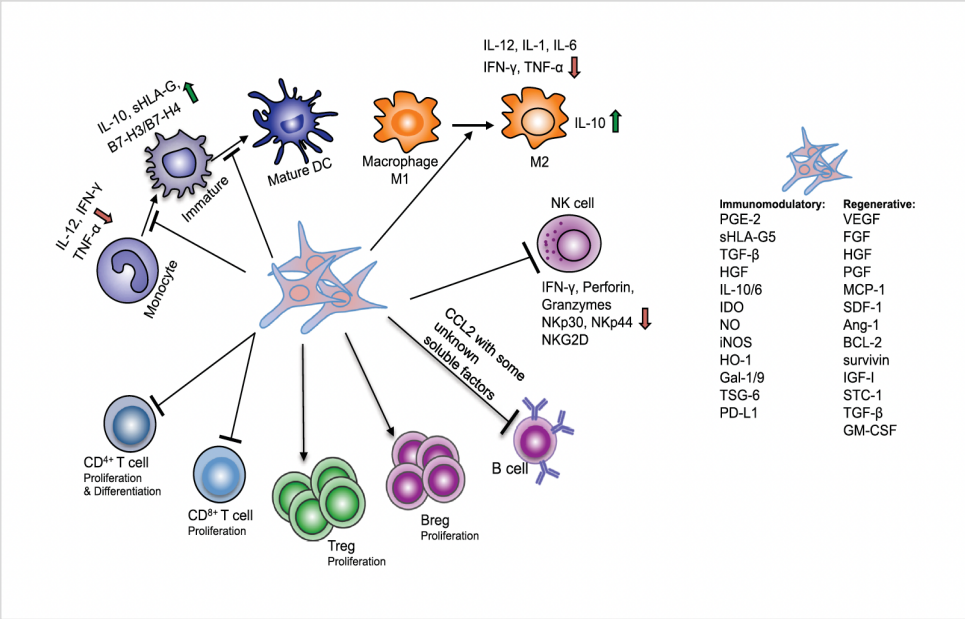

Figure 2: Immunomodulatory mechanisms of mesenchymal stromal cells (MSCs) - MSCs influence the immune system through a combination of direct cell contact and the release of various immune-regulating and regenerative factors. No single molecule is solely responsible for MSCs' therapeutic effects; their immunomodulatory and regenerative actions are the result of a multifaceted, redundant system, with the importance of individual components varying across studies (from [20]).

In what refers to the role of MSCs in AA, published data are controversial, probably due to the intra and inter-heterogeneity between patients included in such studies, as well as to technical differences between research protocols [21-31].

Several studies support that MSCs derived from patients with AA show aberrant morphology, decreased proliferation and clonogenic potential, increased apoptosis, and a propensity to adipogenic in detriment of osteogenic differentiation. Also, gene expression analyses performed on MSCs from patients with aplastic anemia evidenced altered expression of genes involved in cell proliferation, cell division, cell cycling, chemotaxis, hematopoietic cell interactions, adipogenesis, and immune response, in comparison to healthy controls [21,23,27,28].

On the other hand, there are also studies suggesting no difference between MSCs derived from patients with acquired AA in comparison to healthy controls. In accordance, a publication showed that AA derived MSCs retain the capability to form

functional hematopoietic stem cell niche *in vivo*, comparable to MSCs from healthy controls [22,29,30].

Figure 3 represents possible mechanisms contributing to BM niche modulation and immune destruction of hematopoiesis in acquired AA.

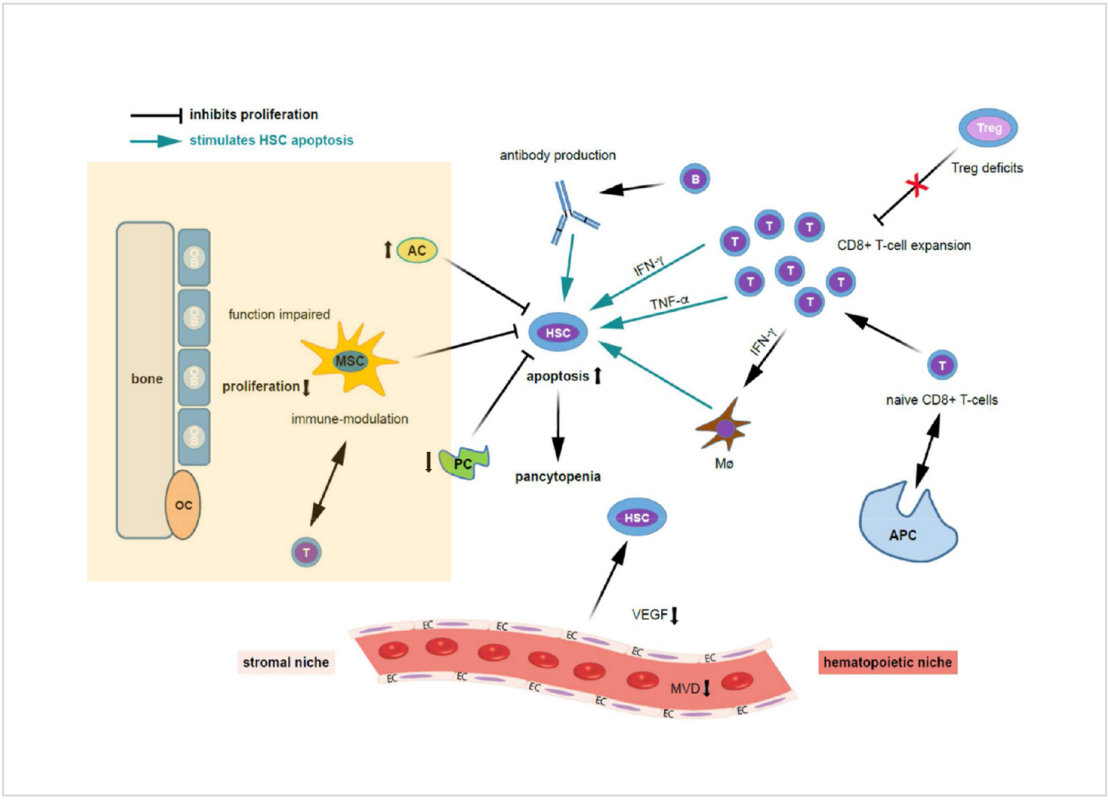

Figure 3: Possible pathophysiological mechanisms involving hematopoietic stem cells (HSC) and mesenchymal stromal cells (MSCs) in aplastic anemia - Acquired aplastic anemia (AA) is characterized by hematopoietic stem cell (HSC) depletion and a dysfunctional bone marrow hematopoietic niche. The pathophysiology involves an autoimmune attack (right side of the figure) where antigen-presenting cells activate naive CD8+ T cells, leading to cytotoxic T cell-mediated apoptosis of bone marrow cells, including HSCs. This is further driven by a polyclonal expansion of dysregulated CD4+ T-cells and oligoclonal expansion of dysregulated CD8+ T-cell populations. Abnormal cytokine production, notably interferon-gamma (IFN-γ), tumor necrosis factor-alpha (TNF-α), and transforming growth factor (TGF), directly induces HSC apoptosis via the Fas/Fas ligand pathway, reducing HSC cycling and viability. Deficiencies in regulatory T cells (Tregs) exacerbate T cell expansion. Additionally, in AA patients increased TNF-α-producing macrophages (Mø) were found in the bone marrow, with IFN-γ-mediated

HSC loss requiring Mø presence, highlighting their role. IFN-γ indirectly impairs HSC function through niche cells like Mø and mesenchymal stem cells (MSCs), contributing to megakaryocyte and HSC loss. Elevated B cells and potential auto-antibody production against HSCs may also be involved. Concurrently with the immune-mediated mechanisms, in AA the stromal niche is compromised through several mechanisms (left side and lower part of the figure). Impairments in osteoblastic, vascular, and perivascular HSC niches might contribute to defective hematopoiesis. Impairment of MSC function may lead to inadequate HSC proliferation and failed suppression of activated T cells, thereby disrupting immune homeostasis. Increased adipocytes and decreased pericytes, along with reduced microvessel density and vascular endothelial growth factor (VEGF) expression, could further suppress hematopoiesis. This underscores that AA pathogenesis extends beyond immune destruction to include significant defects in the non-hematopoietic bone marrow microenvironment. AC, adipocytes; APC, antigen-presenting cell; HSC, hematopoietic stem cell; EC, endothelial cells; INF-γ, interferon-gamma; MVD, microvessel density; Mø, macrophages; MSCs, mesenchymal stromal cells; OB, osteoblasts; OC, osteoclasts; PC, pericytes; TNF-α, tumor necrosis factor-alpha; VEGF, vascular endothelial growth factor (adapted from [15]).

Regarding the therapeutic role of MSCs in AA, data is also conflicting [30-35]. In AA, MSCs have been mainly used in two strategies: given in conjunction with hematopoietic stem cell transplantation, with the goal of preventing graft failure or to shorten time to donor engraftment; or given in monotherapy, to create a BM-microenvironment more supportive of hematopoiesis, also taking advantage from MSCs immunomodulatory properties.

Considering the first strategy, promising results have been attained, with improved donor engraftment, even in transplants from alternative donors (e.g., haploidentical HCT) [31, 32,33,34,36,37]. Considering the second strategy, the published works show that MSCs monotherapy could result in partial response in some AA patients, alleviating the need for transfusions (e.g., by raising hemoglobin and platelet levels to values above transfusion thresholds), but further studies need to be done, since

most of them have been performed with small samples, mainly composed of patients with AA refractory to previous IST therapies [35].

Despite that controversy, the influence of BM microenvironment in the pathogenesis of AA has been a matter of increasing research interest since that knowledge could be relevant to improve therapeutic outcomes, especially in severe cases of AA.

Regarding BM microenvironment role, it is of interest to mention that in patients submitted to HCT in the context of severe AA, the outcomes in terms of survival were superior in those patients receiving BM as stem cell source in comparison to patients receiving peripheral blood (PB) as stem cell source [36,37]. In preliminary publications, that superior outcome was attributed to less acute and chronic GVHD with BM (comparable risk for rejection: 2.5% for mobilized peripheral blood (PB) and 1.5% for BM) while compared to PB as stem cell source. Then, further studies suggested that MSCs and other non-hematopoietic cells present in BM could also contribute to post-transplantation regeneration of BM niche by diverse mechanisms, such as: by providing transient VEGF and cytokine support; by enhancing immune suppression; and by providing stable niche engraftment of donor-derived niche cells [38,39,40].

I.2.2.2. Role of Bone Marrow Adipose Tissue

Bone marrow adipose tissue (BM-AT) contributes to approximately 70% of adult's BM volume and for approximately 10% of total fat in healthy adults above 25 years of age [41,42]. BM adipocytes (BMA) are mainly derived from BM-MSCs. Recent studies have demonstrated that BM-AT is more than a filler of BM empty spaces. As such, it seems to act as an active organ with significant roles in energy storage, endocrine function, bone metabolism, and regulation of tumour growth and bone metastasis [41-48].

Regarding hematopoiesis and hematological disorders, BM-AT have been shown to influence hematopoiesis (e.g., through direct cell contact and secretion of adipocyte-derived factors) as well as the progression of malignant (e.g., leukemia, multiple myeloma) and non-malignant hematologic disorders, such as AA [47,48,49].

As mentioned previously, AA is characterized by hypocellularity and fatty replacement of BM. Small lymphoid aggregates may occur, particularly in the acute phase of disease or when associated with systemic autoimmune diseases (e.g., rheumatoid arthritis or systemic lupus erythematosus). In the BM of patients with AA, the number of adipocytes seems to be higher and the number of osteoblasts lower, which could negatively influence hematopoiesis [50, 51].

Several mechanisms for BM-AT replacement in AA have been suggested. *In vitro* experiments have shown that BM-MSCs derived from patients with AA tend to differentiate into adipocytes in detriment of osteoblasts. Diverse molecules, transcription factors (TF) and signaling pathways have been proposed to take part in this process, as summarized in Table 1 [52-71]:

Table 1 – Mechanisms and players associated with AA-derived BM-MSCs adipogenesis differentiation bias.

Mechanisms	Comments	References
CCAAT/enhancer-binding protein alpha (C/EBPα) and peroxisome proliferator-activated receptor gamma (PPARγ)	- In AA patients, arsenic trioxide (ATO) plus Ciclosporin A (CsA) demonstrated to partially restore the unbalanced differentiation of BM-MSCs by improving the balance between osteogenic and adipogenic differentiation. - ATO showed to inhibit adipogenic differentiation and to promote osteogenic differentiation in healthy BM-MSCs by CCAAT/enhancer-binding protein alpha (C/EBPα) and peroxisome proliferator-activated receptor gamma (PPARγ) regulation.	[52-56]
GATA-2 and peroxisome proliferator-activated receptor gamma (PPARγ)	- GATA-2, expressed in hematopoietic stem cells and early hematopoietic progenitors, is a key transcriptional factor in hematopoiesis, essential for HSPC maintenance, differentiation, proliferation and survival. BM CD34+ cells from patients with AA showed lower expression of GATA-2. - GATA-2 is also involved in the regulation of the hematopoietic microenvironment. It is expressed in preadipocytes and inhibits their terminal differentiation into mature adipocytes by suppressing PPARγ. In AA-derived BM-MSCs, GATA-2 expression showed to be significantly	[57-64]

	lower than in healthy controls, confirmed by lower protein levels of GATA-2 in Western blot analysis; conversely, expression of PPARγ was significantly higher in AA patients.	
Wnt signaling pathway	- Inhibition of differentiation of BM-MSCs into adipocytes mediated by inhibition of PPARγ mRNA expression (Wnt/ß-catenin pathway). - Noncanonical Wnt pathway activates histone methyltransferases leading to the inhibition of PPARγ transactivation of target genes. - In mouse model, Wnt/ß-catenin signal activator (lithium chloride) + CsA has been shown to be more effective in treating AA than CsA only.	[66, 67, 68]
Leptin (LEP)/Leptin receptor (LEP-R)	- Leptin, an adipokine mainly produced by adipocytes, induces proinflammatory stimulus on immune cells. Higher leptin concentration was found in AA-BM in comparison to heathy controls. Additionally, *LEPR* was found to be upregulated on AA-BM T-cells. - In AA mice model, increased LEP levels and decreased LEP-R levels were found in PB and AA-MSCs. It was hypothesized that LEP may increase immune injury in AA mice and that LEP-R decrease could disrupt LEP-mediated regulation of MSCs osteoblast differentiation, consequently leading to increase of BM-AT in AA mice.	[69,70,71]

ATO - arsenic trioxide; CsA - cyclosporin A; C/EBPα - CCAAT/enhancer-binding protein alpha; PPARγ - peroxisome proliferator-activated receptor gamma; LEP - leptin; LEP-R - leptin receptor.

I.2.3. Therapeutic Strategies for AA

I.2.3.1 Pearls and Pitfalls

As mentioned before, the choice of treatment in AA is based on diverse criteria related not only to the characteristics of disease (e.g., AA severity; presence of clonal evolution markers), but also to patient's determinants (e.g., age; performance status; comorbidities; availability of a suitable donor for allogenic HCT).

In adult patients with severe AA, despite the improvements that have been attained in allo-HCT conditioning protocols and supportive therapy, this procedure has been associated with lower survival in older patients (82%, 72%, and 53% for patients aged 1-20, 21-40, and older than 40 years, respectively), due to a higher incidence of

graft failure and GVHD in the older population. Data from EBMT (The European Group for Blood and Marrow Transplantation) for patients grafted from matched siblings (from 2001 to 2010) show the same age effect (86%, 76%, and 55% survival at 10 years, respectively for each group). For that reason, in patients older than 40-50 years with severe AA, regardless of its therapeutic benefit, allo-HCT is not considered first-line, unless in carefully selected cases (e.g., patients with severe disease but with an excellent performance status and a suitable donor) [72].

Regarding immunosuppressive therapy (IST), which is considered first-line therapy for most patients with severe AA above 40-50 years, there is also a significant age effect, with survivals of 82% and 58% for patients younger than 20 or older than 40 years, respectively (A.B., EBMT database, unpublished data). Patients above 50 years of age experience increased toxicities of IST treatment when compared with younger patients, which determines the use of less intense, but also less efficacious regimens, or of supportive therapy only (e.g., transfusional support; antibiotics to treat infections, etc.). Eltrombopag (a thrombopoietin (TPO) nonpeptide agonist, which not only increases platelet counts by binding to and activating the human TPO receptor, but also increases proliferation and differentiation of bone marrow progenitor cells), androgens (e.g., danazol) and granulocyte colony-stimulating factor (G-CSF) have also been used in adjunct to IST standard regimens, or as a mean to avoid toxicities from more intensive regimens (e.g., used in combination with less intense IST regimens or in monotherapy, as supportive therapy), especially in older patients, with variable results.

Despite its efficacy, IST in not devoid of risks. In fact, refractoriness, relapse (estimated to occur in approximately 30% of patients) and clonal evolution must be taken into consideration in patients treated with IST.

In addition, patients diagnosed with AA are at risk of clonal evolution (e.g., clonal mutations or cytogenetic abnormalities) and progression to a clonal hematologic disorder (e.g., myelodysplastic syndrome (MDS), acute myeloid leukemia (AML) or paroxysmal nocturnal hemoglobinuria (PNH)). The likelihood of developing MDS or AML seems to increase over time in patients treated with IST or myeloid growth factors, however it is not clear whether this is due to the therapy, to the underlying disease or to both [73-76].

I.2.3.2. Towards the development of novel regenerative medicine-based therapeutic approaches for AA

According to published data, the main factors affecting the prognosis of AA patients will be the severity of pancytopenia, the response to initial therapy, and the patient's age [1,99].

Despite the best treatment option for severe AA would be allo-HCT (especially using BM as stem cell source), this procedure is not always feasible or well-succeeded, due to several constraints (e.g., unavailability of a suitable donor; risk of toxicity and engraftment failure, especially in older patients; rejection, which is estimated to occur in 5% to 15% of patients with severe AA undergoing bone marrow transplantation).

IST, which is standardly considered the first-line therapy for severe AA patients older than 40-50 years of age and for younger patients without a suitable donor for allo-HCT, has shown to induce hematological recovery in 50% to 70% of cases, with excellent long-term survival among responders. However, in older patients (especially in those over 50 years of age) the outcomes decrease. In addition, among this population, the risk of treatment toxicities and clonal evolution is higher, which contributes to a poorer prognosis.

To circumvent those limitations, an interesting strategy to treat patients with severe AA would be autologous HCT, which could be effective in treating severe AA by promoting recovery of hematopoiesis while avoiding the risks associated with allo-HCT (e.g., toxicity from HCT conditioning regimen; GVHD). That could also be a strategy to circumvent the unavailability of a suitable stem cell donor, which unfortunately is still frequent, especially for ethnic minorities [77,78].

I.2.3.2.1. Autologous HCT – is there a role in AA?

Regarding the application of autologous transplantation in AA (auto-HCT), published data are scarce. Although it seems feasible in some patients [79-81], in a series of nine patients with severe AA in whom peripheral blood stem cell mobilization using G-CSF was attempted, only two attained sufficient mobilization of CD34+ cells to warrant collection [79].

In a case report, auto-HCT (using CD34+ and CD34+/CD90+ cells harvested from PB after mobilization with G-CSF) was performed in a 35 year-age male patient with severe AA initially treated with IST using rabbit ATG and CsA. After the first IST course, transfusion dependency persisted, and a second identical course of IST was administered. After the second IST course, polymorphonuclear (PMN) cell count increase (>2.0 x 109/L) was attained. Then, stem cell mobilization and harvesting (in two large volume leukapheresis procedures) were performed, followed by autologous HCT. 24 months after transplantation, the patient was in complete hematological (peripheral blood and bone marrow) remission, being only on CsA therapy (with dosage tapering from month eight after transplantation) [80].

As proposed, auto-HCT could be a promising therapeutic strategy in severe forms of AA, however, this procedure is limited by insufficient expansion of patient-derived HSPC (AA-HSPC), especially in those cases in which a significant hematological response after IST is not achieved.

In auto-HCT, the optimal doses of stem/progenitor cells (CD34+ cells) to be infused differ according to several variables, such as the type of disease as well as the HCT conditioning protocol. Interestingly, in a recent retrospective study of auto-HCT in multiple myeloma which included patients that received low and very low doses of peripheral blood stem cells (PBSC) (CD34+ cells doses: $3–4 \times 10^6$ [n = 86], $2–2.5 \times 10^6$ [n = 53], $< 2 \times 10^6$ [n = 9] cells per kg body weight), all patients reached hematopoietic reconstitution, even those who received $< 2 \times 10^6$ CD34+ cells/kg body weight. Although low number of reinfused CD34+ cells were associated with prolonged time until leukocyte reconstitution and platelet recovery, no severe adverse events were observed [82].

Assuming that auto-HCT with reinfusion of low doses of PB-derived stem/progenitor cells is feasible, the interest in designing research studies to optimize the mobilization and *ex vivo* expansion of autologous CD34+ from AA patients is strengthened, alongside with the need for a better understanding of AA-BM microenvironment, in particular of AA-derived BM-MSCs, to search for pathophysiological mechanisms that could be targeted or modulated in order to potentiate engraftment and hematological recovery in the context of transplantation or to develop novel therapies for AA.

I.2.3.2.2. *Ex vivo* expansion of autologous HSPC towards auto-HCT for AA treatment

a) Understanding the role of Bone Marrow Niche in the Pathophysiology of AA

A better understanding of BM microenvironment changes in AA, specifically in what concerns extracellular matrix (ECM) composition and cellular crosstalk between HSPC and stromal cells, could contribute to the improvement and development of novel therapeutic strategies, like auto-HCT. The development and optimization of techniques for isolation and expansion of autologous HSPC collected from AA patients would be of utmost importance to circumvent the caveats associated to the reduced AA-HSPC numbers harvested from patients for auto-HCT.

As described above, *in vitro* experiments have shown that BM-MSCs derived from patients with AA tend to differentiate into adipocytes in detriment of osteoblasts, and that diverse molecules and signaling pathways seem to take part in this process (Table 1). However, there is a huge lack of consistent data and improved experimental design is needed towards a better understanding of the potential pathophysiological role of BM microenvironment, namely of BM-MSCs, in AA. One possible strategy would be to modulate AA-MSCs and AA-HSPC culture conditions according to published findings regarding the molecular mechanisms by which BM-derived MSCs seem to be dysfunctional in AA (e.g., biased adipogenic over osteogenic linage differentiation), in comparison to healthy donors. For example, to test the effect of addition of specific molecules (e.g., PPAR pathway modulators) on *in vitro* cell behavior might be a useful strategy to develop and optimize a co-culture model for autologous AA-HSPC expansion. Those data would also be useful to further development of an AA disease model and drug screening platform.

Additionally, although diverse mechanisms by which BM microenvironment might influence the establishment and progression of AA have been proposed, most literature has focused on MSCs only, not considering osteoblasts (OB), which derive from MSCs, as a key element of the osteoblastic niche that influence HSPC fate. Also, the literature on ECM dynamics in the BM niche in AA is very scarce, with a single study demonstrating

that osteonectin is drastically decreased in AA patients, suggesting its involvement in AA pathogenesis [83].

Therefore, to better understand the pathophysiology of AA, it would be relevant to study if the presence of an altered ECM composition in the osteoblastic BM niche (comprising not only MSCs but also osteoblasts differentiated from MSCs) of AA patients could itself induce intrinsic defects in HSPC (e.g., impaired proliferative and differentiative capacity) and contribute to the development of BM failure.

Transcriptomics analysis is a powerful tool to study the expression of genes encoding for matrisome elements acting during osteogenic specification of MSCs [84]. Several recently published RNA-Seq-based studies provided promising insights regarding transcriptomic landscape of hematopoiesis in AA, such as: AA-HSPC lineage-specific alterations in gene expression and transcriptional regulatory networks, suggesting a selective disruption of distinct lineage-committed progenitor pools [85]; distinct HSPC–T cell crosstalk between patients with AA and controls [85]; hematopoiesis failure related with aberrance of B cells [86]; and metabolomic abnormalities of T lymphocytes, mainly on glycolysis and gluconeogenesis, and of natural killer cells, concentrated in oxidative phosphorylation [87].

Accordingly, RNA sequencing (RNA-Seq) can be used to identify factors compromising the hematopoietic supportive capacity of AA-derived BM-MSCs and osteo-induced MSCs. This might involve ECM components mediating cell-matrix interactions, as well as apoptosis-related gene expression signatures.

b) Recreating the Bone Marrow Niche

Over the last years, different strategies have been attempted to expand human HSPC using either liquid cultures, in which small molecules and recombinant factors are exogenously added, or cell-based co-culture approaches. Through expansion, enough HSPC could be generated and, concomitantly, higher numbers of lineage-committed progenitor cells would be produced, which may allow a faster hematopoietic recovery [88, 89].

Only more recently, scientific community has started to understand the complexity of the BM niche, which comprises endosteal, arterial, sinusoidal,

mesenchymal, and neuronal components. Mimicking HSPC interactions in the niche is fundamental to understand and promote *ex vivo* HSPC proliferation without losing multi-lineage differentiation and self-renewal capacities.

Recreation of the BM microenvironment has been attempted in co-cultures of HSPC with MSCs [88, 89]. The IST-iBB team has previously established and optimized a scalable serum-free co-culture system for the expansion of CD34+ enriched cells using BM-MSCs as feeder cells, demonstrating that direct contact is important to support HSPC expansion. Besides the HSPC-MSCs crosstalk, non-cellular ECM elements in the niche display intrinsic cues needed to communicate with and influence cell fate [90-92].

More recently, Branco A et al. [93] published promising results with the optimization of cytokine cocktails (stem cell factor (SCF), FMS-like tyrosine kinase 3 ligand (Flt-3L), and thrombopoietin (TPO)) for *ex vivo* culture platforms targeting the expansion of HSPC. Two expansion platforms for HSPC were studied, a liquid suspension culture system and a co-culture system with BM-derived MSCs. The optimized cocktails comprised concentrations of 64, 61, and 80 ng/mL (liquid suspension culture system) and 90, 82, and 77 ng/mL (co-culture system) for SCF, Flt-3L, and TPO, respectively. The co-culture system outperformed the feeder-free system in 6 of 8 tested experimental measures, showing superior capability of increasing the number of hematopoietic cells while maintaining the expression of HSPC markers (e.g., CD34+ and CD34+CD90+ cells) and multilineage differentiation potential.

The IST-iBB team has also developed decellularized ECM bioscaffolds that preserve specific tissue cues, namely bone signaling cues [94, 95].

More recently, Bianco et al. have successfully established a natural scaffold from decellularized bovine BM and evaluated its suitability as a 3D platform for co-culture of human HSPC and of stromal cell line HS5 [96].

Notwithstanding the widespread use of 2D static culture systems for HSPC expansion, those have shown significant limitations related to their non-homogeneous nature, resulting in concentration gradients (e.g., growth factors, oxygen, etc.) that could affect cell function. To circumvent that, stirred vessels and perfused reactors have shown significant advantages over the commonly used static plates due to a more homogeneous environment and ability to monitor and control critical parameters [97, 98].

I.3. Project Outline

The theoretical framework presented in the previous sections, and the research questions that emerged from it, were the basis of the present doctoral thesis, which relied on a cross-disciplinary strategy, combining Stem Cell Processing, Cell Biology and Hematology (Figure 4).

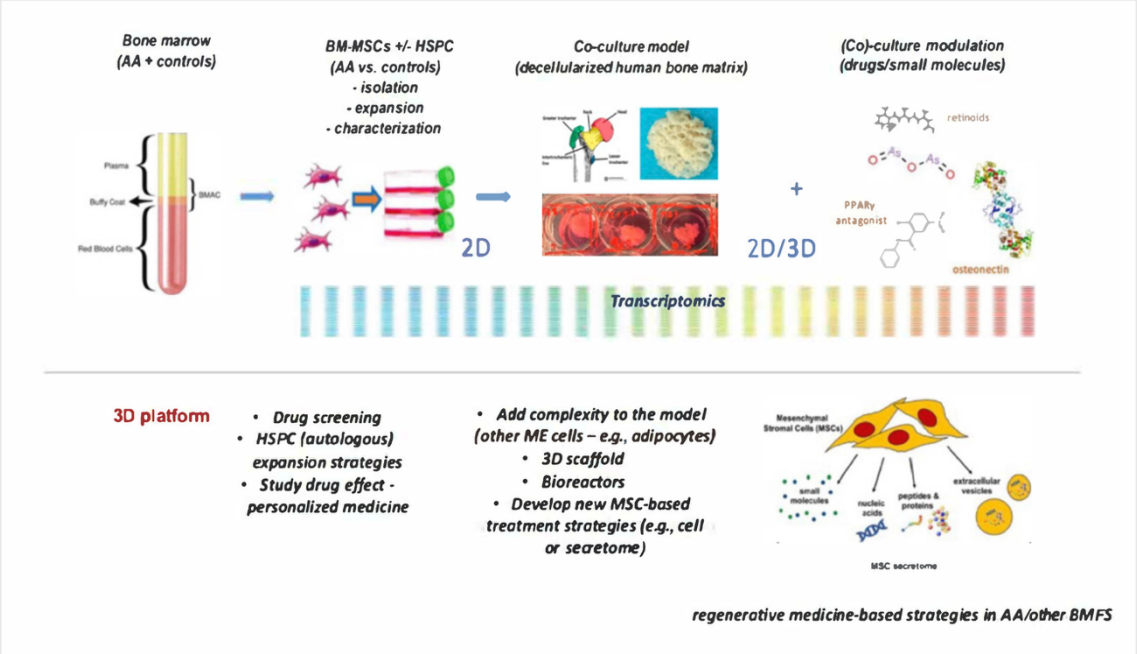

Figure 4: Summary of the project outline and future directions (AA - aplastic anemia; HSPC - human hematopoietic stem and progenitor cells; MSCs - mesenchymal stromal cells; ME – microenvironment; BMFS – bone marrow failure syndromes).

I.3.1. Project Overview

A brief overview of the main objectives of the thesis and respective tasks is provided below.

Task 1

1. Formalization of a collaboration protocol with clinical units, namely Hospital Dona Estefânia - Hematology Unit; Hospital de São Bernardo, Setúbal - Hematology Unit; Hospital CUF Sintra - Orthopedics Unit.
2. Establishment of a cell biobank (in continuous progress) composed of liquid/vapour phase nitrogen cryopreserved mononuclear cells (MNC) isolated from BM aspirates of patients diagnosed with AA and healthy controls (e.g., collected from patients undergoing elective hip arthroplasty or from patients undergoing bone marrow aspirate but with normal results).
3. Isolation, expansion and characterization (morphological, immunophenotypic and functional) of BM-MSCs (AA versus controls). Liquid/vapour phase nitrogen cryopreservation of BM-MSCs in cell biobank.

Task 2

1. RNA extraction from AA and control-derived BM-MSCs for bulk mRNA-Seq, performed at Genomics Unit of Instituto Gulbenkian de Ciência.
2. Bioinformatics analysis of BM-MSCs bulk mRNA-Seq data and RT-qPCR validation of selected candidate genes.
3. Drug-modulation of BM-MSCs (AA and controls) with an available molecule (isotretinoin), selected upon transcriptomics results. Study of proliferative and viability effects after *in vitro* drug exposure of BM-MSCs.

Task 3

1. Isolation by magnetic-activated cell sorting (MACS), expansion and characterization (immunophenotypic and functional) of HSPC from BM control samples. Since AA is a rare, poorly studied disease, for the thesis project, it was opted to primarily study the interactions of AA-derived versus control-derived

BM-MSCs with HSPC derived from healthy donors (control samples), preserving MNC from AA donors for subsequent works, after data consolidation within the doctoral project.

2. (Co-)culture of healthy HSPC on AA-derived versus control-derived BM-MSCs, and without feeder layer support.
3. Comparison of HSPC proliferation according to BM-MSCs feeder-layer source (AA versus control) as a readout of hematopoietic supportive differences between conditions.

Task 4

1. Collection of femoral bone samples from patients undergoing elective hip arthroplasty.
2. Implementation and optimization of a bone decellularization protocol, adapted to human femoral bone samples.
3. Histological characterization of decellularized bone extracellular matrix (dECM) and scanning electron microscopy (SEM).
4. Co-culture of BM-MSCs from control donors on decellularized bone extracellular matrix 3D scaffolds.
5. Assessment of cellular metabolic activity of BM-MSCs + dECM co-culture sets.
6. Histological characterization of BM-MSCs + dECM co-culture sets and SEM.

I.3.2. Project Novelties

The innovative aspects of the thesis are the following:

1. Implies the isolation and expansion of HSPC collected from a homogeneous population of treatment naïve patients newly diagnosed with acquired idiopathic AA, circumventing the caveats of previous studies, performed in heterogeneous sampling groups.
2. Targets a systematic comparison of AA-derived BM-MSCs (known to be dysfunctional) with healthy BM-MSCs (as control), with the focus on the evaluation of a potential adipogenic differentiation bias over osteogenic differentiation, as well as on the study of their hematopoietic supportive capacity.
3. Intends to provide relevant insights in what concerns the therapeutic potential of MSCs as a cell therapy for aplastic anemia (and possibly for other conditions, such as other BM failure syndromes or myelodysplastic syndromes).

I.4. References - Chapter I

1. Kaushansky K, Lichtman MA, Prchal JT, Levi MM, Press OW, Burns LJ, Caligiuri M. eds. *Williams Hematology, 9e, Chapter 35 (*Aplastic Anemia: Acquired and Inherited). New York, NY: McGraw-Hill.
2. Schrier SL, Mentzer WC, Rosmarin AG. Aplastic anemia: Pathogenesis, clinical manifestations, and diagnosis. www.uptodate.com (Literature review current through: May 2019. Topic last updated: Oct 03, 2017).
3. Barbara J. Bain, David M. Clark, Bridget S. Wilkins. Bone marrow pathology, Fifth edition, Chapter 9. Wiley-Blackwell, 2019.
4. Incidence of aplastic anemia: The relevance of diagnostic criteria. By the International Agranulocytosis and Aplastic Anemia Study. Blood 70:1718, 1987.
5. Mary JY, Baumelou E, Guiguet M: Epidemiology of aplastic anemia in France: A prospective multicenter study. Blood 75:1646, 1990.
6. Chongli Y, Ziaobo Z: Incidence survey of aplastic anemia in China. Chin Med Sci J 6:203, 1991.
7. Issaragrisil S: Epidemiology of aplastic anemia in Thailand. Thai Aplastic Anemia Study Group. Int J Hematol 70:137, 1999.
8. Yong AS, Goh AS, Rahman M et al.: Epidemiology of aplastic anemia in the state of Sabah, Malaysia. Med J Malaysia 53:59, 1998.
9. McCahon E, Tang K, Rogers PC et al.: The impact of Asian descent on the incidence of acquired severe aplastic anaemia in children. Br J Haematol 121:170, 2003.
10. Killick SB, Bown N, Cavenagh J, Dokal I, Foukaneli T, Hill A, Hillmen P, Ireland R, Kulasekararaj A, Mufti G, Snowden JA, Samarasinghe S, Wood A, Marsh JC; British Society for Standards in Haematology. Guidelines for the diagnosis and management of adult aplastic anaemia. Br J Haematol. 2016 Jan;172(2):187-207.
11. Young NS, Maciejewski J: Mechanisms of disease: The pathophysiology of acquired aplastic anemia. N Engl J Med 336:1365, 1997.
12. Bacigalupo A. How I treat acquired aplastic anemia. Blood. 2017 Mar 16;129(11):1428-1436.
13. Gupta V, Eapen M, Brazauskas R, et al. Impact of age on outcomes after bone marrow transplantation for acquired aplastic anemia using HLA-matched sibling donors. Haematologica. 2010;95(12):2119-2125.
14. Schrier SL, Mentzer WC, Rosmarin AG. Treatment of aplastic anemia in adults. www.uptodate.com (Literature review current through: May 2019. Topic last updated: Jul 06, 2018).
15. Medinger M, Drexler B, Lengerke C, Passweg J. Pathogenesis of Acquired Aplastic Anemia and the Role of the Bone Marrow Microenvironment. Front Oncol. 2018; 8:587.
16. Wu L, Mo W, Zhang Y, Zhou M, Li Y, Zhou R, et al. Vascular and perivascular niches, but not the osteoblastic niche, are numerically restored following allogeneic hematopoietic stem cell transplantation in patients with aplastic anemia. Int J Hematol. (2017) 106:71–81.
17. Wu L, Mo W, Zhang Y, Deng H, Li Y, Zhou R, et al. Impairment of hematopoietic stem cell niches in patients with aplastic anemia. Int J Hematol. (2015) 102:645–53.
18. Atala, Anthony; Lanza, Robert; Mikos, Antonios G.; Nerem, Robert. Principles or Regenerative Medicine, 3rd edition, Chapters 14 and 15. Elsevier Inc. 2019.

19. Dominici M., Le Blanc K., Mueller I., et al. Minimal criteria for defining multipotent mesenchymal stromal cells. The International Society for Cellular Therapy position statement. *Cytotherapy*. 2006;8(4):315–317.
20. Wu, X., Jiang, J., Gu, Z. et al. Mesenchymal stromal cell therapies: immunomodulatory properties and clinical progress. Stem Cell Res Ther 11, 345 (2020).
21. Hamzic E, Whiting K, Gordon Smith E, Pettengell R. Characterization of bone marrow mesenchymal stromal cells in aplastic anaemia. Br J Haematol. (2015) 169:804–13.
22. Bueno C, Roldan M, Anguita E, Romero-Moya D, Martín-Antonio B, Rosu-Myles M, et al. Bone marrow mesenchymal stem cells from patients with aplastic anemia maintain functional and immune properties and do not contribute to the pathogenesis of the disease. Haematologica (2014) 99:1168– 75.
23. Li J, Yang S, Lu S, Zhao H, Feng J, Li W, et al. Differential gene expression profile associated with the abnormality of bone marrow mesenchymal stem cells in aplastic anemia. PLoS ONE (2012) 7:e47764.
24. Riether C, Schürch CM, Ochsenbein AF. Regulation of hematopoietic and leukemic stem cells by the immune system. Cell Death Differ. (2015) 22:187– 98.
25. Fureder W, Krauth MT, Sperr WR, Sonneck K, Simonitsch-Klupp I, Mullauer L, et al. Evaluation of angiogenesis and vascular endothelial growth factor expression in the bone marrow of patients with aplastic anemia. Am J Pathol. (2006) 168:123–30.
26. Holmberg LA, Seidel K, Leisenring W, Torok-Storb B. Aplastic anemia: analysis of stromal cell function in long-term marrow cultures. Blood (1994) 84:3685–90.
27. Shipounova IN, Petrova TV, Svinareva DA, Momotuk KS, Mikhailova EA, Drize NI. Alterations in hematopoietic microenvironment in patients with aplastic anemia. Clin Transl Sci. (2009) 2:67–74.
28. Chao YH, Peng CT, Harn HJ, Chan CK, Wu KH. Poor potential of proliferation and differentiation in bone marrow mesenchymal stem cells derived from children with severe aplastic anemia. Ann Hematol. (2010) 89:715–23.
29. Michelozzi IM, Pievani A, Pagni F, Antolini L, Verna M, Corti P, et al. Human aplastic anaemia-derived mesenchymal stromal cells form functional haematopoietic stem cell niche in vivo. Br J Haematol. (2017) 179:669–73.
30. Broglie L, Margolis D, Medin JA. Yin and Yang of mesenchymal stem cells and aplastic anemia. World J Stem Cells. 2017 Dec 26;9(12):219-226.
31. Gonzaga VF, Wenceslau CV, Lisboa GS, Frare EO, Kerkis I. Mesenchymal Stem Cell Benefits Observed in Bone Marrow Failure and Acquired Aplastic Anemia. Stem Cells Int. 2017; 2017:8076529.
32. LiuZ,ZhangY,XiaoH,YaoZ,ZhangH,LiuQ,WuB,NieD,LiY,PangY,FanZ,LiL,JiangZ,DuanF,LiH,ZhangP,GaoY, Ouyang L, Yue C, Xie M, Shi C, Xiao Y, Wang S. Cotransplantation of bone marrow-derived mesenchymal stem cells in haploidentical hematopoietic stem cell transplantation in patients with severe aplastic anemia: an interim summary for a multicenter phase II trial results. Bone Marrow Transplant 2017; 52: 1080.
33. Luan C, Chen R, Chen B, Ding J, Ni M. Umbilical cord blood transplantation supplemented with the infusion of mesenchymal stem cell for an adolescent patient with severe aplastic anemia: a case report and review of literature. Patient Prefer Adherence 2015; 9: 759-765.

34. Clé DV, Santana-Lemos B, Tellechea MF, Prata KL, Orellana MD, Covas DT, Calado RT. Intravenous infusion of allogeneic mesenchymal stromal cells in refractory or relapsed aplastic anemia. Cytotherapy 2015; 17: 1696-1705.
35. Pang Y, Xiao HW, Zhang H, Liu ZH, Li L, Gao Y, Li HB, Jiang ZJ, Tan H, Lin JR, Du X, Weng JY, Nie DN, Lin DJ, Zhang XZ, Liu QF, Xu DR, Chen HJ, Ge XH, Wang XY, Xiao Y. Allogeneic Bone Marrow-Derived Mesenchymal Stromal Cells Expanded In Vitro for Treatment of Aplastic Anemia: A Multicenter Phase II Trial. Stem Cells Transl Med 2017; 6: 1569-1575.
36. Bacigalupo A, Socié G, Schrezenmeier H, Tichelli A, Locasciulli A, Fuehrer M, et al. Aplastic Anemia Working Party of the European Group for Blood and Marrow Transplantation (WPSAA-EBMT). Bone marrow versus peripheral blood as the stem cell source for sibling transplants in acquired aplastic anemia: survival advantage for bone marrow in all age groups. Haematologica (2012) 97:1142–8.
37. Schrezenmeier H, Passweg JR, Marsh JC, Bacigalupo A, Bredeson CN, Bullorsky E, et al. Worse outcome and more chronic GVHD with peripheral blood progenitor cells than bone marrow in HLA-matched sibling donor transplants for young patients with severe acquired aplastic anemia. Blood (2007) 110:1397–400.
38. Gianelli U, Vener C, Raviele PR, Savi F, Somalvico F, Calori R, et al. VEGF expression correlates with microvessel density in Philadelphia chromosome- negative chronic myeloproliferative disorders. Am J Clin Pathol. (2007) 128:966–73.
39. Gerber HP, Malik AK, Solar GP, Sherman D, Liang XH, Meng G, et al. VEGF regulates haematopoietic stem cell survival by an internal autocrine loop mechanism. Nature (2002) 417:954–8.
40. De Felice L, Agostini F, Suriano C, Fraboni D, Gregorj C, Tirindelli MC, et al. Hematopoietic, mesenchymal, and immune cells are more enhanced in bone marrow than in peripheral blood from granulocyte colony-stimulating factor primed healthy donors. Biol Blood Marrow Transl. (2016) 22:1758–64.
41. Wang H, Leng Y, Gong Y. Bone Marrow Fat and Hematopoiesis. Front Endocrinol (Lausanne). 2018; 9:694. Published 2018 Nov 28.
42. Fazeli PK, Horowitz MC, MacDougald OA, Scheller EL, Rodeheffer MS, Rosen CJ, et al. Marrow fat and bone–new perspectives. J Clin Endocrinol Metab. (2013) 98:935–45.
43. Cawthorn WP, Scheller EL, Learman BS, Parlee SD, Simon BR, Mori H, et al. Bone marrow adipose tissue is an endocrine organ that contributes to increased circulating adiponectin during caloric restriction. Cell Metab. (2014) 20:368–75.
44. Li Q, Wu Y, Kang N. Marrow adipose tissue: its origin, function, and regulation in bone remodeling and regeneration. Stem Cells Int. (2018) 2018:7098456.
45. Devlin MJ. Why does starvation make bones fat? Am J Hum Biol. (2011) 23:577–85.
46. van der Eerden B, van Wijnen A. Meeting report of the 2016 bone marrow adiposity meeting. Adipocyte (2017) 6:304–13.
47. Morris EV, Edwards CM. Bone marrow adipose tissue: a new player in cancer metastasis to bone. Front Endocrinol. (Lausanne) (2016) 7:90.
48. *Cuminetti V and Arranz L.* Bone Marrow Adipocytes: The Enigmatic Components of the Hematopoietic Stem Cell Niche. *J. Clin. Med.* 2019, *8*(5), 707.
49. Shipounova IN, Petrova TV, Svinareva DA, Momotuk KS, Mikhailova EA, Drize NI. Alterations in hematopoietic microenvironment in patients with aplastic anemia. Clin Transl Sci. (2009) 2:67–74.

50. Chen YH, Yeh FL, Yeh SP, Ma HT, Hung SC, Hung MC, et al. Myocyte enhancer factor-2 interacting transcriptional repressor (MITR) is a switch that promotes osteogenesis and inhibits adipogenesis of mesenchymal stem cells by inactivating peroxisome proliferator-activated receptor gamma-2. J Biol Chem. (2011) 286:10671–80. Tripathy NK, Singh SP, Nityanand S. Enhanced adipogenicity of bone marrow mesenchymal stem cells in aplastic anemia. Stem Cells Int. (2014) 2014:276862.
51. Wang HY, Ding TL, Xie Y, Xu XP, Yu L, Chen T. Osteogenic and adipogenic differentiation of bone marrow-derived mesenchymal stem cells in patients with aplastic anemia. Zhonghua Nei Ke Za Zhi (2009) 48:39–43.
52. Song Y, Li N, Liu Y, Fang B. Improved outcome of adults with aplastic anaemia treated with arsenic trioxide plus ciclosporin. Br J Haematol. (2013) 160:266–9.
53. Li N, Song Y, Zhou J, Fang B. Arsenic trioxide improves hematopoiesis in refractory severe aplastic anemia. J Hematol Oncol. (2012) 5:61.
54. Zhao J, Wang C, Song Y, Fang B. Arsenic trioxide and microRNA-204 display contrary effects on regulating adipogenic and osteogenic differentiation of mesenchymal stem cells in aplastic anemia. Acta Biochim Biophys Sin (2014) 46:885–93.
55. Song Y, Li N, Liu Y, Fang B. Improved outcome of adults with aplastic anaemia treated with arsenic trioxide plus ciclosporin. Br J Haematol. 2013 Jan;160(2):266-9.
56. Zhao J, Wang C, Song Y, Fang B. Arsenic trioxide and microRNA-204 display contrary effects on regulating adipogenic and osteogenic differentiation of mesenchymal stem cells in aplastic anemia. Acta Biochim Biophys Sin (Shanghai). 2014 Oct;46(10):885-93.
57. Tsai FY, Keller G, Kuo FC, Weiss M, Chen J, Rosenblatt M, et al. An early haematopoietic defect in mice lacking the transcription factor GATA-2. Nature (1994) 371:221–6.
58. Ling KW, Ottersbach K, van Hamburg JP, Oziemlak A, Tsai FY, Orkin SH, et al. GATA-2 plays two functionally distinct roles during the ontogeny of hematopoietic stem cells. J Exp Med. (2004) 200:871–82.
59. Rodrigues NP, Janzen V, Forkert R, Dombkowski DM, Boyd AS, Orkin SH, et al. Haploinsufficiency of GATA-2 perturbs adult hematopoietic stem-cell homeostasis. Blood (2005) 106:477–84.
60. Fujimaki S, Harigae H, Sugawara T, Takasawa N, Sasaki T, Kaku M. Decreased expression of transcription factor GATA-2 in haematopoietic stem cells in patients with aplastic anaemia. Br J Haematol. (2001) 113:52–7.
61. Zeng W, Chen G, Kajigaya S, Nunez O, Charrow A, Billings EM, et al. Gene expression profiling in CD34 cells to identify differences between aplastic anemia patients and healthy volunteers. Blood (2004) 103:325–32.
62. Tong Q, Tsai J, Hotamisligil GS. GATA transcription factors and fat cell formation. Drug News Perspect. (2003) 16:585–8.
63. Xu Y, Takahashi Y, Wang Y, Hama A, Nishio N, Muramatsu H, et al. Downregulation of GATA-2 and overexpression of adipogenic gene- PPARgamma in mesenchymal stem cells from patients with aplastic anemia. Exp Hematol. (2009) 37:1393–9.
64. Kamata M, Okitsu Y, Fujiwara T, Kanehira M, Nakajima S, Takahashi T, et al. GATA2 regulates differentiation of bone marrow-derived mesenchymal stem cells. Haematologica (2014) 99:1686–96.

65. Birbrair A, Frenette PS. Niche heterogeneity in the bone marrow. Ann N Y Acad Sci. (2016) 1370:82–96.
66. Takada I, Kouzmenko AP, Kato S. Wnt and PPARgamma signaling in osteoblastogenesis and adipogenesis. Nat Rev Rheumatol. 2009;5(8):442-447. doi:10.1038/nrrheum.2009.137
67. Yuan Z, Li Q, Luo S, et al. PPARγ and Wnt Signaling in Adipogenic and Osteogenic Differentiation of Mesenchymal Stem Cells. Curr Stem Cell Res Ther. 2016;11(3):216-225. doi:10.2174/1574888x10666150519093429
68. Zhang N, Dai YL, Huang LF, Liu WL. Zhongguo Shi Yan Xue Ye Xue Za Zhi. [Therapeutic effect of lithium chloride combined with cyclosporine A on mouse model with aplastic anemia]. 2012;20(3):654-657
69. Gao M, Ge M, Huo J, et al. Leptin-mediated proinflammatory bone marrow environment in acquired aplastic anemia. Cytokine. 2022;152:155829. doi:10.1016/j.cyto.2022.155829
70. Chen Q, Shou P, Zheng C, et al. Fate decision of mesenchymal stem cells: adipocytes or osteoblasts?. Cell Death Differ. 2016;23(7):1128-1139. doi:10.1038/cdd.2015.168
71. Yin X, Yang J, Liu Y, et al. Altered expression of leptin and leptin receptor in the development of immune-mediated aplastic anemia in mice. Exp Ther Med. 2019;18(2):1047-1056. doi:10.3892/etm.2019.7660
72. Socié G, Henry-Amar M, Bacigalupo A, et al. European Bone Marrow Transplantation-Severe Aplastic Anaemia Working Party. Malignant tumors occurring after treatment of aplastic anemia. N Engl J Med. 1993;329(16):1152-1157.
73. Kim SY, Le Rademacher J, Antin JH, et al. Myelodysplastic syndrome evolving from aplastic anemia treated with immunosuppressive therapy: efficacy of hematopoietic stem cell transplantation. Haematologica. 2014;99(12):1868-1875.
74. Babushok DV. A brief, but comprehensive, guide to clonal evolution in aplastic anemia. Hematology Am Soc Hematol Educ Program. 2018 Nov 30;2018(1):457-466.
75. Scheinberg P. Aplastic anemia: therapeutic updates in immunosuppression and transplantation. Hematology Am Soc Hematol Educ Program. 2012; 2012:292-300.
76. Young NS. Aplastic anaemia. Lancet. 1995 Jul 22;346(8969):228-32.
77. Fingrut, Warren. The Need for Ethnically Diverse Stem Cell Donors. UBCMJ. 2015: 7.1 (44-47).
78. Anthias C, Shaw BE, Bruce JG, et al. Role of Race/Ethnicity in Donor Decisions about Unrelated Hematopoietic Progenitor Cell Donation: Exploring Reasons for Higher Attrition among Racial/Ethnic Minorities. Biol Blood Marrow Transplant. 2020;26(3):593-599.
79. Sloand EM, Read EJ, Scheinberg P, Tang Y, More K, Leitman SF, Maciejewski J, Young NS. Mobilization, collection, and immunomagnetic selection of peripheral blood CD34 cells in recovered aplastic anemia patients. Transfusion. 2007 Jul;47(7):1250-3.
80. Balint B, Stamatovic D, Todorovic M, Elez M, Vojvodic D, Pavlovic M, Cucuz-Jokic M. Autologous transplant in the treatment of severe aplastic anemia - a case report. Transfus Apher Sci. 2011 Oct;45(2):137-41.

81. Rosa M et al. Successful Bone Marrow Recovery After an Immunoablative Regimen with Autologous Cord Blood Transplant in a Child with Idiopathic Severe Aplastic Anemia: A Case Report. Transplant Proc. 2020 Mar;52(2):653-656.
82. Sauer, S., Pavel, P., Schmitt, A. et al. Low-dose peripheral blood stem cell graft after high-dose chemotherapy - an evaluation of hematopoietic reconstitution. BMC Cancer 20, 353 (2020).
83. Park M, Park CJ, Jang S, Kim DY, Lee JH, Lee JH, Lee KH, Hwang K, Lee YH. Reduced expression of osteonectin and increased natural killer cells may contribute to the pathophysiology of aplastic anemia. Appl Immunohistochem Mol Morphol. 2015 Feb;23(2):139-45.
84. Shaik, S., Martin, E.C., Hayes, D.J., Gimble, J, V. Devireddyal, R. Transcriptomic Profiling of Adipose Derived Stem Cells Undergoing Osteogenesis by RNA-Seq. Sci Rep 9, 11800 (2019).
85. Zhu C, Lian Y, Wang C, Wu P, Li X, Gao Y, Fan S, Ai L, Fang L, Pan H, Cheng T, Shi J, Zhu P. Single-cell transcriptomics dissects hematopoietic cell destruction and T-cell engagement in aplastic anemia. Blood. 2021 Jul 8;138(1):23-33.
86. Tonglin H, Yanna Z, Xiaoling Y, Ruilan G, Liming Y. Single-Cell RNA-Seq of Bone Marrow Cells in Aplastic Anemia. Front Genet. 2022 Jan 3;12:745483.
87. Zhou Q, Huang L, Liu Y, Huang J, Wen L, Yang J, Liang J, Chen Y, Chen C. Single-cell RNA sequencing depicts metabolic changes in children with aplastic anemia. Front Oncol. 2023 Mar 29;13:1075408.
88. Branco A, Rayabaram J, Miranda CC, et al. Advances in ex vivo expansion of hematopoietic stem and progenitor cells for clinical applications. Front Bioeng Biotechnol. 2024;12:1380950.
89. Andrade, P.Z., et al., Stem cell bioengineering strategies to widen the therapeutic applications of haematopoietic stem/progenitor cells from umbilical cord blood. J Tissue Eng Regen Med, 2015. 9(9): p. 988-1003.
90. Andrade PZ, dos Santos F, Almeida-Porada G, da Silva CL, S Cabral JM. Systematic delineation of optimal cytokine concentrations to expand hematopoietic stem/progenitor cells in co-culture with mesenchymal stem cells. Mol Biosyst. 2010 Jul;6(7):1207-15.
91. da Silva CL, Gonçalves R, dos Santos F, Andrade PZ, Almeida-Porada G, Cabral JMS. Dynamic cell–cell interactions between cord blood haematopoietic progenitors and the cellular niche are essential for the expansion of CD34+, CD34+CD38- and early lymphoid CD7+ cells. J Tissue Eng and Reg Med. 2010. 4:149-158.
92. Andrade PZ, de Soure AM, Dos Santos F, Paiva A, Cabral JM, da Silva CL. Ex vivo expansion of cord blood haematopoietic stem/progenitor cells under physiological oxygen tensions: clear-cut effects on cell proliferation, differentiation and metabolism. J Tissue Eng Regen Med. 2013.
93. Branco A, Bucar S, Moura-Sampaio J, Lilaia C, Cabral JMS, Fernandes-Platzgummer A, Lobato da Silva C. Tailored Cytokine Optimization for ex vivo Culture Platforms Targeting the Expansion of Human Hematopoietic Stem/Progenitor Cells. Front Bioeng Biotechnol. 2020 Sep 25;8:573282.
94. Carvalho MS, Poundarik AA, Cabral JMS, da Silva CL, Vashishth D. Biomimetic matrices for rapidly forming mineralized bone tissue based on stem cell-mediated osteogenesis. Sci Rep 2018 8:14388 2018.

95. Simões, I.N., et al., Acellular Urethra Bioscaffold: Decellularization of Whole Urethras for Tissue Engineering Applications. Sci Rep, 2017. 7: p. 41934.
96. Bianco, J.E.R., et al., Characterization of a novel decellularized bone marrow scaffold as an inductive environment for hematopoietic stem cells. Biomater Sci, 2019. 7(4): p. 1516-1528.
97. Cabrita, G., Ferreira, BS, Lobato da Silva, C, Gonçalves, R, Almeida-Porada, G, Cabral, JMS, Hematopoietic stem cells: from the bone to the bioreactor. TRENDS in Biotechnology, 2003. 21(5): p. 233-240.
98. de Almeida Fuzeta, M., et al., Addressing the Manufacturing Challenges of Cell-Based Therapies. Adv Biochem Eng Biotechnol, 2020. 171: p. 225-278.
99. Hossain MJ, Xie S. Patient features and survival of pediatric aplastic anemia in the USA: a large institution experience. J Public Health (Oxf). 2019 Jun 1;41(2):329-337.

II. Materials and Methods

II.1. Sampling inclusion criteria, access and collection

All the samples were accessed upon establishment of collaboration protocols with the following clinical units: Pediatrics Hematology Unit, Hospital Dona Estefânia, ULS de São José (principal collaborating physician - Paula Kjöllerström, MD); Hematology Unit, Hospital de São Bernardo, ULS da Arrábida (principal collaborating physician - Joana Santos, MD); Orthopedics and Traumatology Unit, CUF Sintra Hospital (principal collaborating physician - João Sarmento Esteves, MD); Hematology Unit - CUF Sintra Hospital.

BM samples were provided after informed donor consent and under ethical agreement within the clinical institutions involved.

Untreated, SAA and VSAA donors were selected and included, according to the diagnostic criteria of British Society for Haematology [28]: severe AA (SAA): marrow cellularity <25% [or 25–50% with <30% residual hematopoietic cells], plus at least 2 of (i) neutrophils <0.5 x10^9/L, (ii) platelets <20 x 10^9/L (iii) reticulocyte count <20 x 10^9/L; very severe AA (VSAA): as for SAA but neutrophils <0.2 x 10^9/L. An exception was accepted for sample M08A22, collected from a late-relapsed patient (more than six months without therapy), with idiopathic acquired SAA after IST + related allo-HCT, with loss of chimerism of donor cells.

AA-derived samples were collected during posterior superior iliac spine (PSIS) BM aspiration procedure performed for diagnostic purposes.

Control samples were provided either from patients undergoing superior iliac spine (PSIS) BM aspiration for diagnostic purposes but whose results were normal (no disease), and from orthopedics patients undergoing elective hip arthroplasty (excluded patients with bone disease such as bone osteonecrosis, bone fracture, infection, cancer).

Both for disease and control groups, an average volume of 6-8 ml was provided in K2 EDTA tubes. Human immunodeficiency virus 1 and 2 (HIV 1/2) and hepatitis C virus (HCV) status were tested, being an exclusion criterion if positive. In addition, possible causes of AA (e.g., infection, bone marrow failure syndrome associated with inherited germline gene mutation, autoimmune disorder, etc.) were also assessed as exclusion criteria.

For the decellularization experiment, femoral head/neck bone samples were collected from patients undergoing elective hip arthroplasty (excluded patients with bone disease such as bone osteonecrosis, bone fracture, infection, cancer), and stored in a sterile container filled with normal saline.

All BM samples were hand-picked on-site and processed in the same day of BM aspiration procedure at Stem Cell Laboratory of Stem Cell Engineering Research Group (SCERG) of iBB-IST at Taguspark *campus*, Porto Salvo, Oeiras.

II.2. Human BM-MNC fraction isolation

BM mononuclear cells (MNC) fraction was separated and collected using HetaSep™, STEMCELL Technologies, an erythrocyte aggregation agent used to quickly separate nucleated cells from red blood cells (RBC). Centrifugation method was used, according to the following protocol:

1) BM samples, transported in 4 ml K2EDTA tubes, were transferred into a 15 ml Falcon® Conical Tube using a Pasteur pipette and the total volume of bone marrow (BM) sample was determined for each donor.
2) HetaSep™ was added to the whole BM sample at a 1:5 (HetaSep™:BM) ratio, based on the volume determined in step 1, and gently mixed by pipetting.
3) The HetaSep™ BM mixture was then centrifuged at 90 x g at room temperature (15 - 25°C) with the brake off. A 5-minute centrifugation time was used, as recommended by the product information sheet, given the average fresh BM sample volume of approximately 6-8 mL.
4) After centrifugation and careful removal from the centrifuge, the HetaSep™ BM mixture was placed in a tube rack inside the flow hood to sit undisturbed at room temperature for 10 minutes. This step allows for further sedimentation of the RBCs and improves the recovery of nucleated cells.
5) The leukocyte-rich supernatant was then harvested into a sterile 50 mL conical tube with a Pasteur pipette.
6) The harvested fraction was washed with a 4-fold volume of filtered phosphate-buffered saline (PBS) by centrifugation at 120 x g for 10 minutes at room

temperature (15 - 25°C) with the brake off. Subsequently, the supernatant was carefully removed, yielding a cell pellet containing the cells of interest.

7) For samples with significant residual RBCs, an additional step of RBC lysis with ammonium chloride solution was performed. The cells were gently resuspended in 1 mL of PBS, followed by the addition of 4 mL of ammonium chloride solution, and gently mixed by pipetting. The mixture was incubated on ice for 10 minutes and then washed with a 4-fold volume of filtered PBS by centrifuging at 300 x g for 10 minutes at room temperature (15 - 25°C) with the brake off. The supernatant was then carefully removed.
8) After careful removal of the supernatant, as described for steps 6) or 7), cells were resuspended in 3 mL of Dulbecco's Modified Eagle Medium (DMEM) supplemented with 10% Fetal Bovine Serum (FBS) and 1% Antibiotic-Antimycotic (A/A) solution (pre-warmed at room temperature). The type of FBS was chosen according to the following criteria: for sequential BM-MSCs isolation and expansion, MSC-qualified FBS was selected; in case of MNC liquid/vapour phase nitrogen cryopreservation or sequential isolation of CD34+ cells, non-MSC-qualified FBS was chosen.
9) Conventional cell counting with a hemacytometer (Neubauer chamber) and trypan blue (Thermo Fisher Scientific) was performed to assess the total cell number and viability. The Trypan blue exclusion method relies on the entry of Trypan blue dye into cells with compromised membrane integrity, staining dead cells blue.

II.3. Cell cryopreservation and thawing

Cell cryopreservation protocol

A cell cryopreservation protocol was performed either to immediately preserve the mononuclear cells (MNC) separated from whole bone marrow (BM) samples (section II.2) or after BM-MSCs harvesting following culture expansion. For both purposes, the cell cryopreservation protocol was the following:

1) Either after MNC separation from whole BM or upon harvesting of BM-MSCs from culture, conventional cell counting with a hemacytometer (Neubauer chamber) and trypan blue (Thermo Fisher Scientific) was performed to assess the total cell number and viability.
2) To pellet the cells, samples were centrifuged as follows: MNCs at 300 x g for 10 minutes at 15°C, and MSCs at 300 x g for 5 minutes at room temperature (15 - 25°C).
3) Then, the number of cryovials for each sample was planned according to the desired cell storage concentration (0.5 - 10 x 10^6 MNC/mL; up to 1×10^6 BM-MSCs/mL). Labeling of the cryovials was performed, indicating the sample identification, the cryopreservation medium, the cell passage number (if applicable), and the date of cryopreservation.
4) The freezing medium was prepared by combining 10% dimethyl sulfoxide (DMSO) with 90% cell culture medium. The specific cell culture medium varied by cell type: for MNCs, it was 10% FBS-DMEM (containing 1% Antibiotic-Antimycotic solution) with non-MSC-qualified FBS; for MSCs, 10% FBS-DMEM (containing 1% Antibiotic-Antimycotic solution) using MSC-qualified FBS was employed. This prepared medium was then kept cold (on ice or at 4°C). The volume of freezing medium required was calculated based on the number of samples, the initial cell count, and the desired final cell concentration per cryovial. On average, 1 to 1.5 mL of freezing medium was used per cryovial for each sample.
5) Cells were gently resuspended in the prepared freezing medium to achieve the desired cell storage concentration. Aliquots of 1 to 1.5 mL were then dispensed into 1.8-mL cryovials (Abdos®).
6) The filled cryovials were then placed into a gradual freezing container (e.g., Mr. Frosty, Nalgene®, 12-place capacity). To ensure proper thermal mass and uniform cooling, empty slots were filled with balancing tubes. The container was then transferred to a -80°C freezer for a minimum of 12 hours. This step facilitates a gradual cooling rate (approximately 1°C/min), which is critical for preventing the formation of damaging intracellular ice crystals and improving overall cell survival during cryopreservation.

7) After the gradual freezing process, the cryovials were transferred into a liquid/vapour phase nitrogen storage tank for long-term storage. At the Stem Cell Laboratory of SCERG, iBB-IST, cryopreserved cells are stored according to specific internal rules. These rules dictate storage based on cell type and cell passage number (P). Specifically, P0 corresponds to MSCs harvested immediately after isolation from MNCs. Pn corresponds to subsequent passages, where 'n' equals the number of cell culture and harvesting cycles. It is important to note that the passage number increases by one each time cells are thawed and re-seeded (e.g., P = Pn as labeled in the cryovial + 1). For this project, MNC and low passage number BM-MSCs were preferentially stored in a master cell liquid/vapour phase nitrogen bank to ensure better stock preservation of primary samples. BM-MSCs under study were stored in a working cell bank in a liquid/vapour phase nitrogen container.

Cell thawing protocol

The cryopreserved MNC and BM-MSC samples were thawed using a common protocol, detailed below:

1) For thawing, the cryovial(s) of interest were swiftly transferred from the liquid/vapour phase nitrogen tank to a 37°C water bath. The cell suspension was continuously monitored until completely thawed. This rapid thawing procedure is critical to prevent ice crystal formation and to ensure maximum cell viability.
2) Then, in a laminar flow hood, the cell suspension was harvested using a 1 mL pipette and transferred into a 15 mL conical tube, taking care to avoid the introduction of bubbles during the transfer.
3) A volume of 3 to 5 mL (dependent on the cryopreserved cell concentration) of 10% FBS-DMEM (1% Antibiotic-Antimycotic solution) medium, pre-warmed to room temperature, was added to the conical tube containing the cell suspension. The mixture was then gently mixed by slowly pipetting up and down (two to three times) to avoid introducing bubbles.

4) Thawed cells were pelleted by centrifugation at 300 x g for 5 minutes at room temperature (15-25°C). The supernatant was then aspirated, and the resulting cell pellet was resuspended in 3 to 5 mL of pre-warmed 10% FBS-DMEM (1% Antibiotic-Antimycotic solution) medium. The resuspension volume was adjusted based on the initial cryopreserved cell concentration.
5) Conventional cell counting with a hemacytometer (Neubauer chamber) and trypan blue was performed to assess the total cell number and viability. This information was then used to determine the appropriate cell seeding strategy. For the initial isolation of BM-MSCs from the MNC fraction, the seeding density was set at 2×10^5 cells/cm^2. For subsequent expansion of BM-MSCs, a seeding density of 3×10^3 cells/cm^2 was used.

To minimize the potential effects of cryopreservation on cell function, all experiments involving phenotypical and functional assays of BM-MSCs and molecular studies (e.g., cell RNA extraction), were performed after the cells had undergone one passage following thawing, as detailed in subsequent sections.

II.4. Establishment of a Human BM-MNC and BM-MSCs cell biobank

A cell biobank composed of MNC and BM-MSCs isolated from both BM samples collected from AA and control donors was established at Stem Cell Laboratory of iBB-IST at Taguspark *campus* and has been continuously expanded.

Samples were allocated in the biobank according to the following rules:

1) All samples were identified by pseudonymization according to the following standard rule – F = female/M = male(gender) | # # (year of birth) | A # # (year of collection). For example, M10A22 refers to a male donor, born in 2010, whose sample was collected in 2022.
2) A complete database detailing cell type (e.g. BM-MNC; BM-MSCs), sample source (e.g. PSIS; femoral head/neck), number of available cryostored vials from each donor, including passage number cell concentration and liquid/vapour phase nitrogen tank location, was generated and has been continuously updated.

3) Subsequent data from cytogenetic and molecular studies performed on diseased samples within the context of AA diagnostic guidelines were provided by the clinical unit and added to the database under the 'Observations' entry for each AA patient. Notably, for all patients diagnosed with AA, a next-generation sequencing (NGS) panel designed to evaluate genes associated with various forms of bone marrow failure syndromes (including Fanconi anemia, dyskeratosis congenita, and Diamond-Blackfan anemia) was performed at diagnosis. No mutations were detected.

Presently, the biobank includes samples from: five patients *de novo* diagnosed with severe acquired idiopathic AA (median age = 13 years; minimum = 2 years; maximum = 35 years); one relapsed patient with severe acquired idiopathic AA after allo-HCT from a related donor; one patient in partial response after IST therapy with ATG + CsA; sixteen control (healthy) donors (median age = 57 years; minimum = 4 years; maximum = 73 years).

MSCs studies

II.5. Human BM-MSCs isolation and expansion

BM-MSCs isolation and expansion protocol

1) Previously isolated MNC (HetaSep™, STEMCELL Technologies) were seeded in 6 or 12-well plates (depending on sampling amount) at a density of 200000 MNC/cm^2 and cultured in 10% FBS MSCs-qualified + DMEM + 1% A/A (pre-warmed at room temperature) medium at 37°C with 5% CO_2 in a humidified chamber. For BM-MSCs isolation, different coating strategies were used: no coating; gelatin 0.1% coating (G1393 gelatin solution, Sigma-Aldrich®); laminin-521 (LN521) coating (Biolaminin 521 LN, BioLamina). After filtered-PBS dilution of coating agent, culture wells were homogeneously coated, and plates were incubated at 37°C for 1 hour. Supernatant was then aspirated, and plates were additionally washed (genly rinse) with PBS in order to remove any unbounded coating.

2) Medium changes were performed each 72h and cells were harvested at 70% confluence. For cell harvesting, supernatant medium was removed and an appropriate volume of 0.05% trypsin-EDTA solution (working solution: 1 ml trypsin 2.5% + 100 μL EDTA 0.5M + 48.9 ml PBS) to cover the cell monolayer was added. After 10 min incubation at 37°C cells were observed in optical microscope in order to ascertain if detachment was attained. Then, culture medium in a 2:1 ration was added to inhibit trypsin effect and cell mixture was collected by gently pipetting the cell suspension up and down to dislodge any remaining cells.
3) Cell suspension was transferred into a sterile conical centrifuge tube and centrifugated at 300 x g for 5 minutes at room temperature (15 - 25°C). After resuspension in 10% FBS-DMEM (1% A/A) MSCs-qualified medium (pre-warmed at room temperature), conventional cell counting with a hemacytometer (Neubauer chamber) and trypan blue was performed to assess the total cell number and viability.
4) After BM-MSCs isolation, cells were replated (in passage 0 [P0] stage) on uncoated T-Flasks at a cell density of 3000 cells/cm^2. T-flask area was chosen according to sampling amount. Cells were incubated at 37°C with 5% CO_2 in a humidified chamber.
5) Medium changes where performed each 72h and cells were harvested at 70% confluence. Conventional cell counting with a hemacytometer (Neubauer chamber) and trypan blue was performed to assess the total cell number and viability.

Proliferation rate comparisons between AA and control-derived BM-MSCs was performed by either assessing the number of days until 70% confluence, in case of BM-MSCs isolation, or by calculation of the fold increase (FI) of cell number at 70% confluence harvesting (FI = number of cells harvested at 70% confluence divided by the seeding cell number), in case of BM-MSCs expansion after isolation. Results were plotted in bar charts (designed with Microsoft Excel).

For both three AA-derived (M15, M10, M87) and control-derived (F18, M11, M78) BM-MSCs samples replated after one passage post-thawing on 12-well plates

at a density of 3000 cell/cm^2, *in vitro* proliferative kinetics was daily assessed. The experiment was performed for 7 days. Cells were seeded in 21 wells (7 wells [one for each day of counting] x technical triplicates) of 12-well plates, and the cell number for each day (D0 = day of cell seeding) was determined by the total number of cells harvested from the respective well and counted with a hemacytometer on bright-field microscope. Results were plotted by means of a line graph (designed with Microsoft Excel).

For each experimental setup, proliferative analysis was performed in technical triplicates, and the mean of results (±SE of the mean) was graphically represented.

After BM-MSCs isolation and expansion, cells were immunophenotypically and functionally characterized, as described below. Liquid/vapour phase nitrogen cryopreservation of BM-MSCs was performed in order to establish a cell biobank of AA and control-derived BM-MSCs.

II.6. Human BM-MSCs multilineage differentiation assays

To confirm osteogenic, chondrogenic and adipogenic differentiation capacity of BM-MSCs isolated and expanded from each single donor BM sample, differentiation assays and respective stainings were performed (technical triplicates for each sample), as below.

Osteogenic differentiation assay:

1) BM-MSCs were seeded on 12-well plates at a cell density of 3000 cell/cm^2 and expanded in 10% FBS-DMEM (1% A/A) medium (pre-warmed at room temperature) at 37°C with 5% CO_2 in a humidified chamber until 80-90% cell confluency.
2) Culture medium was aspirated and replaced by 1 ml of MesenCult™ Osteogenic Differentiation supplemented medium (STEMCELL Technologies) + 1% A/A (pre-warmed at room temperature) and cells were incubated at 37°C with 5% CO_2 in a humidified chamber
3) Differentiation medium was changed every 3 days until 14 days of culture time for cell differentiation.

4) Osteogenic differentiation of MSCs was visualized by staining with alkaline phosphatase (ALP), to assess osteoblast activity, and silver nitrate (von Kossa), to assess the presence of calcium deposits.
5) ALP staining (sequential steps) - remove the media from the wells; wash once with PBS (200µl); fix the cells in 4% PFA (200µl) for 30 minutes at room temperature (RT) and protected from light; wash the wells twice with PBS (200µl) for 5 minutes at room temperature; keep the cells in distilled water for 15 minutes (200µl); mix an aliquot of Fast Violet (Sigma-Aldrich) (1.5ml) with 60µl of naphtol (Sigma-Aldrich), add 200µl to cover the well surface and incubate for 45 minutes at room temperature, protected from light; wash three times with PBS (200µl); keep in distilled water and take photos on bright-field microscope (Olympus IX51 Inverted Microscope) equipped with an attached digital camera.
6) von Kossa (VK) staining (sequential steps) – this protocol is to be performed after the protocol for ALP staining; wash cells with distilled water (200µl); stain cells with 200 µL of 2.5% silver nitrate solution (Sigma-Aldrich) for 30 minutes, at RT; wash three times with PBS (200µl); keep in distilled water and take photos on bright-field microscope (Olympus IX51 Inverted Microscope equipped with an attached digital camera).

Adipogenic differentiation assay:

1) BM-MSCs were seeded on 12-well plates at a cell density of 3000 cell/cm^2 and expanded in 10% FBS-DMEM (1% A/A) medium (pre-warmed at room temperature) at 37°C with 5% CO_2 in a humidified chamber until 80-90% cell confluency.
2) Culture medium was aspirated and replaced by 1 ml of MesenCult™ Adipogenic Differentiation supplemented medium (STEMCELL Technologies) + 1% A/A (pre-warmed at room temperature) and cells were incubated at 37°C with 5% CO_2 in a humidified chamber.
3) Differentiation medium was changed every 3 days until 14 days of culture time for cell differentiation.

4) Adipogenic differentiation of MSCs was visualized by Oil Red O staining, used to stain neutral lipids with red color, but not differentiating distinct types of lipids (e.g., triglycerides, cholesterol esters). Upon availability, in last experiments AdipoRed™ Assay Reagent (Lonza), a fluorescent dye designed to stain intracellular lipid droplets, relatively specific to neutral lipids, was also applied. Both Oil Red O and AdipoRed™ are relatively specific to neutral lipids and, despite at a lesser extent, could stain some phospholipids or other intracellular hydrophobic molecules, which should be considered for results interpretation.

7) Oil Red O staining (sequential steps) – wash the cells twice with PBS (200µl); fix the cells in 4% PFA (200µl) for 30 minutes at room temperature and protected from light; 3) wash three times with PBS (200µl); incubate the cells with 0.3% Oil Red-O (Sigma-Aldrich) solution for 1 hour at room temperature; wash the wells twice with PBS (200µl); keep in distilled water and take photos on bright-field microscope (Olympus IX51 Inverted Microscope with an attached digital camera).

   To make Oil Red O working solution, a 0.5% stock solution of Oil Red O was prepared by dissolving 0.5 grams of Oil Red O powder (Sigma-Aldrich) in 100 ml of 100% isopropanol. To dissolve the powder, the solution was stirred thoroughly and allowed to sit undisturbed for 20 minutes. Working solution was stored in the fridge (4°C). Whenever Oil Red O staining was to be performed, a fresh 0.3% working solution was prepared from the stock solution (e.g. 30 ml of the 0.5% Oil Red O stock solution diluted 20 ml of distilled water). After dilution, the working solution must be well stirred and allowed to sit undisturbed for 10 minutes. Then, before being applied over cells, it must be filtered (e.g. with a Whatman® qualitative filter paper, Grade 1, or a syringe filter) to remove any undissolved particles.

8) AdipoRed™ (Lonza) protocol (sequential steps) – remove the culture medium and gently wash the cells with PBS; add 5 µL of AdipoRed™ (Lonza) directly to each well containing 1 ml of PBS; pipette gently to ensure even distribution of the reagent; incubate the cells in the dark at room

temperature for 15 minutes (do not exceed the recommended incubation time to avoid increase of background fluorescence); visualize cells and take photos on a fluorescence microscope (Olympus IX51 Inverted Microscope equipped with an attached digital camera).

Chondrogenic differentiation assay:

1) After centrifugation of MSCs to obtain a cell pellet, supernatant was removed letting a small residual volume, then mixed with the cell pellet.
2) Micromass cell cultures were generated by seeding 5 μL droplets of cell concentrate in ultra-low attachment 24-well plate (Corning®). About five droplets were seeded at symmetrically distanced points (e.g. one drop at the upper-middle, one drop at lower-middle, one drop at right-middle, one drop at left-middle, one drop at the center).
5) Plates were then incubated at 37°C with 5% CO_2 in a humidified chamber for 1 hour.
6) 1 ml of StemPro® Chondrogenesis Differentiation supplemented medium (Gibco) (pre-warmed at room temperature) was gently added to each cell-seeded well, followed by plate incubation at 37°C with 5% CO_2 in a humidified chamber.
7) Cultures were refeeded with differentiation (about 250 μL) medium every 3 days until 21 days of culture time for cell differentiation.
8) Chondrogenic differentiation of MSCs was visualized by Alcian Blue stain, used to assess proteoglycan synthesis (blue-colored) by chondrocytes.
9) Alcian Blue staining (sequential steps) – remove media from culture well and rinse once with PBS (200 μL); fix cells with 4% PFA solution (200 μL) for 30 minutes; after fixation, rinse wells with PBS (200 μL) and stain cells with 1% Alcian Blue (Alcian Blue 8GX, Sigma-Aldrich) prepared in 0.1 N HCL for 30 minutes (200 μL); rinse wells three times with 0.1 N HCL and add 200 μL of distilled water to neutralize acidity; visualize cells and take photos on bright-field microscope (Olympus IX51 Inverted Microscope equipped with an attached digital camera).

II.7. Human BM-MSCs immunophenotypic characterization by Flow Cytometry

For all samples, immunophenotypic characterization was performed by flow cytometry, firstly on a FACSCalibur™ flow cytometer (BD Biosciences) and more recently on a FACSCanto™ II (BD Biosciences), due to equipment replacement.

Flow cytometry protocol for BM-MSCs

1) Previously harvested BM-MSCs were homogeneously distributed by four flow cytometry tubes at a cell concentration between $5x10^4$ to $10x10^4$ cells per tube (depending on the available cell numbers for each experiment) and washed with PBS (until 2 ml).
2) Cells were firstly stained with Far Red LIVE/DEAD™ Fixable Dead Cell Stain Kit (Thermo Fisher Scientific) viability dye and then, after 15 minutes of incubation in the dark at room temperature and PBS washing (2 ml), with a multicolor previously titrated antibody panel (BioLegend) for cell surface markers, combined in three tubes (Tube 1 - CD73 FITC; CD90 PE; CD44 PerCP-Cy5.5; live/dead; Tube 2 – CD34 FITC, CD14 PE, CD105 PerCP-Cy5.5, CD19 APC; Tube 3 – HLA-DR FITC, CD80 PE, CD45 PerCP-Cy5.5, CD11b APC; Tube 4 - unstained).
3) After a 15-minute period of incubation in the dark at room temperature and PBS washing (2 ml), cells were immediately analyzed in the flow cytometer (a yield of 10000 events per tube was established). To notice that, despite unstained, the fourth tube was processed in the same way as the other ones (except for staining), in order to achieve more accurate and comparable results.

The flow cytometry panel was designed according to a pre-established panel for MSCs characterization (positive markers: CD73, CD90, CD44, CD105; negative markers: CD34, CD14, CD19, HLA-DR, CD80, CD45, CD11b) and flow cytometer settings were performed for both cytometers as needed (e.g., after technical maintenance of the equipment; after change of the lot number of

BD® Cytometer Setup and Tracking (CS&T) beads; after specific experimental settings that could change cell properties).

Flow cytometry data was analyzed with FCS Express™7 (De Novo Software by Dotmatics). Cell surface marker expression was determined by both determining the percentage (%) of cells expressing positive/negative markers and by mean fluorescence intensity (MFI; mean geometric mean was used). Representative images of flow cytometry analysis of BM-MSCs samples using FCS Express™7 [De Novo Software by Dotmatics] are included in chapter X.ii., Appendix B (B.1. and B.2.).

II.8. Human BM-MSCs RNA extraction and cDNA synthesis

RNA extraction was performed by using High Pure RNA Isolation Kit (Roche) and according to the manufacturer's protocol, which briefly consists of:

1) Cell lysis and homogenization in the presence of chaotropic salts (lysis buffer) and RNAses inactivation.
2) Nucleic acids binding to glass fibers pre-packed in High Pure Filter Tube.
3) Digestion of residual contaminating DNA by DNAse I .
4) Washing (by centrifugation) of bound nucleic acids with a specially developed Wash Buffer to get rid of RT-PCR inhibitory contaminants.
5) Further washing of bound nucleic acids for salts, proteins and other cellular impurities purification.
6) RNA recovery in a new collecting tube by using the Elution Buffer (applied into the High Pure Filter Tube containing the RNA) and after centrifugation.

RNA quantification was performed with NanoDrop® (Thermo Fisher Scientific). For quality control, A260/A280 ratio (indicating protein contamination) between 1.8 to 2.0 and A260/A230 ratio (indicating contamination with organic compounds) between 2.0-2.2 were checked and all samples were in the optimal range. In each experiment, RNA concentration of different samples was normalized (e.g., by further dilution with Elution Buffer, if needed) before cDNA synthesis. After normalization, RNA concentration was further confirmed with NanoDrop® (Thermo

Fisher Scientific). RNA samples were then stored in 1.5. ml microtubes, properly identified, at -80°C freezer or sequentially converted in cDNA.

cDNA synthesis was performed by using High-Capacity cDNA Reverse Transcription Kit (Applied Biosystems™) according to the manufacturer's protocol, on cold, as described below:

1) Thawing of kit components (10X RT Buffer, 25X dNTP Mix (100 mM), 10X RT Random Primers and MultiScribe™ Reverse Transcriptase) on ice.
2) Calculation of the volume of components needed to prepare the required number of reactions. The final volume of master mix per reaction must be of 10 μL. Nuclease-free water (4.2 μL per reaction) is added to attain the desired volume.
3) Gently mixing of the 2X RT master mix and placement on ice.
4) Pipetting of 10 μL of 2X RT master mix into individual PCR tubes.
5) Pipetting of 10 μL of RNA sample into each tube, mixing up and down for two times.
6) Placing the tubes on ice until readiness to load the thermal cycler (VWR® PCR thermal cycler XT96 and Bio-Rad T100 Thermal Cycler were used).
7) Programming of the thermal cycler (Step 1 at 25°C for 10 minutes; Step 2 at 37°C for 120 minutes; Step 3 at 85°C for 5 minutes; Step 4 at 4°C, hold).
8) Setting of the reaction volume to 20 μL.
9) Loading of reaction tubes into thermal cycler and starting the thermal cycler running.

After cDNA synthesis samples were stored at -20°C freezer or sequentially used for RT-qPCR analysis.

II.9. Human BM-MSCs RT-qPCR analysis

RT-qPCR analysis was performed with NZYSpeedy qPCR Green Master Mix (2x), ROX plus (NZYtech) in StepOnePlus™ (Applied Biosystems™) and System Quant Studio™ 5 Real-Time PCR System (Applied Biosystems™), by delta-delta Ct (ΔΔCt) method. cDNA amount per reaction was optimized in order maximize the usage of available cDNA, without compromising sensitivity and results reproducibility. As so, about 50 ng of cDNA was used per reaction.

Results, represented by AA versus controls log2 fold change (L2FC; FC = $2^{-\Delta\Delta Ct}$), were plotted on bar graphs (designed in Microsoft Excel).

RT-qPCR genes and respective primer sequences are shown in Table 2, below.

Table 2 – Studied genes and RT-qPCR primer sequences.

Gene	Primer Sequence (5' to 3')
GAPDH_FW (housekeeping gene)	GTCTCCTCTGACTTCAACAGCG
GAPDH_RV (housekeeping gene)	ACCACCCTGTTGCTGTAGCCAA
ACTB_FW (housekeeping gene)	CACCATTGGCAATGAGCGGTTC
ACTB_RV (housekeeping gene)	AGGTCTTTGCGGATGTCCACGT
APOL4_FW	CCTGGAAGAGATTTGTGCGTGTG
APOL4_RV	AACCACTCCCTAAACTGCTGTTC
BHLHE41_FW	CTGGGACATCTGGAGAAAGCTG
BHLHE41_RV	AGTGGAACGCATCCAAGTCGGA
CD74_FW	AAGCCTGTGAGCAAGATGCGCA
CD74_RV	AGCAGGTGCATCACATGGTCCT
HOTAIR_FW	CCAGAGAACGCTGGAAAAACCTG
HOTAIR_RV	GGAGATGATAAGAAGAGCAAGGAA
TNFSF9_FW	GCCTCTTGGACCTGCGGCAG
TNFSF9_RV	CGTGTCCTCTTTGTAGCTCAGG
MYBL1_FW	CGTGGAGGCAAACGCTGTGTTA
MYBL1_RV	GGTGGATTTGATAGGAGAAGCAG
WNT5A_FW	TACGAGAGTGCTCGCATCCTCA
WNT5A_RV	TGTCTTCAGGCTACATGAGCCG
KCTD9_FW	GCCGCTGTAATCTTGCACATGC
KCTD9_RV	CAGTTTCAGGGATGCTCCTTCTG

SOCS2_FW	GGTCGGCGGAGGAGCCATCC
SOCS2_RV	GAAAGTTCCTTCTGGTGCCTCTT
SOCS3_FW	CATCTCTGTCGGAAGACCGTCA
SOCS3_RV	GCATCGTACTGGTCCAGGAACT
RBP1_FW	ACGGAGACAAGCTCCAGTGTGT
RBP1_RV	GACCACACCTTCCACTCTCATC
SPARC_FW	ACATGGGTGGACACGG
SPARC_RV	CCAACAGCCTAATGTGAA
PPARG_FW	TCTGCAAACATATCACAAGAAATGA
PPARG_RV	TCCACGGAGCTGATCCCAA
FABP4_FW	GACAGGAAAGTCAAGAGCACCATA
FABP4_RV	GACGCATTCCACCACCAGTT
GATA2_FW	CAGCAAGGCTCGTTCCTGTT
GATA2_RV	GGCTTGATGAGTGGTCGGT
BGLAP_FW	CGCTACCTGTATCAATGGCTGG
BGLAP_RV	CTCCTGAAAGCCGATGTGGTCA
SPP1_FW	CGAGGTGATAGTGTGGTTTATGG
SPP1_RV	GCACCATTCAACTCCTCGCTTTC
CEBPA_FW	AGGAGGATGAAGCCAAGCAGCT
CEBPA_RV	AGTGCGCGATCTGGAACTGCAG
RARA_FW	AGCACCAGCTTCCAGTTAGTGG
RARA_RV	CAAAGCAAGGCTTGTAGATGCGG
ARID5A_FW	TGGCAAGCAGAACGGAATCCAG
ARID5A_RV	CTTGTAGAGGCTGACCAGGAAG
LEPR_FW	GCAGTCTATGCTGTTCAGGTGC
LEPR_RV	CCAAAATTCAGGTCCTCTCATAGG

II.10. Human BM-MSCs absolute telomere length quantification by RT-qPCR

BM-MSCs absolute telomere length was performed by RT-qPCR with Absolute Human Telomere Length Quantification qPCR Assay Kit (ScienCell™), according to the manufacturer's protocol. The kit contains a single copy reference (SCR) primer set that recognizes and amplifies a 100 bp-long region on human chromosome 17,

serving as reference for data normalization, and a reference genomic DNA sample with known telomere length used as reference for calculating the telomere length of the target samples. Also included is the 2X GoldNStart TaqGreen qPCR Master Mix, a SYBR®Green dye-based qPCR master mix with a "hot-start" property (for maximal inhibition of primer dimer formation), containing SYBR®Green, dNTPs, Taq DNA polymerase, and an inert gold-color loading indicator in a single tube (allows for better visualization and tracking of sample loading in qPCR plates or tubes).

The quantification method was performed by comparative ΔΔCt method, as follows:

1) For telomere (TEL), ΔCt (TEL) is the quantification cycle number difference of TEL between the target and the reference genomic DNA samples.

   → ΔCt (TEL) = Ct (TEL, target sample) - Ct (TEL, reference sample)

2) For single copy reference (SCR), ΔCt (SCR) is the quantification cycle number difference of SCR between the target and the reference genomic DNA samples.

   → ΔCt (SCR) = Ct (SCR, target sample) - Ct (SCR, reference sample)

3) ΔΔCt = ΔCt (TEL) - ΔCt (SCR)
4) Relative telomere length of the target sample to the reference sample (fold) = $2^{-\Delta\Delta Ct}$
5) Considering reference sample telomere length of 1.23 ± 0.09 Mb, the total telomere length of the target sample = (1.23 ± 0.09 Mb) x $2^{-\Delta\Delta Ct}$
6) As there are 92 chromosome ends in one diploid cell, average telomere length on each chromosome end = (1.23 ± 0.09 Mb) x $2^{-\Delta\Delta Ct}$/92
7) Results were expressed in kilobase (kb).

II.11. Human BM-MSCs bulk-mRNA sequencing

BM-MSCs absolute bulk-mRNA sequencing of both AA and control samples was performed at Genomic Unit of Instituto Gulbenkian Ciência, Oeiras. Sampling metadata are shown in Table 3, below.

Table 3 – RNA samples for bulk mRNA-Seq: identification (ID) and characteristics of aplastic anemia (AA) and control bone marrow (BM) donors; disease severity and treatment status; source of MSCs; passage number of MSCs at RNA extraction; and RNA quantification after extraction (measured in NanoDrop®).

Samples	Sample ID	Age (years)	Gender	Disease Severity and Treatment Status	MSCs source	MSCs passage number	RNA quantification [after dilution]
AA donors (disease)	AM15	7	Male	*De novo*, previously untreated, SAA	Bone Marrow (PSIS)	P5	301 ng/μl [54.2 ng/μl]
	AM10	12	Male	*De novo*, previously untreated, SAA	Bone Marrow (PSIS)	P3	291 ng/μl [55.3. ng/μl]
	AM08	14	Male	SAA Relapse post IST + related allogeneic-HCT (relapse after more than six months without therapy; loss of chimerism of donor cells)	Bone Marrow (PSIS)	P6	398 ng/μl [62.6 ng/μl]
	AM87	35	Male	*De novo*, previously untreated, SAA	Bone Marrow (PSIS)	P4	252 ng/μl [69.3 ng/μl]
Healthy donors (controls)	CF18	4	Female	Febrile syndrome - hematologic disorder excluded	Bone Marrow (PSIS)	P5	716 ng/μl [91.3 ng/μl]
	CM11	11	Male	Elective orthopedic surgery for benign condition	Bone Marrow (femoral head/neck)	P2	384 ng/μl [66.2 ng/μl]

	CF10	12	Female	Elective orthopedic surgery for benign condition	Bone Marrow (vertebral body)	P6	191 ng/μl [61.6 ng/μl]
	CM78	44	Male	Elective BM aspirate for diagnostic purposes - hematologic disorder excluded	Bone Marrow (PSIS)	P2	71.6 ng/μl [not diluted]

AA – aplastic anemia; BM – bone marrow; HCT - hematopoietic cell transplantation; PSIS – posterior superior iliac spine; IST – immunosuppressive therapy; SAA – severe aplastic anemia; Sample ID - Sample Identification. AM15 – biobank's sample M15A22; AM10 - biobank's sample M10A22; AM08 - biobank's sample M08A22; AM87 - biobank's sample M87A22; CF18 - biobank's sample F18A22; CM11 - biobank's sample M11A22; CF10 - biobank's sample F10A22; CM78 - biobank's sample M78A22.

Bulk mRNA-Seq protocol

1) RNA extraction was performed by using High Pure RNA Isolation Kit (Roche) and according to the manufacturer's protocol. Extraction was performed immediately after MSCs harvesting. RNA quantification was performed with NanoDrop® (Thermo Fisher Scientific). According to the guidelines of Genomics Unit, the concentration of RNA samples was normalized to a maximum range of 100 ng/μl. For each sample, a quality control (QC) aliquot was prepared to be analyzed in Fragment Analyzer™ system (Agilent Technologies).
2) RNA samples were stored at -80ºC for a maximum period of 5 days, the necessary time to complete RNA extraction for all samples. RNA samples (Total RNA) were packaged in dry ice and directly transported (in less than 30 minutes) to the Genomics Unit at Instituto Gulbenkian Ciência (IGC).
3) Quality control of RNA samples was performed by using Fragment Analyzer™ (Agilent Technologies), an automated parallel capillary electrophoresis system, and analyzed with ProSize data analysis software 4.0.2.7. All samples passed QC.
4) Full-length cDNAs were generated following the SMART-Seq2 protocol as described by Picelli, 2014 [1]. Quality control of cDNA was performed by using Fragment Analyzer™ (Agilent Technologies) and ProSize data analysis software 4.0.2.7. All samples passed QC.

5) Library preparation was performed following the Nextera library preparation protocol (Nextera® XT DNA Library Preparation kit, Illumina), as previously described by Baym, 2015 [2]. Libraries were confirmed by Fragment Analyzer™ (Agilent Technologies) and then sequenced in NextSeq2000 (Illumina) using NextSeq 1000/2000 P2 Reagents (100 Cycles) v3 (Illumina, reference 20046811). With this method, 100 bp single-end reads were obtained.
6) For the experiment, a yield of about 25 million reads per sample was requested. Sequence information was extracted in FASTQ format, using Illumina DRAGEN FASTQ Generation v3.8.4. Library preparation and sequencing were performed and optimized at Genomics Unit of IGC.

II.12. Bulk mRNA-Seq data analysis

Bioinformatics analysis protocol

1) After sequencing, for each sample, a ". fastq" file was provided. Quality control was performed with FastQC, with adequate results (Table A.1, Appendix A).
2) Genome indexing and reads alignment onto human reference genome (GRCh38 [3, 4]) were then performed by using STAR (2.7.11a --- 2023/08/15 ::: STARdiploid) [5,6] (mapping statistics summarized in Table A.2, Appendix A). Data quality showed to be adequate for all samples and variation between samples was low.
3) By using RSamtools [7], index BAM files (.bai) were generated. After fixing file names and BAM indexing, feature counting was performed. Generation of a count matrix table with counts for all samples (genes in rows; samples in columns) was performed in RStudio Software (R version 4.2.3) [6], by applying "GenomicFeatures" and "GenomicAlignments" BioConductor's packages [8].
4) Hierarchical clustering was performed by applying DSEq2 package [9]. Variance stabilizing transformation (VST) function was used (to yield a matrix of approximately homoskedastic values, with constant variance

along the range of mean values, normalized with respect to library size). VST-transformed counts matrix with the 500 most variable genes was then generated and values were scaled (z-score) to be plotted by means of a heatmap. Plotting was performed with R package “gplots” [10].

5) Principal component analysis (PCA) was performed by applying prcomp() function and graphic visualization of PCA analysis was generated with R package “factoextra” [11].
6) Differential gene expression analysis (DGE) was then performed by using DESeq2 package [9] and graphically represented in a volcano plot, designed with “EnhancedVolcano” R package [13]. In order to make the estimates more robust also for genes with low read counts, lfcShrink() function and “apelglm” R package (apeglm provides Bayesian shrinkage estimators for effect sizes for a variety of generalized linear models (GLM)) were applied [1212]. This step was of particular importance in this experiment, taking into consideration the limited number of samples and consequent heavily rely on the L2FC values for downstream analysis. Therefore, “apeglm” provides Bayesian shrinkage estimators for effect sizes for a variety of GLM models, using approximation of the posterior for individual coefficients.
7) Functional enrichment analysis was then performed, either by means of Gene Ontology (GO) Over Representation Analysis (ORA) and Gene Set Enrichment Analysis (GSEA), using “clusterProfiler” [14, 15] and "org.Hs.eg.db" R packages [16]. Complimentary functional enrichment analysis and conversion of gene lists was performed with g:Profiler [17].
8) A deeper exploratory analysis (manual datamining) was subsequently done, in order to identify gene subsets associated to functional groups of interest in the context of AA. For that purpose, GeneCards – the human gene database [18], Enrichr [19] and PubMed were systematically consulted.
9) For visualization of DGE by functional group, heatmaps and stripcharts were drawn with “ggplot2” R package [20].

II.13. Human BM-MSCs *in vitro* drug-modulation with isotretinoin

Drug-modulation of both AA and control-derived BM-MSCs with isotretinoin, selected upon the results of transcriptomics analysis (which suggested significant expression differences in *RARA* and functionally related genes), was performed. Isotretinoin, used to treat acne, may act as a prodrug, being intracellularly converted into retinoic acid receptors (RARs) and retinoid X receptors (RXRs) agonist activators. Five isotretinoin metabolites are known: all-trans retinoic acid (ATRA), 13-cis-4-oxo-retinoic acid, all-trans-4-oxo-retinoic acid, 9-cis-retinoic acid and 9-cis-4-oxoretinoic acid. In sebaceous glands of patients with acne, isotretinoin enhances expression of proapoptotic transcription factors, as p53, hence induction of sebocyte apoptosis and depletion of sebocyte progenitor cells, which leads to its sebum-suppressive effect [21].

For drug-modulation, AA and control BM-MSCs were seeded at a cell density of 3000 cell/cm^2 on 24-well plates (technical triplicates were performed) and expanded in either 0.1 μM, 1 μM or 10 μM isotretinoin or no-drug + 10% FBS-DMEM (1% A/A) MSCs-qualified medium (pre-warmed at room temperature) at 37°C with 5% CO_2 in a humidified chamber.

II.14. Viability assay using a resazurin-based solution

After 24h of BM-MSCs exposure to isotretinoin, PrestoBlue™(Thermo Fisher Scientific) resazurin-based viability assay was performed. Conceptually, PrestoBlue™(Thermo Fisher Scientific)-exposed living cells will take up resazurin (blue-colored, non-fluorescent compound). Cell metabolic activity will then convert resazurin to resorufin, a pink-colored fluorescence compound. As a result, the more the living cells, the more resorufin is produced, increasing the fluorescence signal.

Viability assay protocol (sequential steps)

1) Preparation of 10% PrestoBlue™(Thermo Fisher Scientific) working solution, diluted in 10% FBS-DMEM (1% A/A) MSCs-qualified medium (pre-warmed at room temperature).

2) Addition of 500μL of working solution to each well and incubation at 37°C with 5% CO_2 in a humidified chamber for 2 hours. Negative control (medium only) was included.
3) Fluorescence measurements in 96-well plate (Falcon® 96-well Black Flat Bottom), performed on Infinite® M200 PRO (Tecan®) microplate reader (technical triplicates, with 100 μL per well), according to PrestoBlue™ (Thermo Fisher Scientific) manufacturer's manual specifications (excitation/emission = 560/590 nm). Experiment was set to optimal gain. Relative fluorescence units (RFU), either absolute values or after normalization for negative control (medium only) RFU, were compared for the four different experimental conditions (no-drug; isotretinoin at 0.1 μM, 1 μM or 10 μM) and plotted in bar charts (designed with Microsoft Excel).

II.15. RT-qPCR after human BM-MSCs *in vitro* drug-modulation with isotretinoin

1) AA and control-derived BM-MSCs were seeded at a cell density of 3000 cell/cm^2 on T25 culture flasks and cultured in either 10 μM isotretinoin or no-drug + 10% FBS-DMEM (1% A/A) MSCs-qualified medium (pre-warmed at room temperature) at 37°C with 5% CO_2 in a humidified chamber for 6 days.
2) Cells were then harvested with trypsin-EDTA solution for RNA extraction and cDNA synthesis (as previously described in section II.8.).
3) RT-qPCR for *RARA*, *CEBPA*, *PPARG*, *WNT5A*, *APOL4* and *SOCS3* genes was performed (as in section II.9).
4) Results (log2 fold change (L2FC)) for both experimental conditions (no-drug; isotretinoin 10 μM) were compared and contrasted according to disease status (AA versus control-derived BM-MSCs). Results were plotted in bar charts (designed with Microsoft Excel).

HSPC studies

II.16. Human HSPC isolation by Magnetic-Activated Cell Sorting (MACS)

HSPC isolation from BM mononuclear cells fraction (MNC) of control (healthy) donors was performed by magnetic-activated cell sorting (MACS). Positive selection of CD34+ cells was performed using Human CD34 MicroBead Kit UltraPure (Miltenyi Biotec), which contains MicroBeads directly conjugated to CD34 antibodies for magnetic labeling of CD34 expressing cells (e.g., BM is expected to contain about 0.5% to 3% CD34+ hematopoietic progenitor cells), according to manufacturer's instructions, summarized below:

1) Centrifugation of mononuclear cells at 300 x g for 10 minutes and supernatant aspiration.
2) Cell pellet resuspension in 300 μL of MACS buffer (a solution containing PBS, pH 7.2, 0.5% bovine serum albumin (BSA), and 2 mM EDTA maintained at +2 to +8 °C) per 10^8 total cells.
3) Addition of 100 μL of FcR Blocking Reagent for up to 10^8 total cells.
4) Addition of 100 μL of CD34 MicroBeads UltraPure, human per 10^8 total cells.
5) Mixing and incubation for 30 minutes in the refrigerator (+2 to +8 °C).
6) Washing the cells in 5-10 ml of MACS buffer (a solution containing PBS, pH 7.2, 0.5% bovine serum albumin (BSA), and 2 mM EDTA maintained at +2 to +8 °C) and centrifugation at 300 x g for 10 minutes.
7) Supernatant aspiration and resuspension (up to 10^8 cells) in 500 μL of MACS buffer.
8) Magnetic separation with LS columns (appropriate for the MidiMACS separator, Miltenyi Biotec; maximum number of labeled cells of 10^8). Pre-separation filter was used to remove any cell clumps and debris from single-cell suspensions before they were applied to the MACS column. Column was firstly prepared by rinsing with 3 ml of MACS buffer. Cell suspension was then applied onto the column and flow-through containing unlabeled cells was collected. Column was then washed with 3

ml of MACS buffer for three times and flow-through containing unlabeled cells was collected.

9) Removal of the magnetic column from the separator and placing on a 15 ml conical collection tube.
10) Pipetting 5 ml of MACS buffer onto the column (placed over the collection tube) and immediately flush out of the magnetically labeled cells (CD34+ cells) by firmly pushing the plunger into de column.
11) Total nucleated cell counting (TNC) with hemacytometer and trypan blue exclusion method, to determine total nucleated cell number and viability.
12) Immunophenotypic analysis of sorted CD34+ enriched cells by flow cytometry. In case of multiple donors, immunophenotypic analysis after MACS was performed in the pool sample (all sorted samples together). Flow cytometry method similar to the protocol described in section II.18.
13) To complement the TNC counting of CD34+ enriched cells, an additional calculation was performed to adjust those values to the correspondent percentage of CD34+CD45RA- cells determined by flow cytometry.
14) CD34+ selected cells were immediately used for HSPC expansion, as described below.

According to results from previous works and manufacturer's data a purity of >95% is expected after MACS CD34+ cells sorting.

In this study a range of 68% to 80% of CD34+ cells were obtained after MACS, as described in Table 5 (Section IV.3.1.).

II.17. HSPC expansion

HSPC expansion was performed according to previously established protocols [22, 23], as follows.

1) To assess the effect of AA versus control-derived BM-MSCs feeder layers on HSPC (healthy donors) expansion, CD34+ cells sorted from either single donor MNC or from a pool of donors (used to obtain the adequate number of CD34+ cells needed for each experiment) were seeded (technical

triplicates were performed) on 12-well plates at a density of 30000 cells/ml, using 1 mL of StemSpan™ Serum-free Expansion Medium II (StemCell Technologies) per well supplemented with 1% A/A and a previously defined cytokine cocktail [23] composed of SCF (90 ng/mL), Flt-3L (82 ng/mL) and TPO (77 ng/mL) (PeproTech). Basic fibroblast growth factor (bFGF) (PeproTech) at a concentration of 5 ng/mL was also added to support BM-MSCs feeder layer cells.

2) Before HSPC seeding, BM-MSCs feeder layers were established in the 12-well plate(s) to be used for HSPC expansion, by seeding AA or control-derived BM-MSCs at a density of 3000 cells/cm^2 and culturing them with 10% FBS MSCs-qualified + DMEM + 1% A/A (pre-warmed at room temperature) medium at 37°C with 5% CO_2 in a humidified chamber, until 90 to 100% of confluency.
3) For all BM-MSCs samples, cell seeding for feeder layer establishment was performed after one cell passage post-thawing, to avoid confounding effects of cryopreservation on MSCs functional properties. As the experimental goal was to compare the effect of BM-MSCs feeder layers from different donors, namely AA versus control donors, it was decided not to perform Mitomycin C-mediated cell growth arrest to avoid potential effects of the compound (Mitomycin C is a DNA crosslinker with the capacity to inhibit DNA replication and transcription, leading to cell cycle arrest and eventually, at higher exposures, to cell death) on the experimental results.
4) After establishment of feeder layers, HSPC (CD34+ enriched cells) were gently seeded on the top of them. HSPC expansion was performed during 7 days at 37°C with 5% CO_2 in a humidified chamber.

Since AA is a rare, poorly studied disease, for the thesis project it was opted to study the interactions of AA and control-derived BM-MSCs with HSPC derived from control samples, preserving MNC (and consequently HSPC isolation) from AA donors for subsequent works, after data consolidation and protocols' optimization performed in the context of the doctoral project.

II.18. Human HSPC quantification and immunophenotypic characterization

After HSPC 7-day expansion, cells were harvested through forced pipetting. Conventional (manual) counting by trypan blue exclusion method was performed to determine the total nucleated cell number (TNC) fold increase, calculated by dividing the cell number harvested at day 7 by the initial seeding cell number.

For all experiments, immunophenotypic characterization of HSPC was performed by flow cytometry, firstly on a FACSCalibur™ flow cytometer (BD Biosciences) and more recently on a FACSCanto™ II (BD Biosciences), due to equipment replacement.

Flow cytometry protocol for HSPC

1) Harvested HSPC were homogeneously distributed by two flow cytometry tubes at a cell concentration between $5x10^4$ to $10x10^4$ cells per tube (depending on the available cell numbers) and washed with PBS (until 2 ml).
2) Cells were firstly stained with Far Red LIVE/DEAD™ Fixable Dead Cell Stain Kit (Thermo Fisher Scientific) viability dye and then, after a 15-minute period of incubation in the dark at room temperature and PBS washing (2 ml), with a multicolor previously titrated antibody panel (BioLegend) for cell surface markers, combined in one tube (Tube 1 - CD45RA FITC; CD90 PE; CD34 PerCP-Cy5.5).
3) After a 15-minute period of incubation in the dark at room temperature and PBS washing (2 ml), cells were immediately analyzed in the flow cytometer (a yield of 10000 events per tube was established). An unstained tube was processed in the same manner (except for staining).

The flow cytometry panel was designed according to a pre-established panel for HSPC characterization (positive markers: CD34 [a marker expressed in HSPC, whose expression levels are highest in most primitive HSPC, decreasing with differentiation], CD90 [expressed in a subset of more primitive, less differentiated HSPC, with greater self-renewal and long-term repopulation capacity]; negative marker: CD45RA [low or negative expression in HSPC with greatest self-renewal

capacity and long term repopulation potential]) and flow cytometer settings and proper compensations for each fluorochrome were performed for both cytometers, as needed (e.g., after technical maintenance of the equipment; after change of the lot number of BD® Cytometer Setup and Tracking (CS&T) beads; after specific experimental settings that could change cell properties).

Flow cytometry data was analyzed by using FCS Express™7 (De Novo Software by Dotmatics). Representative image included in chapter X.ii., Appendix B, B.5.).

To complement the TNC counting performed manually, an additional calculation was performed to adjust those values to the correspondent percentage of CD34+CD45RA- cells (HSPC) determined by flow cytometry, to correct for possible overestimation of the cell numbers counted on hemacytometer (e.g., by confounding feeder layer MSCs with HSPC due to possible mixing during cell harvesting and morphological configuration change of MSCs in suspension). Upon that, CD34+ cells fold increase was calculated by dividing the cell number of CD34+ cells harvested at day 7 by the initial seeding number of CD34+ cells (measured as described in Section II.16.).

For each experimental setup, proliferative analysis was performed in technical triplicates and the mean of results (±SE of the mean) was plotted in bar charts (designed with Microsoft Excel).

II.19. Human HSPC *in vitro* clonogenic assays

In vitro clonogenic assay was performed in order to functionally characterize HSPC according to their capacity to differentiate into several hematopoietic lineages. Results were analyzed taking into consideration the experimental conditions (e.g., BM-MSCs feeder layer source), to ascertain if there was any functional effect associated to each one of them.

Colony-forming unit (CFU) assay was performed in 24-well plate (in technical triplicates), upon adaptation of the manufacturer's protocol, as below:

1) HSPC harvested after 7-day cell expansion were resuspended in MethoCult™ methylcellulose-based medium (STEMCELL Technologies) at a

cell concentration of 1000 cells in 2 ml of medium. The suspension tube was vortexed for at least 4 seconds to mix thoroughly.

2) The tube was left to stand for about 5 minutes to allow bubbles to rise to the top.
3) The mixture was carefully collected from the tube, to avoid formation of air-bubbles, with a 16-gauge blunt-end needle attached to a sterile luer lock syringe. For each tube plated (containing cells from a single expansion condition) a new needle and syringe were used.
4) A volume of 500 μL was dispensed on the center of each well and evenly distributed by gently tilting the plate to allow the medium to attach to the wall of the well on all sides.
5) To maintain humidity, 2 ml of sterile water was added to the remnant free wells, and the plate was covered and incubated at 37°C with 5% CO_2 in a humidified chamber for 14 days.
6) Colony identification and counting was performed by visual inspection using bright-field microscopy (Olympus CK40). Formed colonies were classified as: erythroid burst-forming unit (BFU-E), colony forming unit granulocyte-monocyte (CFU-GM), colony-forming unit-granulocyte, erythrocyte, monocyte or megakaryocyte (CFU-GEMM). Average colony count for each experimental condition was calculated. Colony number was normalized by the number of MethoCult™ seeded cells and multiplied by the total number of CD34+ cells harvested on Day 7 of HSPC expansion. Results were plotted in graph bars (designed with Microsoft Excel).

Bone decellularization

II.20. Human femoral bone decellularization protocol

Decellularization of human bone from femoral head/neck collected after informed consent from patients undergoing elective hip replacement surgery was performed, based on a previously published protocol [24], specifically adapted and optimized for human femoral bone samples.

Decellularization protocol

1) Pieces of the medullary component of freshly collected bone samples were separated (as much as feasible) with the aid of a punch biopsy needle. Different needle diameters (5 mm, 10 mm, 15 mm) were tried. The bone sectioning area was preferentially located at the interface between cortical and medullary bone (for easier topographical orientation) with a fragment thickness of about of 3 to 5 mm. To clean samples before separation, surgical bone pieces were washed with 10 mM PBS buffer (pH 7.4) [PBS1x] under orbital agitation (VWR® Standard Analog Shaker) for three times (10 minutes each) at RT.

2) Protocol solutions were prepared, as described below:

   a) Solution #1: 10 mM PBS buffer (pH 7.4) [PBS1x]
   b) Solution #2: 10 mM Tris Base + 1.5% phenylmethanesulphonylfluoride (PMSF) + 0.1% ethylenediaminetetraacetic acid (EDTA) (pH 7.4)
   c) Freezing buffer solution: 10 mM Tris Base + 5 mM EDTA (pH 8.0)
   d) Enzymatic solution no.1: 0.25% trypsin (for cell detachment) + 0.5% EDTA
   e) Enzymatic solution no.2: 10 mM Tris Base (pH 8.0) + 20 U/mL of Benzonase (a nuclease that breaks down DNA and RNA) (Sigma-Aldrich – 250 U/µL)
   f) Polar solvent #1: 50% of 99.9% isopropanol + 50% of normal saline
   g) Polar solvent #2: 99.9% isopropanol (only)

3) Bone decellularization was performed for 4 days, as described in the Table 4, below.

Table 4 – Human femoral bone decellularization protocol.

Day (no.)	Processing stages
1	1. Rinse in solution #1, 10 mM PBS buffer (pH 7.4) for three times (10 min) at RT. 2. Wash in solution #2 for three times (10 min) at RT. 3. Three cycles of freeze–thaw (−80°C to 37°C) in freezing buffer solution. 4. Centrifuge in solution #1 – 500 x g for 5 min at 25°C. In case of large fragments, not possible to centrifuge in 50 ml conical tubes, washing under agitation was performed. 5. Incubate in solution #2 for 18 h at 4°C (overnight).
2	1. Wash in solution #1 for three times (10 min) at RT. 2. Incubate in enzymatic digestion solution #1 for 5 h at 37°C under agitation (75 rpm). 3. Wash in solution #2 for two times (10 min) at RT under agitation (50 rpm). 4. Keep in solution #1 until the following day (overnight).
3	1. Centrifuge in solution #1 – 500 x g for 5 min at 25°C. 2. Incubate in enzymatic digestion solution #2 for 6h at RT under agitation (50 rpm). 3. Wash in solution #1 for three times (10 min). 4. Polar solvent extraction with polar solvent #1 for 1 h at 37°C under agitation (300 rpm on Thermomixer comfort [Eppendorf]). 5. Centrifuge the sample with polar solvent #1 – 500 x g for 5 min at 25°C. Steps 4. and 5. were repeated for 3 times.
4	1. Polar solvent extraction with polar solvent #2 for 1 h at 37°C under agitation (300 rpm on Thermomixer comfort [Eppendorf]). 2. Centrifuge the sample with polar solvent #2 – 500 x g for 5 min at 25°C. Steps 1. and 2. were repeated for 3 to 4 times until the material appeared clear with no lipid content. 3. Decellularized bone pieces where then stored in 100% ethanol at 4°C.

PBS - Phosphate-Buffered Saline; RT - room temperature; rpm - revolutions per minute; g -relative centrifugal force.

After decellularization, bone pieces from each donor, prepared simultaneously under the same experimental conditions, were processed in one of three ways (e.g. for the same donor, decellularized bone pieces were distributed for each one of the following procedures):

1) Decalcification, for sequential histological processing (paraffin embedding and sectioning) and staining, serving as a control sample for comparative histological analysis after co-culture of BM-MSCs on decellularized human femoral bone scaffold from the same donor.
2) Sequential *ex vivo* co-culture of BM-MSCs on decellularized human femoral bone scaffold.
3) Scanning electron microscopy (SEM), performed at MicroLab - Electron Microscopy Laboratory of Instituto Superior Técnico, Lisbon.

Decalcification protocol was performed in order to allow paraffin sectioning. Previous attempts without decalcification were unsuccessful due to sectioning destruction and loss of bone structural integrity. Decalcification was performed based on previously published protocols [25, 26] for BM trephine biopsy processing, as follows:

1) Fixation step in 10% neutral buffered formalin filled (60 ml) container for about 12-24 hours.
2) Immersion of bone piece into Gooding and Stewart's decalcification solution (10% formic acid + 5% formaldehyde, diluted in distilled water) for about 6 hours at 37°C (without agitation).
3) Decellularized and decalcified bone samples were then immersed into a new 10% neutral buffered formalin filled (60 ml) container and transported in person to the Histopathology Unit at the Gulbenkian Institute of Molecular Medicine (GIMM), Lisbon, where paraffin embedding and sectioning, as well as Hematoxylin and eosin (H&E) and immunocytochemistry stainings were performed and optimized.

II.21. BM-MSCs *ex vivo* culture in decellularized human femoral bone scaffolds

BM-MSCs seeding and expansion in decellularized human bone matrix scaffolds was performed according to the following protocol:

1) A cell pellet of about 3 million control-derived BM-MSCs (F18A22, at passage number 5; M78A22, at passage number 3) was established after *in*

vitro culture, cell harvesting and centrifugation, and aspiration of cell supernatant.

2) Cells were homogeneously resuspended in 100 μL of 10% FBS MSCs-qualified + DMEM + 1% A/A (pre-warmed at room temperature), at a concentration of about 300000 cells/10μL.
3) Decellularized bone scaffolds generated from a single healthy donor (F59A23) were placed at the middle of ultra-low attachment 24-well plate (Corning®) wells (one scaffold per well). To prevent microbiological contamination, the day before cell seeding all decellularized scaffolds were washed with PBS + 3% A/A and left overnight (for about 12 hours) on 12-well sterile plates inside laminar flow hood under UV-C light. Considering the exploratory proof-of-concept aim of the experiment, and to prevent reproducibility limitations possibly associated to the intrinsic heterogeneity of biological scaffolds, it was decided to use scaffolds from the same donor at this first stage.
4) To evaluate the impact of cross-sectional surface area of the scaffold on cell attachment and proliferation, scaffolds with 5 mm, 10 mm and 15 mm of diameter were used.
5) Cell seeding was performed by pipetting 10 μL of the BM-MSCs suspension (after gently mixing for homogenization) over 4, 3 or 2 evenly distributed spots at the upper surface (opposite to the lower surface, in direct contact with the bottom of the well) of each 15 mm, 10 mm or 5 mm diameter scaffold, respectively.
6) After seeding, cells were incubated at 37°C with 5% CO_2 in a humidified chamber for 2 hours.
7) Then, about 2 ml of 10% FBS MSCs-qualified + DMEM + 2% A/A (pre-warmed at room temperature) were gently added throughout the edges of each well (to avoid cell detachment), covering the upper surface of the scaffold.
8) BM-MSCs + dECM scaffold sets were then incubated at 37°C with 5% CO_2 in a humidified chamber for a period of 17 days. Medium changes were carefully performed every 4 days.

II.22. Viability assay of BM-MSCs cultured on decellularized human bone scaffolds

Viability assay of BM-MSCs cultured on each decellularized bone scaffold was performed using PrestoBlue™(Thermo Fisher Scientific), at days 1, 5, 9 and 17 after cell seeding.

Viability assay protocol (sequential steps)

1) Preparation of 10% PrestoBlue™(Thermo Fisher Scientific) working solution, diluted in 10% FBS-DMEM (1% A/A) MSCs-qualified medium (pre-warmed at room temperature).
2) Addition of 1 ml of working solution to each well and incubation at 37°C with 5% CO_2 in a humidified chamber for 2 hours. Negative controls (decellularized bone scaffold without seeded cells and medium only) were included.
3) Fluorescence measurements in 96-well plate (Falcon® 96-well Black Flat Bottom), performed on Infinite® M200 PRO (Tecan®) microplate reader (technical triplicates, with 100 μL per well), according to PrestoBlue™(Thermo Fisher Scientific) manufacturer's manual specifications (excitation/emission = 560/590 nm). Experiment was set to optimal gain.

Relative fluorescence units (RFU), either absolute values or after normalization for medium only RFU (control), were compared for the following conditions: 5 mm, 10 mm and 15 mm decellularized bone scaffold + BM-MSCs sets; decellularized bone scaffold without seeded BM-MSCs. Results were plotted in bar charts (designed with Microsoft Excel).

II.23. Histological processing and staining of decellularized bone scaffolds

Processing of decellularized and decalcified bone was performed at the Histopathology Unit at the Gulbenkian Institute of Molecular Medicine (GIMM), Lisbon, where paraffin embedding and sectioning, as well as Hematoxylin and eosin (H&E), and immunohistochemistry stainings (with human-reactive polyclonal antibodies [host/isotype - rabbit/IgG]: collagen type I, fibronectin and Stromal cell–derived factor 1, Thermo Fisher Scientific) were performed and optimized, according to previously published protocols [27], as follows.

1) Tissue samples were sectioned at a thickness of 5µm using a microtome (Minot Microtome Leica RM2145) to proceed to an immunohistochemistry staining protocol.
2) Sections were deparaffinized and hydrated with no antigen retrieval being required.
3) Endogenous peroxidase was blocked by incubation with 3% H_2O_2 in methanol.
4) Before primary antibody was incubated for 1h at RT total proteins were blocked with protein block serum free (Dako; Ref. X0909).
5) Anti-rabbit EnVision+HRP (horseradish peroxidase) was used as a secondary antibody, for 30 min at RT (ref. K4003, Dako, Glostrup, Denmark).
6) Brown positive cells were revealed by enzymatic substrate with horseradish peroxidase DAB solution (containing diaminobenzadine-tetrahydrochloride - ref K346811-2, Dako).
7) All slides were counterstained with Harris' Hematoxylin (Bio-Optica) and mounted with Entellan medium (Sigma ref. 1.00869.0500).
8) Stainings were imaged in Olympus IX51 Inverted Microscope and recorded by an attached digital camera.

II.24. Scanning electron microscopy of decellularized human bone scaffolds

In order to inspect 3D structure of bone extracellular matrix, both previously and after BM-MSCs *ex vivo* co-culture, scanning electron microscopy (SEM) was performed at MicroLab - Electron Microscopy Laboratory of Instituto Superior Técnico, Lisbon.

Samples were placed on an Al stub using double-sided carbon tape and sputter coated with a thin gold/palladium (Au/Pd) film in a Quorum Technologies coater, model Q150T ES, and then then analyzed in a Hitachi scanning electron microscope (SEM), model S2400, with digital image acquisition by Bruker, software Quantax Esprit 1.9.

II.25. Overall data analysis

Data analysis was performed by using a combination of statistical resources from RStudio Software (R version 4.2.3) [6], Microsoft Excel (namely, two-tailed t-test, assuming unequal variances) and FCS Express™7 (De Novo Software by Dotmatics).

II.26. References - Chapter II

1. Picelli S, Faridani OR, Björklund AK, Winberg G, Sagasser S, Sandberg R. Full-length RNA-seq from single cells using Smart-seq2. Nat Protoc. 2014;9(1):171-181. doi:10.1038/nprot.2014.006
2. Baym M, Kryazhimskiy S, Lieberman TD, Chung H, Desai MM, Kishony R. Inexpensive multiplexed library preparation for megabase-sized genomes [published correction appears in PLoS One. 2015 Jun 18;10(6):e0131262. doi: 10.1371/journal.pone.0131262]. PLoS One. 2015;10(5):e0128036. Published 2015 May 22. doi:10.1371/journal.pone.0128036
3. Genome sequence, primary assembly (GRCh38): https://ftp.ebi.ac.uk/pub/databases/gencode/Gencode_human/release_44/GRCh38.primary_assembly.genome.fa.gz.
4. Comprehensive gene annotation (GRCh38): https://ftp.ebi.ac.uk/pub/databases/gencode/Gencode_human/release_44/gencode.v44.primary_assembly.annotation.gtf.gz.
5. Dobin A, Davis CA, Schlesinger F, et al. STAR: ultrafast universal RNA-seq aligner. Bioinformatics. 2013;29(1):15-21.doi:10.1093/bioinformatics/bts635 (https://github.com/alexdobin/STAR/releases/tag/2.7.11a)
6. R Core Team (2021) R: A Language and Environment for Statistical Computing. R Foundation for Statistical Computing, Vienna. https://www.R-project.org
7. Morgan M, Pagès H, Obenchain V, Hayden N (2024). Rsamtools: Binary alignment (BAM), FASTA, variant call (BCF), and tabix file import. R package version 2.20.0, https://bioconductor.org/packages/Rsamtools
8. Lawrence M, Huber W, Pagès H, Aboyoun P, Carlson M, Gentleman R, Morgan M, Carey V (2013). "Software for Computing and Annotating Genomic Ranges." PLoS Computational Biology, 9. doi:10.1371/journal.pcbi.1003118, http://www.ploscompbiol.org/article/info%3Adoi%2F10.1371%2Fjournal.pcbi.1003118
9. Love MI, Huber W, Anders S (2014). "Moderated estimation of fold change and dispersion for RNA-seq data with DESeq2." Genome Biology, 15, 550. doi:10.1186/s13059-014-0550-8
10. Warnes, G. R., Bolker, B., Bonebakker, L., Gentleman, R., Liaw, W. H. A., Lumley, T., Maechler, M., Magnusson, A., Moeller, S., Schwartz, M., & Venables, B. 1 (2023). gplots: Various R Programming Tools for Plotting Data. R package version 3.1.3. https://CRAN.R-project.org/package=gplots
11. Kassambara, A., & Mundt, F. (2020). factoextra: Extract and Visualize the Results of Multivariate Data Analyses. R package version 1.0.7
12. Zhu, A., Ibrahim, J. G., & Love, M. I. (2019). Heavy-tailed prior distributions for sequence count data: removing the noise and preserving large differences. Bioinformatics, 35(12), 2084-2092
13. Kevin Blighe, Sharmila Rana & Myles Lewis (2023). EnhancedVolcano: Publication-ready volcano plots with enhanced colouring and labeling. R package version 1.16.0. https://github.com/kevinblighe/EnhancedVolcano
14. Wu T, Hu E, Xu S, Chen M, Guo P, Dai Z, Feng T, Zhou L, Tang W, Zhan L, Fu x, Liu S, Bo X, Yu G (2021). "clusterProfiler 4.0: A universal enrichment tool for interpreting omics data." The Innovation, 2(3), 100141. doi:10.1016/j.xinn.2021.100141.

15. Yu G, Wang L, Han Y, He Q (2012). “clusterProfiler: an R package for comparing biological themes among gene clusters.” OMICS: A Journal of Integrative Biology, 16(5), 284-287. doi:10.1089/omi.2011.0118
16. Carlson M (2019). org.Hs.eg.db: Genome wide annotation for Human. R package version 3.8.2.
17. Raudvere, U., Kolberg, L., Kuzmin, I., Arak, T., Adler, P., Peterson, H., & Vilo, J. (2019). g:Profiler: a web server for functional enrichment analysis and conversions of gene lists (2019 update). Nucleic Acids Research, 47(W1), W191-W198
18. Stelzer, G., Rosen, N., Plaschkes, I., Zimmerman, S., Twik, M., Fishilevich, S., ... & Lancet, D. (2016). The GeneCards Suite: From Gene Data Mining to Disease Genome Sequence Analyses. Current Protocols in Bioinformatics, 54(1), 1.30.1-1.30.33
19. Kuleshov, M. V., Jones, M. R., Rouillard, A. D., Fernandez, N. F., Duan, Q., Wang, Z., ... & Ma'ayan, A. (2016). Enrichr: a comprehensive gene set enrichment analysis web server 2016 update. Nucleic acids research, 44(W1), W90-W97
20. Wickham H (2016). ggplot2: Elegant Graphics for Data Analysis. Springer-Verlag New York. ISBN 978-3-319-24277-4, https://ggplot2.tidyverse.org
21. Melnik BC. Acne Transcriptomics: Fundamentals of Acne Pathogenesis and Isotretinoin Treatment. Cells. 2023;12(22):2600. Published 2023 Nov 10.
22. dos Santos F., Andrade P. Z., Boura J. S., Abecasis M. M., da Silva C. L., Cabral J. M. S. (2010). Ex vivo expansion of human mesenchymal stem cells: a more effective cell proliferation kinetics and metabolism under hypoxia. J. Cell. Physiol. 223 27–35.
23. Branco A, Bucar S, Moura-Sampaio J, et al. Tailored Cytokine Optimization for ex vivo Culture Platforms Targeting the Expansion of Human Hematopoietic Stem/Progenitor Cells. Front Bioeng Biotechnol. 2020;8:573282.
24. Bianco JER , Rosa RG , Congrains-Castillo A , et al. Characterization of a novel decellularized bone marrow scaffold as an inductive environment for hematopoietic stem cells. Biomater Sci. 2019;7(4):1516-1528.
25. Naresh KN, Lampert I, Hasserjian R, et al. Optimal processing of bone marrow trephine biopsy: the Hammersmith Protocol. J Clin Pathol. 2006;59(9):903-911.
26. Torlakovic EE, Brynes RK, Hyjek E, et al. ICSH guidelines for the standardization of bone marrow immunohistochemistry. Int J Lab Hematol. 2015;37(4):431-449.
27. Ana M Biscaia Santos, Ana M Cristóvão Pinto, Ana R Pires, Joana G Antunes 2024. Immunohistochemistry protocol optimized at iMM-JLA. protocols.io. https://dx.doi.org/10.17504/protocols.io.j8nlkon2wv5r/v1
28. Killick SB, Bown N, Cavenagh J, Dokal I, Foukaneli T, Hill A, Hillmen P, Ireland R, Kulasekararaj A, Mufti G, Snowden JA, Samarasinghe S, Wood A, Marsh JC; British Society for Standards in Haematology. Guidelines for the diagnosis and management of adult aplastic anaemia. Br J Haematol. 2016 Jan;172(2):187-207.

III. Head-to-head comparison of phenotypic and functional properties between AA-derived and control-derived BM-MSCs

III.1. Summary

Despite several reports demonstrating abnormal function of key bone marrow (BM) elements, particularly dysfunctional mesenchymal stromal cells (MSCs), in aplastic anemia (AA), published results are scarce and controversial. Therefore, further studies are needed to address these limitations and improve our understanding of the role of BM-MSCs in AA. To this end, a comparative analysis of morphological and functional properties of AA-derived (number of donors = 4; median age = 13 years; minimum = 7 years; maximum = 35 years) and control-derived (number of donors =7; median age = 40 years; minimum = 4 years; maximum = 69 years) BM-MSCs, isolated from age-matched donors, was performed. No significant differences in morphological and immunophenotypic properties were identified between groups.

Trilineage differentiation capacity was assessed and confirmed for both AA and control-derived BM-MSCs. Some of the AA-derived BM-MSCs cells visualized on bright-field microscopy after Oil Red O staining (Sigma-Aldrich) showed a significant amount of intense-red-colored fat cells.

Proliferative rates between AA-derived and control-derived BM-MSCs were similar, either at BM-MSCs isolation from MNC or after expansion of previously isolated BM-MSCs, cryopreserved in liquid/vapour phase nitrogen. For both AA and controls, MNC isolation of BM-MSCs on gelatin 0.1% coating or laminin-521 (LN521) was faster in comparison with no coating, with a mean number of days to 70% confluency of 9 days (n=6; minimum = 8 days; maximum = 10 days) and 14 days (n=5; minimum =12 days; maximum = 16 days), respectively.

AA-derived BM-MSCs telomere length (n=11; mean of average telomere length on each chromosome end = 16.04 kb; minimum = 4.32 kb; maximum = 35.84 kb) was not shorter in comparison to controls (n=11; mean of average telomere length on each chromosome end = 10.68 kb; minimum = 6.90 kb; maximum = 19.03 kb) (p = 0.14). BM-MSCs from older donors and at higher passage number presented lower telomere length.

Telomere absolute length assay by RT-qPCR showed to be feasible in a clinical context, aiding in diagnostic support of bone marrow failure syndromes, especially in case of variants of uncertain significance (VUS) in telomeropathies-related genes.

III.2. Background

As referred in Chapter I, several reports have demonstrated an abnormal function of key BM elements in AA, namely the existence of dysfunctional MSCs [1,2,3]. However, published data are contradictory [4, 5] and of low reproducibility.

Idiopathic acquired aplastic anemia (AA) is a rare disease, treated at few reference units of hematology, which poses limitations to sampling assess. Moreover, pancytopenia is not specific for AA, meaning that there will be cases of *de novo* idiopathic acquired AA which will be misdiagnosed, delaying patient referral and correct diagnosis. There are even cases in which patients are empirically started on corticosteroids, without a previous BM examination, especially in geographical areas or medical contexts with poor assess to hematology units.

Alongside with those limitations, it is the fact that the research studies on AA-derived BM-MSCs that have been performed were limited by a significative heterogeneity between studied patients, either between works, or even in the same study (e.g., including a wide spectrum of disease severity stages, from non-severe to very severe forms of AA; not clearly defined “idiopathic acquired” classification; not treatment-naïve patients). To this inter and intra-study sampling heterogeneity, adds technical discrepancies, namely regarding methodological approach and experimental setup, which limits results comparison and data sampling scaling up.

A possible confounding effect of previously published data is also the donor age-matching. Proliferative and osteogenic impairment of MSCs isolated from older donors (e.g. 60 and 80 years old) compared to younger ones (e.g., 30 and 45 years old) has been demonstrated [7]. As so, it is important to take this into account while analyzing results from experiments performed in conditions with multiple peaks of age incidence, as is the case of AA. In this project, which involved both pediatrics and adult clinical units, an effort was made in order to age-match samples for each experimental setup, as far as possible upon sample availability.

Taking those determinants into consideration, and with the aim to establish an as consistent as possible dataset for present and future works, isolation, expansion and characterization of age-matched BM-MSCs derived from idiopathic

acquired severe and very severe AA and healthy controls was performed, after careful donor selection.

To further characterize AA-derived BM-MSCs, telomere length was also assessed. The rational follows.

Telomeres consist of repetitive DNA sequences at the ends of chromosomes, functioning as protective caps, preventing damage and fusion. At each cell division, telomeres shorten, as a natural part of aging. Critically short telomeres can trigger cellular senescence or apoptosis [19,22].

In MSCs, telomere length varies, depending on age of donor, tissue source and culture conditions. MSCs from older-aged donors will have shorter telomeres in comparison to younger donors, which reflects their overall aging process and influences their functional properties. As so, shorter telomeres associate with lower replicative capacity and differentiation potential, leading to reduced functionality and impaired therapeutic potential [20, 21].

Telomere length is maintained by telomerase, an enzyme that can add DNA to telomeres, counteracting telomere shortening and cellular senescence. In humans, this enzyme is highly active in germ cells and embryonic cells, ensuring the transmission of intact chromosomes to offspring and supporting rapid cell division during development. In addition, certain adult stem cells (e.g., hematopoietic stem cells; germline stem cells; hair follicle stem cells), responsible for tissue renewal and repair, express telomerase to maintain proliferative capacity [19,20,21].

Most adult somatic cells will have low or undetectable telomerase activity, which limits their replicative capacity, and will contribute to cellular senescence. On the contrary, in the vast majority of cancer cells, telomerase will be upregulated, which contributes to uncontrolled proliferation and aggressiveness of cancer cells [22, 23].

MSCs maintain some level of telomerase activity, however it is not sufficient to completely prevent telomere shortening overtime. Moreover, the level of telomerase activity is influenced by donor age and MSCs source (e.g., UC-MSCs and AT-MSCs present higher levels of telomerase in comparison to BM-MSCs). As telomerase will prevent telomere shortening, its activity is essential for preserving

MSCs self-renewal and differentiation properties. Due to this fact, telomerase has been under investigation for improvement of MSCs expansion and application in regenerative medicine [21,24,25].

Regarding aplastic anemia, telomere length seems to play a significant role in disease severity and prognosis, even in case of acquired AA and not just in inherited forms associated with germline mutations of telomeropathies-related genes [26,27,28]. In a cohort of patients with severe aplastic anemia receiving immunosuppressive therapy, telomere length inversely correlated with the risk of relapse, clonal evolution, and overall survival. Genetic defect in *TERC* or *TERT* was identified in only 1 patient [26].

III.3. Results and discussion

III.3.1. Comparative analysis of morphologic and immunophenotypic characteristics between AA-derived and control-derived BM-MSCs

Comparison of BM-MSCs derived both from AA and control donors, visualized on bright-field microscope at serial magnifications (4x, 10x, 20x), did not show significant differences between both groups. Cell morphology was compared for different passage numbers and days in culture. Figure 5 is a representative image of AA-derived (M15, M87) and control-derived (F18, M78) age-matched samples cultivated with expansion medium (10%FBS-DMEM (1% A/A).

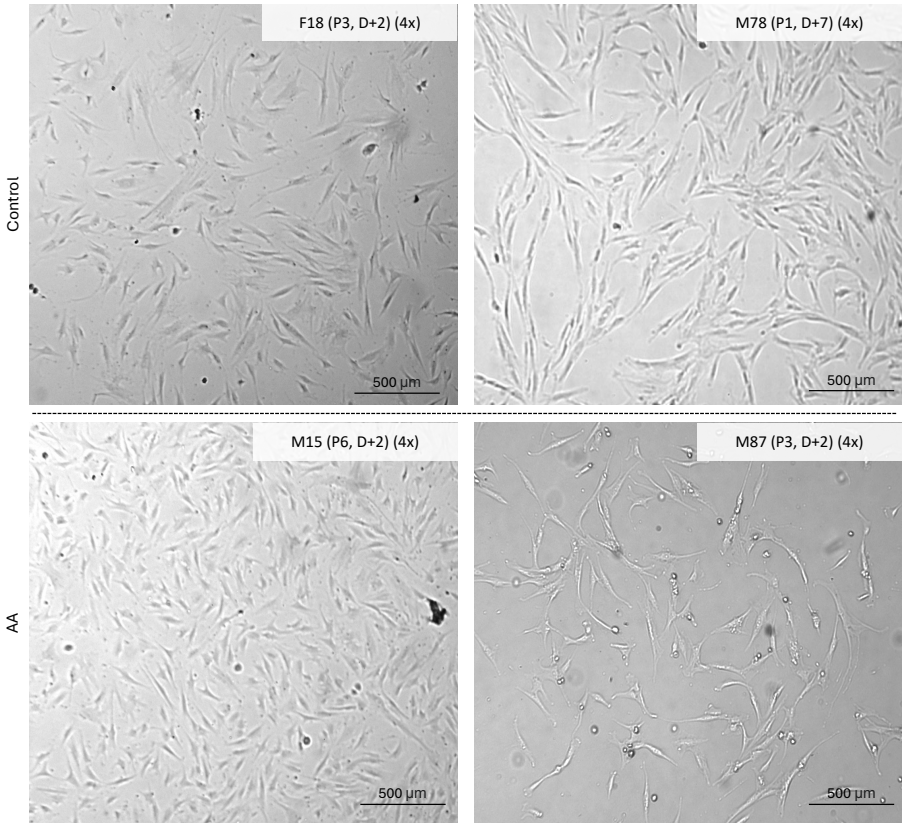

Figure 5: Fibroblastic, spindle-shape morphology of AA and healthy control-derived BM-MSCs cultured under expansion conditions. Representative image of cell morphology of both disease and healthy samples imaged at 4x magnification on bright-field microscope (Olympus IX51 Inverted Microscope equipped with an attached digital camera). P = cell passage number; D = day number of cell culture (the day of BM-MSCs seeding was considered D0).

Immunophenotypic profile, performed by flow cytometry, did not show significant differences in expression of positive and negative cell surface markers, as measured by percentage of cell expression (%) ($p > 0.05$) and mean fluorescence intensity (MFI) ($p > 0.05$), between AA-derived and control-derived BM-MSCs.

For both groups, no significant differences attributable to sampling source (PSIS-derived versus femoral head/neck-derived BM-MSCs), cell passage number or donor age were detected. Viability was similar between groups.

Data acquired with either FACSCalibur™ (BD Biosciences) (Figure 6) or FACSCanto™ II (BD Biosciences) (Figure 7) flow cytometers are plotted below (representative images of flow cytometry analysis of BM-MSCs samples using FCS Express™7 (De Novo Software by Dotmatics) are included in chapter X.ii., Appendix B, B.1. and B.2.; mean fluorescence intensity (MFI) plots included in chapter X.i., Appendix B, B.3. and B.4.).

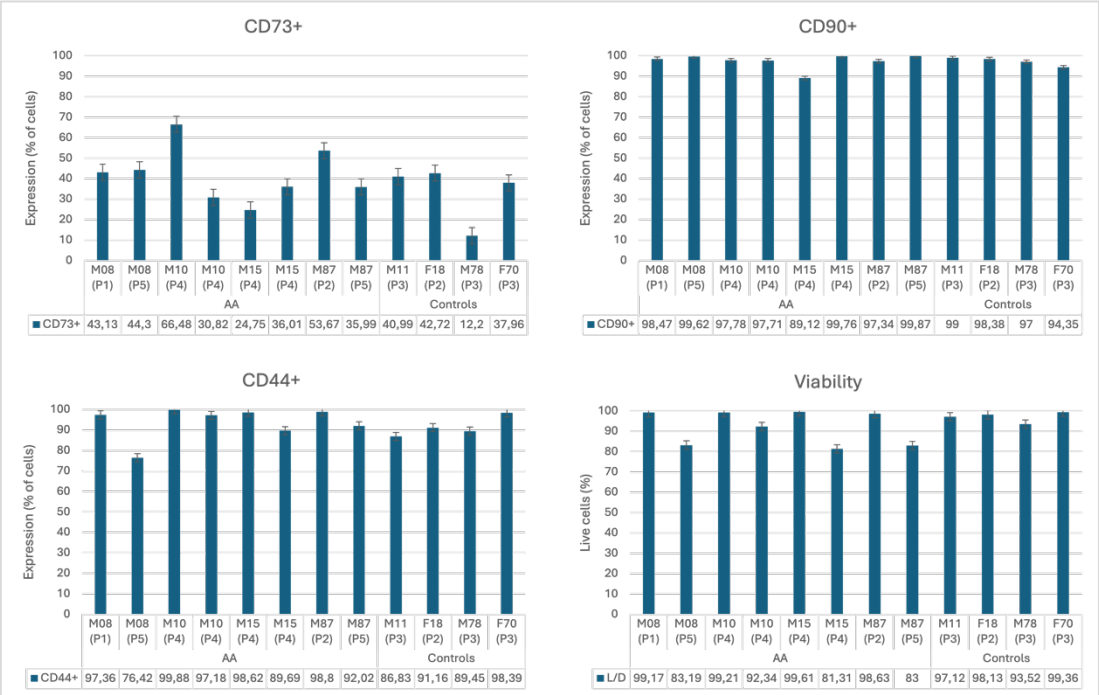

Figure 6: AA-derived and control-derived BM-MSCs immunophenotypic profile - % of cells expressing cell surface positive markers for MSCs identification (CD73, CD90, CD44) (±SE mean); % of live cells (±SE mean). All samples were negative for CD34, CD14, CD19, HLA-DR (data not shown). Data acquisition performed with FACSCalibur™ flow cytometer (BD Biosciences). P = cell passage number.

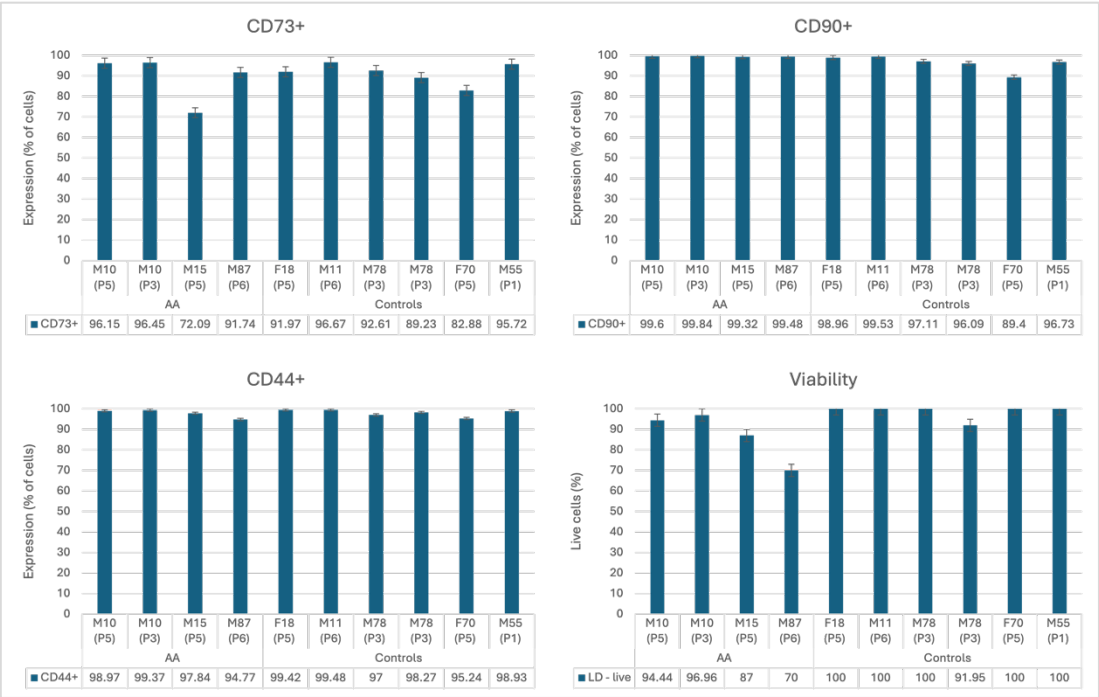

Figure 7: AA-derived and control-derived BM-MSCs immunophenotypic profile - % of cells expressing cell surface positive markers for MSCs identification (CD73, CD90, CD44) (±SE mean); % of live cells (±SE mean). All samples were negative for CD34, CD14, CD19, HLA-DR (data not shown). Data acquisition performed with FACSCanto™ II (BD Biosciences). P = cell passage number.

As depicted, expression of CD73, CD90 and CD44, which are positive cell surface markers that characterize BM-MSCs, was consistent between AA-derived and control-derived BM-MSCs.

An exception was verified for CD105, which is a common marker used for MSCs immunophenotyping. Under the conditions of this study, CD105 expression among BM-MSCs from both groups was highly variable, even for cells from the same donor (chapter X.ii., Appendix B, B.3. and B.4.).

CD105 corresponds to endoglin, a cell surface positive marker for MSCs, that was hypothesized to predict MSCs chondrogenic potential [8, 9], however not confirmed in posterior studies [10]. More recently, human adipose tissue-derived (AT-MSCs) and human umbilical cord-derived (UC-MSCs) MSCs were studied for CD105 expression, with identification of a subpopulation of CD105 negative AT-

MSCs and UC-MSCs with a stronger immunomodulatory capacity, possible related to autocrine production of TGF-beta 1 [11].

CD105 is a labile, short half-life, marker, whose expression rapidly varies in response to physiological or pathological conditions. Endoglin is a transmembrane glycoprotein making part of the transforming growth factor-beta (TGF-β) receptor complex [12]. It is primarily expressed on vascular endothelial cells, playing a role in angiogenesis [13], in synctiotrophoblasts (of term placenta) and, less abundantly, in monocytes, fibroblasts, chondrocytes, and hematopoietic progenitor cells. In MSCs its expression is labile and depends on cell culture variables, making it a tricky cell marker for MSCs labeling, especially *in vivo* [15].

Changes in CD105 expression could either vary according to biological (e.g., activation, differentiation or proliferative stage) or technical issues (e.g., sample handling or storage variations). Despite optimization of flow cytometry settings and proper compensations for each fluorochrome, specifically determined for both cytometers, as needed (e.g., after technical maintenance of the equipment; after change of the lot number of BD® Cytometer Setup), it was not possible to capture reproducible results of CD105 expression. Consequently, it was not possible to conclude if the observed variability was related to functional differences between BM-MSCs, to technical issues, or both.

In regard to MFI results (chapter X.ii., Appendix B, B.3. and B.4.), it was not possible to identify a significantly distinct pattern between AA and control groups. MFI coefficient of variation (CV) was acceptable and relatively stable for all markers, across samples, again with a higher variability for CD105, as would be expected upon its expression profile, as previously discussed.

III.3.2. Multilineage differentiation assay (osteogenic, adipogenic and chondrogenic) of AA-derived and control-derived BM-MSCs - comparative analysis

To confirm the differentiation capacity of BM-MSCs, trilineage differentiation assay was performed for both AA-derived and control-derived BM-MSCs.

As depicted below, trilineage differentiation capacity was confirmed for all samples, either AA-derived (Figure 8) or control-derived (Figure 9). Despite the staining strategy (on bright-field) did not allow to obtain quantitative data (e.g., as measured by fluorescence), upon imaged data, AA-derived BM-MSCs did not seem to have lower osteogenic capacity in comparison to control-derived samples. To notice, M55 control appeared to have a lower differentiation capacity, namely of osteogenic differentiation, possible related to older age of donor (69 years old) [7].

On the other hand, AA-derived BM-MSCs seemed to have a higher adipogenic differentiation in comparison to control-derived BM-MSCs, with the exception of F18 control sample, with a high adipogenic differentiation capacity, which could be possible related to the impact of donor younger age (4 years old donor).

Differently from osteogenic differentiation, adipogenic differentiation potential have been shown to remain on the same level throughout the ageing process of MSCs [7, 16], which is important to take into account, especially when comparing older-age matched samples. This reinforces the hypothesis of an adipogenic bias in AA-derived BM-MSCs, as previously described [17].

Despite promising, these results still lack robustness and must be confirmed by increasing age-matched sampling numbers as well as by applying quantitative methodologies.

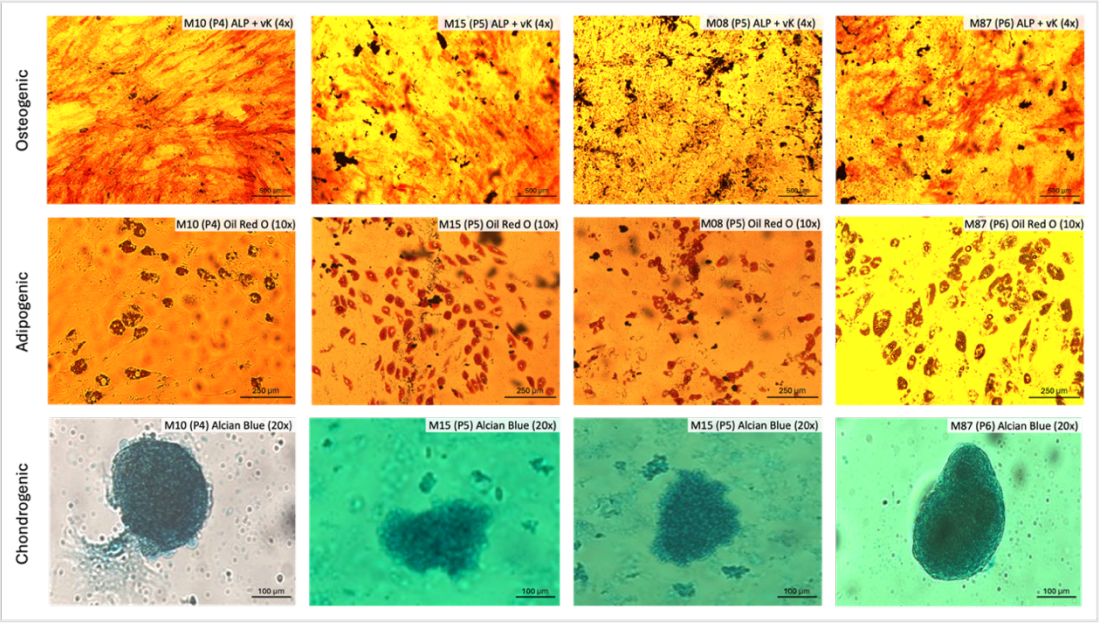

Figure 8: AA-derived BM-MSCs trilineage differentiation assay - osteogenic, adipogenic and chondrogenic differentiation. Samples imaged on bright-field microscope (Olympus IX51 Inverted Microscope equipped with an attached digital camera). Representative images of cells are shown.

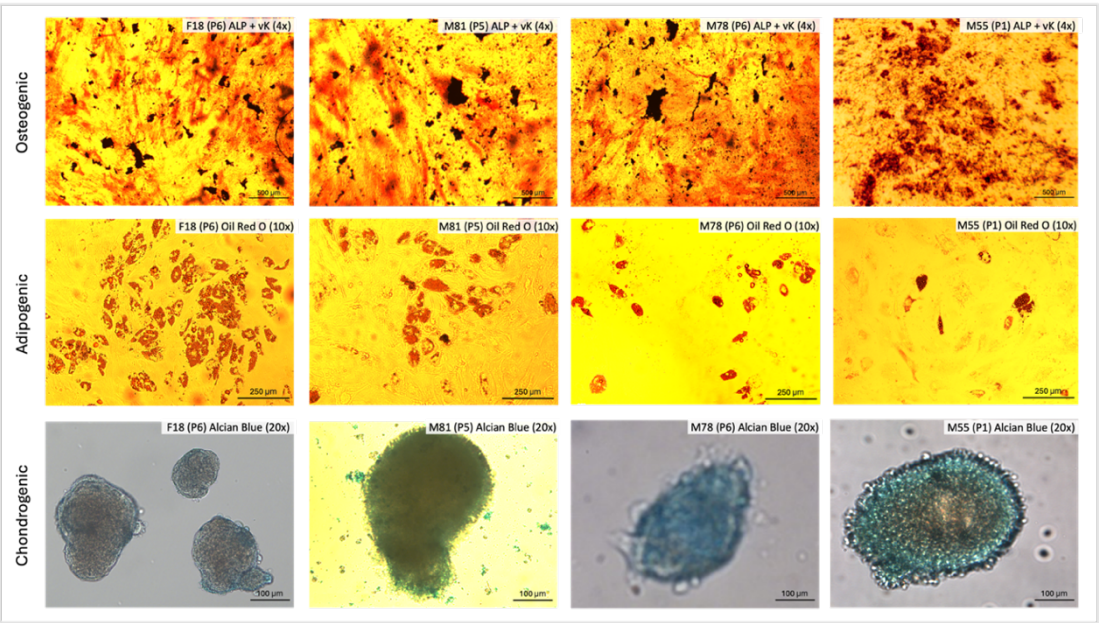

Figure 9: Healthy control-derived BM-MSCs trilineage differentiation assay - osteogenic, adipogenic and chondrogenic differentiation. Samples imaged on bright-field microscope (Olympus IX51 Inverted Microscope equipped with an attached digital camera). Representative images of cells are shown.

In latest experiments, AdipoRed™ Assay Reagent (Lonza), a fluorescent dye designed to stain intracellular lipid droplets, relatively specific to neutral lipids, was also applied. Both Oil Red O and AdipoRed™ are relatively specific to neutral lipids and at a lesser extent could stain some phospholipids or other intracellular hydrophobic molecules, which should be considered for results interpretation.

Below (Figure 10) is shown a representative image of AA-derived and control-derived adipogenic differentiation assay after AdipoRed™ staining. Despite this was just a proof-of-concept experiment, it was interesting to notice that fluorescence for either AA-derived (M87) BM-MSCs was lower than for control-derived (M73) BM-MSCs. However, bright-field image suggests the opposite. If this difference relates to biological properties (e.g., distinct lipid content profiles between samples) between groups or to technical issues, which must be optimized in further experiments (e.g., reagent titration), is an interesting research topic to explore.

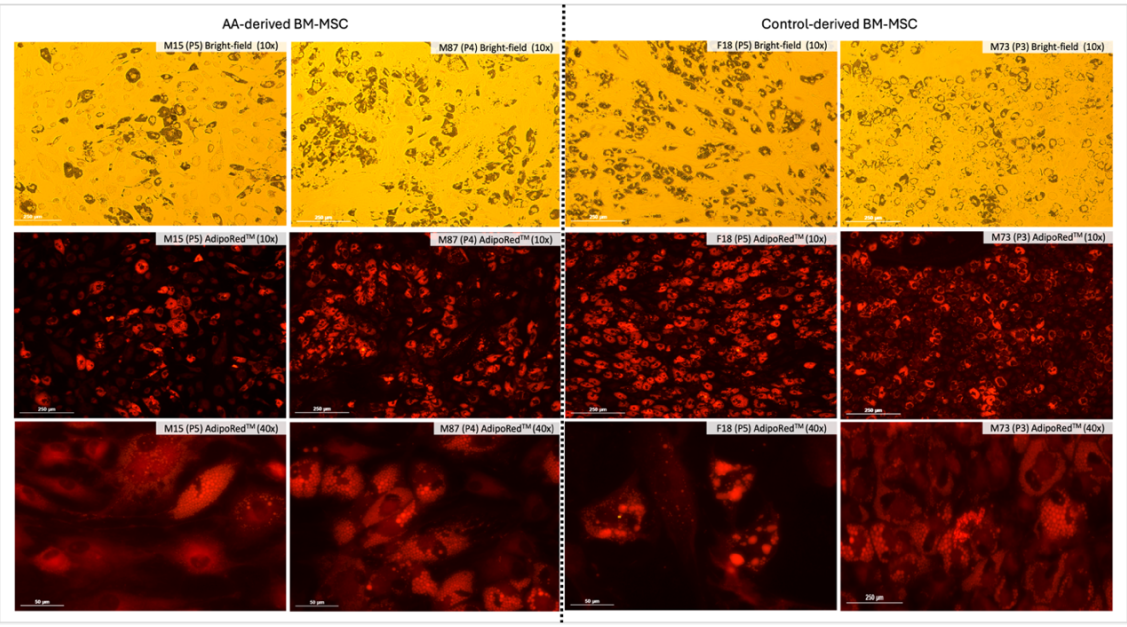

Figure 10: AA-derived and control-derived adipogenic differentiation assay after AdipoRed™ Assay Reagent (Lonza) staining. Samples imaged at 4x magnification on fluorescence microscope (Olympus IX51 Inverted Microscope equipped with an attached digital camera). Representative images of cells are shown.

III.3.3. Proliferative analysis of AA-derived and control-derived BM-MSCs – cell proliferation kinetics and telomere length analysis

Proliferative analysis of AA-derived and control-derived BM-MSCs was performed at different culture stages, namely, upon isolation from MNC layer, expansion after thawing from liquid/vapour phase nitrogen cryopreservation and expansion after a first passage post-thawing. In both groups, cell proliferation was studied for the same sample at different passage numbers, as well as upon seeding (3000 cell/cm^2) on different cell culture surface areas.

BM-MSCs isolation and expansion from MNC

There were no significant differences between time (number of days) to reach 70% confluency (p = 0.82) between AA-derived and control-derived BM-MSCs, as depicted in Figure 11, below.

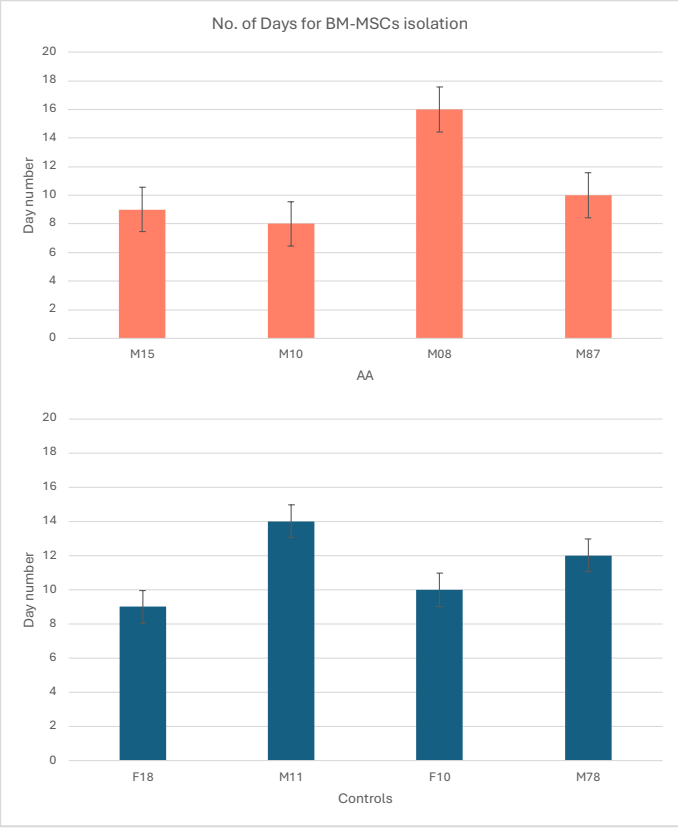

Figure 11: Proliferation performance (defined by the number of days to reach 70% of cell confluency) of AA-derived and control-derived BM-MSCs upon isolation from BM-derived MNC (±SE mean). Samples M78, M11 and M08 were seeded on uncoated cell culture plates. The remaining samples were seeded on gelatin 0.1% coating.

For both conditions, isolation of BM-MSCs on gelatin 0.1% (Sigma-Aldrich®) coated plates was faster in comparison with no coating (p = 0.04), with a mean number of days to 70% confluency of 9 days (n=5; minimum = 8 days; maximum = 10 days) and 14 days (n=3; minimum =12 days; maximum = 16 days), respectively. These results were in accordance with previous works [18].

BM-MSCs expansion after thawing

BM-MSCs proliferation after thawing from liquid/vapour phase nitrogen cryopreservation and culture on 25 cm^2 T-flasks or 75 cm^2 T-flasks, at a seeding density of 3000 cell/cm^2, was not significantly different between AA-derived and control-derived BM-MSCs, as represented in Figure 12 and Figure 13, below.

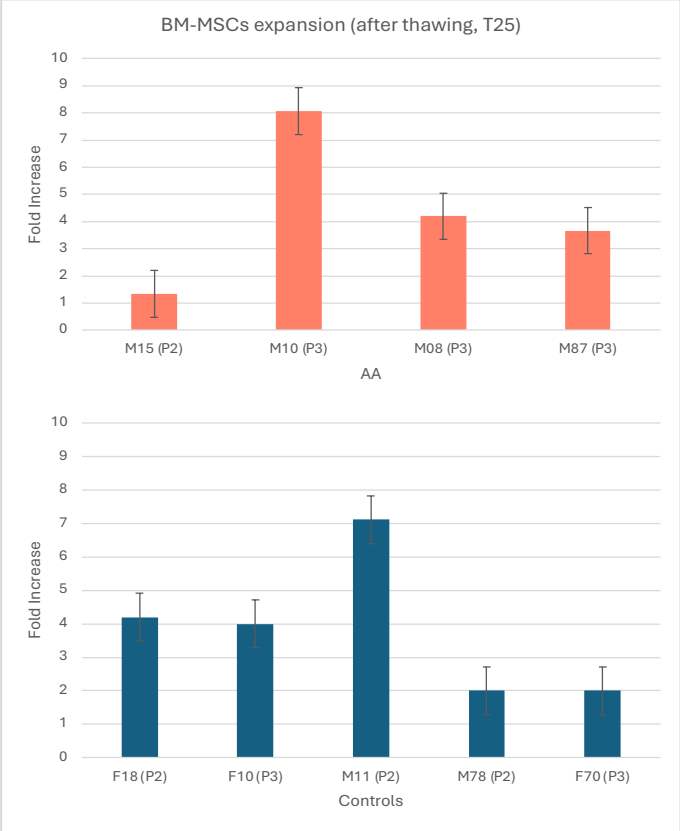

Figure 12: Proliferative rate, defined by Fold Increase (FI) at 70% confluency of AA-derived and control-derived BM-MSCs after thawing and expansion on T-25 flasks (±SE mean). No significant differences between AA and Controls (p = 0.80). P = cell passage number.

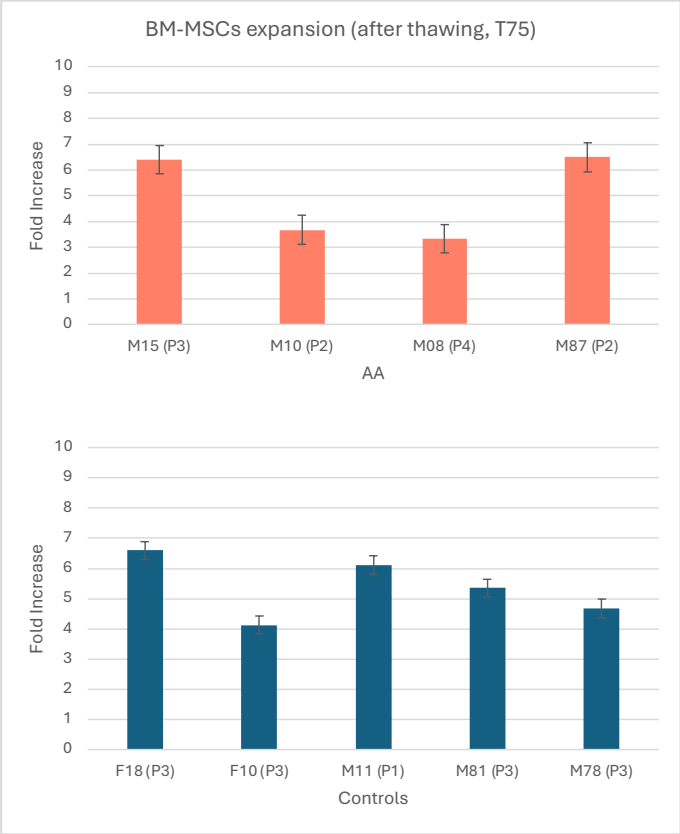

Figure 13: Proliferative rate, defined by Fold Increase (FI) at 70% confluency of AA-derived and control-derived BM-MSCs after thawing and expansion on T-75 flasks (±SE mean). No significant differences between AA and Controls (p = 0.70). P = cell passage number.

In both experimental setups, no viability differences between AA-derived (mean viability = 99%) and control-derived (mean viability = 99%) BM-MSCs were found at cell harvesting (p = 0.51).

To depict if the proliferative profile between groups persisted after at least one cell passage post-thawing, both AA and control-derived BM-MSCs were seeded on 75 cm^2 T-flasks (seeding density = 3000 cell/cm^2) after one passage post-thawing to determine the FI at 70% confluency. No significant differences between AA and Controls (p = 0.48) were found, as depicted in Figure 14, below.

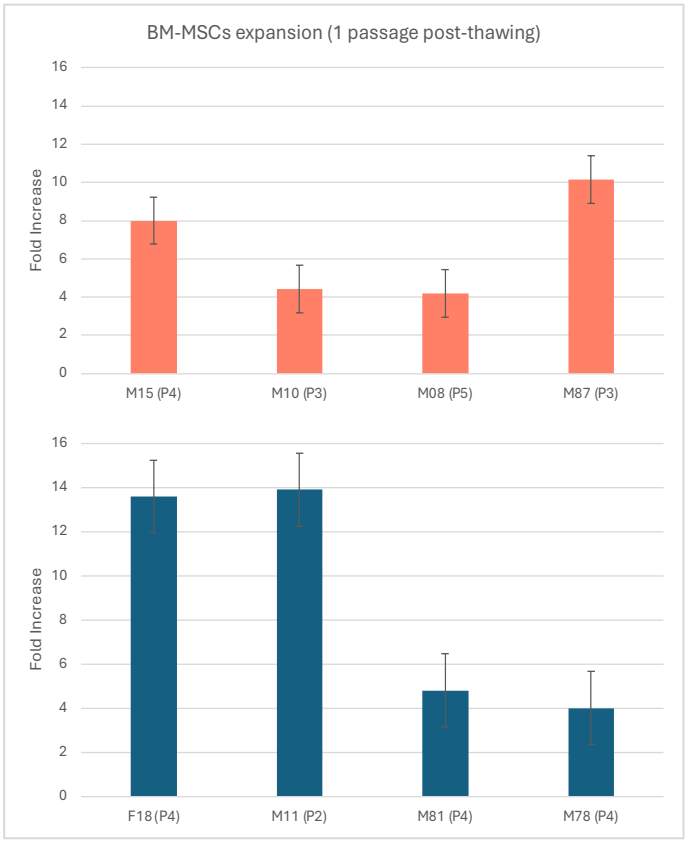

Figure 14: Proliferative rate, defined by Fold Increase (FI) at 70% confluency of AA-derived and control-derived BM-MSCs after one passage post-thawing and expansion on T-75 flasks (±SE mean). No significant differences between AA and Controls (p = 0.48). P = cell passage number.

No viability differences between AA (mean viability = 99%) and control-derived (mean viability = 99%) BM-MSCs were found at cell harvesting (p = 0.55).

Proliferative BM-MSCs kinetics, assessed during a period of 7 day-cell culture (as described in II.5.), did not show significant differences between AA-derived (n=3) and control-derived BM-MSCs (n=3), as represented in Figure 15, below.

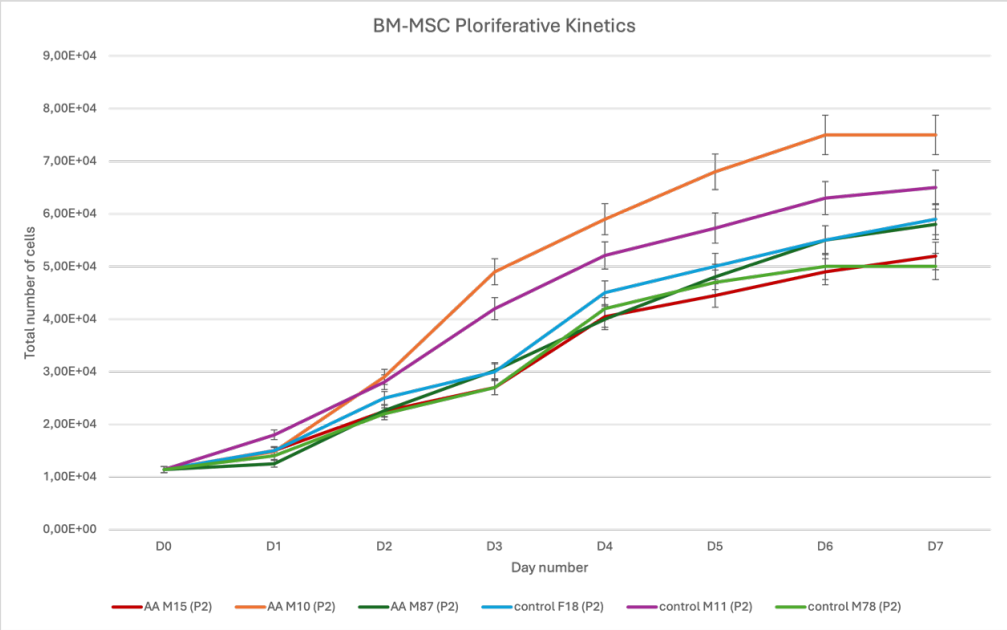

Figure 15: Proliferative kinetics of BM-MSCs (±SE mean). No significant differences between AA-derived and control-derived BM-MSCs (D1, p = 0.35; D2, p = 0.92, D3, p = 0.79, D4, p = 0.99, D5, p = 0.81, D6, p = 0.70, D7, p = 0.68). AA = aplastic anemia; D = day number of cell culture (the day of BM-MSCs seeding was considered D0).

Based on the results, it was concluded that *in vitro* proliferation of AA-derived BM-MSCs did not significantly differ from control-derived BM-MSCs.

In order to determine the impact of cell culture vessel coating on the expansion of BM-MSCs, a laminin-521 (LN521) coating (Biolaminin 521 LN, BioLamina) was tested on AA-derived and control-derived BM-MSCs. According to the manufacturer, Biolaminin 521 LN comprises full-length, human recombinant laminin-521 protein. As an inherent stem cell niche protein, laminin-521 provides a biologically relevant environment, leading to improved survival and efficient cell growth from single-cell cultures to large-scale production.

The experimental setup performed in this project comprised AA-derived (M15) and control-derived (F18 and F70) samples, cultured on LN521 coated versus uncoated 12-well plates, at a seeding density of 3000 cell/cm^2, for 10 days. Expansion rate was assessed by fold increase (FI) at day 10, as represented in Figure 16, below.

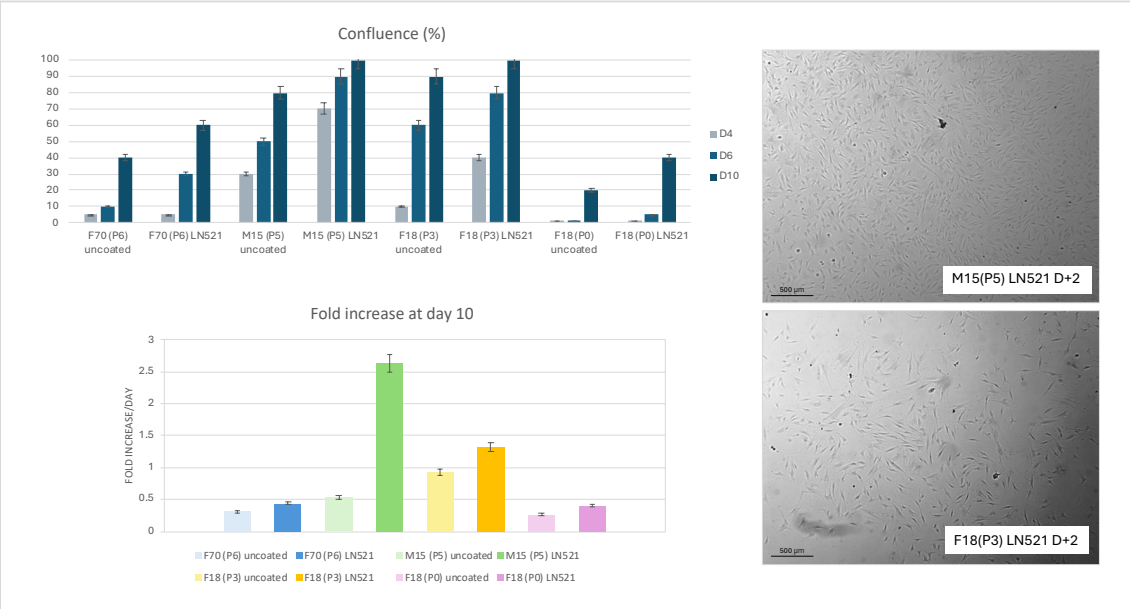

Figure 16: Proliferative rate (defined by confluence (%) and fold increase (FI) at day 10) of AA-derived and control-derived BM-MSCs (±SE mean), cultured on LN521 (Biolaminin 521 LN, BioLamina) coated versus uncoated 12-well plates. At right side, representative morphological image of BM-MSCs cultured on LN521 coated 12-well plates, imaged on bright-field microscope (Olympus IX51 Inverted Microscope equipped with an attached digital camera).

As depicted, LN521 coating led to higher confluence percentage for both AA-derived and control-derived BM-MSCs, resulting in a more expressive fold change at day 10.

In addition, LN521 coating was also used for isolation of BM-MSCs from a control-derived BM-MNC sample (data not shown), with 70% confluence reached at day 9, similarly to gelatin 0.1% coating, as previously mentioned.

Considering the relevance of telomere in MSCs biology and in AA pathophysiology, telomere length of both AA-derived and control-derived BM-MSCs was assessed by RT-qPCR with Absolute Human Telomere Length Quantification qPCR Assay Kit (ScienCellTM), as described previously (section II.10.).

It should be noticed that for all AA samples studied in this project, dyskeratosis congenita/congenital telomeropathies gene mutations were excluded by NGS (*ACD, CTC1, DKC1, NAF1, NHP2, NOP10, OBFC1, PARN, POT1, RPA1, RTEL1, TERC, TERT, TINF2, TPP1, USB1, WRAP53*), as depicted in Materials and Methods.

As represented in Figure 17, AA-derived BM-MSCs telomere length (n=11; mean of average telomere length on each chromosome end = 16.04 kb; minimum = 4.32 kb; maximum = 35.84 kb) was not shorter in comparison to controls (n=11; mean of average telomere length on each chromosome end = 10.68 kb; minimum = 6.90 kb; maximum = 19.03 kb) (p = 0.14). For both groups, telomere length shortens with increase of donor age and passage number.

Despite these results are in accordance with previously publications regarding the influence of telomere length in MSCs biological properties, as described above [20,21,24,25], by this time, and upon literature review, published data about AA-derived BM-MSCs absolute telomere length are scarce and controversial [29], thus requiring further consolidation.

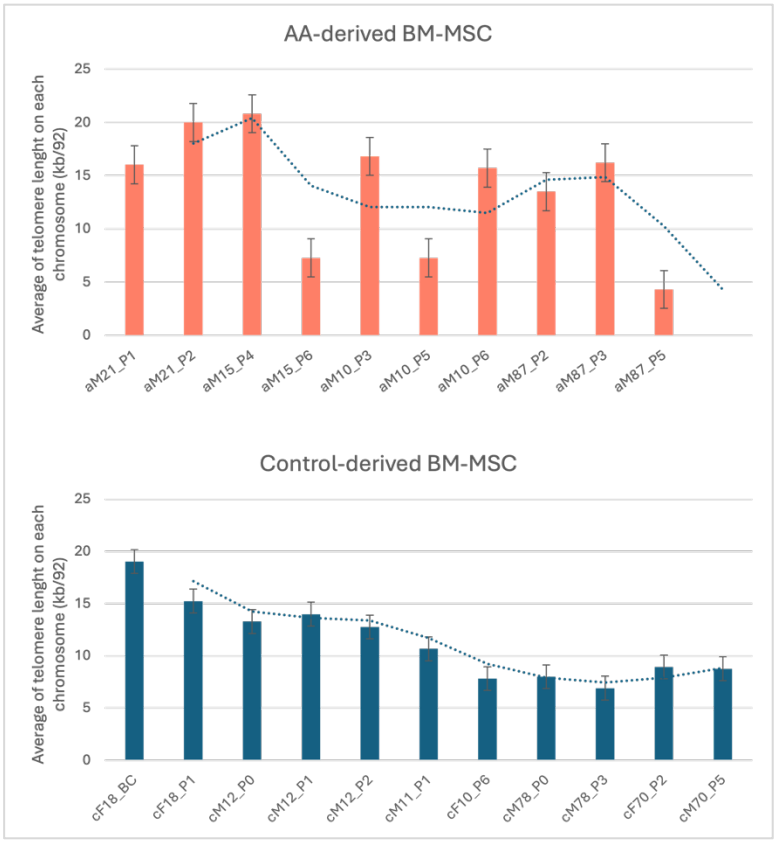

Figure 17: Absolute telomere length for AA-derived and control-derived BM-MSCs. Data is presented as the average of telomere length on each chromosome in kilobase (±SE mean). No significant difference of average telomere length on each chromosome between groups. Donor-age and passage number effect for both groups, with shorter telomere length for older donors and higher cell passage number. kb/92 = average of telomere length on each chromosome in kilobase; a = AA-derived BM-MSCs; c = control-derived BM-MSCs; BC = buffy-coat; P = cell passage number.

In complementarity to telomere length assay performed for BM-MSCs, and in collaboration with Dr. Margarida Coucelo and Dr. Ana Teresa Simões, from Functional Unit of Molecular Hematology, ULS de Coimbra, results of a national Bone Marrow Failure (BMF) group previously analyzed samples were selected and tested by RT-qPCR with Absolute Human Telomere Length Quantification qPCR Assay Kit (ScienCell™).

251 patients were evaluated (2019-2023) using a customized NGS panel including 101 genes, excluding Fanconi Anemia. qPCR Assay for Telomere Length

quantification was performed according to manufacturer's protocol (ScienCell). cDNA samples from BM-derived and PB-derived MNC, stored (-80°C) at biobank of Functional Unit of Molecular Hematology, ULS Coimbra, were used. Patients were grouped as: classic BMF (cBMF, n=58); non-classic BMF/cytopenias (uBMF, n=110); myelodysplastic syndrome/acute leukemia/juvenile myelomonocytic leukemia (MDS/AL/JMML, n=38); AA(n=45).

A total of 63 germline variants were identified: 32 pathogenic, 31 variants of uncertain significance (VUS); and 2 somatic mutations. In the cBMF group the diagnosis was clarified in 20.7% of patients: 4/12 with suspected Diamond-Blackfan anemia (DBA) (2 *RPS19*, *RPL35*, *RPL5*); 6/22 with neutropenia or suspected Shwachman-Bodian-Diamond syndrome (SBDS) (4 *SBDS*, *SRP54*, *GATA2*); 2/24 thrombocytopenia (*WAS*, *GATA2*). In the uBMF group, 15 VUS and 6 pathogenic variants were identified allowing a diagnosis in 5.5% of patients: 2 predisposition syndromes (*SAMD9L*, *DDX41*); telomeropathy (*RTEL1*); DBA-like (GATA1); immunodeficiency (*LIG4*); and Cartilage-hair hypoplasia (*RMRP*). In MDS/LA/LMMJ group, 11 pathogenic variants were identified: 8 associated with a predisposition syndrome (*GATA2*, 2 *RUNX1*, 2 *DDX41*, *ERCCL2*, *TP53*, *NF1*); 1 Shwachman-Diamond syndrome; and 2 immunodeficiency (*STK4*, *RAB27A*); 2 patients had only somatic mutations (*RUNX1*, *NF1*). In the AA group, *TERT* and *MPL* variants were identified in 3 patients, reclassifying them. In 4% of patients (10/251) VUS in telomeropathies-related genes were found, 4 of them with telomere length <1st percentile for age (previously measured by flow cytometry), strengthening the pathogenicity of the variant and supporting a diagnosis.

In conclusion, NGS approach clarified the diagnosis in 12.7% of patients involving 22 different genes. Six uBMF and 3 AA had a genetic diagnosis, and patients were reclassified. Telomere Length assessed by RT-qPCR demonstrated to be a useful complementary assay in patients with VUS in telomeropathies-related genes and allowed to support the diagnosis in 4 other patients, as depicted in Figure 18, below.

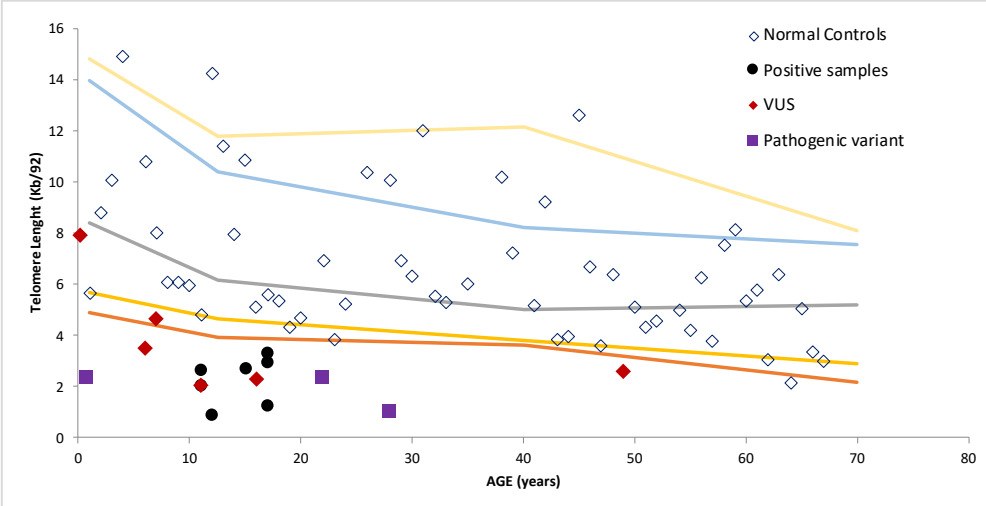

Figure 18: **Absolute telomere length of BMF patients-derived MNC** compared to controls. For each BMF patient with pathogenic variants, average telomere length on each chromosome (kb/92) was under the lower percentile determined for healthy controls. In addition, four patients with VUS in telomeropathies-related genes were identified to be under the lower percentile, demonstrating that RT-qPCR absolute telomere assay is a useful complementary assay for this subset of patients, supporting diagnosis. kb/92 = average of telomere length on each chromosome in kilobase; VUS = variants of uncertain significance.

III.4. Conclusions

Based on the experimental results presented in this chapter, several conclusions were drawn.

The AA-derived BM-MSCs studied did not differ from control-derived BM-MSCs in terms of morphological and immunophenotypic properties.

Regarding differentiation, both AA-derived and control-derived BM-MSCs demonstrated trilineage differentiation capacity. AA-derived BM-MSCs exhibited an adipogenic bias after Oil Red O staining and bright-field microscopy (non-quantitative method). However, an exploratory AdipoRed™ Assay yielded contradictory results, requiring further investigation.

Functionally, the proliferative rate of AA-derived BM-MSCs was comparable to controls. The use of a cell coating agent (e.g., 0.1% gelatin or laminin-521) accelerated the isolation of both AA-derived and control-derived BM-MSCs from MNC.

Regarding telomere length, AA-derived BM-MSCs did not show shorter telomere lengths compared to healthy controls. As expected, based on previous data, BM-MSCs from older donors and at higher passage numbers had shorter telomere lengths.

In the clinical context, the telomere absolute length assay by RT-qPCR proved feasible, demonstrating its potential as a useful complementary assay for diagnosing bone marrow failure syndromes, particularly in patients with variants of uncertain significance (VUS) in telomeropathy-related genes.

III.5. References - Chapter III

1. Medinger M, Drexler B, Lengerke C, Passweg J. Pathogenesis of Acquired Aplastic Anemia and the Role of the Bone Marrow Microenvironment. Front Oncol. 2018; 8:587.
2. Wu L, Mo W, Zhang Y, Zhou M, Li Y, Zhou R, et al. Vascular and perivascular niches, but not the osteoblastic niche, are numerically restored following allogeneic hematopoietic stem cell transplantation in patients with aplastic anemia. Int J Hematol. (2017) 106:71–81.
3. Wu L, Mo W, Zhang Y, Deng H, Li Y, Zhou R, et al. Impairment of hematopoietic stem cell niches in patients with aplastic anemia. Int J Hematol. (2015) 102:645–53.
4. Sharma V, Rawat S, Gupta S, Tamta S, Sharma R, Seth T, Mohanty S. Human Acquired Aplastic Anemia Patients' Bone-Marrow-Derived Mesenchymal Stem Cells Are Not Influenced by Hematopoietic Compartment and Maintain Stemness and Immune Properties. Anemia. 2021 Apr 29;2021:6678067.
5. Bueno C, Roldan M, Anguita E, et al. Bone marrow mesenchymal stem cells from patients with aplastic anemia maintain functional and immune properties and do not contribute to the pathogenesis of the disease. Haematologica. 2014;99(7):1168-1175. doi:10.3324/haematol.2014.103580
6. Killick SB, Bown N, Cavenagh J, Dokal I, Foukaneli T, Hill A, Hillmen P, Ireland R, Kulasekararaj A, Mufti G, Snowden JA, Samarasinghe S, Wood A, Marsh JC; British Society for Standards in Haematology. Guidelines for the diagnosis and management of adult aplastic anaemia. Br J Haematol. 2016 Jan;172(2):187-207.
7. Carvalho MS, Alves L, Bogalho I, Cabral JMS, da Silva CL. Impact of Donor Age on the Osteogenic Supportive Capacity of Mesenchymal Stromal Cell-Derived Extracellular Matrix. Front Cell Dev Biol. 2021 Oct 5;9:747521.
8. Narcisi R, Cleary MA, Brama PA, et al. Long-term expansion, enhanced chondrogenic potential, and suppression of endochondral ossification of adult human MSCs via WNT signaling modulation. Stem Cell Reports. 2015;4(3):459-472.
9. Fan W, Li J, Wang Y, et al. CD105 promotes chondrogenesis of synovium-derived mesenchymal stem cells through Smad2 signaling. Biochem Biophys Res Commun. 2016;474(2):338-344. doi:10.1016/j.bbrc.2016.04.101
10. Cleary MA, Narcisi R, Focke K, van der Linden R, Brama PA, van Osch GJ. Expression of CD105 on expanded mesenchymal stem cells does not predict their chondrogenic potential. Osteoarthritis Cartilage. 2016;24(5):868-872.
11. Pham, L. H., Vu, N. B., Van Pham, P. The subpopulation of CD105 negative mesenchymal stem cells show strong immunomodulation capacity compared to CD105 positive mesenchymal stem cells. 2019. Biomedical Research and Therapy, 6(4), 3131-3140.
12. Barbara NP, Wrana JL, Letarte M. Endoglin is an assessory protein that interacts with the signaling receptor complex of multiple members of the transforming growth factor-beta superfamily. J Biol Chem. 1999;274(2):584-594.
13. Dallas NA, Samuel S, Xia L, et al. Endoglin (CD105): a marker of tumor vasculature and potential target for therapy. Clin Cancer Res. 2008;14(7):1931-1937.
14. Dominici M, Le Blanc K, Mueller I, et al. Minimal criteria for defining multipotent mesenchymal stromal cells. The International Society for Cellular Therapy position statement. Cytotherapy. 2006;8(4):315-317.

15. Lin CS, Xin ZC, Dai J, Lue TF. Commonly used mesenchymal stem cell markers and tracking labels: Limitations and challenges. Histol Histopathol. 2013 Sep;28(9):1109-16.
16. Kornicka K., Marycz K., Tomaszewski K. A., Marędziak M., Śmieszek A. (2015). The effect of age on osteogenic and adipogenic differentiation potential of human adipose derived stromal stem cells (hASCs) and the impact of stress factors in the course of the differentiation process.
17. Tripathy NK, Singh SP, Nityanand S. Enhanced adipogenicity of bone marrow mesenchymal stem cells in aplastic anemia. Stem Cells Int. 2014;2014:276862.
18. Park YH, Yun JI, Han NR, Park HJ, Ahn JY, Kim C, Choi JH, Lee E, Lim JM, Lee ST. Mass production of early-stage bone-marrow-derived mesenchymal stem cells of rat using gelatin-coated matrix. Biomed Res Int. 2013;2013:347618.
19. Hiyama E, Hiyama K. Telomere and telomerase in stem cells. Br J Cancer. 2007;96(7):1020-1024.
20. Serakinci N, Graakjaer J, Kolvraa S. Telomere stability and telomerase in mesenchymal stem cells. Biochimie. 2008;90(1):33-40. doi:10.1016/j.biochi.2007.09.005
21. Jing S, Zhou H, Zou C, et al. Application of telomere biology and telomerase in mesenchymal stem cells. Nano TransMed, 2022, 1(2–4): e9130007.
22. Aubert G, Lansdorp PM. Telomeres and aging. Physiol Rev. 2008;88(2):557-579.
23. Shay JW. Role of Telomeres and Telomerase in Aging and Cancer. Cancer Discov. 2016 Jun;6(6):584-93.
24. Miclau K, Hambright WS, Huard J, Stoddart MJ, Bahney CS. Cellular expansion of MSCs: Shifting the regenerative potential. Aging Cell. 2023 Jan;22(1):e13759.
25. Vasanthan J, Gurusamy N, Rajasingh S, Sigamani V, Kirankumar S, Thomas EL, Rajasingh J. Role of Human Mesenchymal Stem Cells in Regenerative Therapy. Cells. 2020 Dec 31;10(1):54.
26. Scheinberg P, Cooper JN, Sloand EM, Wu CO, Calado RT, Young NS. Association of telomere length of peripheral blood leukocytes with hematopoietic relapse, malignant transformation, and survival in severe aplastic anemia [published correction appears in JAMA. 2010 Nov 3;304(17):1901]. JAMA. 2010;304(12):1358-1364.
27. Wang Y, McReynolds LJ, Dagnall C, Katki HA, Spellman SR, Wang T, Hicks B, Freedman ND, Jones K, Lee SJ, Savage SA, Gadalla SM. Pre-transplant short telomeres are associated with high mortality risk after unrelated donor haematopoietic cell transplant for severe aplastic anaemia. Br J Haematol. 2020 Jan;188(2):309-316.
28. Savage SA, Bertuch AA. The genetics and clinical manifestations of telomere biology disorders. Genet Med. 2010;12(12):753-764.
29. Saxena P, Srivastava J, Rai B, et al. Elevated senescence in the bone marrow mesenchymal stem cells of acquired aplastic anemia patients: A possible implication of DNA damage responses and telomere attrition. Biochim Biophys Acta Mol Basis Dis. 2024;1870(3):167025.
30. Margarida Coucelo, Joana Azevedo, Isabel Bogalho, Ana Teresa Simões et al. OC 4 - NEXT GENERATION SEQUENCING APPROACH TO BONE MARROW FAILURE SYNDROMES – PORTUGUESE EXPERIENCE, EJC Paediatric Oncology, Volume 2, Supplement 1, 2023, 100035.

IV. Comparative analysis between AA and control-derived BM-MSCs feeder layers on HSPC expansion

IV.1. Summary

Ex vivo HSPC expansion has been attempted to obtain high quantity of HSPC to apply in cell and gene therapy for hematological conditions. However, the quality of HSPC for therapeutic purposes depends on their capacity for *ex vivo* proliferation without losing multi-lineage differentiation and self-renewal properties, which is a matter of research. In AA, *ex vivo* expansion of HSPC would be a strategy to circumvent the limited number of donors available for HCT. For that purpose, understanding the role of AA-derived BM-MSCs in HSPC support and expansion will be fundamental to develop strategies to modulate the BM niche in AA, both to improve *ex vivo* expansion and *in vivo* engraftment of HSPC.

In this chapter, a comparative analysis of expansion of HSPC derived from healthy donors (number of donors = 10; median age = 54 years; minimum = 4 years; maximum = 73 years) co-cultured in cell suspension (30000 cells/ml) on AA-derived (number of donors = 4; median age = 13 years; minimum = 7 years; maximum = 35 years) and control-derived (number of donors = 5; median age = 43 years; minimum = 4 years; maximum = 52 years) BM-MSCs feeder layers, or without feeder layer support, was performed. HSPC expansion was significantly higher after both AA-derived and control-derived BM-MSCs co-culture in comparison to no feeder layer. Expansion of HSPC co-cultured on control-derived BM-MSCs was higher than on AA-derived BM-MSCs feeder layers, with statistically significant results attained in two out of four experiments (HSPC Pool#1 experiment, p = 0.02; HSPC Pool#3 experiment, p = 0.02). HSPC viability was similar (>90%) between experiments and groups. Colony forming unit assay (CFU) did not show significant differences regarding clonogenic potential of HSPC expanded on either AA-derived or control-derived BM-MSCs feeder layers. For HSPC cultured without feeder layer, the number of CFU-GEMM was lower in comparison to co-culture with control-derived (p = 0.007) and AA-derived BM-MSCs feeder layers (p = 0.03).

In conclusion, AA-derived BM-MSCs showed lower hematopoietic supportive capacity in comparison to control-derived BM-MSCs, suggesting a dysfunctional role in disease. Understanding the mechanisms behind that would be an important path towards improvement of HSPC expansion in AA.

IV.2. Background

Within BM, MSCs are known to play a significant role in hematopoiesis, either by direct cell-cell contact or by secretion of growth factors and cytokines (e.g. SCF, IL-6, TPO), providing physical support for HSPC and regulating their proliferation and differentiation. BM-MSCs immunomodulatory function also contributes to the maintenance of a balanced hematopoietic environment (e.g., by suppression of immune cell attack to HSPC, thus ensuring their survival and functioning) [1,2]. Interestingly, during embryonic development, MSCs first appear in the aorta-gonad-mesonephros (AGM) region, which is one of the places where definitive HSC are generated. During development, MSCs increase numerically to a plateau level found in adult BM, denoting the co-localization of MSCs to the major hematopoietic tissues [1].

Corroborating the importance on HSPC support, MSCs have been used as a strategy for *ex vivo* expansion of HSPC [3,4], as well as part of hematopoietic stem cell transplantation protocols [2].

Regarding aplastic anemia, several studies suggest that AA-derived BM-MSCs might be involved in functional disruption of AA-HSC [5,6,7], however those results are contradictory [8,9], and thus further research is needed to better understand if there is a pathophysiological role of AA-derived BM-MSCs on hematopoietic support and, consequently, in disease establishment and severity.

Again, the controversy of published data could be in part related to sampling and methodological heterogeneity across studies. Even in the same study, the sampling groups are heterogenous, including patients at distinct stages of AA severity, as well as either treated or untreated, introducing relevant confounding effects for an accurate interpretation of results. Another important consideration is the fact that, from one study to another, different sources of HSPC (e.g. either derived from peripheral blood, BM or cord blood units) were used [6,7,9], which further limits the comparison of results.

In this work, a side-by-side comparison between severe and very severe AA-derived BM-MSCs and control-derived BM-MSCs supportive capacity of *in vitro* expansion of HSPC isolated from BM samples (healthy donors) was performed. In an attempt to circumvent the abovementioned limitations, BM-MSCs samples used in this

work were derived from patients diagnosed with severe and very severe acquired idiopathic AA, age-matched with healthy controls based on sample availability. To increase homogeneity between AA-derived and control-derived BM-MSCs samples, it was opted to preferentially use control-derived MSCs isolated from BM samples collected from PSIS instead of femoral head/neck, whenever possible.

IV.3. Results and discussion

IV.3.1. Analysis of HSPC expansion co-cultured with AA-derived versus control-derived BM-MSCs feeder layers

For a better interpretation, HSPC expansion results will be presented according to the respective experimental setup - BM-MSCs + HSPC from single donor (single donor experiment); BM-MSCs + Pool#1 HSPC (Pool#1 experiment); BM-MSCs + Pool#2 HSPC (Pool#2 experiment); BM-MSCs + Pool#3 HSPC (Pool#3 experiment). The characteristics of HSPC and BM-MSCs samples co-cultured with HSPC as feeder layers are summarized in Table 5 and Table 6, below.

Table 5 – Characterization of HSPC samples.

Sampling group	Sample ID	Donor age (years)	BM source	Pool ID	Percentage of CD34+ cells after MACS (determined by flow cytometry)
Healthy donors	M66	56	PSIS	N/A (single donor experiment)	68%
	F18	4	PSIS	#1	75%
	F70	52	PSIS		
	M12	10	Femoral head/neck	#2	72%
	M72	52	Femoral head/neck		
	F53	69	Femoral head/neck		
	F51	73	Femoral head/neck		
	M66	56	PSIS		
	F91	31	PSIS	#3	80%
	F53	69	Femoral head/neck		

BM - bone marrow; PSIS - posterior superior iliac spine; ID – identification; MACS - Magnetic-activated cell sorting; N/A – not applicable.

Table 6 – Characterization of BM-MSCs feeder layers.

Sampling group	Sample ID	Donor age (years)	BM source	Co-cultured HSPC (single donor/pool ID)
AA	M87 (P4)	35	PSIS	M66 (single donor experiment)
Control	M78 (P2)	44	PSIS	
AA	M15 (P4)	7	PSIS	Pool #1
	M10 (P4)	12	PSIS	
	M08 (P6)	14	PSIS	
	M87 (P4)	35	PSIS	
Control	F18 (P4)	4	PSIS	
	M11 (P4)	11	PSIS	
	M78 (P3)	44	PSIS	
AA	M15 (P3)	7	PSIS	Pool #2
	M10 (P4)	12	PSIS	
	M87 (P6)	35	PSIS	
Control	F18 (P5)	4	PSIS	
	M70 (P6)	52	Femoral head/neck	
	M78 (P4)	44	PSIS	
AA	M15 (P6)	7	PSIS	Pool #3
	M10 (P4)	12	PSIS	
	M87 (P6)	35	PSIS	
Control	F18 (P5)	4	PSIS	
	F81 (P6)	43	PSIS	
	M78 (P6)	44	PSIS	

BM - bone marrow; PSIS - posterior superior iliac spine; ID – identification; HSPC – hematopoietic stem and progenitor cells.

Experimental methodologies are described in Section II (II.16. – II.19.).

Previously from HSPC expansion, feeder layers from both AA-derived and control-derived BM-MSCs were established, after one passage post-thawing, to avoid potential cryopreservation effect on cell growth and functioning. No significant differences in feeder layer establishment (e.g., time to confluence) were detected. Cell distribution and morphology were visualized on bright-field microscope, as represented in Figure 19, below.

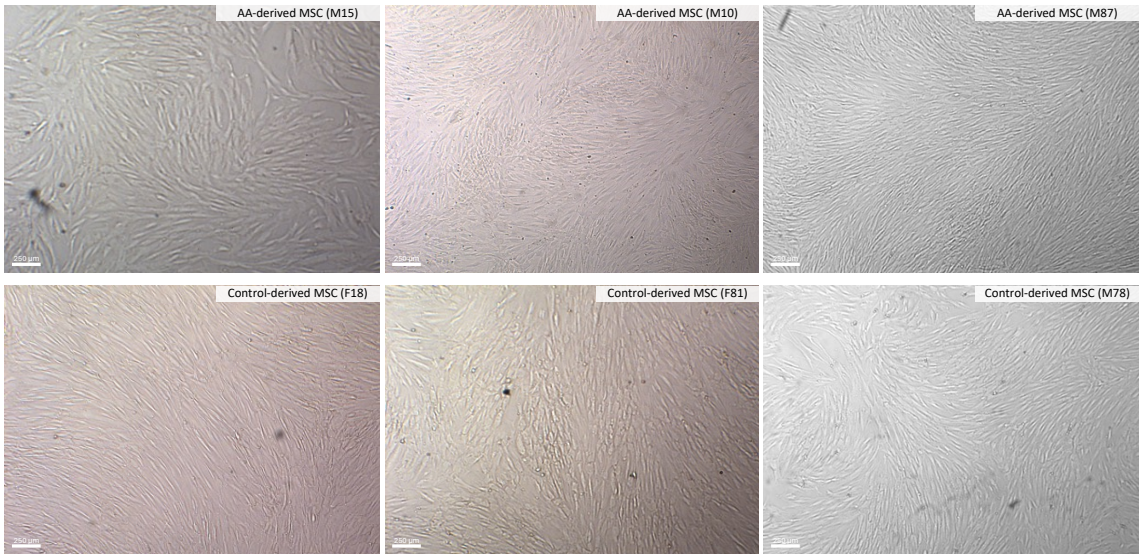

Figure 19: Representative image of AA-derived and control-derived BM-MSCs feeder layers. For both sampling groups it was possible to establish confluent feeder layers for co-culture with HSPC. Samples imaged at 10x magnification on bright-field (Olympus IX51 Inverted Microscope equipped with an attached digital camera). AA = aplastic anemia; HSPC = hematopoietic stem and progenitor cells; BM-MSCs = bone marrow-derived mesenchymal stromal cells.

Globally, HSPC expansion showed a tendency to be higher in co-culture with control-derived BM-MSCs in comparison to AA-derived BM-MSCs. However, statistical significance was only attained in two out of four experimental setups, as detailed next. HSPC expansion was higher after co-culture with either AA or control-derived BM-MSCs in comparison to culture without feeder layer.

In all experiments, HSPC viability was comparable between groups, with rates above 90% of cell viability.

Before HSPC harvesting at Day 7, cells were visualized on bright-field microscope, as represented in Figure 20. As depicted, for HSPC culture without feeder layer, HSPC density appears to be lower in comparison to co-culture with both AA-derived and control-derived BM-MSCs.

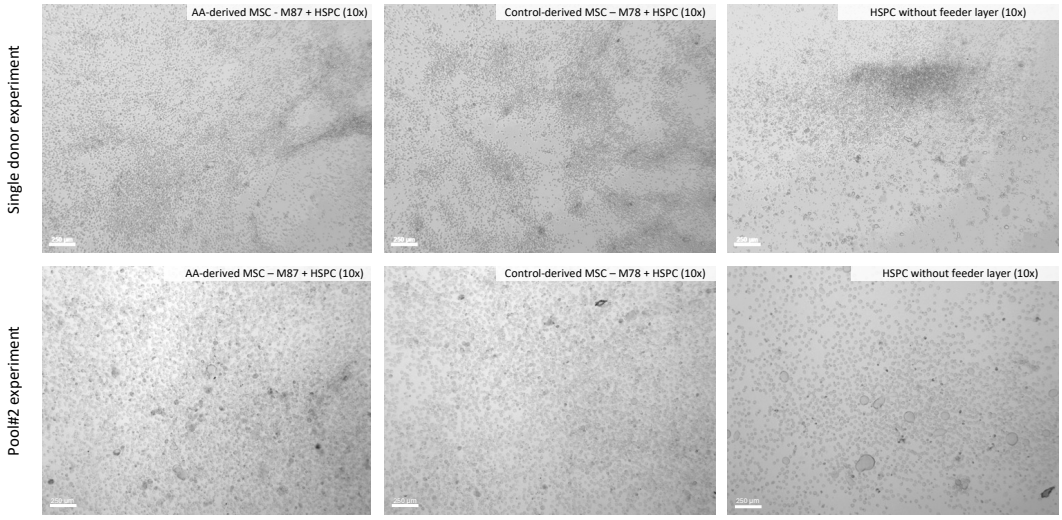

Figure 20: HSPC expansion (co-)cultured with AA-derived and control-derived BM-MSCs feeder layers, or without feeder layer, in the context of: HSPC single donor experiment; Pool#2 experiment. Representative images captured on Day 7 of HSPC expansion. Samples were imaged at 10x magnification on bright-field (Olympus IX51 Inverted Microscope equipped with an attached digital camera). AA = aplastic anemia; HSPC = hematopoietic stem and progenitor cells; BM-MSCs = bone marrow-derived mesenchymal stromal cells.

Results of HSPC expansion after 7-day (co-)culture are represented in Figure 21 and Figure 22, below. For both single donor HSPC experiment and Pool#2 experiment, HSPC expansion in co-culture with AA-derived BM-MSCs was not significantly different from control-derived BM-MSCs co-culture.

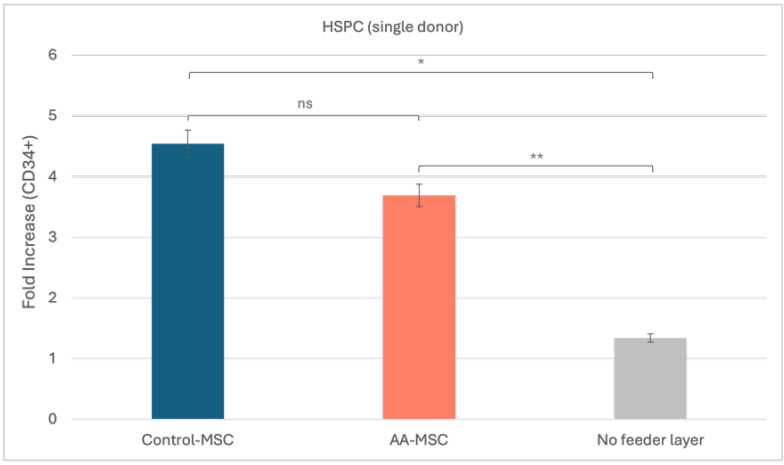

Figure 21: HSPC single donor experiment - HSPC expansion after 7-day (co-)culture with AA-derived (red bar) and control-derived BM-MSCs (blue bar) feeder layers, or without feeder layer (grey bar). * p = 0.006; ** p = 0.04; ns = not significant. Fold increase (FI) represents the fraction of CD34+ cells at Day 7 divided by the number of CD34+ cells enriched sample from single donor (M66) (±SE mean). AA-MSCs = aplastic anemia-derived bone marrow mesenchymal stromal cells; Control-MSCs = control-derived derived bone marrow mesenchymal stromal cells; HSPC = hematopoietic stem and progenitor cells.

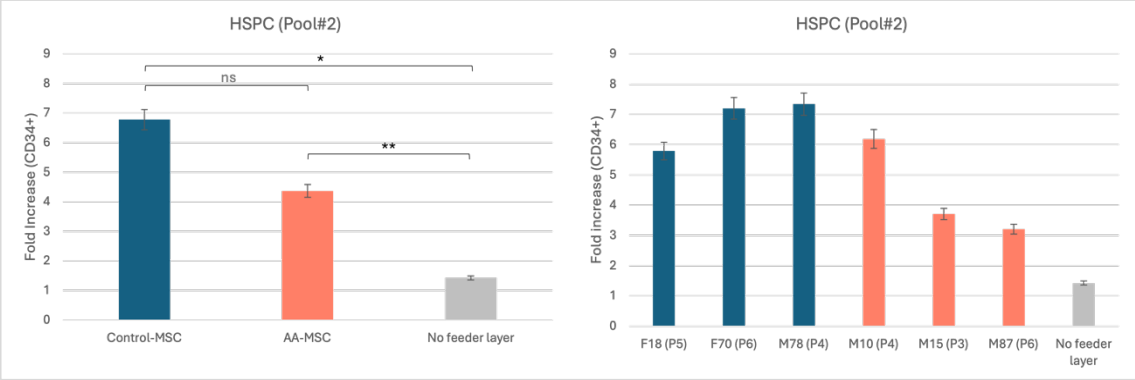

Figure 22: HSPC Pool#2 experiment - HSPC expansion after 7-day (co-)culture with AA-derived (red bars) and control-derived BM-MSCs (blue bars) feeder layers, or without feeder layer (grey bars). * p = 0.003; ** p = 0.03; ns = not significant. Fold increase (FI) represents the fraction of CD34+ cells at Day 7 divided by the number of CD34+ cells enriched Pool#2 (±SE mean). AA-MSCs = aplastic anemia-derived bone marrow mesenchymal stromal cells; Control-MSCs = control-derived derived bone marrow mesenchymal stromal cells; HSPC = hematopoietic stem and progenitor cells.

As represented, HSPC expansion was significantly higher after both AA-derived (p = 0.04 – HSPC single donor experiment; p = 0.03 – HSPC Pool#2 experiment) and control-derived BM-MSCs (p = 0.006 - HSPC single donor experiment; p = 0.003 - HSPC Pool#2 experiment) co-culture, in comparison to no feeder layer.

In order to increase the robustness of this comparative study, two additional experiments were run with HSPC pools (Pool#1 and Pool#3) (co-)cultured over AA-derived and control-derived BM-MSCs, or without feeder layer support.

As performed for HSPC single donor and Pool#2 experiments, both Pool#1 and Pool#3 HSPC were visualized on bright-field microscope at Day 7 of expansion, immediately before HSPC harvesting, and imaged, as shown in Figure 23, below. As verified for the previous experiments (Figure 20), it was not possible to clearly identify a distinctive pattern between HSPC co-culture with both AA-derived and control-derived BM-MSCs upon microscopy. In addition, for HSPC culture without feeder layer, HSPC density appears to be lower in comparison to co-culture with either AA-derived or control-derived BM-MSCs feeder layers.

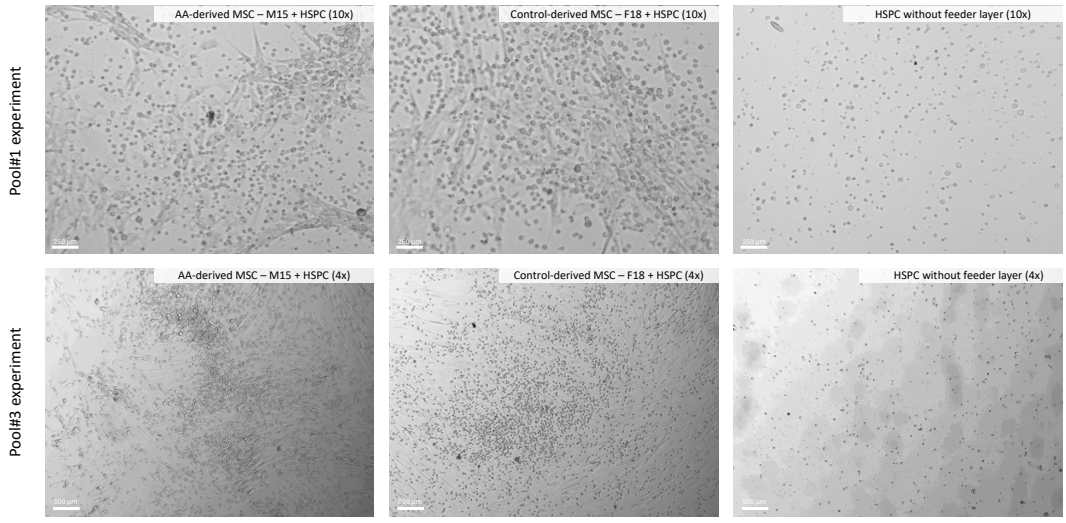

Figure 23: HSPC expansion (co-)cultured with AA-derived and control-derived BM-MSCs feeder layers, or without feeder layer, in the context of: Pool#1 experiment; Pool#3 experiment. Representative images captured on Day 7 of HSPC expansion. Samples were imaged at 10x and magnification, respectively, on bright-field (Olympus IX51 Inverted Microscope equipped with an attached digital camera). AA = aplastic anemia; HSPC = hematopoietic stem and progenitor cells; BM-MSCs = bone marrow-derived mesenchymal stromal cells.

Results of HSPC expansion after 7-day (co-)culture are represented in Figure 24 and Figure 25, below.

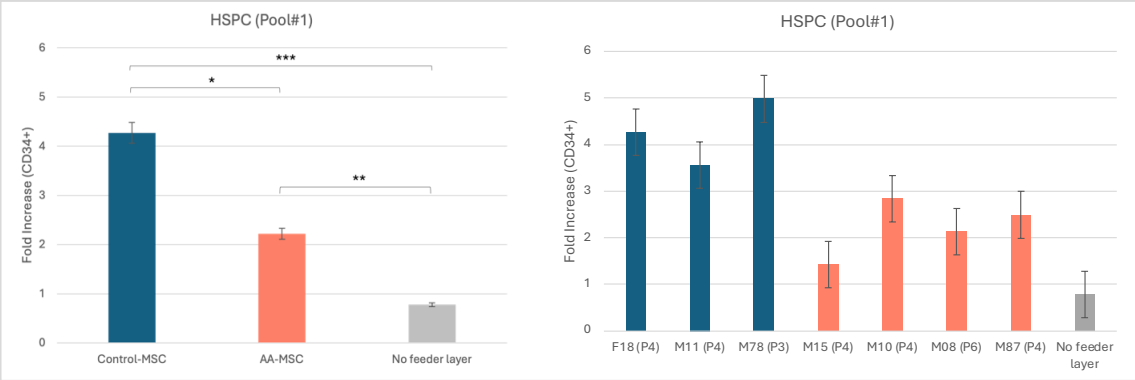

Figure 24: HSPC Pool#1 experiment - HSPC expansion after 7-day (co-)culture with AA-derived (red bars) and control-derived (blue bars) BM-MSCs feeder layers, or without feeder layer (grey bars). * p = 0.02; ** p = 0.02; *** p = 0.01; ns = not significant. Fold increase (FI) represents the fraction of CD34+ cells at Day 7 divided by the number of CD34+ cells enriched Pool#1 (±SE mean). AA-MSCs = aplastic anemia-derived bone marrow mesenchymal stromal cells; Control-MSCs = control-derived derived bone marrow mesenchymal stromal cells; HSPC = hematopoietic stem and progenitor cells.

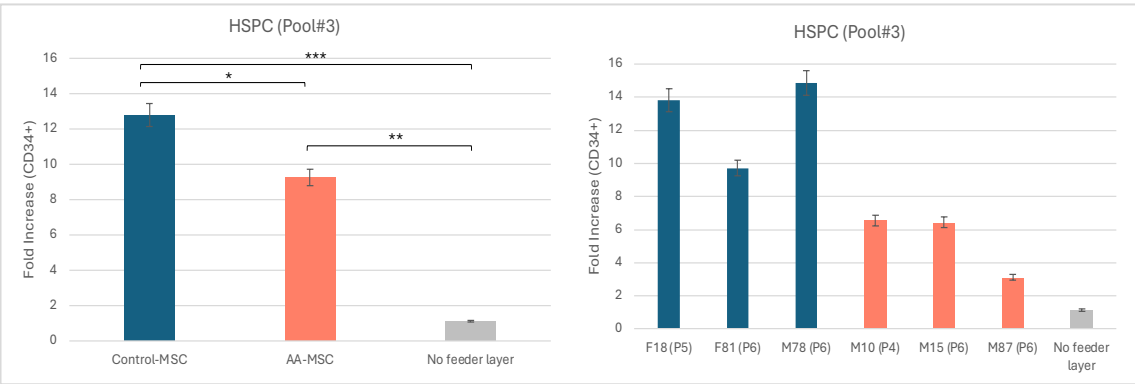

Figure 25: HSPC Pool#3 experiment - HSPC expansion after 7-day (co-)culture with AA-derived (red bars) and control-derived (blue bars) BM-MSCs feeder layers, or without feeder layer (grey bars). * p = 0.02; ** p = 0.03; *** p = 0.02. Fold increase (FI) represents the fraction of CD34+ cells at Day 7 divided by the number of CD34+ cells enriched Pool#3 (±SE mean). AA-MSCs = aplastic anemia-derived bone marrow mesenchymal stromal cells; Control-MSCs = control-derived derived bone marrow mesenchymal stromal cells; HSPC = hematopoietic stem and progenitor cells.

As represented, HSPC expansion was higher after co-culture on AA-derived BM-MSCs feeder layers in comparison to control-derived BM-MSCs feeder layers (p = 0.02 - HSPC Pool#1 experiment; p = 0.02 – HSPC Pool#3 experiment).

In addition, HSPC expansion was significantly higher after both AA-derived (p = 0.02 - HSPC Pool#1 experiment; p = 0.03 - HSPC Pool#3 experiment) and control-derived BM-MSCs (p = 0.01 - HSPC Pool#1 experiment; p = 0.02 - HSPC Pool#3 experiment) co-culture in comparison to no feeder layer.

IV.3.2. Analysis of the clonogenic potential of HSPC expanded in co-culture with AA-derived versus control-derived BM-MSCs feeder layers

Clonogenic potential of HSPC expanded on either AA-derived or control-derived BM-MSCs was similar across experiments (BFU-E, p = 0.08; CFU-GM, p = 0.85; CFU-GEMM, p = 0.10; CFU-E, p = 0.79). For HSPC cultured without feeder layer, the number of CFU-GEMM was lower in comparison to co-culture with control-derived (p = 0.007) or AA-derived BM-MSCs feeder layers (p = 0.03). CFU assay results are represented in Figure 26, below.

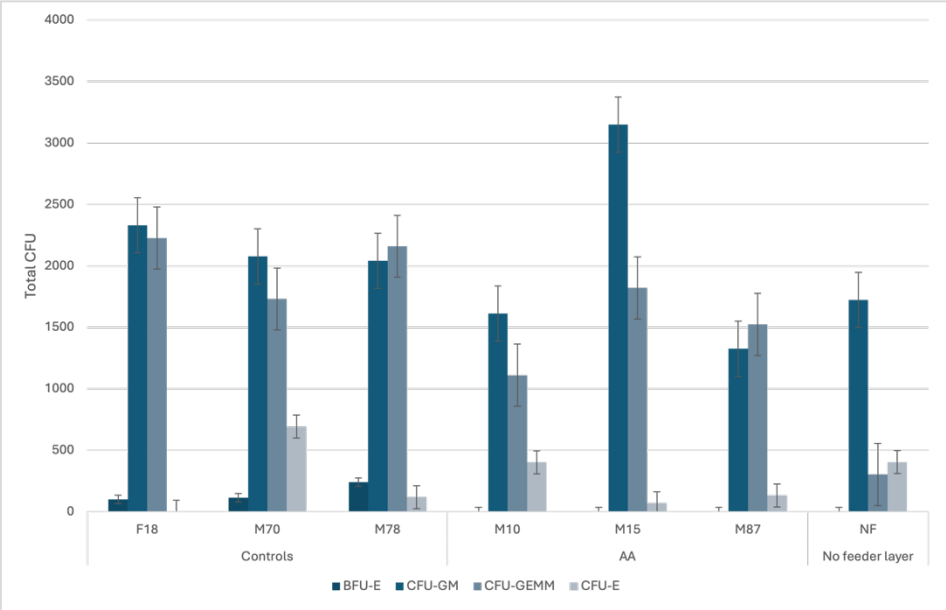

Figure 26: Clonogenic potential of HSPC (co-)cultured with AA-derived and control-derived BM-MSCs feeder layers, or without feeder layer. CFU number was normalized by the number of MethoCult™ seeded cells and multiplied by the total number of CD34+ cells harvested on Day 7 of HSPC expansion. Plotted results correspond to the mean value of total CFU number of Pool#2 experiment, performed in technical triplicates (±SE mean).

Despite apparent consistency across experiments, it is important to notice that the results could had been influenced by the need to use HSPC pool rather than single-donor derived HSPC. In fact, both AA-derived and control-derived BM samples were provided in small volumes of about 6 ml to 8 ml, due to ethical rules and sampling collection

protocols of clinical units, which limited the number of isolated MNC and, consequently, of sorted CD34+ cells per sample.

Because experimental setups were simultaneously performed for several culture conditions, in technical triplicates, it was necessary to increase the number of CD34+ enriched cells by using pools from different donors, a strategy that has been successfully applied in the context of *ex vivo* expansion of CD34 enriched cells isolated from UCB [10,11,12,13].

Another possible confounding effect, alongside with the use of HSPC pools, is the potential variability of HSPC numbers and functional properties (e.g., proliferative and differentiation capacity) related to BM collection site (e.g., posterior superior iliac spine (PSIS) versus femoral head/neck; even peripheral blood, in case of mixing with BM samples during aspiration procedure) [14,15,13].

To circumvent those limitations, further experiments must be performed with more homogeneous HSPC populations (e.g., HSPC isolated from the same patient upon collection of larger volumes of BM, if feasible; samples collected from theoretically equivalent BM locations).

Considering that since the beginning of the project the number of samples in the biobank has been increasing, in close collaboration with the clinical units, it is expected to attain an adequate number of samples to better confirm the present results. Moreover, it is expected to increase the number of AA-derived BM samples, in order to functionally study HSPC from patients.

IV.4. Conclusions

Based on the experimental results presented in this chapter, several conclusions were drawn regarding HSPC expansion and function.

HSPC expansion in co-culture with either control-derived or AA-derived BM-MSCs feeder layers was significantly higher compared to HSPC culture without a feeder layer, consistent with previously published findings.

While HSPC expansion on AA-derived BM-MSCs feeder layers was observed to be lower than that on control-derived BM-MSCs feeder layers, further experiments are required to confirm this observation.

Short-term clonogenic potential was similar between HSPC expanded in co-culture with control-derived and AA-derived BM-MSCs feeder layers. HSPC expanded without a feeder layer exhibited a distinct clonogenic profile compared to those co-cultured on BM-MSCs feeder layers (e.g., lower CFU-GEMM numbers), although this difference showed variability between experiments.

Finally, HSPC sampling heterogeneity was identified as a potential limiting factor for functional HSPC assessment and warrants further investigation in future studies.

IV.5. References - Chapter IV

1. Mendes SC, Robin C, Dzierzak E. Mesenchymal progenitor cells localize within hematopoietic sites throughout ontogeny. Development. 2005;132(5):1127-1136.
2. Crippa S, Santi L, Bosotti R, Porro G, Bernardo ME. Bone Marrow-Derived Mesenchymal Stromal Cells: A Novel Target to Optimize Hematopoietic Stem Cell Transplantation Protocols in Hematological Malignancies and Rare Genetic Disorders. J Clin Med. 2019 Dec 18;9(1):2.
3. da Silva CL, Gonçalves R, dos Santos F, Andrade PZ, Almeida-Porada G, Cabral JM. Dynamic cell-cell interactions between cord blood haematopoietic progenitors and the cellular niche are essential for the expansion of CD34+, CD34+CD38- and early lymphoid CD7+ cells. J Tissue Eng Regen Med. 2010;4(2):149-158.
4. Fernandes-Platzgummer A, Andrade PZ, Cabral JMS, da Silva CL. Scalable Manufacturing of Human Hematopoietic Stem/Progenitor Cells Exploiting a Co-culture Platform with Mesenchymal Stromal Cells. Methods Mol Biol. 2021;2286:107-120.
5. Wang XA, Li JP, Wu KH, Yang SF, Chao YH. Mesenchymal Stem Cells in Acquired Aplastic Anemia: The Spectrum from Basic to Clinical Utility. Int J Mol Sci. 2023 Feb 24;24(5):4464.
6. Chao YH, Lin CW, Pan HH, et al. Increased apoptosis and peripheral blood mononuclear cell suppression of bone marrow mesenchymal stem cells in severe aplastic anemia. Pediatr Blood Cancer. 2018;65(9):e27247.
7. Hamzic E, Whiting K, Gordon Smith E, Pettengell R. Characterization of bone marrow mesenchymal stromal cells in aplastic anaemia. Br J Haematol. 2015;169(6):804-813. doi:10.1111/bjh.13364
8. Michelozzi IM, Pievani A, Pagni F, Antolini L, Verna M, Corti P, et al. Human aplastic anaemia-derived mesenchymal stromal cells form functional haematopoietic stem cell niche in vivo. Br J Haematol. (2017) 179:669–73.
9. Bueno C, Roldan M, Anguita E, et al. Bone marrow mesenchymal stem cells from patients with aplastic anemia maintain functional and immune properties and do not contribute to the pathogenesis of the disease. Haematologica. 2014;99(7):1168-1175.
10. Gary L. Gilmore, Darlene K. DePasquale, John Lister, Richard K. Shadduck. Selection of CD34+ HSC from Pooled Cord Blood Samples Does Not Result in Co-Purification of Potential Alloreactive CD3+ T Cells. Blood, Volume 106, Issue 11, 2005, Page 5263, ISSN 0006-4971.
11. Gilmore GL, DePasquale DK, Lister J, Shadduck RK. Ex vivo expansion of human umbilical cord blood and peripheral blood CD34(+) hematopoietic stem cells. Exp Hematol. 2000;28(11):1297-1305.
12. Bucar S, Branco ADM, Mata MF, Milhano JC, Caramalho Í, Cabral JMS, Fernandes-Platzgummer A, da Silva CL. Influence of the mesenchymal stromal cell source on the hematopoietic supportive capacity of umbilical cord blood-derived CD34+-enriched cells. Stem Cell Res Ther. 2021 Jul 13;12(1):399.
13. Sandhya R. Panch, James Szymanski, Bipin N. Savani, David F. Stroncek. Sources of Hematopoietic Stem and Progenitor Cells and Methods to Optimize Yields for Clinical Cell Therapy. Biology of Blood and Marrow Transplantation. Volume 23, Issue 8, 2017, Pages 1241-1249, ISSN 1083-8791.

14. Kumar S, Geiger H. HSC Niche Biology and HSC Expansion Ex Vivo. Trends Mol Med. 2017 Sep;23(9):799-819. doi: 10.1016/j.molmed.2017.07.003.
15. Kwon M, Kim BS, Yoon S, Oh SO, Lee D. Hematopoietic Stem Cells and Their Niche in Bone Marrow. Int J Mol Sci. 2024 Jun 21;25(13):6837.

V. Transcriptomics analysis of AA-derived versus control-derived BM-MSCs

V.1. Summary

AA is a rare disorder, characterized by BM failure with severe reduction in the number of HSPC and BM microenvironment disturbances (e.g., BM replacement by fat cells). Besides cytotoxic T-cell–mediated attack to CD34+ HSPC, stem cell niche modulation has been implicated in pathophysiology of AA. Several reports have demonstrated an abnormal function of key BM elements, namely dysfunctional MSCs, however with scarce and heterogeneous data, and controversial results.

In this work, bulk messenger ribonucleic acid sequencing (bulk mRNA-Seq) of BM-derived MSCs (BM-MSCs) from both severe acquired idiopathic AA (SAA) patients (n= 4; median age = 13 years; minimum = 7 years; maximum = 35 years) and healthy controls (n=4; median age = 11.5 years; minimum = 4 years; maximum = 44 years) was performed to search for candidate (differently expressed) genes that might be related to the pathophysiology of disease and, consequently, become potential therapeutic targets.

Upon data analysis, molecular patterns related to immune response, adipogenesis, lipid metabolism, osteoblast and osteoclast differentiation and activity, cell-ECM interactions/ECM remodeling, hematopoietic support, angiogenesis, DNA repair/DNA damage response, and stress response, were identified.

Additionally, gene expression profiles related to key signaling pathways, namely Wnt/β-catenin, MAPK, PI3K/AKT, JAK-STAT, NF-kB, were identified, however with inconsistent results.

No significant gene expression differences were identified for genes previously associated with MSCs disfunction in AA, namely, *GATA2*, *CEBPA*, *RUNX1*, *LEP*, *LEPR*. Interestingly, contrarily to what was expected from previously published results, *PPARG* was downregulated in AA-derived BM-MSCs in comparison to healthy controls.

Transcriptomics results of a selected subset of genes were confirmed by RT-qPCR. Regarding genes with significant different gene expression (DGE) results in transcriptomics analysis, gene expression profiles between AA and control-derived BM-MSCs showed a similar pattern (of either up or down regulation) between bulk mRNA-Seq and RT-qPCR, with the exception of *TNFSF9* (downregulated in RT-qPCR). For genes without significant DGE results in transcriptomics analysis but of potential interest in AA

biology, RT-qPCR results were less consistent with transcriptomics data. Results must be consolidated in further experiments.

In vitro drug-modulation of AA and control-derived BM-MSCs with isotretinoin, a drug that could modulate the expression of several genes with potential influence on AA pathophysiology, was performed. Drug was selected based on the molecular analysis results. Gene expression profile of *CEBPA*, *PPARG*, *RARA*, *WNT5A*, *APOL4* and *SOCS3*, assessed by RT-qPCR after a 6-day period of drug exposure of AA and control-derived BM-MSCs, suggested and effect of isotretinoin on *CEBPA* (upregulation), *PPARG* (downregulation), *RARA* (downregulation), *WNT5A* (downregulation) and *APOL4* (upregulation) expression, observed in global and individual analysis of either AA or control samples. However, upon comparison of gene expression profiles in either treated and untreated groups contrasting by disease (AA versus control), no differences were found either before or after drug exposure, with a possible exception for *CEBPA* (upregulation) and *SOCS3* (upregulation), which must be confirmed in further experiments.

In both AA and control samples, cellular metabolic activity at 24h of drug exposure was significantly lower for cells exposed to drug concentrations of both 1 μM ($p = 0.004$) and 10 μM ($p = 0.002$) in comparison to no drug. However, no significant differences between the three different drug concentrations were found ($p = 0.21$, for 0.1 μM versus 1 μM; $p = 0.13$, for 0.1 μM versus 10 μM; $p = 0.76$ for 1 μM versus 10 μM). Globally, proliferative rate of BM-MSCs exposed to the drug, calculated by cell number fold increase (FI) at day 6 of exposure, appeared to be lower for increasing concentrations of drug in comparison to no drug exposure, with significance attained for 10 μM of isotretinoin concentration ($p = 0.15$, for 1 μM versus no drug; $p = 0.03$ for 10 μM versus no drug; $p = 0.42$ for 1 μM versus 10 μM).

Overall, the results obtained provided valuable insights on altered patterns of BM microenvironment in AA, unveiling pathways for *ex vivo* modeling of disease towards development of regenerative medicine-based diagnostic and therapeutic strategies.

V.2. Background

AA is a life-threatening hematologic syndrome characterized by pancytopenia and bone marrow (BM) failure associated with fatty replacement of BM and near absence of hematopoietic precursors cells [1,2].

The role of BM microenvironment in the pathogenesis of AA has been a matter of increasing research interest, aiming to improve therapeutic outcomes in AA [3-32]. Histological examination of BM from AA patients evidences a higher number of adipocytes and a lower number of osteoblasts, which could negatively influence hematopoiesis.

Several mechanisms for BM-adipose tissue replacement in AA have been proposed. *In vitro* experiments have shown that BM-MSCs derived from patients with AA tend to differentiate into adipocytes in detriment of osteoblasts, and diverse molecules, transcription factors (TF) and signaling pathways were proposed to take part in this process. As summarized in Table 1 (section I.2.2.2.), *PPARγ* upregulation, *GATA2* downregulation, Wnt signaling pathway inhibition, increased leptin levels and downregulation of leptin receptor in MSCs, have been suggested to be present in AA [33,45].

Despite interesting, those results are limited by the scarcity and heterogeneity of studies (e.g., heterogeneous sampling groups; different methodological approaches; studies performed in animal model), and consequent lack of reproducibility.

Motivated by the purpose of studying molecular patters of AA-derived BM-MSCs, while circumventing sampling heterogeneity, transcriptomics analysis was performed in order to search for the presence of differently expressed genes that could be related to AA pathophysiological mechanisms. The choice of bulk mRNA-Seq was based on the high-throughput nature of the methodology, allowing the capture and quantification of the expression of thousands of genes simultaneously, thus providing a comprehensive and efficient view of the transcriptome.

MSCs transcriptomics analysis demonstrated to be a powerful tool to study the expression of genes encoding for matrisome elements throughout osteogenic specification of MSCs [46]. More recently, single-cell RNA sequencing analysis of human BM-MSCs have been performed, allowing identification of functional

subpopulations, providing novel insights into biological features of MSCs at the single-cell level [47].

In the context of AA, several single-cell RNA-Seq studies performed on HSPC/mononuclear cells presented relevant data regarding transcriptomic landscape of hematopoiesis in AA, such as: AA-HSPC lineage-specific alterations in gene expression and transcriptional regulatory networks, suggesting selective disruption of distinct lineage-committed progenitor pools; distinct HSPC-T cell crosstalk between AA patients and controls [48]; hematopoiesis disruption associated with aberrance of B cells [49]; or metabolomic abnormalities of T and NK cells, namely on glycolysis/gluconeogenesis and oxidative phosphorylation, respectively [50].

Regarding AA-derived BM-MSCs transcriptomics analysis, published results are scarce, with only one recent publication identified, evidencing BM-MSCs significant different expression of senescence-associated genes and pathways, as well as of DNA damage response and telomere maintenance genes, hypothesized to be possible contributors to impairment of hematopoiesis support in AA [51].

V.3. Results and discussion

For a better data visualization, results were identified according to Sample ID as represented in Table 3 (section II.11.).

V.3.1. Gene expression clustering according to BM-MSCs source (AA versus control samples)

Figure 27 shows sample clustering by disease status (AA vs. healthy controls), except for AM08 and CF10 samples.

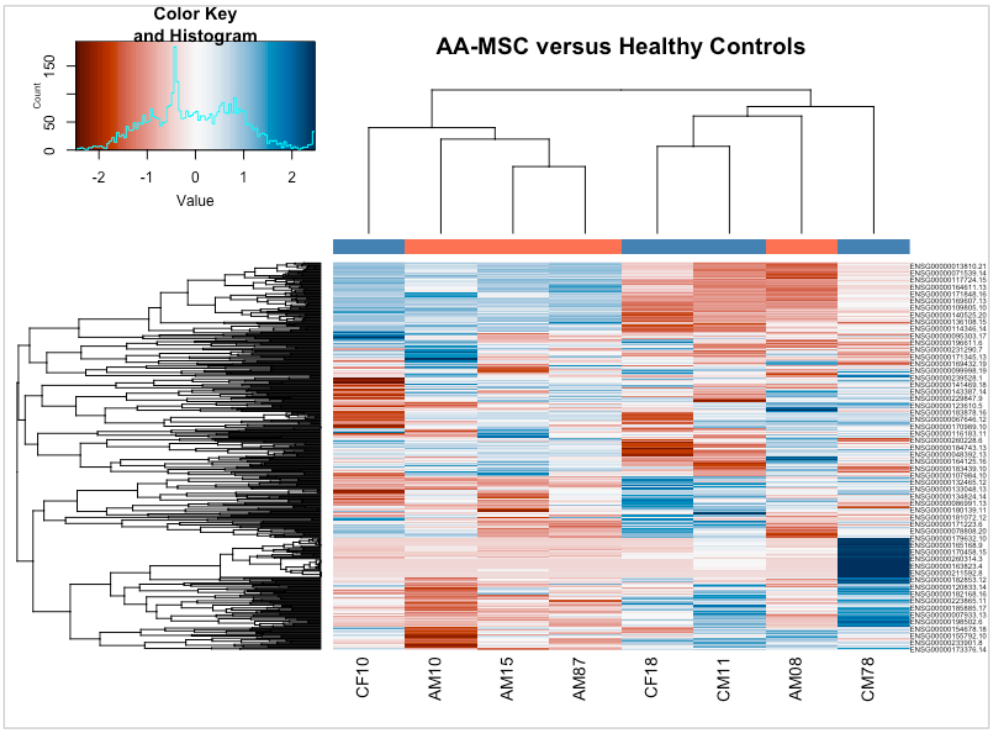

Figure 27: Heatmap and dendrogram designed from scaled (z-score) VST-transformed counts matrix of the 500 most variable genes. Clustering of samples by gene expression. Gene identification (GENCODE ID) shown along the right axis. Aplastic anemia (AA) samples: AM10, AM15, AM08, and AM87 (dendrogram orange bars). Control samples: CF18, CM11, CF10, CM78 (dendrogram blue bars). Heatmap Color key: Blue indicates increased expression; red indicates decreased expression.

The fact that CF10 bone marrow sample was collected from a vertebral body (a less typical location for BM collection), raised the hypothesis that its unusual origin

might be influencing the hierarchical clustering results. Consequently, it was decided to remove CF10 for downstream analysis. After CF10 removal, all remaining samples clustered according to disease status (Figure 28).

To investigate whether AM08, the only sample derived from a patient diagnosed with severe aplastic anemia (SAA) relapsed after allogeneic haematopoietic cell transplantation (allo-HCT), could be also interfering with the results of hierarchical clustering, further analyses were performed. The patient relapsed approximately seven months after undergoing allo-HCT from a sibling donor. This relapse occurred following six months without prior therapy and was associated with complete loss of donor cell chimerism. Removal of AM08, or AM08 and CF10 in combination (Appendix C, Figures C.1 and C.2), was tested. AM08 removal alone did not affect the clustering pattern.

Due to the potential for misleading results from the CF10 sample, it was excluded from all downstream analyses (Figure 28).

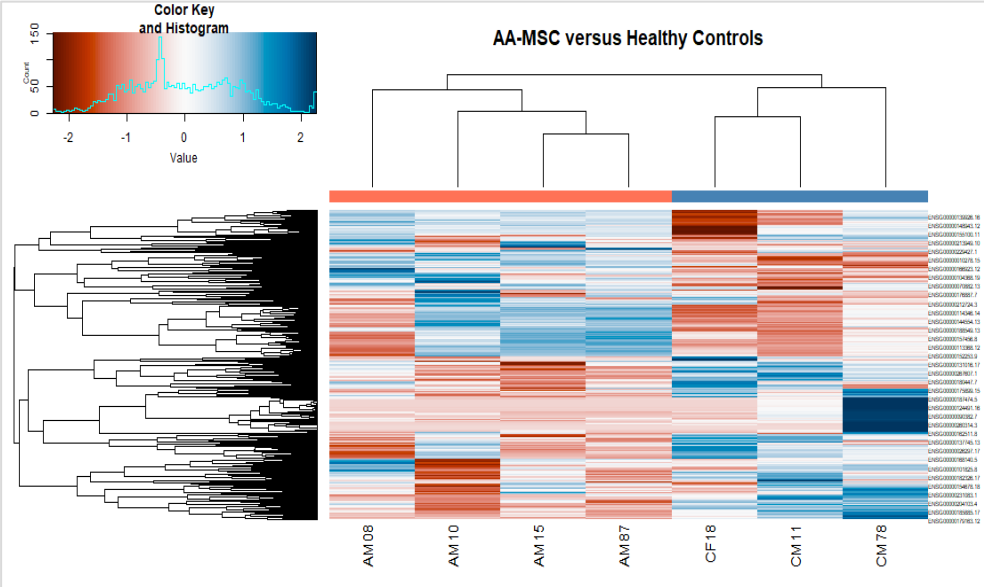

Figure 28: Heatmap and dendrogram designed from scaled (z-score) VST-transformed counts matrix of the 500 most variable genes. Clustering of samples by gene expression. CF10 sample removed. Gene identification (GENCODE ID) shown along the right axis. Aplastic anemia (AA) samples: AM10, AM15, AM08, and AM87 (dendrogram orange bar). Control samples: CF18, CM11, CM78 (dendrogram blue bar). Heatmap Color key: Blue indicates increased expression; red indicates decreased expression.

Principal component analysis (PCA)

Principal component analysis (PCA; Figure 29) revealed that PC1 and PC2 effectively differentiated AA and control-derived BM-MSCs, accounting for 63.5% of the total variance (42% [PC1], 21.5% [PC2]). Eigenvalues and PCA score distributions (PC1-PC4) are detailed in Appendix C, Figures C.3 and C.4.

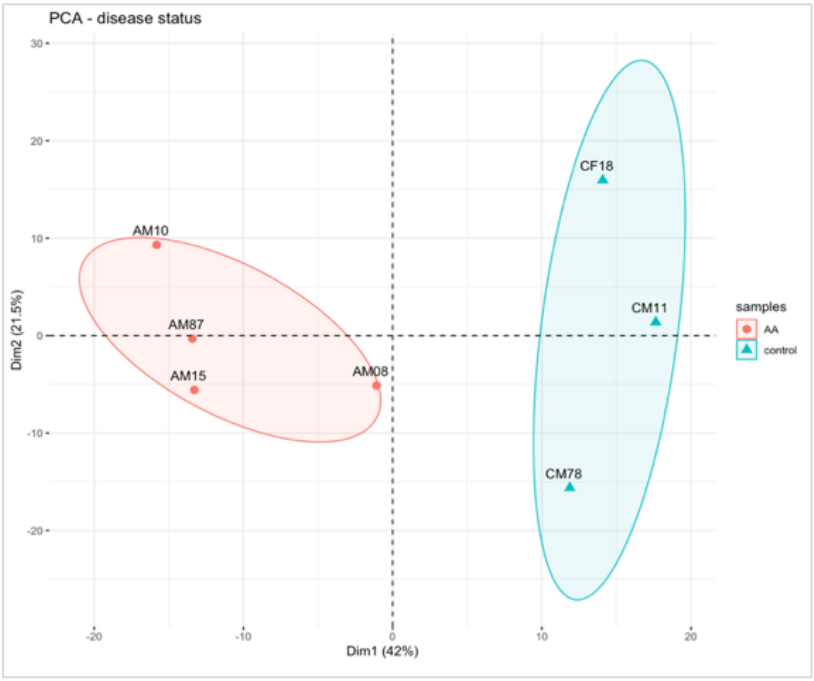

Figure 29: Principal component analysis (PCA) - Principal component analysis (PCA) revealed that PC1 and PC2 segregated AA and control samples, explaining 63.5% of the variance (42% [PC1], 21.5% [PC2]).

V.3.2. Identification of BM-MSCs candidate genes potentially related to pathophysiological mechanisms of idiopathic AA

Differential gene expression analysis (DGE) of AA versus control samples

Considering padj < 0.05 and log2 fold change (L2FC) cutoff of <-1.5 for AA downregulated genes and of >1.5 for AA upregulated genes, 306 differentially expressed genes were identified. Of those, 188 genes were downregulated, and 118 genes upregulated. DGE results (AA versus controls) are plotted in Figure 30 (volcano plot).

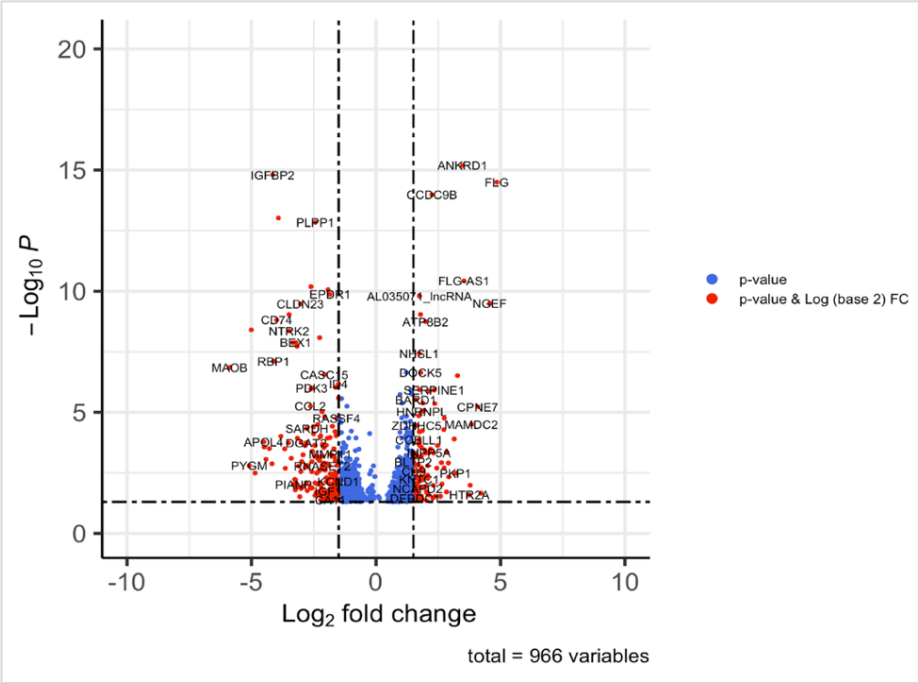

Figure 30: Volcano plot representing differently expressed genes between AA versus control samples (padj < 0.05; L2FC cutoff of <-1.5 and >1.5). n=966 refers to the total number of differently expressed genes (padj < 0.05) before filtering for L2FC threshold of <-1.5 and >1.5, for down and upregulated genes, respectively.

Functional enrichment analysis

Gene Ontology (GO) analysis for upregulated and downregulated genes by means of Gene Set Enrichement Analysis (GSEA) method is represented in Figure 31. As depicted, genes related to DNA repair and immunoregulation seem to play a role in disease.

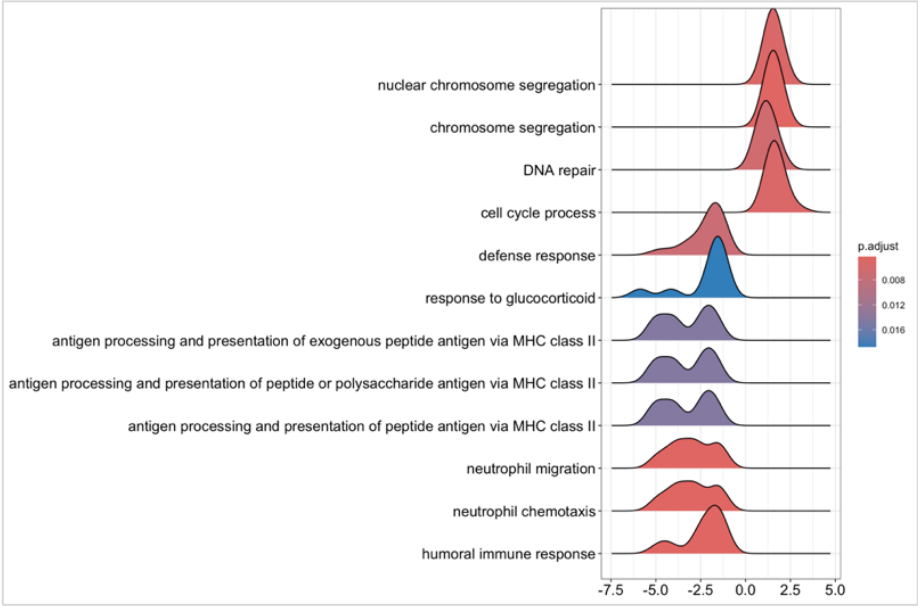

Figure 31: GO enrichment analysis (GSEA) representing downregulated and upregulated genes accordingly to biological function (AA versus control samples). Genes related to DNA repair and immunoregulation seem to play a role in disease.

Data Mining results

Taking the gene sets of up and downregulated genes and considering the present knowledge about AA pathophysiological mechanisms and its biological traits, an exploratory analysis for each single gene was performed, in order to identify the seemingly most suitable candidates for downstream analysis. Afterwards, a deeper analysis of selected genes was performed, resulting in the identification of several functional groups of interest, namely: immune response (two gene patterns identified: pro-inflammatory; immunomodulatory), adipogenesis (two gene patterns identified: adipogenesis promotion; adipogenesis inhibition), lipid metabolism, osteoblast and osteoclast differentiation and activity, hematopoietic

support, ECM remodeling and cell-ECM interactions, DNA repair and DNA damage response, stress response, angiogenesis, and cell signaling pathways. To better represent those groups and identify the genes belonging to each functional subset, heatmaps contrasting AA and controls by biological function were plotted, as shown in Figures 32-42 (corresponding stripcharts and tables with padj and L2FC for each functional gene subset are shown in Appendix D, Figures D.1-D.11, and Appendix E, Tables E.1-E.11, respectively).

Immune response

Two distinct molecular patterns related to immune response were identified.

A pro-inflammatory pattern (Figure 32), characterized by AA-derived BM-MSCs up-regulation of pro-inflammatory genes and down-regulation of anti-inflammatory genes in comparison to controls. Given the inflammatory nature of AA, this pattern suggests that BM-MSCs may exacerbate the immune-mediated destruction of HSPC in AA, potentially contributing to disease pathogenesis.

Conversely, an immunomodulatory pattern was also identified (Figure 33). In this pattern, AA-derived cells exhibited down-regulation of pro-inflammatory genes and up-regulation of anti-inflammatory genes relative to controls. Given the known immunoregulatory functions of MSCs, this pattern may represent an adaptive response by AA-derived BM-MSCs to mitigate the immune-mediated destruction of HSPC in AA.

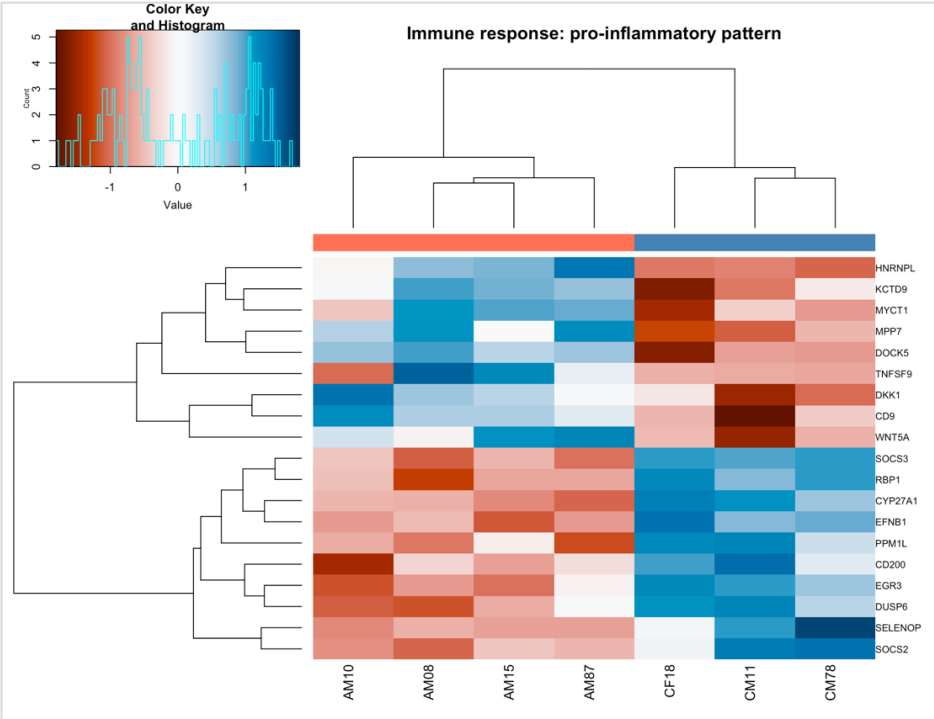

Figure 32: Heatmap of differently expressed genes (AA versus controls) by biological function - immune response-related genes (pro-inflammatory pattern): AA-derived BM-MSCs showing up-regulation of pro-inflammatory genes and down-regulation of anti-inflammatory genes in comparison to controls [detailed references Appendix G, Table – G.1.]. Gene symbols shown along the right axis. Aplastic anemia (AA) samples: AM10, AM15, AM08, and AM87 (dendrogram orange bar). Control samples: CF18, CM11, CM78 (dendrogram blue bar). Heatmap Color key: Blue indicates increased expression; red indicates decreased expression.

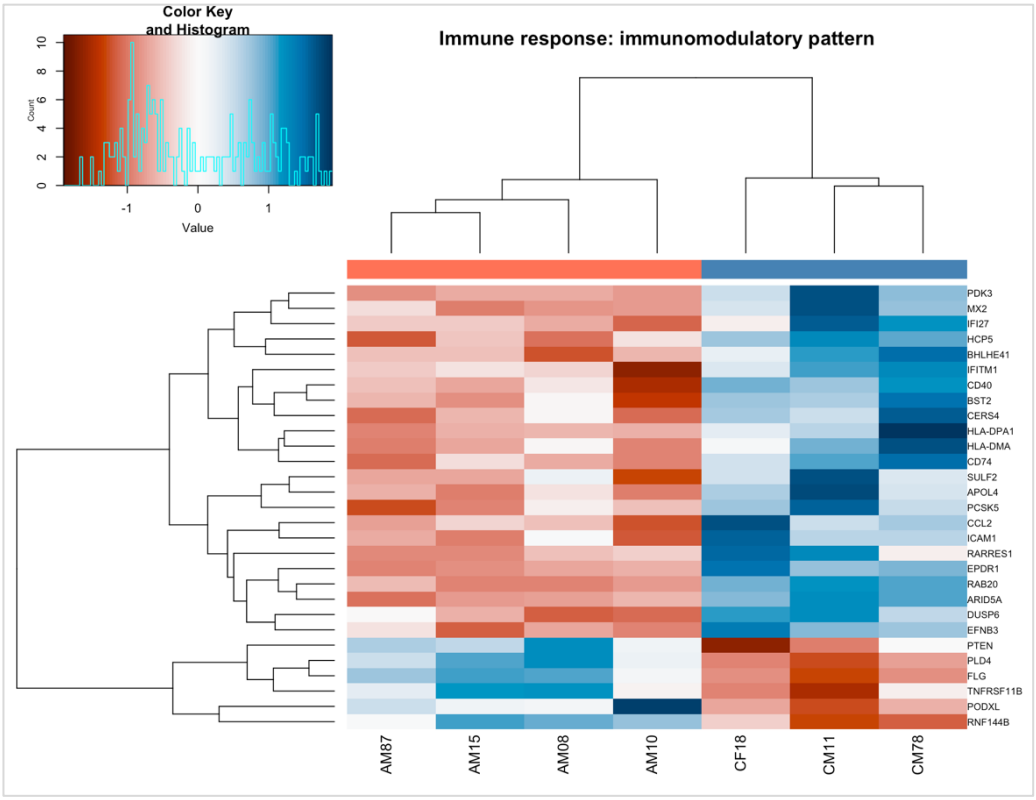

Figure 33: Heatmap of differently expressed genes (AA versus controls) by biological function - immune response-related genes (immunomodulatory pattern): AA-derived BM-MSCs showing down-regulation of pro-inflammatory genes and up-regulation of anti-inflammatory genes in comparison to controls [detailed references in Appendix G, Table – G.2.]. Gene symbols shown along the right axis. Aplastic anemia (AA) samples: AM10, AM15, AM08, and AM87 (dendrogram orange bar). Control samples: CF18, CM11, CM78 (dendrogram blue bar). Heatmap Color key: Blue indicates increased expression; red indicates decreased expression.

Adipogenesis and Lipid metabolism

Consistent with immune response patterns, AA-derived BM-MSCs exhibited two opposing adipogenic phenotypes (Figure 34): promotion, aligning with bone marrow adipose tissue (BM-AT) replacement observed in AA bone marrow and potentially associated with disease establishment/maintenance; and inhibition, which may reflect a compensatory response by AA-derived BM-MSCs to counteract disease-related disruption of the AA bone marrow niche.

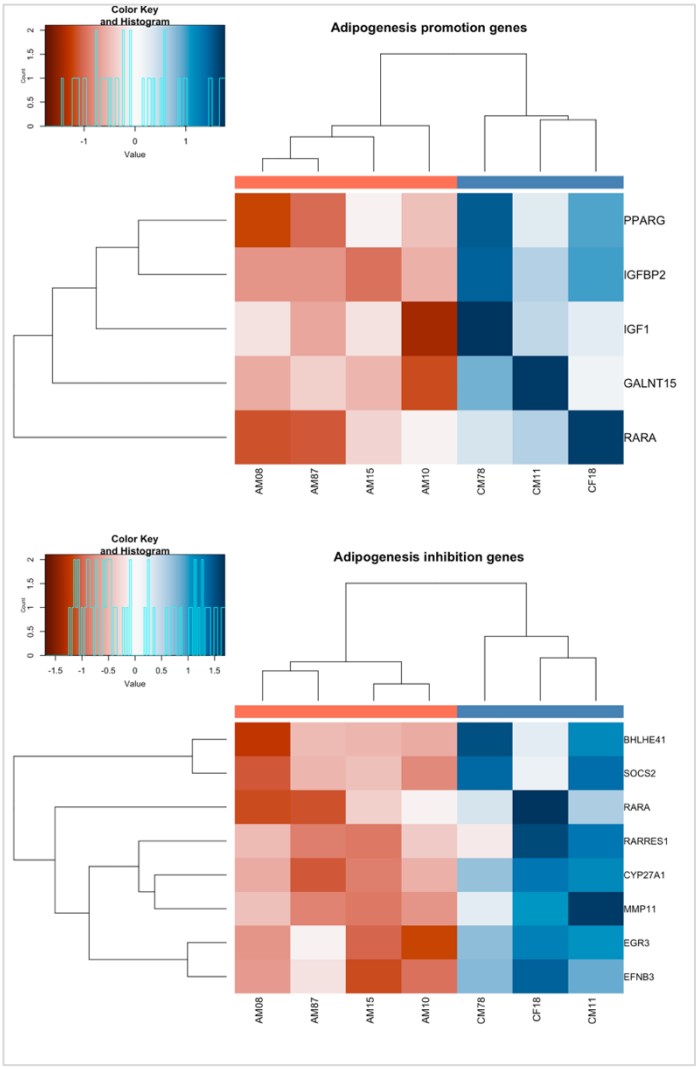

Figure 34: Heatmap of differently expressed genes (AA versus controls) by biological function - adipogenesis-related genes: AA-derived BM-MSCs showing down-regulation of both adipogenesis promotion and adipogenesis inhibition genes, in comparison to controls [detailed references in Appendix G, Table G.3. and Table G.4.]. Gene symbols shown along the right axis. Aplastic anemia (AA) samples: AM10, AM15, AM08, and AM87 (dendrogram orange bar). Control samples: CF18, CM11, CM78 (dendrogram blue bar). Heatmap Color key: Blue indicates increased expression; red indicates decreased expression.

Analysis of lipid metabolism genes (Figure 35) revealed that aplastic anemia AA-derived BM-MSCs exhibited significant downregulation of genes that could functionally translate into: increased lipolysis and lipoprotein lipase (LPL) activity; decreased triglyceride synthesis, fatty acid uptake and storage, and lipogenesis; reduced very long

chain fatty acid (VLCFA) biosynthesis; and increased lipid transport proteins. Conversely, AA-derived BM-MSCs showed upregulation of genes related to cell membrane phospholipid composition and organization, suggesting potential impacts on cell signaling and interactions.

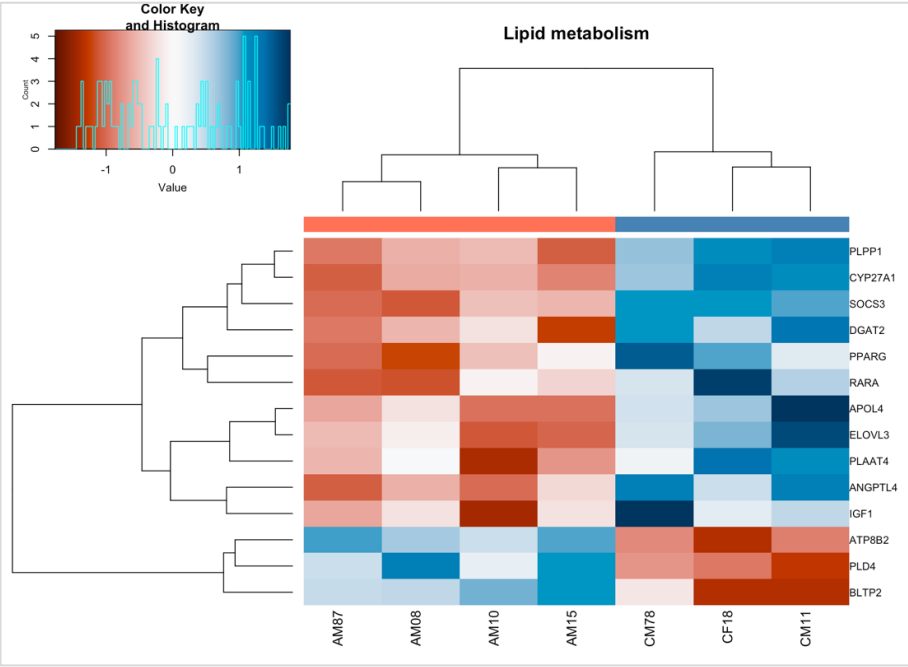

Figure 35: Heatmap of differently expressed genes (AA versus controls) by biological function - lipid metabolism-related genes. AA-derived BM-MSCs showing downregulation of genes that could functionally translate into increase of lipolysis and lipoprotein lipase (LPL) activity, decrease in triglyceride synthesis, decrease in uptake and storage of fatty-acids, decrease in lipogenesis, decrease in biosynthesis of very long chain fatty acids (VLCFA) and increase in lipid transport proteins. AA-derived BM-MSCs upregulated genes related to cell membrane phospholipid composition and organization [detailed references in Appendix G, Table G.5.]. Gene symbols shown along the right axis. Aplastic anemia (AA) samples: AM10, AM15, AM08, and AM87 (dendrogram orange bar). Control samples: CF18, CM11, CM78 (dendrogram blue bar). Heatmap Color key: Blue indicates increased expression; red indicates decreased expression.

Osteoblast and osteoclast differentiation and activity

In what refers to osteoblast and osteoclast differentiation and activity, different gene expression profiles between AA and controls were found.

Several downregulated AA-derived BM-MSCs osteoblast-related genes were identified (Figure 36a.), which could functionally translate into a decreased promotion of osteoblast differentiation and activity, impairment of ECM remodeling, necessary for osteoblast activity, unbalance between bone formation and resorption and impairment of osteoblast protection against oxidative stress. In addition, a subset of upregulated AA-derived BM-MSCs osteoblast-related genes whose expression could also result in inhibition of osteoblast differentiation and activity was found, suggesting an overall disruption of bone matrix production and mineralization in AA, and consequent impairment of hematopoietic support.

Regarding osteoclastogenesis and osteoclast activity, a group of AA-derived BM-MSCs downregulated genes that could functionally translate into a decreased inhibition of osteoclast differentiation and activity in disease, thus promoting osteoclast activity, was identified (Figure 36b.). AA-derived BM-MSCs upregulated genes related to promotion of osteoclast adhesion and bone resorption activity were also found. Considering those data, we hypothesize that increased osteoclast activity might negatively affect the hematopoietic support in AA, possibly contributing as a pathophysiological mechanism.

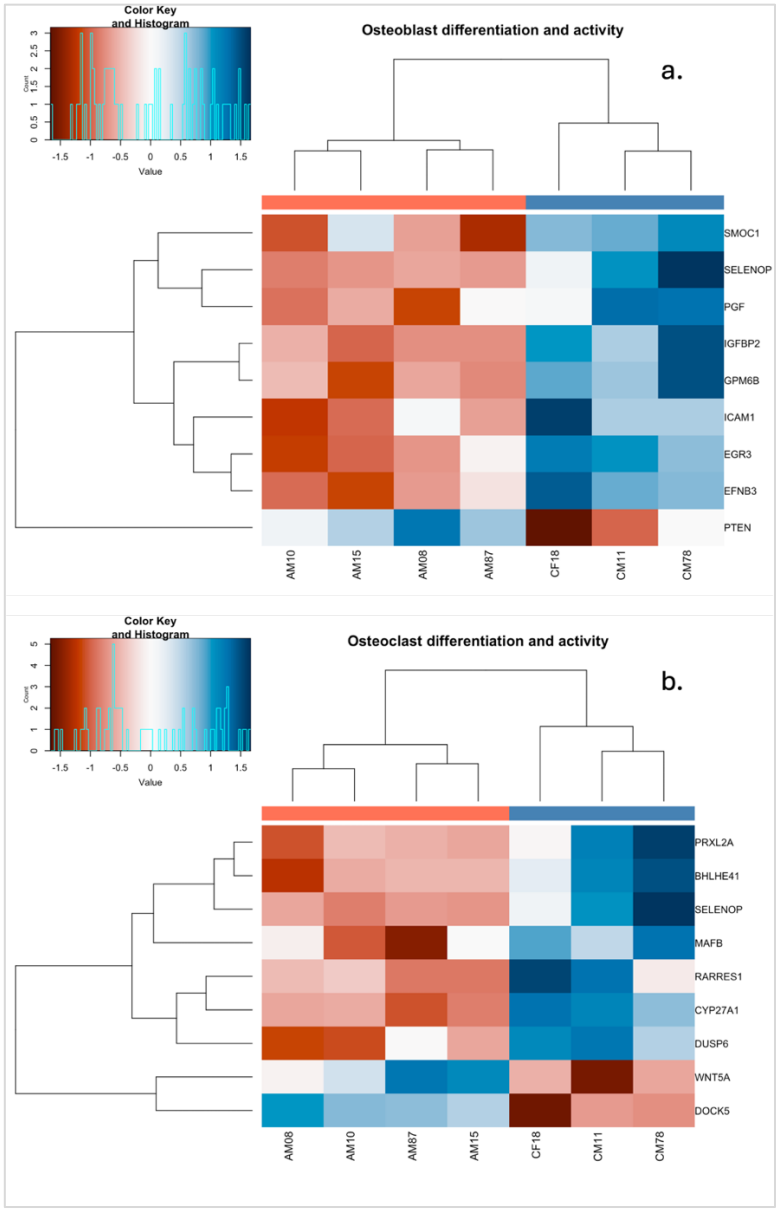

Figure 36: Heatmap of differently expressed genes (AA versus controls) by biological function. 36a. Osteoblast differentiation and activity - AA-derived BM-MSCs downregulation of genes involved in promotion of osteoblast differentiation and activity and upregulation of genes involved in inhibition of osteoblast differentiation and activity. 36b. Osteoclast differentiation and activity - AA-derived BM-MSCs downregulation of genes involved in inhibition of osteoclast differentiation and activity and upregulation of genes involved in osteoclast activation [detailed references in Appendix G, Table G.6. and Table G.7.]. Gene symbols shown along the right axis. Aplastic anemia (AA) samples: AM10, AM15, AM08, and AM87 (dendrogram orange bar). Control samples: CF18, CM11, CM78 (dendrogram blue bar). Heatmap Color key: Blue indicates increased expression; red indicates decreased expression.

Hematopoietic support

As depicted in Figure 37, several genes related to HSPC balance between self-renewal, differentiation and proliferation were identified, as well as genes interfering and regulating HSPC mobilization and homing. Overall, both listed down and upregulated genes in AA-derived BM-MSCs could phenotypically translate into impairment of BM niche support of HSPC (e.g., HSPC survival and maintenance disruption) and into lineage differentiation bias (e.g., decreased myeloid, erythroid and megakaryocyte differentiation; increased lymphoid lineage commitment).

Regarding HSPC mobilization and homing, transcriptomics data raised up the hypothesis of an unbalance between both mechanisms in AA, but the results were heterogenous, and thus it was not possible to predict a functional effect solely based on DGE results. To notice that *CCL2* (also known as Monocyte Chemoattractant Protein-1 (*MCL-1*)) downregulation in AA-derived BM-MSCs should be interpreted widely. CCL2 is a pro-inflammatory chemokine, and its downregulation in AA-derived BM-MSCs could also translate an immunomodulatory effect of MSCs against the lymphocytotoxic BM environment present in AA.

Interestingly, contrarily to previously published data (Table 1, section I.2.2.2.), *PPARG* was downregulated in AA-derived BM-MSCs. Besides adipogenesis promotion, *PPARG* also plays a role in HSPC regulation (e.g. quiescence and proliferation), lineage commitment, possibly favoring myeloid lineage instead of lymphoid differentiation, as well as in immune regulation (e.g. anti-inflammatory effects). Therefore, it could be hypothesized that *PPARG* downregulation could also functionally contribute to disease pathophysiology, however by different mechanisms from those that have been suggested [127,128,129].

Another gene of interest identified in this experiment was *FRZB* (*SFRP3*), a Wnt signaling inhibitor, downregulated in AA-derived BM-MSCs. Wnt signaling plays an important role in embryonic and adult hematopoiesis, regulating HSPC self-renewal and differentiation in a context-dependent manner, as well as influencing committed lymphoid progenitor cells (e.g., pro-B cells and pre-B cells in BM), immature thymocytes and mature T cells, as well as nonlymphoid lineages (e.g. megakaryocyte differentiation and platelet production) [72,73]. Downregulation of *FRZB* and, consequently, of functionally related genes, suggests an impairment of HSPC self-renewal capacity in AA,

as well as a trend to lymphocyte differentiation and proliferation, which could be mediated, at least in part, by diseased AA-derived BM-MSCs.

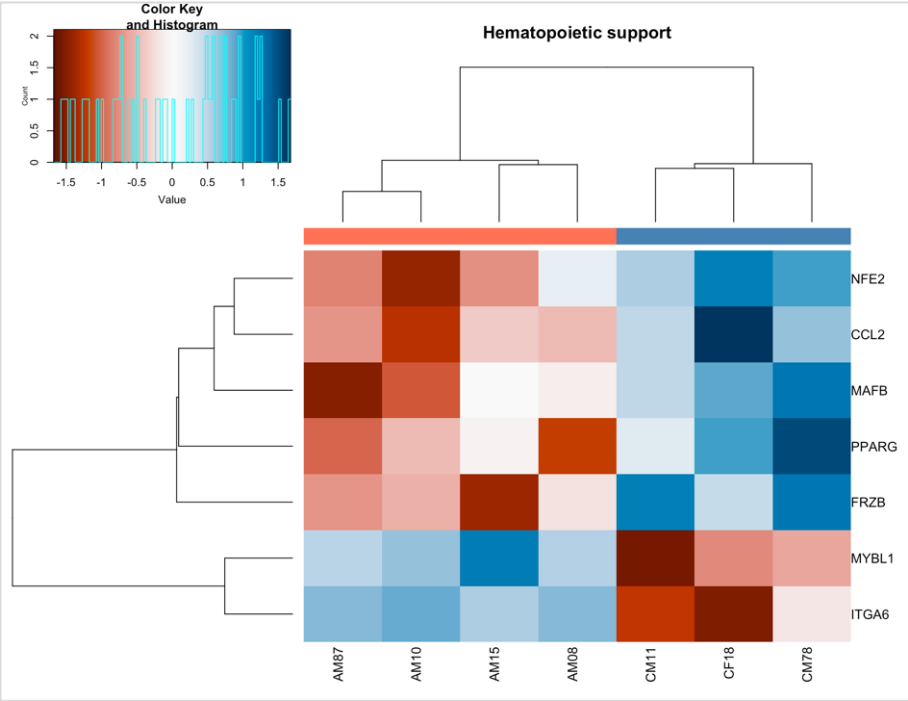

Figure 37: Heatmap of differently expressed genes (AA versus controls) by biological function - hematopoietic support-related genes. AA-derived BM-MSCs showing downregulated and upregulated genes that could phenotypically translate into impairment of BM niche support of HSPC and/or be involved in HSPC lineage differentiation bias [detailed references in Appendix G, Table G.8.]. Gene symbols shown along the right axis. Aplastic anemia (AA) samples: AM10, AM15, AM08, and AM87 (dendrogram orange bar). Control samples: CF18, CM11, CM78 (dendrogram blue bar). Heatmap Color key: Blue indicates increased expression; red indicates decreased expression.

ECM remodeling and cell-ECM interactions

ECM provides structural and functional support to cells throughout the body, influencing a variety of biological processes, such as tissue development and remodeling, tissue repair and regeneration, barrier function, cell adhesion and migration, cell differentiation, and cell signaling. Its functioning is regulated by a complex and dynamic process involving protein synthesis and degradation, remodeling (e.g., degradation of old components and synthesis of new ones), cell-ECM interactions (either through cell surface receptors, such as integrins, or mediated by growth factors and other signaling molecules), as well as mechanical (e.g., regulation of ECM synthesis and degradation through cell mechanoreceptors in response to mechanical forces) and epigenetic regulation (e.g., regulation of ECM-related gene expression by DNA methylation and histone modification).

As depicted in Figure 38, below, differently expressed genes functionally related to ECM and cell-ECM interactions were identified. The subset of AA-derived BM-MSCs downregulated genes relates to cell-ECM interactions as well as ECM remodeling, suggesting a BM niche unbalance in disease and consequently a less supportive environment for hematopoiesis and immune regulation. Regarding AA-derived BM-MSCs upregulated genes, the results showed low consistency between diseased samples, despite significant L2FC and padj. Among the upregulated genes, some of them relate to cell-ECM interaction, in particular to cell adhesiveness (e.g., *PODXL*, promoting MSCs migration and homing to injury sites [74]; *MAMDC2*, involved in cell adhesion, migration, and signaling processes, such as MAPK pathway attenuating effect [75, 76]).

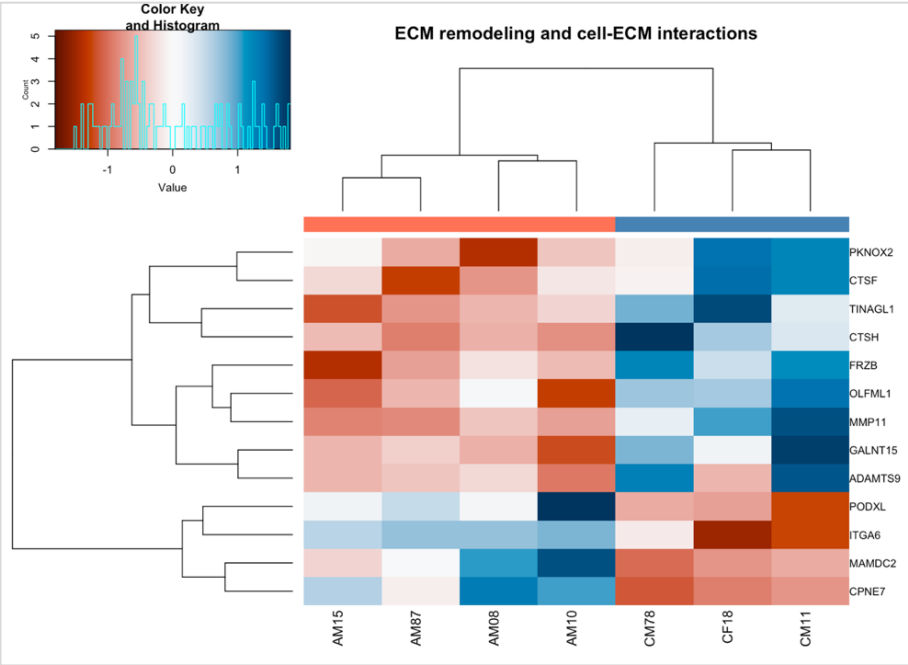

Figure 38: Heatmap of differently expressed genes (AA versus controls) by biological function - ECM remodeling and cell-ECM interactions. AA-derived BM-MSCs downregulation of genes related to cell-ECM interactions and ECM remodeling, suggesting a BM niche unbalance and, consequently, a less supportive environment for hematopoiesis and immune regulation in AA [detailed references in Appendix G, Table G.9.]. Gene symbols shown along the right axis. Aplastic anemia (AA) samples: AM10, AM15, AM08, and AM87 (dendrogram orange bar). Control samples: CF18, CM11, CM78 (dendrogram blue bar). Heatmap Color key: Blue indicates increased expression; red indicates decreased expression.

DNA repair and DNA damage response

A subset of genes related to DNA repair and damage response were identified, as shown in Figure 39. Both AA-derived BM-MSCs up and downregulated genes functionally associate with DNA damage response, cell cycle checkpoint control and apoptosis. Whether this pattern represents an AA-derived BM-MSCs response to the immune cytotoxic attack over BM, or to a disruption in DNA repair and damage response capacity of AA-derived BM-MSCs, thus contributing to disease phenotype, is not possible to ascertain here. Overall, the results from this experiment suggested that DNA repair and DNA damage response mechanisms might be significant in AA, and thus an

important topic for research (e.g., *RGCC* gene, a regulator of cell cycle progression, induced by p53 in response to DNA damage [77], was into the lowest L2FC range [L2FC -4.18]).

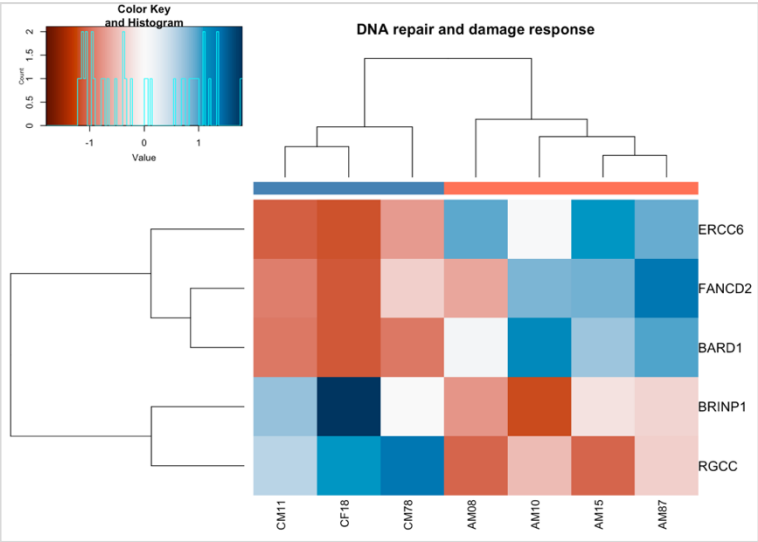

Figure 39: Heatmap of differently expressed genes (AA versus controls) by biological function - DNA repair and DNA damage response. AA-derived BM-MSCs showing upregulation and downregulation of genes functionally associated with DNA damage response, cell cycle checkpoint control and apoptosis [detailed in references Appendix G, Table G.10.]. Gene symbols shown along the right axis. Aplastic anemia (AA) samples: AM10, AM15, AM08, and AM87 (dendrogram orange bar). Control samples: CF18, CM11, CM78 (dendrogram blue bar). Heatmap Color key: Blue indicates increased expression; red indicates decreased expression.

Stress response

Results evidenced an AA-derived BM-MSCs downregulation of genes involved in response to oxidative stress, hypoxia and nutrient deprivation, as well as of genes involved in regulation of stress response (e.g., *DUSP6* and *PPM1L*, related to dampening of stress response, promoting cell adaptation and survival under stress conditions[78,79]), as shown in Figure 40.

Significantly downregulated AA-derived BM-MSCs genes, as *SELENOP* and *PRXL2A* (L2FC -3.34, padj $1.32x10^{-8}$ and L2FC -4.28, padj 0.0003, respectively), that play an important role in reactive oxygen species (ROS) scavenging, especially in inflammatory

context, were identified in AA samples [80]. In addition, the downregulation of both *SELENOP* and *SELENBP1* might suggest a pattern of selenium transport and metabolism dysregulation in AA [81], which may also be a relevant research topic to explore in further studies.

Considering stress response genes upregulated in AA samples, both *ANKRD1* and *FLG-AS1* were identified within the higher L2FC range (L2FC 3.47, padj $6.38x10^{-16}$ and L2FC 3.43, padj $3.75x10^{-11}$, respectively). Those genes have been involved in mechanical stress response and remodeling of muscle tissues (e.g., cardiomyocytes) under stress conditions [82] and in regulation of cellular responses to oxidative and inflammatory stress (e.g. diabetic retinopathy) and skin barrier disruption [83], respectively.

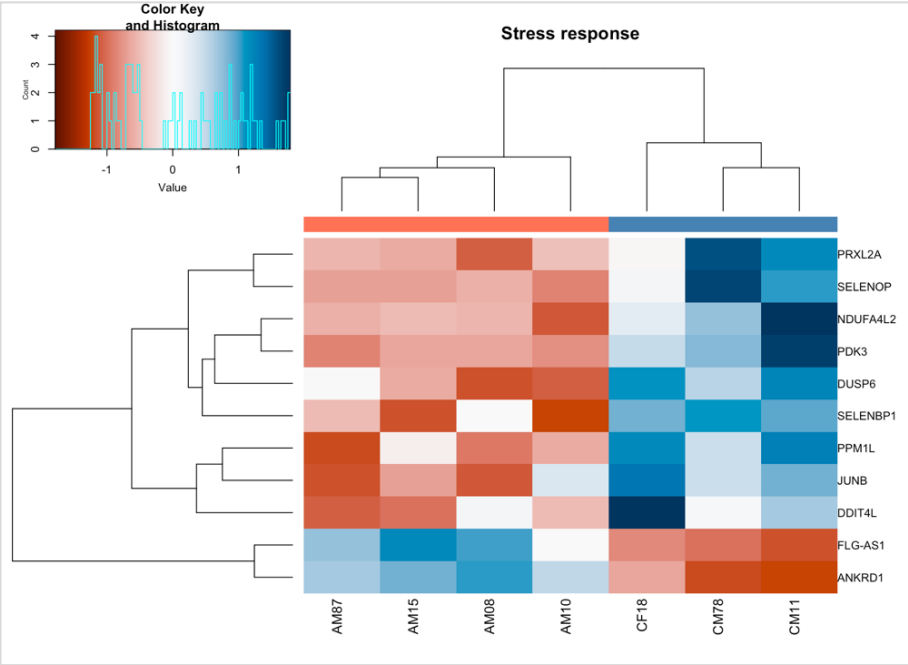

Figure 40: Heatmap of differently expressed genes (AA versus controls) by biological function - Stress response. AA-derived BM-MSCs showing downregulation of genes involved in response to oxidative stress, hypoxia and nutrient deprivation [detailed references in Appendix G, Table G.11.]. Gene symbols shown along the right axis. Aplastic anemia (AA) samples: AM10, AM15, AM08, and AM87 (dendrogram orange bar). Control samples: CF18, CM11, CM78 (dendrogram blue bar). Heatmap Color key: Blue indicates increased expression; red indicates decreased expression.

Angiogenesis

Angiogenesis is a dynamic and context-dependent process, intrinsically linked to hematopoiesis [168]. Figure 41 lists the most significant genes related to angiogenesis differently expressed in this experiment.

Several pro-angiogenic genes were identified to be downregulated in AA-derived BM-MSCs, which could theoretically affect the hematopoietic support provided by the bone marrow niche in healthy conditions.

Oppositely, despite in a more heterogeneous pattern between samples, pro-angiogenic AA-derived BM-MSCs upregulated genes were also identified. Upregulation of pro-angiogenic genes could occur in pro-inflammatory conditions and facilitate immune cell infiltration (e.g., through increasing the access of inflammatory cells into tissues, as mediated by endothelial expression of cell adhesion molecules and chemokines) [8484] and thus be hypothesized as an adjuvant disease mechanism in AA.

TNFSF9 (also known as 4-1BB Ligand or CD137L), noticed to be upregulated in AA-derived BM-MSCs (with the exception of AM10) within the highest L2FC range (L2FC 4.22, padj 0.02), has been related to immune activation by T cell co-stimulation trough interaction with 4-1BB receptor (CD137), enhancing T cell proliferation, cytokine production, and survival. It also mediates a bidirectional signaling, transmitting back signals into the cells where it is expressed, promoting their activation and survival [85,86]. *TNFSF9* has been implicated in serval diseases (e.g., cancer; auto-immune diseases) [87,88] and might be a relevant gene to explore in AA studies.

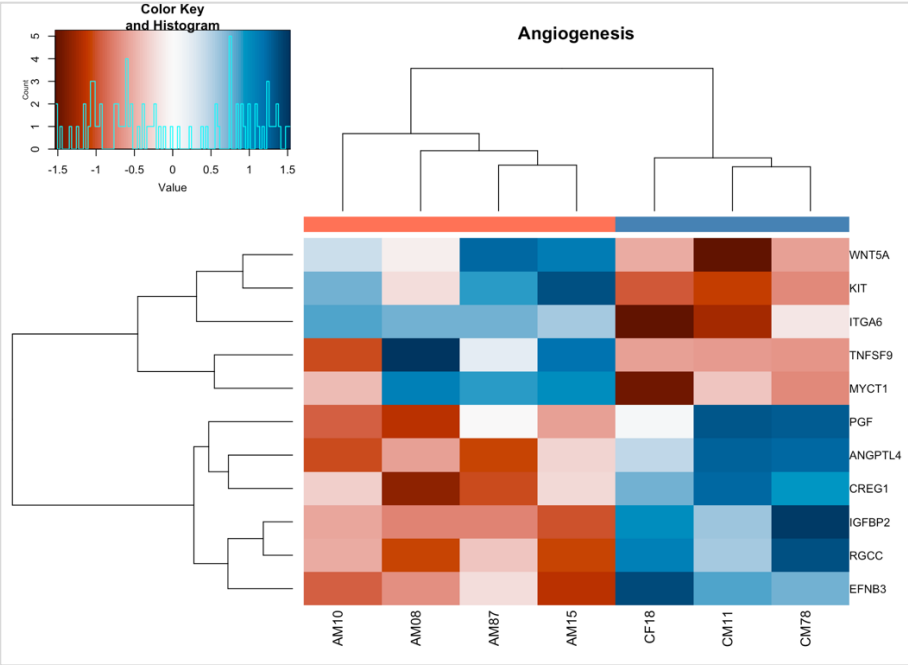

Figure 41: Heatmap of differently expressed genes (AA versus controls) by biological function - Angiogenesis. AA-derived BM-MSCs showing either up or downregulation of pro-angiogenic genes [detailed references Appendix G, Table G.12.]. Gene symbols shown along the right axis. Aplastic anemia (AA) samples: AM10, AM15, AM08, and AM87 (dendrogram orange bar). Control samples: CF18, CM11, CM78 (dendrogram blue bar). Heatmap Color key: Blue indicates increased expression; red indicates decreased expression.

Cell signaling

From each previous functional group, a subset of genes (Figure 42) directly implicated in cell signaling pathways of interest in AA, such as Wnt/ß-catenin, Wnt (noncanonical), MAPK, PI3K/Akt, NF-kB and JAK-STAT, was identified.

As depicted in UMAP plot (Figure 43), both up and downregulation of genes similarly involved in the same cell signaling pathway were observed, as is the case of genes involved in activation or inhibition of Wnt/ß-catenin pathways. An exception was noticed for noncanonical Wnt pathway, represented by *WNT5A*. This gene was upregulated in AA-derived BM-MSCs, suggesting an activation of Wnt pathway in AA samples. WNT5A influences several cellular processes, as cell polarity, migration,

adhesion and differentiation, and has been implicated in disease, such as cancer, inflammation and organ fibrosis [8989,123,124,125,126].

MAPK and PI3K/Akt pathways play an important crosstalk for MSCs functioning and response to various stimulus, regulating proliferation, differentiation, migration, immunomodulation (e.g., these pathways have been implicated in mediating the immunosuppressive effects of MSCs) and survival, in a context-dependent manner [90,91,92].

In this experiment, AA-derived BM-MSCs evidenced downregulation of genes involved in MAPK inhibition and upregulation of genes involved in MAPK and PI3K/Akt pathways activation. Considering the inflammatory BM microenvironment in AA, this overall MAPK and PI3K/Akt activation pattern may reflect a response mechanism of MSCs to disease-related injury. Whether this response occurs *in vivo* and promotes disease resolution or exacerbates severity remains a key question for further research and therapeutic development.

NF-kB pathway is a key regulator of immune and inflammatory responses [93] and its activation in BM-MSCs has been associated with inflammation and ineffective hematopoiesis in hematological diseases, such as myelodysplastic syndromes [9494]. In this analysis, several genes implicated in NF-kB pathway were identified, with contradictory results, meaning up and downregulation of genes with activation or inhibitory effects for both AA and control samples. To notice is *AHNAK2* gene, upregulated in AA-derived BM-MSCs samples (L2FC 1.92; padj $8.43x10^{-06}$), which has been associated with NF-kB activation, especially in cancer, contributing to disease aggressiveness and progression [95,96,97,98]. More recently, *AHNAK2* was implicated in regulation of immune infiltration in pancreatic cancer [99]. This gene also modulates other cell signaling pathways, such as PI3K/Akt pathway [100], promoting cell proliferation and migration, and inhibiting apoptosis.

JAK-STAT is an important cell signaling pathway, implicated in several biological processes, such as immune system development and function (e.g., induces differentiation, proliferation and activation of immune cells, as T and B lymphocytes and macrophages; mediates the effects of cytokines involved in immune responses and inflammation), cell growth and differentiation, as well as hematopoiesis [101,102].

It has been implicated in regulation of MSCs proliferation, differentiation, immunomodulation, migration and tissue repair. Regarding MSCs immunosuppressive function, it has been reported that MSCs-derived factor indoleamine 2,3-dioxygenase (IDO) is involved in GVHD prevention by inhibiting T cell proliferation trough tryptophan degradation, and that interferon-gamma (IFN-γ) production by activated T-cells is related to the IDO induction in MSCs through the IFN-γ-JAK-STAT1 pathway [103,104].

In addition, JAK-STAT signaling has been implicated in cancer (either solid and hematological malignancies) and immune diseases, and several inhibitors have been developed for targeted therapy in such conditions [105,106,107].

Considering this experiment, in AA-derived BM-MSCs samples, both *SOCS2* (L2FC -2.62; padj $1.08x10^{-06}$) and *SOCS3* (L2FC -1.92; padj $8.66x10^{-11}$) were downregulated in comparison to controls. These genes code for intracellular proteins belonging to SOCS protein family, and their expression is induced by STATs (Signal Transducer and Activator of Transcription). They function as negative regulators of JAK-STAT pathway, by preventing phosphorylation and activation of STATs [101,102].

Accordingly, this gives rise to the hypothesis that JAK-STAT signaling could be activated in AA, supporting that JAK inhibitors might be potential therapeutic adjuncts in AA [108]. However, in further studies, the specificity of JAK inhibitors must be taken into consideration, especially in the context of AA, due to their impact on hematopoiesis [109].

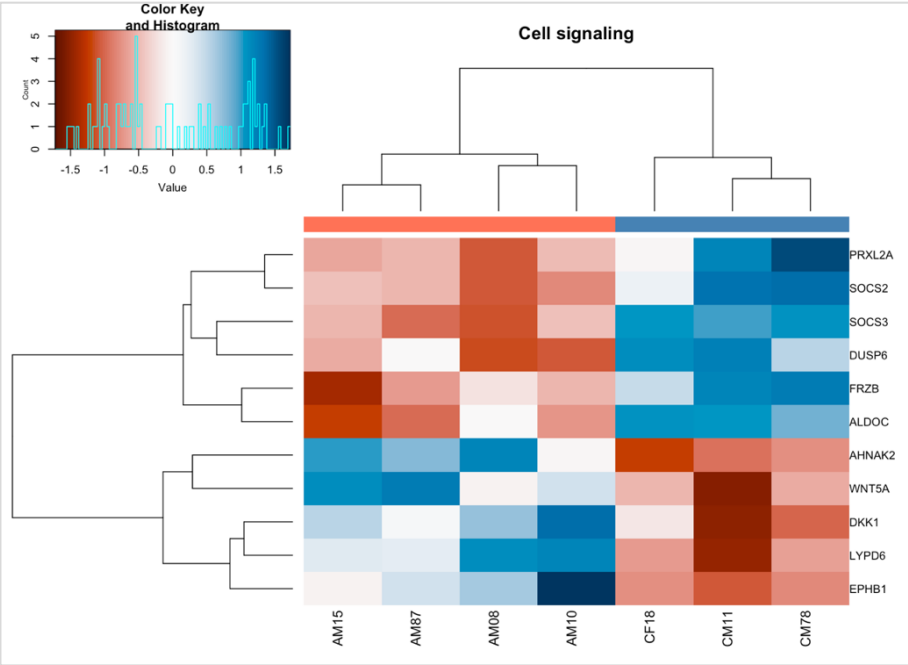

Figure 42: Heatmap of differently expressed genes (AA versus controls) by biological function - Cell signaling. AA-derived BM-MSCs showing - downregulation of genes related to MAPK inhibition, JAK-STAT inhibition, Wnt/ß-catenin inhibition or activation; upregulation of genes related to MAPK, PI3K/Akt and NF-kB activation, Wnt/ß-catenin inhibition or activation, Wnt (noncanonical) activation. As shown, the simultaneous up- and downregulation of genes within the same signaling pathway highlights the intricate nature of cellular signaling interactions. This complexity underscores the challenges in interpreting transcriptomic results and their biological significance [detailed references in Appendix G, Table G.13.]. Gene symbols shown along the right axis. Aplastic anemia (AA) samples: AM10, AM15, AM08, and AM87 (dendrogram orange bar). Control samples: CF18, CM11, CM78 (dendrogram blue bar). Heatmap Color key: Blue indicates increased expression; red indicates decreased expression.

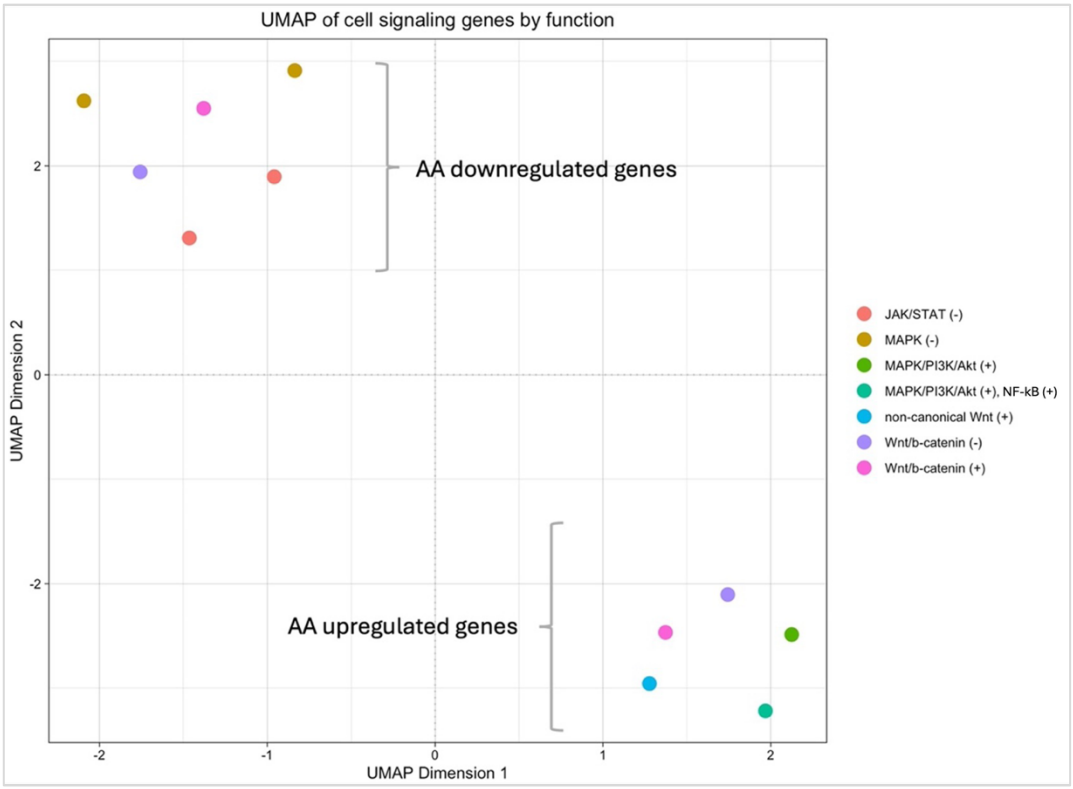

Figure 43: Uniform Manifold Approximation and Projection (UMAP) of differently expressed genes (AA versus controls) by biological function. Two distinct molecular patterns were observed in AA-derived BM-MSCs: downregulation of genes related to MAPK inhibition, JAK-STAT inhibition, Wnt/ß-catenin inhibition or activation; upregulation of genes related to MAPK, PI3K/Akt or NF-kB activation, Wnt/ß-catenin inhibition or activation, Wnt (noncanonical) activation. Symbols: (-) indicates pathway inhibition; (+) indicates pathway activation.

Other genes of interest in AA – not identified in transcriptomics analysis

DGE analysis results for genes that, accordingly to previously published data, could be implicated in some of the abovementioned biological functions, such as *BGLAP* (osteocalcin), *SPARC* (osteonectin), *SPP1* (osteopontin), *FN1* (fibronectin), *RUNX1*, *RUNX2*, *CTNNB1* (beta-catenin), *CEBPA*, *SALL4*, *VEGFA*, *FGF2*, *HGF*, *ANGPT1*, *PDGFA*, *PDGFB* and *TGFB1*, were reviewed, with no significant differences between AA and controls.

Considering genes coding for cytokines produced by MSCs, either anti-inflammatory or pro-inflammatory, such as *IL-10*, *PGE2*, *IDO*, *HLA-G5*, and *IL-6*, *IL-8*, *IL-*

1b, respectively, and genes coding for MSCs-derived adipokines, as *ADIPOQ* (adiponectin), *RETN* (resistin), *NAMPT* (visfastin), *APLN* (apelin), *LEP* (leptin) and *LEPR* (leptin receptor), no significant differences between AA and controls were found.

Moreover, for genes associated with inherited AA, such as *TERC*, *TERT*, *DKC1*, *TINF2*, *FANCA*, *FANCB*, *GATA2*, *SRP72*, or associated to somatic mutations and clonal hematopoiesis in AA [110], such as *DNMT3A*, *ASXL1*, *BCOR*, *BCORL1*, no significant differences between AA and controls were identified. Gene list presented in chapter X.vi., Appendix F (Table F.1).

Conclusion of bulk mRNA-Seq analysis

This study, while providing novel insights, acknowledges several limitations that could influence results and data interpretation. Firstly, the rarity of aplastic anemia limited the availability of AA-derived samples (n= 4), particularly from newly diagnosed patients. A larger cohort of both AA and control samples would enhance the robustness of our findings. Secondly, RNA extraction was performed after *in vitro* BM-MSCs expansion, which may have altered cell properties and consequently impacted the results. Factors such as plastic adherence and prolonged cell culture, involving repeated passaging, can induce significant alterations in MSCs phenotypic and functional characteristics, including their gene expression profiles [169,170].

Despite these limitations, this study contributes valuable information regarding BM-MSCs in acquired idiopathic AA, complementing previous transcriptomic studies that primarily focused on bone marrow and peripheral blood-derived mononuclear cells [48,49,50].

The key findings of this study, summarized in Figure 44, suggest two potential roles for MSCs in aplastic anemia.

Firstly, the observed immunomodulatory, adipogenesis-inhibitory, and enhanced DNA damage response molecular patterns in AA-derived BM-MSCs may represent a compensatory mechanism against the AA-associated immune attack on the hematopoietic niche. This suggests a protective and potentially regenerative function of MSCs in AA.

Conversely, the concurrent presence of pro-inflammatory, pro-adipogenic, osteoblast-inhibitory, osteoclast-activating, extracellular matrix remodeling and angiogenesis-disruptive, impaired DNA damage response/stress response, and dysregulated cell signaling molecular patterns indicates a dysfunctional state of MSCs. This dysfunction could contribute to AA pathogenesis, potentially arising as a secondary consequence of disease-associated cytotoxic insult to the BM and thereby influencing disease severity and therapeutic response variability.

Previous studies, as thoroughly reviewed elsewhere [6,16,171], have identified several molecular patterns associated with MSCs in aplastic anemia (AA). However, by capturing the comprehensive transcriptional profile of disease-derived MSCs compared to healthy controls, this work provides crucial insights into the complex interplay of concomitant mechanisms. Our findings suggest that the disease phenotype in AA may reflect a delicate balance between opposing molecular patterns. Furthermore, we have identified several novel candidate genes, not previously reported in the context of AA, opening new avenues for investigating the molecular mechanisms underlying AA.

To validate these findings and to clarify the precise contribution of BM-MSCs dysfunction to AA pathogenesis and therapeutic outcomes, future research is crucial. This should include *in vivo* studies and investigation of larger patient cohorts, ultimately paving the way for targeted and innovative therapeutic strategies.

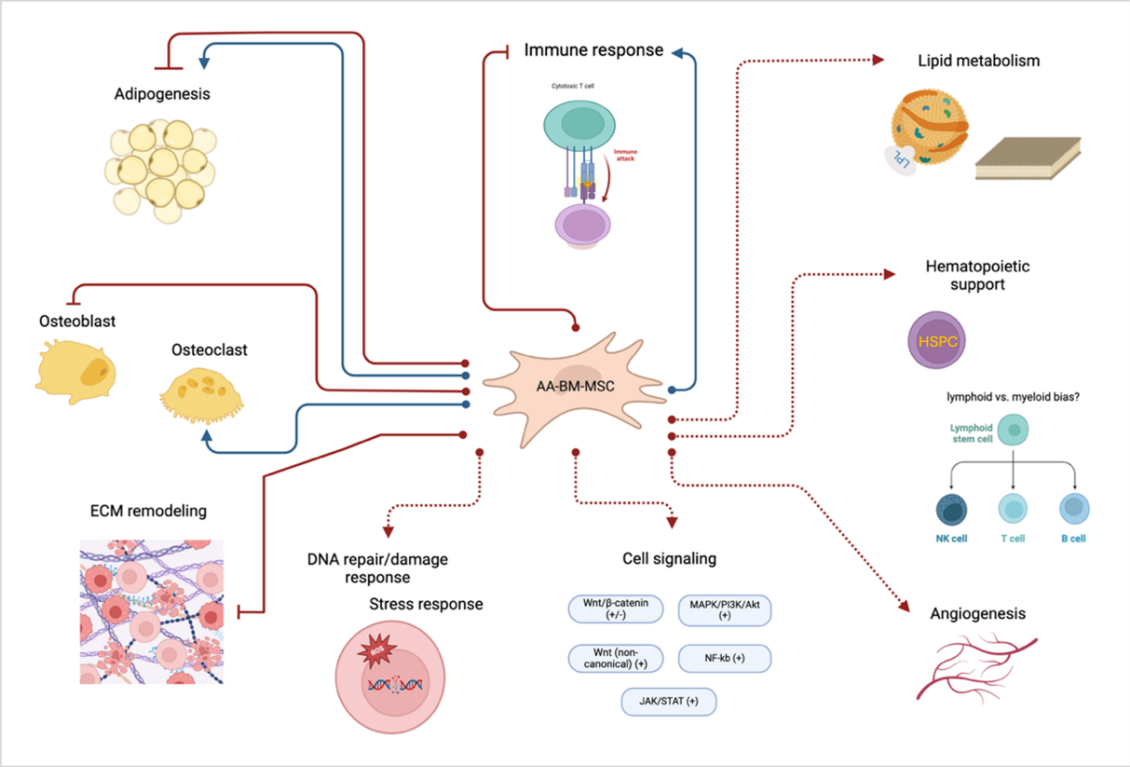

Figure 44: Summary of bulk transcriptomic analysis comparing AA-derived BM-MSCs to healthy controls. Solid blue line: activation; solid red line: inhibition; dashed red line: functional disruption; cell signaling (+): activation; cell signaling (-): inhibition; cell signaling (+/-): either activation or inhibition. AA-BM-MSCs: bone marrow-derived mesenchymal stromal cells from aplastic anemia patients; ECM: extracellular matrix; HSPC: hematopoietic stem and progenitor cells. Created with BioRender.com. Lira, K. (2024) BioRender.com/g26e388.

V.3.3. Validation of transcriptomics results for selected candidate genes by RT-qPCR

For a subset of selected candidate genes, namely *SPARC*, *BGLAP*, *SPP1*, *PPARG*, *FABP4*, *LEPR*, *GATA2*, *CEBPA*, *RARA*, *ARID5*, *ADIPOQ*, *BIRC5*, *SFRP1*, *TNFSF9*, *WNT5A*, *BHLHE41*, *MYBL1*, *APOL4*, *KCTD9*, *HOTAIR*, *SOCS2*, *SOCS3*, *RBP1*, *CD74*, gene expression profiles were confirmed by RT-qPCR, for both AA-derived and control-derived BM-MSCs.

Genes studied by RT-qPCR were selected based on their functional properties and potential role in the context of AA biology, as well as on the L2FC value and statistical significance (padj) obtained from transcriptomics analysis, as depicted in Table 7 and Table 8, below.

Table 7 – Genes selected for RT-qPCR according to biological function and DGE analysis results.

Gene symbol	Biological function	L2FC	padj
RARA [117]	Regulation of adipogenesis (adipogenesis inhibitor); lipid metabolism.	-1.662	0.007
ARID5 [118,119,120]	Pro-inflammatory; adipose tissue homeostasis (e.g., repression of *PPARG* transcription).	-1.501	2.567×10^{-6}
TNFSF9 [121,122]	Pro-inflammatory.	4.219	0.022
WNT5A [123,124,125,126]	Wnt noncanonical pathways activator; bone resorption promotion; angiogenesis.	2.478	0.0002
PPARG [127,128,129]	Adipogenesis promotion; lipid metabolism; hematopoietic support.	-1.996	0.007
BHLHE41 [130,131,132]	Anti-inflammatory; adipogenesis inhibition.	-3.669	0.0003
MYBL1 [132,133]	Hematopoiesis regulation (balance between self-renewal and differentiation).	2.739	0.0005
APOL4 [134,135,136]	Pro-inflammatory; lipid metabolism.	-4.508	0.0002

HOTAIR [111]	Gene regulation, chromatin remodeling, cancer progression, angiogenesis, inflammation.	-3.920	$9.507X10^{-14}$
SOCS2 [101,102,112,113]	Anti-inflammatory; adipogenesis inhibition; JAK-STAT cell signaling.	-2.621	$1.086x10^{-6}$
SOCS3 [101,102,113,114]	Lipid metabolism; JAK-STAT cell signaling.	-1.925	8.664x10-^{11}
RBP1 [115,137]	Immunomodulation.	-4.113	7.795x10-8
CD74 [116]	Immunomodulation.	-3.988	$1.551x10^{-9}$

L2FC – Log2 fold change; padj – adjusted p-value.

Table 8 – Genes selected for RT-qPCR according to potential biological relevance in the context of AA biology, but with no significant DGE results in transcriptomics analysis.

Gene symbol	Biological function	L2FC	padj
SPARC (osteonectin) [138]	ECM synthesis regulation; differentiation and maturation of osteoblasts; bone mineralization.	-0.018	0.966
BGLAP (osteocalcin) [139]	Bone formation and remodeling by regulation of osteoblasts and osteoclasts activity; bone mineralization.	-0.008	NA
SPP1 (osteopontin) [140,141]	Bone remodeling; inflammation (pro-inflammatory).	0.130	0.459
FABP4 [142,143]	Lipid metabolism; inflammation.	-1.431	0.766
LEPR [143,144,145]	Hematopoiesis (e.g., secretion of HSPC supportive growth factors by LepR+ stromal cells; marker for functional long-term HSC); inflammation.	-0.040	NA
GATA2 [146,147]	Hematopoiesis (HSC self-renewal and hematopoietic lineage determination).	-1.458	0.051
CEBPA [148,149,150,151,152]	Hematopoiesis (e.g., induction of myeloid versus erythroid differentiation);	-0.123	0.238

	adipogenesis (e.g., PPARG synergism with CEBPA).		
ADIPOQ (adiponectin) [153,154]	Hematopoiesis (HSC self-renewal and proliferation - pool expansion); anti-inflammatory.	0.022	NA
BIRC5 (survivin) [155,156]	Hematopoiesis (e.g., HSPC maintenance, proliferation, differentiation and survival; erythroid differentiation); apoptosis inhibitor.	1.768	0.068
SFRP1 [157,158,159,160]	Wnt signaling modulator (soluble inhibitor); hematopoiesis (e.g., HSC self-renewal and differentiation; regulation of the balance between HSC quiescence and activation); osteoblast inhibitor.	-1.211	0.461
KCTD9 [161,162,163,164]	Pro-inflammatory (e.g., NK cell activity enhancement); Wnt/β-catenin pathway inhibitor (e.g., colorectal cancer tumor suppressor).	0.967	0.023

L2FC – Log2 fold change; padj – adjusted p-value; ECM – extracellular matrix; HSC – hematopoietic stem cells; HSPC – hematopoietic stem and progenitor cells; NK – natural killer cells.

As depicted in Figure 45, below, for genes with significant DGE results in transcriptomics analysis (Table 7), RT-qPCR gene expression profiles between AA and control-derived BM-MSCs showed a similar pattern of either up or down regulation in comparison to bulk mRNA-Seq data, with the exception of *TNFSF9*, which was downregulated in RT-qPCR assessment (RT-qPCR L2FC = -0.233 versus bulk mRNA-Seq L2FC = 4.219).

For genes without significant DGE results in transcriptomics analysis but of potential interest in AA biology (Table 8), RT-qPCR results were less consistent with transcriptomics data, namely for *LEPR* (RT-qPCR L2FC = -2.795 versus bulk mRNA-Seq L2FC = -0.040); *GATA2* (RT-qPCR L2FC = -1.936 versus bulk mRNA-Seq L2FC = -1.458); *ADIPOQ* (RT-qPCR L2FC = -3.055 versus bulk mRNA-Seq L2FC = 0.022); *BIRC5* (RT-qPCR L2FC = 3.595 versus bulk mRNA-Seq L2FC = 1.758); *SFRP1* (RT-qPCR L2FC = -2,585 versus bulk mRNA-Seq L2FC = -1.211).

Despite RT-qPCR results seem to reinforce expression differences for genes with potential interest in AA but not significantly captured by bulk mRNA-Seq, it is not possible to infer if those results are biologically meaningful or result from methodological discrepancies. As so, RT-qPCR results must be interpreted carefully, especially for genes without DGE significance in transcriptomics analysis.

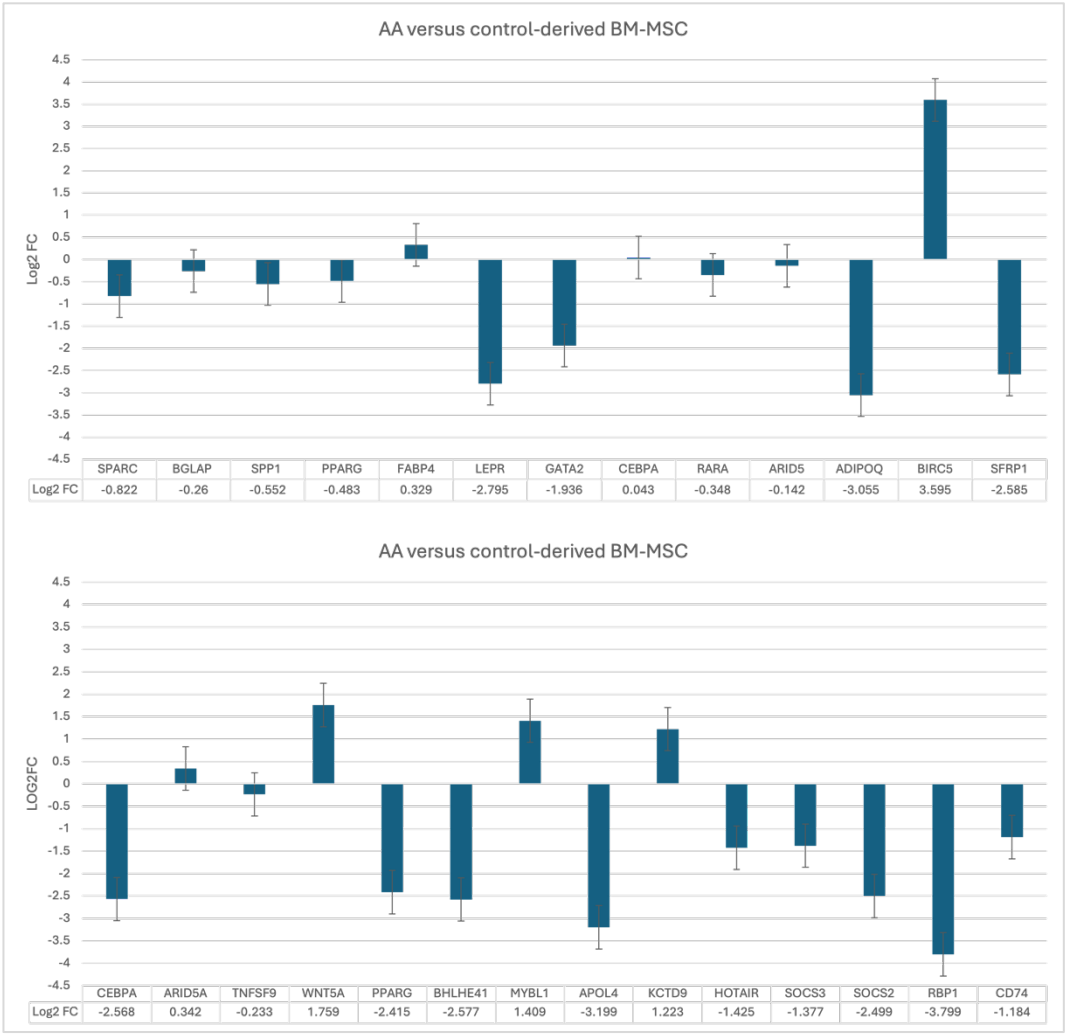

Figure 45: RT-qPCR results for genes selected according to functional properties, transcriptomics analysis and AA biology. Results determined by delta-delta Ct (ΔΔCt) method and plotted as Log2 fold change (L2FC; FC = $2^{-\Delta\Delta Ct}$) between AA and control-derived BM-MSCs (±SE mean). AA - aplastic anemia.

Limitations of gene expression analysis and future perspectives

Gene expression analysis is hugely sensitive to experimental variables (e.g., cell processing, culture conditions, cell passage number, RNA quality, etc.) as well as to methodological approaches.

From one side, RT-qPCR reproducibility could be limited by its relative quantification nature (to a reference housekeeping gene) as well as by the fact of being a targeted approach, depending on primer design quality for higher sensitivity and specificity [165]. On the other side, despite mRNA-Seq allows higher sensitivity and precision (e.g., absolute quantification of RNA molecules) [166], results could also be affected by processing errors and sampling variability.

In this work, RT-qPCR experiments were performed in samples derived from the same donors used for bulk mRNA-Seq experience, at an identical passage number, but unfortunately it was not possible to perform RT-qPCR on the same RNA extracted for transcriptomics, due to limitation of sample quantity. Consequently, reproducibility of results could had been limited by this fact.

One strategy to circumvent those limitations would be to enlarge the number of both AA and control donors for transcriptomics analysis, either by bulk or single-cell mRNA-Seq, with the purpose of increasing data robustness.

Another methodological approach of interest would be to perform protein analysis (e.g., by Western Blot) in both AA and control-derived BM-MSCs, in order to better ascertain the phenotypic impact of different gene expression profiles on cells. In future experiments, Western blot analysis is planned to be performed, based on the DGE data presented in this chapter.

V.3.4. BM-MSCs *in vitro* drug-modulation with isotretinoin - analysis of treatment effect on cell survival and gene expression

As described previously (sections II.13., II.14. and II.15.), *in vitro* drug-modulation with isotretinoin was performed in both AA and control-derived BM-MSCs. Regarding samples used for this experiment, AA group was similar to the groups used for gene expression analysis, with the exception of M08, not included. Control group similarly included F18, but not the other controls. Instead, control F81 (age = 43 years old; BM

source = PSIS; passage number = 6) was added. This difference was imposed by limitations regarding sample availability. However, considering the exploratory purpose of the experiment, it was decided to proceed.

Expression profile of selected genes after 6-day BM-MSCs culture under drug exposure

Gene expression profile of *CEBPA*, *PPARG*, *RARA*, *WNT5A*, *APOL4* and *SOCS3*, determined by RT-qPCR after *in vitro* 6-day culture of AA and control-derived BM-MSCs under 10μM isotretinoin exposure, was performed.

Considering global and individual analysis of both AA and control samples, isotretinoin exposure seemed to influence the expression of *CEBPA* (upregulation), *PPARG* (downregulation), *RARA* (downregulation); *WNT5A* (downregulation) and *APOL4* (upregulation) in comparison to untreated samples (L2FC cutoff ± 0.5), as depicted in Figure 46, below.

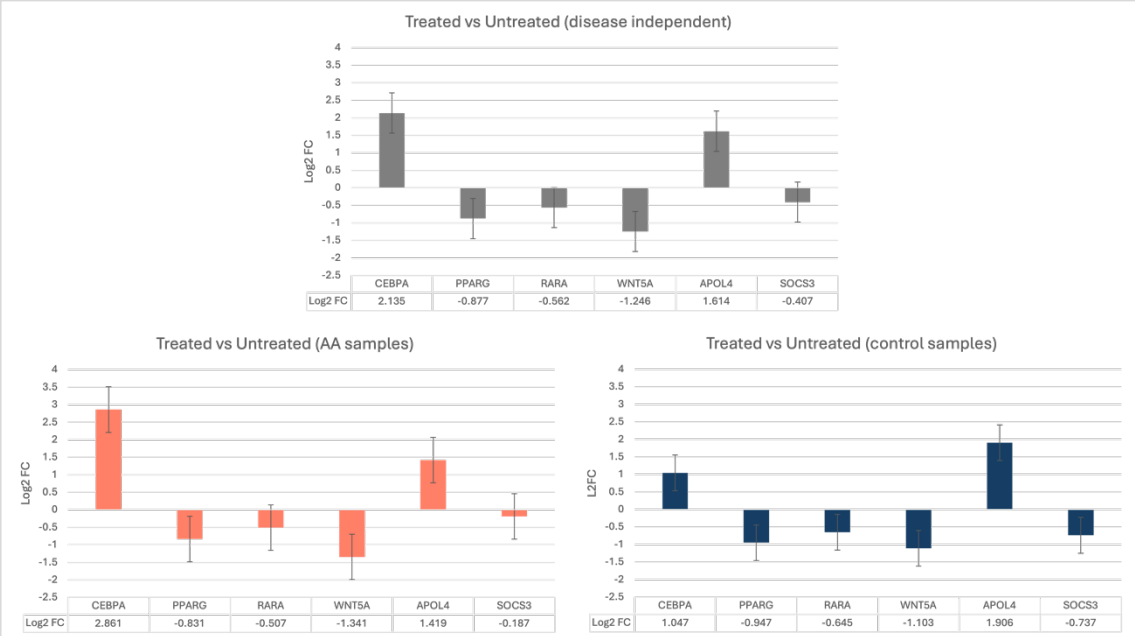

Figure 46: RT-qPCR results for selected genes after 6-day exposure of AA and control-derived BM-MSCs to isotretinoin (10μM). Results determined by delta-delta Ct (ΔΔCt) method and plotted as Log2 fold change (L2FC; FC = $2^{-\Delta\Delta Ct}$) between treated and untreated samples (±SE mean). AA - aplastic anemia.

However, upon comparison of gene expression profiles between treated and untreated samples contrasting by disease status (AA versus controls), no significant differences were found either before or after drug exposure, as represented in Figure 47, below. An exception could be hypothesized for *CEBPA* (upregulation) and *SOCS3* (upregulation) but must be confirmed in further experiments.

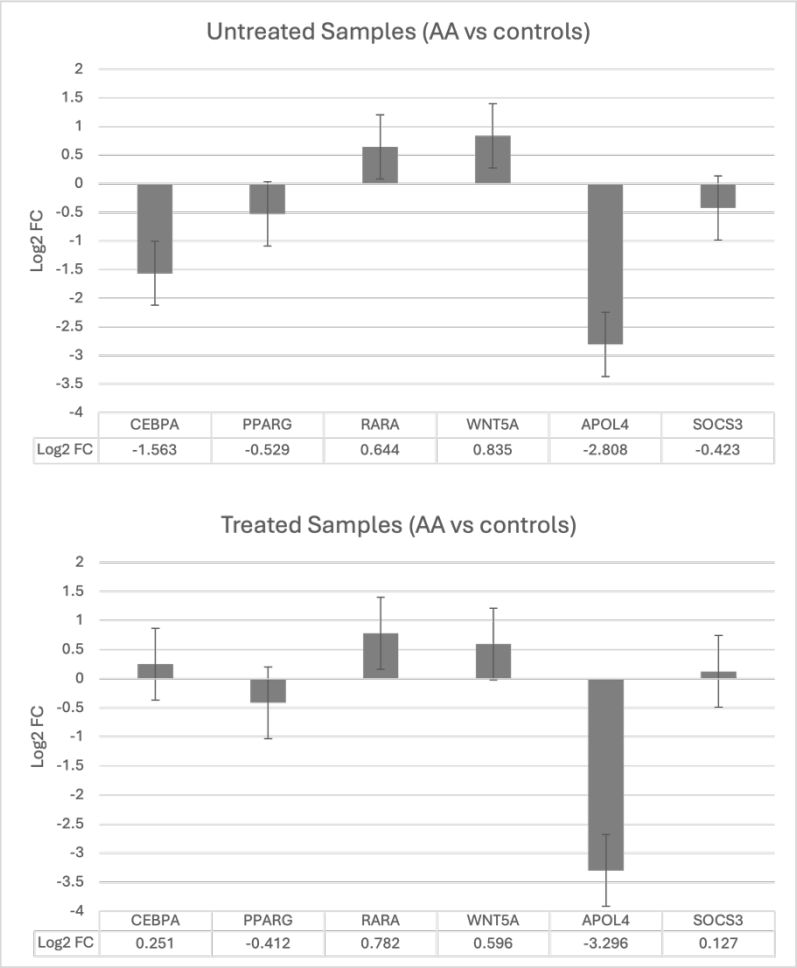

Figure 47: RT-qPCR results for selected genes after 6-day exposure of AA and control-derived BM-MSCs to isotretinoin (10μM). Results determined by delta-delta Ct (ΔΔCt) method and plotted as Log2 fold change (L2FC; FC = $2^{-\Delta\Delta Ct}$) between treated and untreated samples contrasting by disease status – AA versus controls (±SE mean). AA - aplastic anemia.

Cellular metabolic activity after 24 hours of drug exposure

Cellular metabolic activity at 24 hours after *in vitro* AA and control-derived BM-MSCs drug-modulation with isotretinoin (0.1 μM, 1 μM, 10 μM) was assessed, as depicted in Figure 48, below.

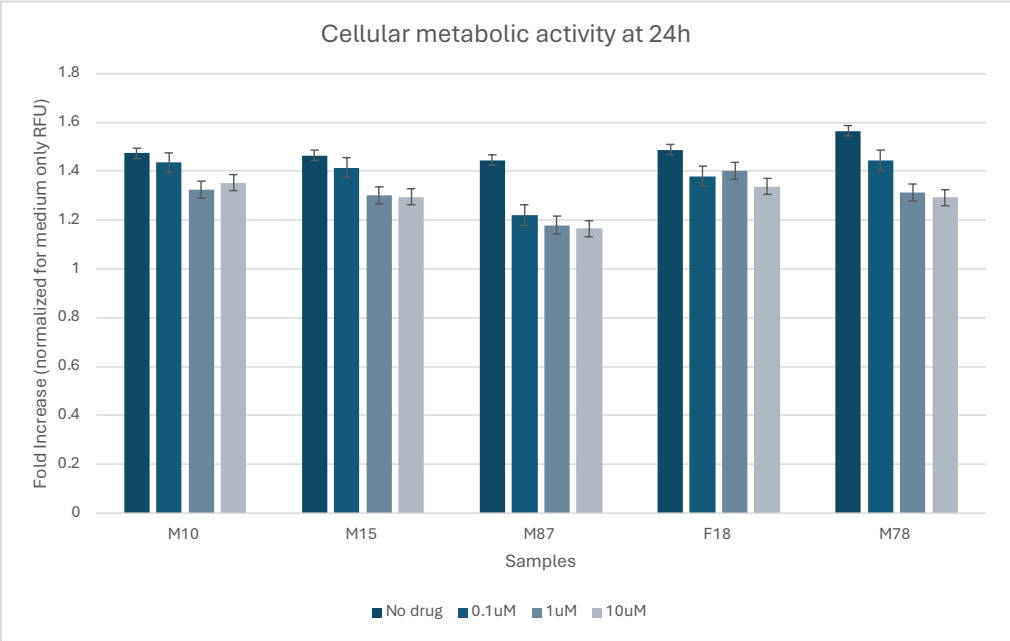

Figure 48: Cellular metabolic activity at 24 hours after *in vitro* AA and control-derived BM-MSCs drug-modulation with isotretinoin (0.1 μM, 1 μM, 10 μM). Viability/metabolic assay performed with PrestoBlue™. Results expressed as mean fold increase of relative fluorescence units (RFU), normalized for negative control (cell medium) (±SE mean). AA - aplastic anemia.

In both groups, fluorescence fold increase (a readout of cellular metabolic activity) at 24h of drug exposure was significantly lower for cells exposed to drug concentrations of both 1 μM (p = 0.004) and 10 μM (p = 0.002), in comparison to no-drug. However, no significant differences were identified between the three different drug concentrations (p = 0.21, for 0.1 μM versus 1 μM; p = 0.13, for 0.1 μM versus 10 μM; p = 0.76 for 1 μM versus 10 μM).

Proliferative rate of AA and control-derived BM-MSCs after *in vitro* 6-day culture under drug exposure

Proliferative rate of AA and control-derived BM-MSCs after *in vitro* 6-day culture with isotretinoin at different concentrations (no drug, 1 μM, 10 μM), calculated by cell number fold increase (FI), was determined by the end of day 6.

As depicted in Figure 49, proliferative rate appeared to be lower for increasing concentrations of drug in comparison with no drug exposure, with significance attained for 10 μM isotretinoin concentration (p = 0.15, for 1 μM versus no drug; p = 0.03 for 10 μM versus no drug; p = 0.42 for 1 μM versus 10 μM).

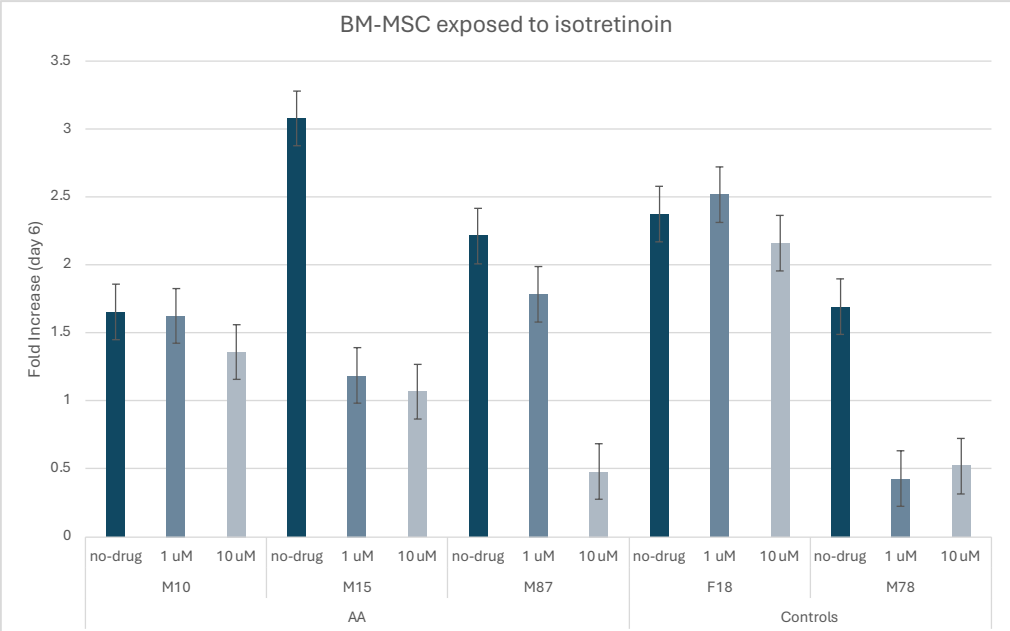

Figure 49: Proliferative rate by day 6 of *in vitro* AA and control-derived BM-MSCs drug-modulation with isotretinoin (no drug, 1 μM, 10 μM). Significance attained for 10 μM isotretinoin concentration (p = 0.15, for 1 μM versus no drug; p = 0.03 for 10 μM versus no drug; p = 0.42 for 1 μM versus 10 μM). Results expressed by mean fold increase (FI) of cell number by day 6 (±SE mean). AA - aplastic anemia.

Despite the exploratory character of the drug experiment with isotretinoin, whose results must be consolidated, this was a preliminary approach to drug modulation that will be further optimized and extended to other molecules of interest. The ultimate goal will be to establish an AA model for disease study and drug testing.

V.4. Conclusions

Transcriptomics analysis provided valuable insights on altered patterns of BM microenvironment in AA, thus contributing to a better understanding of disease mechanisms.

Molecular patterns related to immune response, adipogenesis, lipid metabolism, osteoblast and osteoclast differentiation and activity, cell-ECM interactions/ECM remodeling, hematopoietic support, angiogenesis, DNA repair/DNA damage response, stress response, and cell signaling were identified.

Based on the gene expression profile differences unveiled by bulk mRNA-Seq data, two opposite roles for BM-MSCs in AA were hypothesized:

1) A protective and regenerative role against cytotoxic-mediated immune attack on the hematopoietic niche (e.g., immunomodulatory, adipogenesis inhibitory and DNA damage responsive molecular patterns).
2) An adjunctive pathophysiological role, which might influence disease establishment or severity and therapeutic outcomes (e.g., pro-inflammatory, pro-adipogenic, osteoblast inhibitor, osteoclast activator, ECM remodeling and angiogenesis disruptive, DNA repair/stress response impairing, and cell signaling deregulatory molecular patterns).

Contrarily to previously published data, *PPARG* upregulation was not identified. In addition, despite *GATA2* seemed to be downregulated in AA samples, statistical significance was not attained.

Among candidate genes, the upregulation of *WNT5A* and downregulation of *SOCS2*, *SOCS3*, *RARA* and *RBP1* was particularly relevant, since these genes could be interesting targets for *ex vivo* BM-MSCs culture modulation (e.g., for improvement of BM-MSCs-mediated support of HSPC expansion) or to development of novel therapeutical approaches for AA, some of them already clinically approved for the treatment of other hematological conditions (e.g., counteraction of *SOCS2* and *SOCS3* downregulation by a JAK inhibitor, such as ruxolitinib - a JAK1/2 inhibitor, approved for myelofibrosis, refractory polycythemia vera or steroid refractory acute GVHD [167]; compensation of *RARA* and *RBP1* downregulation with retinoids, such as all-trans

retinoic acid (ATRA), a drug approved for treatment of acute promyelocytic leukemia, or isotretinoin).

In general, transcriptomics results were adequately validated by RT-qPCR and showed a similar pattern of up and downregulation between AA and controls, reproduced in RNA samples extracted at different timepoints.

In vitro drug-modulation of BM-MSCs with a molecule selected upon gene expression analysis showed to be feasible. This approach will be optimized for disease modeling and drug testing.

V.5. References - Chapter V

1. Kaushansky K, Lichtman MA, Prchal JT, Levi MM, Press OW, Burns LJ, Caligiuri M. eds. Williams Hematology, 9e, Chapter 35 (Aplastic Anemia: Acquired and Inherited). New York, NY: McGraw-Hill
2. Barbara J. Bain, David M. Clark, Bridget S. Wilkins. Bone marrow pathology, Fifth edition, Chapter 9. Wiley-Blackwell, 2019
3. Young NS, Maciejewski J. The pathophysiology of acquired aplastic anemia. N Engl J Med. 1997;336(19):1365-1372. doi:10.1056/NEJM199705083361906
4. Bacigalupo A. How I treat acquired aplastic anemia. Blood. 2017;129(11):1428-1436. doi:10.1182/blood-2016-08-693481
5. Gupta V, Eapen M, Brazauskas R, et al. Impact of age on outcomes after bone marrow transplantation for acquired aplastic anemia using HLA-matched sibling donors. Haematologica. 2010;95(12):2119-2125. doi:10.3324/haematol.2010.026682
6. Medinger M, Drexler B, Lengerke C, Passweg J. Pathogenesis of Acquired Aplastic Anemia and the Role of the Bone Marrow Microenvironment. Front Oncol. 2018;8:587. Published 2018 Dec 5. doi:10.3389/fonc.2018.00587
7. Wu L, Mo W, Zhang Y, et al. Vascular and perivascular niches, but not the osteoblastic niche, are numerically restored following allogeneic hematopoietic stem cell transplantation in patients with aplastic anemia. Int J Hematol. 2017;106(1):71-81. doi:10.1007/s12185-017-2217-1
8. Wu L, Mo W, Zhang Y, et al. Impairment of hematopoietic stem cell niches in patients with aplastic anemia. Int J Hematol. 2015;102(6):645-653. doi:10.1007/s12185-015-1881-2
9. Dominici M, Le Blanc K, Mueller I, et al. Minimal criteria for defining multipotent mesenchymal stromal cells. The International Society for Cellular Therapy position statement. Cytotherapy. 2006;8(4):315-317. doi:10.1080/14653240600855905
10. Wu X, Jiang J, Gu Z, Zhang J, Chen Y, Liu X. Mesenchymal stromal cell therapies: immunomodulatory properties and clinical progress. Stem Cell Res Ther. 2020;11(1):345. Published 2020 Aug 8. doi:10.1186/s13287-020-01855-9
11. Hamzic E, Whiting K, Gordon Smith E, Pettengell R. Characterization of bone marrow mesenchymal stromal cells in aplastic anaemia. Br J Haematol. 2015;169(6):804-813. doi:10.1111/bjh.13364
12. Li J, Yang S, Lu S, et al. Differential gene expression profile associated with the abnormality of bone marrow mesenchymal stem cells in aplastic anemia. PLoS One. 2012;7(11):e47764. doi:10.1371/journal.pone.0047764
13. Holmberg LA, Seidel K, Leisenring W, Torok-Storb B. Aplastic anemia: analysis of stromal cell function in long-term marrow cultures. Blood. 1994;84(11):3685-3690
14. Shipounova IN, Petrova TV, Svinareva DA, Momotuk KS, Mikhailova EA, Drize NI. Alterations in hematopoietic microenvironment in patients with aplastic anemia. Clin Transl Sci. 2009;2(1):67-74. doi:10.1111/j.1752-8062.2008.00074.x
15. Chao YH, Peng CT, Harn HJ, Chan CK, Wu KH. Poor potential of proliferation and differentiation in bone marrow mesenchymal stem cells derived from children with severe aplastic anemia. Ann Hematol. 2010;89(7):715-723. doi:10.1007/s00277-009-0892-6

16. Broglie L, Margolis D, Medin JA. Yin and Yang of mesenchymal stem cells and aplastic anemia. World J Stem Cells. 2017;9(12):219-226. doi:10.4252/wjsc.v9.i12.219
17. Bueno C, Roldan M, Anguita E, et al. Bone marrow mesenchymal stem cells from patients with aplastic anemia maintain functional and immune properties and do not contribute to the pathogenesis of the disease. Haematologica. 2014;99(7):1168-1175. doi:10.3324/haematol.2014.103580
18. Michelozzi IM, Pievani A, Pagni F, et al. Human aplastic anaemia-derived mesenchymal stromal cells form functional haematopoietic stem cell niche in vivo. Br J Haematol. 2017;179(4):669-673. doi:10.1111/bjh.14234
19. Bacigalupo A, Socié G, Schrezenmeier H, et al. Bone marrow versus peripheral blood as the stem cell source for sibling transplants in acquired aplastic anemia: survival advantage for bone marrow in all age groups. Haematologica. 2012;97(8):1142-1148. doi:10.3324/haematol.2011.054841
20. Schrezenmeier H, Passweg JR, Marsh JC, et al. Worse outcome and more chronic GVHD with peripheral blood progenitor cells than bone marrow in HLA-matched sibling donor transplants for young patients with severe acquired aplastic anemia. Blood. 2007;110(4):1397-1400. doi:10.1182/blood-2007-03-081596
21. Crippa S, Santi L, Bosotti R, Porro G, Bernardo ME. Bone Marrow-Derived Mesenchymal Stromal Cells: A Novel Target to Optimize Hematopoietic Stem Cell Transplantation Protocols in Hematological Malignancies and Rare Genetic Disorders. J Clin Med. 2019;9(1):2. Published 2019 Dec 18. doi:10.3390/jcm9010002
22. Liu Z, Zhang Y, Xiao H, et al. Cotransplantation of bone marrow-derived mesenchymal stem cells in haploidentical hematopoietic stem cell transplantation in patients with severe aplastic anemia: an interim summary for a multicenter phase II trial results [published correction appears in Bone Marrow Transplant. 2017 Jul;52(7):1080. doi: 10.1038/bmt.2017.85]. Bone Marrow Transplant. 2017;52(5):704-710. doi:10.1038/bmt.2016.347
23. Sebo ZL, Rendina-Ruedy E, Ables GP, et al. Bone Marrow Adiposity: Basic and Clinical Implications. Endocr Rev. 2019;40(5):1187-1206. doi:10.1210/er.2018-00138
24. Cuminetti V, Arranz L. Bone Marrow Adipocytes: The Enigmatic Components of the Hematopoietic Stem Cell Niche. J Clin Med. 2019;8(5):707. Published 2019 May 18. doi:10.3390/jcm8050707
25. Naveiras O, Nardi V, Wenzel PL, Hauschka PV, Fahey F, Daley GQ. Bone-marrow adipocytes as negative regulators of the haematopoietic microenvironment. Nature. 2009;460(7252):259-263. doi:10.1038/nature08099
26. Ambrosi TH, Scialdone A, Graja A, et al. Adipocyte Accumulation in the Bone Marrow during Obesity and Aging Impairs Stem Cell-Based Hematopoietic and Bone Regeneration. Cell Stem Cell. 2017;20(6):771-784.e6. doi:10.1016/j.stem.2017.02.009
27. Mattiucci D, Maurizi G, Izzi V, et al. Bone marrow adipocytes support hematopoietic stem cell survival. J Cell Physiol. 2018;233(2):1500-1511. doi:10.1002/jcp.26037
28. Wang H, Leng Y, Gong Y. Bone Marrow Fat and Hematopoiesis. Front Endocrinol (Lausanne). 2018;9:694. Published 2018 Nov 28. doi:10.3389/fendo.2018.00694

29. Tripathy NK, Singh SP, Nityanand S. Enhanced adipogenicity of bone marrow mesenchymal stem cells in aplastic anemia. Stem Cells Int. 2014;2014:276862. doi:10.1155/2014/276862
30. Osorio EY, Gugala Z, Patterson GT, et al. Inflammatory stimuli alter bone marrow composition and compromise bone health in the malnourished host. Front Immunol. 2022;13:846246. Published 2022 Aug 2. doi:10.3389/fimmu.2022.846246
31. Wan S, Xie J, Liang Y, Yu X. Pathological roles of bone marrow adipocyte-derived monocyte chemotactic protein-1 in type 2 diabetic mice. Cell Death Discov. 2023;9(1):412. Published 2023 Nov 13. doi:10.1038/s41420-023-01708-3
32. Gonzaga VF, Wenceslau CV, Lisboa GS, Frare EO, Kerkis I. Mesenchymal Stem Cell Benefits Observed in Bone Marrow Failure and Acquired Aplastic Anemia. Stem Cells Int. 2017;2017:8076529. doi:10.1155/2017/8076529
33. Song Y, Li N, Liu Y, Fang B. Improved outcome of adults with aplastic anaemia treated with arsenic trioxide plus ciclosporin. Br J Haematol. 2013;160(2):266-269. doi:10.1111/bjh.12110
34. Li N, Song Y, Zhou J, Fang B. Arsenic trioxide improves hematopoiesis in refractory severe aplastic anemia. J Hematol Oncol. 2012;5:61. Published 2012 Oct 9. doi:10.1186/1756-8722-5-61
35. Zhao J, Wang C, Song Y, Fang B. Arsenic trioxide and microRNA-204 display contrary effects on regulating adipogenic and osteogenic differentiation of mesenchymal stem cells in aplastic anemia. Acta Biochim Biophys Sin (Shanghai). 2014;46(10):885-893. doi:10.1093/abbs/gmu082
36. Fujimaki S, Harigae H, Sugawara T, Takasawa N, Sasaki T, Kaku M. Decreased expression of transcription factor GATA-2 in haematopoietic stem cells in patients with aplastic anaemia. Br J Haematol. 2001;113(1):52-57. doi:10.1046/j.1365-2141.2001.02736.x
37. Zeng W, Chen G, Kajigaya S, et al. Gene expression profiling in CD34 cells to identify differences between aplastic anemia patients and healthy volunteers. Blood. 2004;103(1):325-332. doi:10.1182/blood-2003-02-0490
38. Xu Y, Takahashi Y, Wang Y, et al. Downregulation of GATA-2 and overexpression of adipogenic gene-PPARgamma in mesenchymal stem cells from patients with aplastic anemia. Exp Hematol. 2009;37(12):1393-1399. doi:10.1016/j.exphem.2009.09.005
39. Kamata M, Okitsu Y, Fujiwara T, et al. GATA2 regulates differentiation of bone marrow-derived mesenchymal stem cells. Haematologica. 2014;99(11):1686-1696. doi:10.3324/haematol.2014.105692
40. Takada I, Kouzmenko AP, Kato S. Wnt and PPARgamma signaling in osteoblastogenesis and adipogenesis. Nat Rev Rheumatol. 2009;5(8):442-447. doi:10.1038/nrrheum.2009.137
41. Yuan Z, Li Q, Luo S, et al. PPARγ and Wnt Signaling in Adipogenic and Osteogenic Differentiation of Mesenchymal Stem Cells. Curr Stem Cell Res Ther. 2016;11(3):216-225. doi:10.2174/1574888x10666150519093429
42. Zhang N, Dai YL, Huang LF, Liu WL. Zhongguo Shi Yan Xue Ye Xue Za Zhi. [Therapeutic effect of lithium chloride combined with cyclosporine A on mouse model with aplastic anemia]. 2012;20(3):654-657

43. Gao M, Ge M, Huo J, et al. Leptin-mediated proinflammatory bone marrow environment in acquired aplastic anemia. Cytokine. 2022;152:155829. doi:10.1016/j.cyto.2022.155829
44. Chen Q, Shou P, Zheng C, et al. Fate decision of mesenchymal stem cells: adipocytes or osteoblasts?. Cell Death Differ. 2016;23(7):1128-1139. doi:10.1038/cdd.2015.168
45. Yin X, Yang J, Liu Y, et al. Altered expression of leptin and leptin receptor in the development of immune-mediated aplastic anemia in mice. Exp Ther Med. 2019;18(2):1047-1056. doi:10.3892/etm.2019.7660
46. Shaik S, Martin EC, Hayes DJ, Gimble JM, Devireddy RV. Transcriptomic Profiling of Adipose Derived Stem Cells Undergoing Osteogenesis by RNA-Seq. Sci Rep. 2019 Aug 13;9(1):11800. doi: 10.1038/s41598-019-48089-1. PMID: 31409848; PMCID: PMC6692320.
47. Xie, Z., Yu, W., Ye, G. et al. Single-cell RNA sequencing analysis of human bone-marrow-derived mesenchymal stem cells and functional subpopulation identification. Exp Mol Med 54, 483–492 (2022).
48. Zhu C, Lian Y, Wang C, et al. Single-cell transcriptomics dissects hematopoietic cell destruction and T-cell engagement in aplastic anemia. Blood. 2021;138(1):23-33. doi:10.1182/blood.2020008966
49. Tonglin H, Yanna Z, Xiaoling Y, Ruilan G, Liming Y. Single-Cell RNA-Seq of Bone Marrow Cells in Aplastic Anemia. Front Genet. 2022;12:745483. Published 2022 Jan 3. doi:10.3389/fgene.2021.745483
50. Zhou Q, Huang L, Liu Y, et al. Single-cell RNA sequencing depicts metabolic changes in children with aplastic anemia. Front Oncol. 2023;13:1075408. Published 2023 Mar 29. doi:10.3389/fonc.2023.1075408
51. Saxena P, Srivastava J, Rai B, et al. Elevated senescence in the bone marrow mesenchymal stem cells of acquired aplastic anemia patients: A possible implication of DNA damage responses and telomere attrition. Biochim Biophys Acta Mol Basis Dis. 2024;1870(3):167025.
52. Picelli S, Faridani OR, Björklund AK, Winberg G, Sagasser S, Sandberg R. Full-length RNA-seq from single cells using Smart-seq2. Nat Protoc. 2014;9(1):171-181. doi:10.1038/nprot.2014.006
53. Baym M, Kryazhimskiy S, Lieberman TD, Chung H, Desai MM, Kishony R. Inexpensive multiplexed library preparation for megabase-sized genomes [published correction appears in PLoS One. 2015 Jun 18;10(6):e0131262. doi: 10.1371/journal.pone.0131262]. PLoS One. 2015;10(5):e0128036. Published 2015 May 22. doi:10.1371/journal.pone.0128036
54. Genome sequence, primary assembly (GRCh38): https://ftp.ebi.ac.uk/pub/databases/gencode/Gencode_human/release_44/GRCh38.primary_assembly.genome.fa.gz.
55. Comprehensive gene annotation (GRCh38): https://ftp.ebi.ac.uk/pub/databases/gencode/Gencode_human/release_44/gencode.v44.primary_assembly.annotation.gtf.gz.
56. Dobin A, Davis CA, Schlesinger F, et al. STAR: ultrafast universal RNA-seq aligner. Bioinformatics. 2013;29(1):15-21.doi:10.1093/bioinformatics/bts635 (https://github.com/alexdobin/STAR/releases/tag/2.7.11a)

57. R Core Team (2021) R: A Language and Environment for Statistical Computing. R Foundation for Statistical Computing, Vienna. https://www.R-project.org
58. Morgan M, Pagès H, Obenchain V, Hayden N (2024). Rsamtools: Binary alignment (BAM), FASTA, variant call (BCF), and tabix file import. R package version 2.20.0, https://bioconductor.org/packages/Rsamtools
59. Lawrence M, Huber W, Pagès H, Aboyoun P, Carlson M, Gentleman R, Morgan M, Carey V (2013). "Software for Computing and Annotating Genomic Ranges." PLoS Computational
Biology, 9. doi:10.1371/journal.pcbi.1003118, http://www.ploscompbiol.org/article/info%3Adoi%2F10.1371%2Fjournal.pcbi.1003118
60. Love MI, Huber W, Anders S (2014). "Moderated estimation of fold change and dispersion for RNA-seq data with DESeq2." Genome Biology, 15, 550. doi:10.1186/s13059-014-0550-8
61. Warnes, G. R., Bolker, B., Bonebakker, L., Gentleman, R., Liaw, W. H. A., Lumley, T., Maechler, M., Magnusson, A., Moeller, S., Schwartz, M., & Venables, B. 1 (2023). gplots: Various R Programming Tools for Plotting Data. R package version 3.1.3. https://CRAN.R-project.org/package=gplots
62. Kassambara, A., & Mundt, F. (2020). factoextra: Extract and Visualize the Results of Multivariate Data Analyses. R package version 1.0.7
63. Zhu, A., Ibrahim, J. G., & Love, M. I. (2019). Heavy-tailed prior distributions for sequence count data: removing the noise and preserving large differences. Bioinformatics, 35(12), 2084-2092
64. Kevin Blighe, Sharmila Rana & Myles Lewis (2023). EnhancedVolcano: Publication-ready volcano plots with enhanced colouring and labeling. R package version 1.16.0. https://github.com/kevinblighe/EnhancedVolcano
65. Wu T, Hu E, Xu S, Chen M, Guo P, Dai Z, Feng T, Zhou L, Tang W, Zhan L, Fu x, Liu S, Bo X, Yu G (2021). "clusterProfiler 4.0: A universal enrichment tool for interpreting omics data." The Innovation, 2(3), 100141. doi:10.1016/j.xinn.2021.100141.
66. Yu G, Wang L, Han Y, He Q (2012). "clusterProfiler: an R package for comparing biological themes among gene clusters." OMICS: A Journal of Integrative Biology, 16(5), 284-287. doi:10.1089/omi.2011.0118
67. Carlson M (2019). org.Hs.eg.db: Genome wide annotation for Human. R package version 3.8.2.
68. Raudvere, U., Kolberg, L., Kuzmin, I., Arak, T., Adler, P., Peterson, H., & Vilo, J. (2019). g:Profiler: a web server for functional enrichment analysis and conversions of gene lists (2019 update). Nucleic Acids Research, 47(W1), W191-W198
69. Stelzer, G., Rosen, N., Plaschkes, I., Zimmerman, S., Twik, M., Fishilevich, S., ... & Lancet, D. (2016). The GeneCards Suite: From Gene Data Mining to Disease Genome Sequence Analyses. Current Protocols in Bioinformatics, 54(1), 1.30.1-1.30.33
70. Kuleshov, M. V., Jones, M. R., Rouillard, A. D., Fernandez, N. F., Duan, Q., Wang, Z., ... & Ma'ayan, A. (2016). Enrichr: a comprehensive gene set enrichment analysis web server 2016 update. Nucleic acids research, 44(W1), W90-W97
71. Wickham H (2016). ggplot2: Elegant Graphics for Data Analysis. Springer-Verlag New York. ISBN 978-3-319-24277-4, https://ggplot2.tidyverse.org

72. Staal FJ, Clevers HC. WNT signalling and haematopoiesis: a WNT-WNT situation. Nat Rev Immunol. 2005;5(1):21-30. doi:10.1038/nri1529
73. Lento W, Congdon K, Voermans C, Kritzik M, Reya T. Wnt signaling in normal and malignant hematopoiesis. Cold Spring Harb Perspect Biol. 2013;5(2):a008011. Published 2013 Feb 1. doi:10.1101/cshperspect.a008011
74. Lee RH, Seo MJ, Pulin AA, Gregory CA, Ylostalo J, Prockop DJ. The CD34-like protein PODXL and alpha6-integrin (CD49f) identify early progenitor MSCs with increased clonogenicity and migration to infarcted heart in mice. Blood. 2009;113(4):816-826.
75. Lin WD, Liao WL, Chen WC, Liu TY, Chen YC, Tsai FJ. Genome-wide association study identifies novel susceptible loci and evaluation of polygenic risk score for chronic obstructive pulmonary disease in a Taiwanese population. BMC Genomics. 2024;25(1):607. Published 2024 Jun 17.
76. Lee H, Park BC, Soon Kang J, Cheon Y, Lee S, Jae Maeng P. MAM domain containing 2 is a potential breast cancer biomarker that exhibits tumour-suppressive activity. Cell Prolif. 2020;53(9):e12883.
77. Gene [Internet]. Bethesda (MD): National Library of Medicine (US), National Center for Biotechnology Information; 2004 - [cited 2025 Jan 10]. Assession No. 28984, regulator of cell cycle (RGCC), Homo sapiens. Available from: https://www.ncbi.nlm.nih.gov/gene/28984
78. Ahmad MK, Abdollah NA, Shafie NH, Yusof NM, Razak SRA. Dual-specificity phosphatase 6 (DUSP6): a review of its molecular characteristics and clinical relevance in cancer. Cancer Biol Med. 2018;15(1):14-28.
79. Lu G, Ota A, Ren S, et al. PPM1l encodes an inositol requiring-protein 1 (IRE1) specific phosphatase that regulates the functional outcome of the ER stress response. Mol Metab. 2013;2(4):405-416. Published 2013 Aug 3.
80. Ren X, Ma L, Wang N, et al. Antioxidant Gene Signature Impacts the Immune Infiltration and Predicts the Prognosis of Kidney Renal Clear Cell Carcinoma. Front Genet. 2021;12:721252. Published 2021 Aug 19.
81. Oo SM, Oo HK, Takayama H, et al. Selenoprotein P-mediated reductive stress impairs cold-induced thermogenesis in brown fat. Cell Rep. 2022;38(13):110566.
82. Boskovic S, Marín Juez R, Stamenkovic N, Radojkovic D, Stainier DY, Kojic S. The stress responsive gene ankrd1a is dynamically regulated during skeletal muscle development and upregulated following cardiac injury in border zone cardiomyocytes in adult zebrafish. Gene. 2021;792:145725.
83. Luo R, Li L, Xiao F, Fu J. LncRNA FLG-AS1 Mitigates Diabetic Retinopathy by Regulating Retinal Epithelial Cell Inflammation, Oxidative Stress, and Apoptosis via miR-380-3p/SOCS6 Axis. Inflammation. 2022;45(5):1936-1949. doi:10.1007/s10753-022-01665-6
84. Stucker S, Chen J, Watt FE, Kusumbe AP. Bone Angiogenesis and Vascular Niche Remodeling in Stress, Aging, and Diseases. Front Cell Dev Biol. 2020;8:602269. Published 2020 Nov 26. doi:10.3389/fcell.2020.602269
85. Croft M, Duan W, Choi H, Eun SY, Madireddi S, Mehta A. TNF superfamily in inflammatory disease: translating basic insights. Trends Immunol. 2012;33(3):144-152. doi:10.1016/j.it.2011.10.004

86. Wu J, Wang Y. Role of TNFSF9 bidirectional signal transduction in antitumor immunotherapy. Eur J Pharmacol. 2022;928:175097. doi:10.1016/j.ejphar.2022.175097
87. Wong HY, Schwarz H. CD137 / CD137 ligand signalling regulates the immune balance: A potential target for novel immunotherapy of autoimmune diseases. J Autoimmun. 2020;112:102499. doi:10.1016/j.jaut.2020.102499
88. Wu J, Wang Y, Jiang Z. TNFSF9 Is a Prognostic Biomarker and Correlated with Immune Infiltrates in Pancreatic Cancer. J Gastrointest Cancer. 2021;52(1):150-159. doi:10.1007/s12029-020-00371-6
89. Kumawat K, Gosens R. WNT-5A: signaling and functions in health and disease. Cell Mol Life Sci. 2016;73(3):567-587. doi:10.1007/s00018-015-2076-y
90. Chen J, Crawford R, Chen C, Xiao Y. The key regulatory roles of the PI3K/Akt signaling pathway in the functionalities of mesenchymal stem cells and applications in tissue regeneration. Tissue Eng Part B Rev. 2013;19(6):516-528. doi:10.1089/ten.TEB.2012.0672
91. Xu C, Feng C, Huang P, et al. TNFα and IFNγ rapidly activate PI3K-AKT signaling to drive glycolysis that confers mesenchymal stem cells enhanced anti-inflammatory property. Stem Cell Res Ther. 2022;13(1):491. Published 2022 Oct 4. doi:10.1186/s13287-022-03178-3
92. Neo SH, Her Z, Othman R, et al. Expansion of human bone marrow-derived mesenchymal stromal cells with enhanced immunomodulatory properties. Stem Cell Res Ther. 2023;14(1):259. Published 2023 Sep 19. doi:10.1186/s13287-023-03481-7
93. Liu T, Zhang L, Joo D, Sun SC. NF-κB signaling in inflammation. Signal Transduct Target Ther. 2017;2:17023-. doi:10.1038/sigtrans.2017.23
94. Ping Z, Chen S, Hermans SJF, et al. Activation of NF-κB driven inflammatory programs in mesenchymal elements attenuates hematopoiesis in low-risk myelodysplastic syndromes. Leukemia. 2019;33(2):536-541. doi:10.1038/s41375-018-0267-x
95. Zhang S, Cai Z, Li H. AHNAKs roles in physiology and malignant tumors. Front Oncol. 2023;13:1258951. Published 2023 Nov 14. doi:10.3389/fonc.2023.1258951
96. Tang NN, Xu RB, Jiang B, et al. AHNAK2 Regulates NF-κB/MMP-9 Signaling to Promote Pancreatic Cancer Progression. Biochem Genet. Published online June 12, 2024. doi:10.1007/s10528-024-10844-z
97. Li X, Li H, Shao MM, Miao J, Fu Y, Hu B. Downregulation of AHNAK2 inhibits cell cycle of lung adenocarcinoma cells by interacting with RUVBL1. Thorac Cancer. 2023;14(22):2093-2104. doi:10.1111/1759-7714.14989
98. Ye R, Liu D, Guan H, et al. AHNAK2 promotes thyroid carcinoma progression by activating the NF-κB pathway. Life Sci. 2021;286:120032. doi:10.1016/j.lfs.2021.120032
99. Ou G, Tian Z, Su M, Yu M, Gong J, Chen Y. Identification of gemcitabine resistance-related AHNAK2 gene associated with prognosis and immune infiltration in pancreatic cancer. Heliyon. 2024;10(13):e33687. Published 2024 Jun 27. doi:10.1016/j.heliyon.2024.e33687
100. Xu M, Wen J, Xu Q, et al. AHNAK2 Promotes the Progression of Differentiated Thyroid Cancer through PI3K/AKT Signaling Pathway. Curr Cancer Drug Targets. 2024;24(2):220-229.

101. Hu X, Li J, Fu M, Zhao X, Wang W. The JAK/STAT signaling pathway: from bench to clinic. Signal Transduct Target Ther. 2021;6(1):402. Published 2021 Nov 26.
102. Lv Y, Qi J, Babon JJ, et al. The JAK-STAT pathway: from structural biology to cytokine engineering. Signal Transduct Target Ther. 2024;9(1):221. Published 2024 Aug 21.
103. Mirfakhraie R, Ardakani MT, Hajifathali A, et al. Highlighting the interaction between immunomodulatory properties of mesenchymal stem cells and signaling pathways contribute to Graft Versus Host Disease management. Transpl Immunol. 2022;71:101524.
104. Kim DS, Jang IK, Lee MW, et al. Enhanced Immunosuppressive Properties of Human Mesenchymal Stem Cells Primed by Interferon-γ. EBioMedicine. 2018;28:261-273.
105. Xue C, Yao Q, Gu X, et al. Evolving cognition of the JAK-STAT signaling pathway: autoimmune disorders and cancer. Signal Transduct Target Ther. 2023;8(1):204. Published 2023 May 19. doi:10.1038/s41392-023-01468-7
106. Hu Q, Bian Q, Rong D, et al. JAK/STAT pathway: Extracellular signals, diseases, immunity, and therapeutic regimens. Front Bioeng Biotechnol. 2023;11:1110765. Published 2023 Feb 23.
107. Rah B, Rather RA, Bhat GR, et al. JAK/STAT Signaling: Molecular Targets, Therapeutic Opportunities, and Limitations of Targeted Inhibitions in Solid Malignancies. Front Pharmacol. 2022;13:821344. Published 2022 Mar 24.
108. Groarke EM, Feng X, Aggarwal N, et al. Efficacy of JAK1/2 inhibition in murine immune bone marrow failure. Blood. 2023;141(1):72-89.
109. Lin CM, Cooles FA, Isaacs JD. Basic Mechanisms of JAK Inhibition. Mediterr J Rheumatol. 2020;31(Suppl 1):100-104. Published 2020 Jun 11.
110. Yoshizato T, Dumitriu B, Hosokawa K, et al. Somatic Mutations and Clonal Hematopoiesis in Aplastic Anemia. N Engl J Med. 2015;373(1):35-47. doi:10.1056/NEJMoa1414799
111. Raju GSR, Pavitra E, Bandaru SS, et al. HOTAIR: a potential metastatic, drug-resistant and prognostic regulator of breast cancer. Mol Cancer. 2023;22(1):65. Published 2023 Mar 30.
112. Val CH, de Oliveira MC, Lacerda DR, et al. SOCS2 modulates adipose tissue inflammation and expansion in mice. J Nutr Biochem. 2020;76:108304.
113. Alexander WS. Suppressors of cytokine signalling (SOCS) in the immune system. Nat Rev Immunol. 2002;2(6):410-416.
114. Liu W, Wang X. Research Advances on Suppressor of Cytokine Signaling 3 (SOCS3) in Animal Carbohydrate and Lipid Metabolism Processes. Pak J Biol Sci. 2022;25(12):1100-1108.
115. Bradshaw, D., Cashin, C.H., Kennedy, A.J. (1984). Anti-Inflammatory Effects of the Retinoids. In: Cunliffe, W.J., Miller, A.J. (eds) Retinoid Therapy. Springer, Dordrecht.
116. Su, H., Na, N., Zhang, X. et al. The biological function and significance of CD74 in immune diseases. Inflamm. Res. 66, 209–216 (2017).
117. Cassim Bawa FN, Hu S, Gopoju R, et al. Adipocyte retinoic acid receptor α prevents obesity and steatohepatitis by regulating energy expenditure and lipogenesis. Obesity (Silver Spring). 2024;32(1):120-130.

118. Nyati KK, Agarwal RG, Sharma P, Kishimoto T. Arid5a Regulation and the Roles of Arid5a in the Inflammatory Response and Disease. Front Immunol. 2019;10:2790. Published 2019 Dec 5.
119. Nyati KK, Kishimoto T. Recent Advances in the Role of Arid5a in Immune Diseases and Cancer. Front Immunol. 2022 Jan 19;12:827611.
120. Chalise JP, Hashimoto S, Parajuli G, et al. Feedback regulation of Arid5a and Ppar-γ2 maintains adipose tissue homeostasis. Proc Natl Acad Sci U S A. 2019;116(30):15128-15133.
121. Aggarwal BB, Gupta SC, Kim JH. Historical perspectives on tumor necrosis factor and its superfamily: 25 years later, a golden journey. Blood. 2012 Jan 19;119(3):651-65.
122. Singh R, Kim YH, Lee SJ, Eom HS, Choi BK. 4-1BB immunotherapy: advances and hurdles. Exp Mol Med. 2024;56(1):32-39.
123. Maeda K, Kobayashi Y, Koide M, Uehara S, Okamoto M, Ishihara A, Kayama T, Saito M, Marumo K. The Regulation of Bone Metabolism and Disorders by Wnt Signaling. Int J Mol Sci. 2019 Nov 6;20(22):5525.
124. Lojk J, Marc J. Roles of Non-Canonical Wnt Signalling Pathways in Bone Biology. Int J Mol Sci. 2021 Oct 7;22(19):10840.
125. Roberts JL, Liu G, Paglia DN, et al. Deletion of Wnt5a in osteoclasts results in bone loss through decreased bone formation. Ann N Y Acad Sci. 2020;1463(1):45-59.
126. Shi YN, Zhu N, Liu C, et al. Wnt5a and its signaling pathway in angiogenesis. Clin Chim Acta. 2017;471:263-269.
127. Zhuang H, Zhang X, Zhu C, et al. Molecular Mechanisms of PPAR-γ Governing MSCs Osteogenic and Adipogenic Differentiation. Curr Stem Cell Res Ther. 2016;11(3):255-264. doi:10.2174/1574888x10666150531173309
128. Guo B, Huang X, Lee MR, Lee SA, Broxmeyer HE. Antagonism of PPAR-γ signaling expands human hematopoietic stem and progenitor cells by enhancing glycolysis. Nat Med. 2018 Mar;24(3):360-367.
129. Greene ME, Pitts J, McCarville MA, et al. PPARgamma: observations in the hematopoietic system. Prostaglandins Other Lipid Mediat. 2000;62(1):45-73.
130. Podleśny-Drabiniok, A., Novikova, G., Liu, Y. et al. BHLHE40/41 regulate microglia and peripheral macrophage responses associated with Alzheimer's disease and other disorders of lipid-rich tissues. Nat Commun 15, 2058 (2024).
131. Kreslavsky T, Vilagos B, Tagoh H, et al. Essential role for the transcription factor Bhlhe41 in regulating the development, self-renewal and BCR repertoire of B-1a cells. Nat Immunol. 2017;18(4):442-455.
132. Gulbagci NT, Li L, Ling B, et al. SHARP1/DEC2 inhibits adipogenic differentiation by regulating the activity of C/EBP. EMBO Rep. 2009;10(1):79-86.
133. Baker SJ, Ma'ayan A, Lieu YK, John P, Reddy MV, Chen EY, Duan Q, Snoeck HW, Reddy EP. B-myb is an essential regulator of hematopoietic stem cell and myeloid progenitor cell development. Proc Natl Acad Sci U S A. 2014 Feb 25;111(8):3122-7.
134. Gal Ophir, Ninette Amariglio, Jasmine Jacob-Hirsch, Ran Elkon, Gideon Rechavi, Daniel M. Michaelson. Apolipoprotein E4 enhances brain inflammation by modulation of the NF-κB signaling cascade, Neurobiology of Disease. Volume 20, Issue 3, 2005, Pages 709-718, ISSN 0969-9961.

135. Zhu H, Hu X, Feng S, Li Y, Zhang Y, Qiu S, Chen R, Ye Y, Gu L, Jian Z, Xu X, Xiong X. APOL4, a Novel Immune-Related Prognostic Biomarker for Glioma. J Clin Med. 2022 Sep 29;11(19):5765.
136. Vanhollebeke B, Pays E. The function of apolipoproteins L. Cell Mol Life Sci. 2006;63(17):1937-1944.
137. Wang Y, Zhang L, Chen H, Yang J, Cui Y, Wang H. Coronary artery disease-associated immune gene RBP1 and its pan-cancer analysis. Front Cardiovasc Med. 2023 Mar 9;10:1091950.
138. Zhu YS, Mo TT, Jiang C, Zhang JN. Osteonectin bidirectionally regulates osteoblast mineralization. J Orthop Surg Res. 2023 Oct 8;18(1):761.
139. Zoch ML, Clemens TL, Riddle RC. New insights into the biology of osteocalcin. Bone. 2016 Jan;82:42-9.
140. Lund SA, Giachelli CM, Scatena M. The role of osteopontin in inflammatory processes. J Cell Commun Signal. 2009 Dec;3(3-4):311-22.
141. Kusuyama J, Bandow K, Ohnishi T, Hisadome M, Shima K, Semba I, Matsuguchi T. Osteopontin inhibits osteoblast responsiveness through the down-regulation of focal adhesion kinase mediated by the induction of low-molecular weight protein tyrosine phosphatase. Mol Biol Cell. 2017 May 15;28(10):1326-1336.
142. Furuhashi M, Saitoh S, Shimamoto K, Miura T. Fatty Acid-Binding Protein 4 (FABP4): Pathophysiological Insights and Potent Clinical Biomarker of Metabolic and Cardiovascular Diseases. Clin Med Insights Cardiol. 2015 Feb 2;8(Suppl 3):23-33.
143. Kagawa, Y., Low, Y.L., Pyun, J. et al. Fatty Acid-Binding Protein 4 is Essential for the Inflammatory and Metabolic Response of Microglia to Lipopolysaccharide. J Neuroimmune Pharmacol 18, 448–461 (2023).
144. Trinh T, Ropa J, Aljoufi A, et al. Leptin receptor, a surface marker for a subset of highly engrafting long-term functional hematopoietic stem cells. Leukemia. 2021;35(7):2064-2075.
145. Fantuzzi G, Faggioni R. Leptin in the regulation of immunity, inflammation, and hematopoiesis. J Leukoc Biol. 2000;68(4):437-446. Pérez-Pérez A, Sánchez-Jiménez F, Vilariño-García T, Sánchez-Margalet V. Role of Leptin in Inflammation and Vice Versa. Int J Mol Sci. 2020 Aug 16;21(16):5887.
146. Peters IJA, de Pater E, Zhang W. The role of GATA2 in adult hematopoiesis and cell fate determination. Front Cell Dev Biol. 2023 Nov 14;11:1250827.
147. Ganapathi KA, Townsley DM, Hsu AP, et al. GATA2 deficiency-associated bone marrow disorder differs from idiopathic aplastic anemia. Blood. 2015;125(1):56-70.
148. Suh HC, Gooya J, Renn K, Friedman AD, Johnson PF, Keller JR. C/EBPalpha determines hematopoietic cell fate in multipotential progenitor cells by inhibiting erythroid differentiation and inducing myeloid differentiation. Blood. 2006 Jun 1;107(11):4308-16.
149. Friedman AD. C/EBPα in normal and malignant myelopoiesis. Int J Hematol. 2015;101(4):330-341. doi:10.1007/s12185-015-1764-6.
150. Roberto Avellino, Ruud Delwel; Expression and regulation of C/EBPα in normal myelopoiesis and in malignant transformation. *Blood* 2017; 129 (15): 2083–2091.

151. Rosen ED, Hsu CH, Wang X, Sakai S, Freeman MW, Gonzalez FJ, Spiegelman BM. C/EBPalpha induces adipogenesis through PPARgamma: a unified pathway. Genes Dev. 2002 Jan 1;16(1):22-6.
152. Madsen MS, Siersbæk R, Boergesen M, Nielsen R, Mandrup S. Peroxisome proliferator-activated receptor γ and C/EBPα synergistically activate key metabolic adipocyte genes by assisted loading. Mol Cell Biol. 2014 Mar;34(6):939-54.
153. Robinson, K., Prins, J. & Venkatesh, B. Clinical review: Adiponectin biology and its role in inflammation and critical illness. Crit Care 15, 221 (2011).
154. DiMascio L, Voermans C, Uqoezwa M, et al. Identification of adiponectin as a novel hemopoietic stem cell growth factor. J Immunol. 2007;178(6):3511-3520.
155. Gil-Kulik P, Krzyżanowski A, Dudzińska E, Karwat J, Chomik P, Świstowska M, Kondracka A, Kwaśniewska A, Cioch M, Jojczuk M, Nogalski A, Kocki J. Potential Involvement of BIRC5 in Maintaining Pluripotency and Cell Differentiation of Human Stem Cells. Oxid Med Cell Longev. 2019 Jan 10;2019:8727925.
156. Leung CG, Xu Y, Mularski B, Liu H, Gurbuxani S, Crispino JD. Requirements for survivin in terminal differentiation of erythroid cells and maintenance of hematopoietic stem and progenitor cells. J Exp Med. 2007;204(7):1603-1611.
157. Hettler F, Schreck C, Marquez SR, Engleitner T, Vilne B, Landspersky T, Weidner H, Hausinger R, Mishra R, Oellinger R, Rauner M, Naumann R, Peschel C, Bassermann F, Rad R, Istvanffy R, Oostendorp RAJ. Osteoprogenitor SFRP1 prevents exhaustion of hematopoietic stem cells via PP2A-PR72/130-mediated regulation of p300. Haematologica. 2023 Feb 1;108(2):490-501.
158. Yao W, Cheng Z, Shahnazari M, Dai W, Johnson ML, Lane NE. Overexpression of secreted frizzled-related protein 1 inhibits bone formation and attenuates parathyroid hormone bone anabolic effects. J Bone Miner Res. 2010 Feb;25(2):190-9.
159. Peter V. N. Bodine, Weiguang Zhao, Yogendra P. Kharode, Frederick J. Bex, Andre-Jean Lambert, Mary Beth Goad, Tripti Gaur, Gary S. Stein, Jane B. Lian, Barry S. Komm, The Wnt Antagonist Secreted Frizzled-Related Protein-1 Is a Negative Regulator of Trabecular Bone Formation in Adult Mice, Molecular Endocrinology, Volume 18, Issue 5, 1 May 2004, Pages 1222–1237.
160. Moorer MC, Riddle RC. Regulation of Osteoblast Metabolism by Wnt Signaling. Endocrinol Metab (Seoul). 2018 Sep;33(3):318-330.
161. Zhang X, Wang P, Chen T, et al. Kctd9 Deficiency Impairs Natural Killer Cell Development and Effector Function. Front Immunol. 2019;10:744. Published 2019 Apr 10.
162. Yao, H., Ren, D., Wang, Y. et al. KCTD9 inhibits the Wnt/β-catenin pathway by decreasing the level of β-catenin in colorectal cancer. Cell Death Dis 13, 761 (2022).
163. Angrisani, A., Di Fiore, A., De Smaele, E. et al. The emerging role of the KCTD proteins in cancer. Cell Commun Signal 19, 56 (2021).
164. Jiang J, Li X, Zhang C, Wang J, Li J. Anti-cancer effects of Coix seed extract through KCTD9-mediated ubiquitination of TOP2A in lung adenocarcinoma. Cell Div. 2024;19(1):6. Published 2024 Feb 20.
165. Wagner EM. Monitoring gene expression: quantitative real-time rt-PCR. Methods Mol Biol. 2013;1027:19-45.

166. Tzec-Interián JA, González-Padilla D, Góngora-Castillo EB. Bioinformatics perspectives on transcriptomics: a comprehensive review of bulk and single-cell RNA sequencing analyses. Quantitative Biology. 2025;e78.
167. Groarke EM, Feng X, Aggarwal N, et al. Efficacy of JAK1/2 inhibition in murine immune bone marrow failure. Blood. 2023;141(1):72-89.
168. Kwon M, Kim BS, Yoon S, Oh SO, Lee D. Hematopoietic Stem Cells and Their Niche in Bone Marrow. Int J Mol Sci. 2024 Jun 21;25(13):6837. doi: 10.3390/ijms25136837.
169. Carmona-Luque M, Ballesteros-Ribelles A, Millán-López A, Blanco A, Nogueras S, Herrera C. The Effect of Cell Culture Passage on the Efficacy of Mesenchymal Stromal Cells as a Cell Therapy Treatment. J Clin Med. 2024 Apr 24;13(9):2480. doi: 10.3390/jcm13092480.
170. Hughes AM, Kuek V, Oommen J, Kotecha RS, Cheung LC. Murine bone-derived mesenchymal stem cells undergo molecular changes after a single passage in culture. Sci Rep. 2024 May 29;14(1):12396. doi: 10.1038/s41598-024-63009-8.
171. Wang XA, Li JP, Wu KH, Yang SF, Chao YH. Mesenchymal Stem Cells in Acquired Aplastic Anemia: The Spectrum from Basic to Clinical Utility. Int J Mol Sci. 2023 Feb 24;24(5):4464. doi: 10.3390/ijms24054464.

VI. Development of a decellularized human bone marrow scaffold for *ex vivo* disease modelling

VI.1. Summary

Bone marrow microenvironment (BMME) plays a critical role in the development and function of blood cells. In AA, BMME disruption has been shown to contribute to disease pathophysiology and severity. Consequently, to better understand the mechanisms of disease it is relevant to develop a model that incorporates structural and biochemical cues of the natural BM microenvironment in order to circumvent the limitations of plastic-based 2D culture systems.

Considering that, aiming at the development of a 3D biological culture system that better represents the human BM microenvironment ultrastructural and chemical complexity, a human bone (femoral head/neck) detergent-free decellularization protocol was established and optimized.

Healthy bone samples collected in the context of elective hip replacement surgery (n=5; median age = 59 years; minimum = 52 years; maximum = 65 years) were decellularized and characterized by histochemistry (H&E), immunohistochemistry (collagen type I, fibronectin, stromal cell–derived factor 1) and scanning electron microscopy (SEM).

Ex vivo co-culture of control-derived BM-MSCs in decellularized bone extracellular matrix (dECM) scaffolds (5 mm, 10 mm and 15 mm of diameter) was performed for 17 days. Cellular viability assay, performed at different timepoints, showed an increase in cellular metabolic activity of scaffold plus BM-MSCs in comparison to controls (empty scaffold or medium only). A plateau was attained at day 10.

BM-MSCs expansion and extracellular matrix formation were demonstrated by microscopy. It was noticed that cell expansion in dECM scaffold was heterogeneous, with higher cell densities and ECM deposition identified in the upper half of the scaffold. This was hypothesized to be related to cell seeding methodology and/or to scaffold mineralization.

Overall, decellularization protocol showed to be feasible, while maintaining significant physiological properties of human bone (e.g., 3D structural integrity; ECM biochemical properties). The successful culture of BM-MSCs onto the human dECM scaffold is relevant as a preliminary result to proceed towards the development of an *ex vivo* human BM model for disease study and modulation.

VI.2. Background

Human bone is composed of an outer layer of compact (cortical) bone, organized in osteons (Haversian systems), inside of which is the spongy (cancellous) bone, composed of trabeculae (thin bony struts) arranged in a network that provides strength while minimizing weight. Trabeculae form interconnected spaces, where BM cells and niche elements reside [1]. HSPC are preferentially localized to trabecular bone area [2].

The BM niche is a complex microenvironment, composed of cellular (e.g., MSCs, osteoblasts, osteoclasts, endothelial cells, adipocytes, macrophages, sympathetic nerves) and ECM components (e.g., glycoproteins, as fibronectin, osteonectin, laminin; collagens, as collagen type I; proteoglycans and hyaluronan), which provide biophysical and signaling cues, influencing cell proliferation, differentiation, adhesion and migration, thus regulating HSPC functioning and hematopoiesis [3].

Adding to this, physical factors, such as oxygen tension (e.g., HSPC reside in areas with low oxygen levels) [4] and shear stress (e.g., blood flow creates mechanical forces that could influence HSPC functioning) [5], increase the level of complexity of BM microenvironment, further contributing to the limitations of current experimental approaches to study HSPC and BM niche and to their low reproducibility *in vivo* [6].

Figure 50 depicts BM niche is composed of distinct functional areas – the endosteal niche, also known as the osteoblastic niche, which provides osteoblast-secreted cytokines and ECM proteins, essential for HSC maintenance and self-renewal; and the perisinusoidal vascular niche, adjacent to blood vessels lined by endothelial cells and perivascular cells such as MSCs, which provides HSPC with nutrients, oxygen and signaling molecules essential for proliferation, differentiation and survival [7]. More recently, a periarteriolar niche maintained by mechanical stimulation (through mechanosensitive ion channel PIEZO1) was described, appearing to play a role in osteogenesis and lymphopoiesis [8].

Over the years, to improve bone tissue research, 3D cell culture models have been developed, such as synthetic scaffolds [9-12], bio-functionalized scaffolds [13-16], natural or synthetic polymers-based hydrogels [9,11,17], microspheres or organoids [18,21], 3D printing [22,23], as well as decellularized ECM (obtained by decellularization of ECM produced by stromal cells *in vitro*) [24].

Despite those advances, *in vitro* recreation of the intricate BM niche has been challenging, with no optimal system attained. To circumvent those limitations, BM decellularization models have been attempted, with increasing interest, based on the hypothesis that biological, naturally derived, ECM scaffolds would better recreate the structural and chemical complexity of the BM niche.

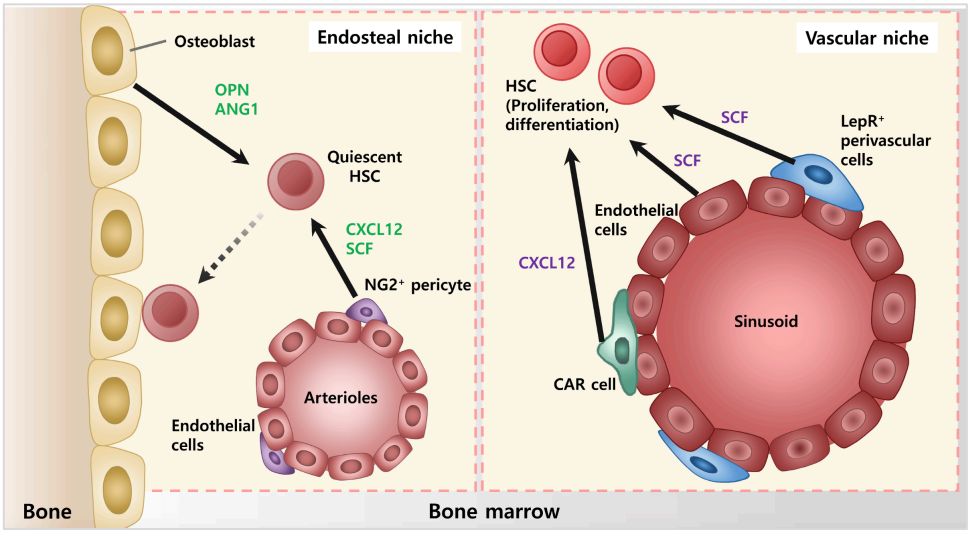

Figure 50: Bone marrow microenvironment. The bone marrow (BM) hosts two crucial hematopoietic stem cell (HSC) microenvironments: the endosteal and vascular niches. The endosteal niche, located at the bone surface, is recognized as the "osteoblastic niche" due to the significant role of osteoblasts in promoting HSC quiescence and self-renewal. In parallel, the vascular niche, positioned alongside blood vessels, serves to stimulate HSC proliferation and differentiation through its rich supply of nutrients and signaling factors. This latter niche comprises endothelial cells, pericytes, and smooth muscle cells. Collectively, these distinct niches are fundamental to regulating HSC maintenance and activity within the BM. HSC: hematopoietic stem cells; CAR cell: CXCL12-abundant reticular stromal cells; LepR+: leptin receptor positive perivascular stromal cells; NG2+: neuroglial antigen 2 stromal pericytes. OPN: Osteopontin. ANG1: Angiopoietin-1, SCF: Stem cell factor (from [7]).

According to published data, decellularized bone marrow scaffolds were successfully established in bovine [25] and porcine [26] samples, either by detergent-free or high-hydrostatic pressurization method, respectively. More recently, a

decellularized human bone (femoral head) 3D platform was developed [27] and applied to study human BM-MSCs subjected to dynamic culture (e.g., sheer and compressive stress) in a bioreactor system. In comparison to static controls, both dynamic conditions improved cell repopulation within the scaffold and boosted ECM production [28].

Despite promising, decellularization protocols between studies are heterogeneous and sometimes omissive, which limits their application. On the other hand, human bone size and consistency differs from animal tissues, which difficult strict application of those protocols into human samples.

As discussed in previous sections, interpretation of 2D cell culture experiments should be performed cautiously, since those models lack architectural and biochemical properties of biological tissues, as is the case of BM microenvironment, with all its complexity and cues that influence cellular functioning and crosstalk.

The need for optimization of a research model in AA, as concluded from previously published data as well as from the experiments performed in the context of this project, was the basis for the development of a decellularized human bone marrow platform to be applied in further research steps, aiming to provide a BM platform for disease study and modulation.

To establish that model, a previously published detergent-free free bovine bone decellularization protocol, involving mechanical disruption (agitation; freeze-thawing), enzymatic digestion (trypsin; benzonase), chemical washing (EDTA - chelating agent; Tris Base - buffer) and polar solvent extraction (isopropanol), was adapted and optimized for human bone (femoral head/neck) [25]. The option for a detergent-free methodology was related to the fact that detergents, even in low dose, were shown to be able to denature collagen molecules [31] and were detected in residual amounts in decellularized tissues, disrupting the ECM biochemical composition and topographical ligand landscape, with adverse cell seeding behaviour [32].

VI.3. Results and discussion

VI.3.1. Optimization of a human bone marrow decellularization protocol

As described previously (section II.20.), a human bone marrow decellularization protocol was performed and optimized in healthy bone samples (n=5; median age = 59 years; minimum = 52 years; maximum = 65 years) collected in the context of elective hip replacement surgery.

Macroscopic appearance of femoral bone fragments after surgical collection and decellularization are represented in Figure 51.

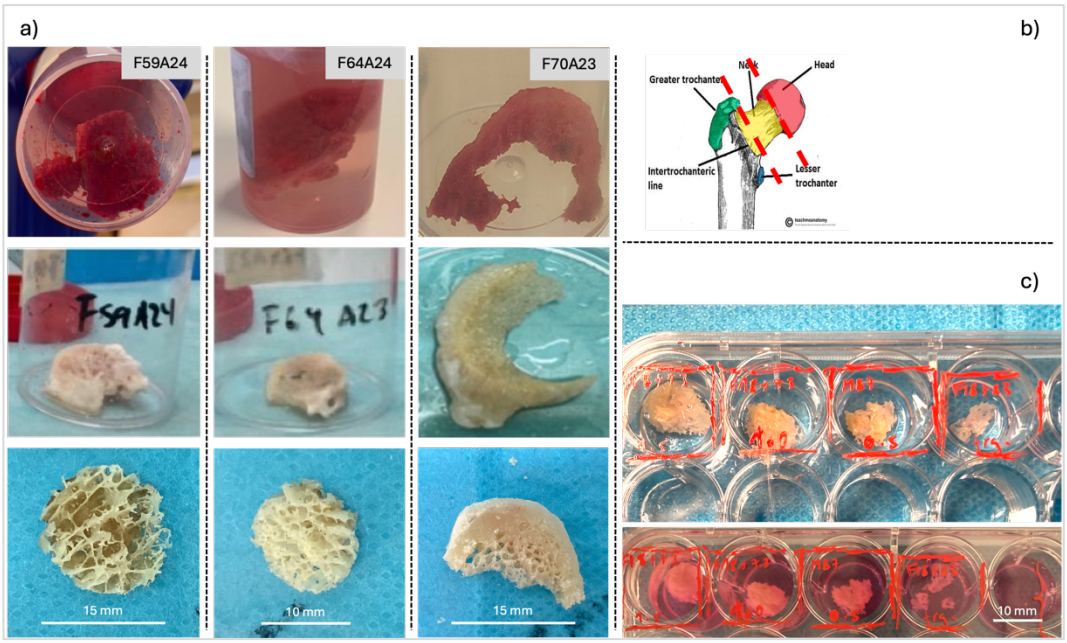

Figure 51: Human femoral bone samples – **a)** after surgical collection (upper row), after PBS (1x) washing of the surgical piece, before bone separation in smaller fragments and decellularization (middle row), and after decellularization (lower row); **b)** schematic representation of bone sample collection area (between the dashed red lines) **c)** representative image of decellularized femoral bone scaffolds placed in ultra-low attachment 24-well plate - empty scaffolds (upper row); BM-MSCs seeded scaffolds embed in 10% FBS MSCs-qualified supplemented medium (lower row).

It is important to notice that, despite EDTA washings, bone fragments maintained their stiffness and hardness, even after the decellularization protocol, which limited the capacity to obtain homogeneous scaffolds, even using a punch biopsy needle of similar diameter (5 mm, 10 mm, 15 mm diameters were tried). In addition, scaffold thickness varied between 3 to 5 mm, with some degree of bone crushing at the cutting limits. To circumvent those limitations, an attempt of EDTA-based decalcification either before or after decellularization protocol was made, however with poor and time-consuming results, even for smaller bone samples, thus implying the application of more tissue aggressive chemicals, such as formic acid and formaldehyde [33,34]. This was the reason why decalcification protocol was performed only before histological processing (paraffin embedding and sectioning), therefore not influencing BM-MSCs + dECM co-culture.

In research context, bone decalcification (removal of bone mineral component, namely hydroxyapatite) is mainly performed to increase bone matrix porosity, thus enhancing cellular infiltration and bone regeneration; to improve biocompatibility, since decalcification is related to exposure of bone bioactive molecules (e.g., bone morphogenetic protein), promoting cell adhesion, proliferation and differentiation; and to reduce stiffness and increase bone tissue flexibility, which is relevant for scaffold shape according to specific experimental determinants. However, decalcification could also have negative impact on bone mechanical (e.g., demineralization weakens bone structural integrity) and biochemical (e.g., damage to organic compounds, such as collagen and other proteins, altering the topographical landscape and thus bone regenerative cues) properties, which implies a balanced demineralization strategy according to the research purpose [35,36].

In this experiment, it was decided to avoid aggressive decalcification methods as part of the decellularization protocol, in order to prevent disruption of bone matrix structure and biochemical cues that could affect experimental results in the context of a disease modeling approach. However, due to the biological nature of human femur, which is a long and strong bone, playing an important role in body weight support and locomotion, it was hard to separate bone fragments in a

reproducible manner, an issue that must be improved for the optimization of the decellularized BM platform under development.

The effectiveness of bone decellularization protocol was confirmed by histochemistry (H&E). As represented in Figure 52, ECM integrity showed to be preserved after decellularization, reinforcing the adequacy and further applicability of the protocol.

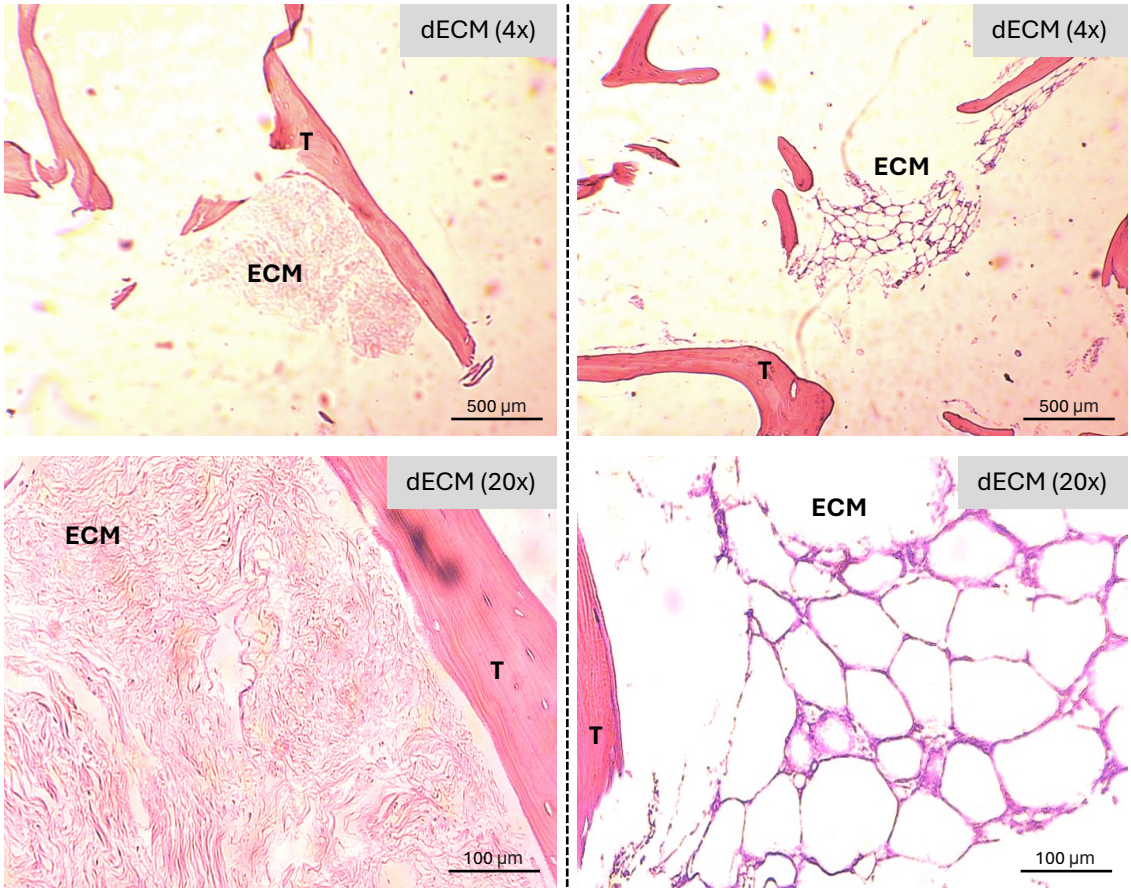

Figure 52: Representative H&E stainings of decellularized human bone (femoral head/neck) scaffolds. Eosin staining (pink-red color) representing preservation of extracellular matrix (ECM) components and bone trabeculae (T) after decellularization. Absence of blue-purple staining representative of cell nuclei (as would be revealed by hematoxylin). Histological samples imaged at 4x and 20x magnification on bright-field microscope (Olympus IX51 Inverted Microscope equipped with an attached digital camera).

The analysis of biochemical composition of dECM, assessed by immunohistochemistry, confirmed the presence of collagen type I and fibronectin (FN) after decellularization, as depicted in Figure 53.

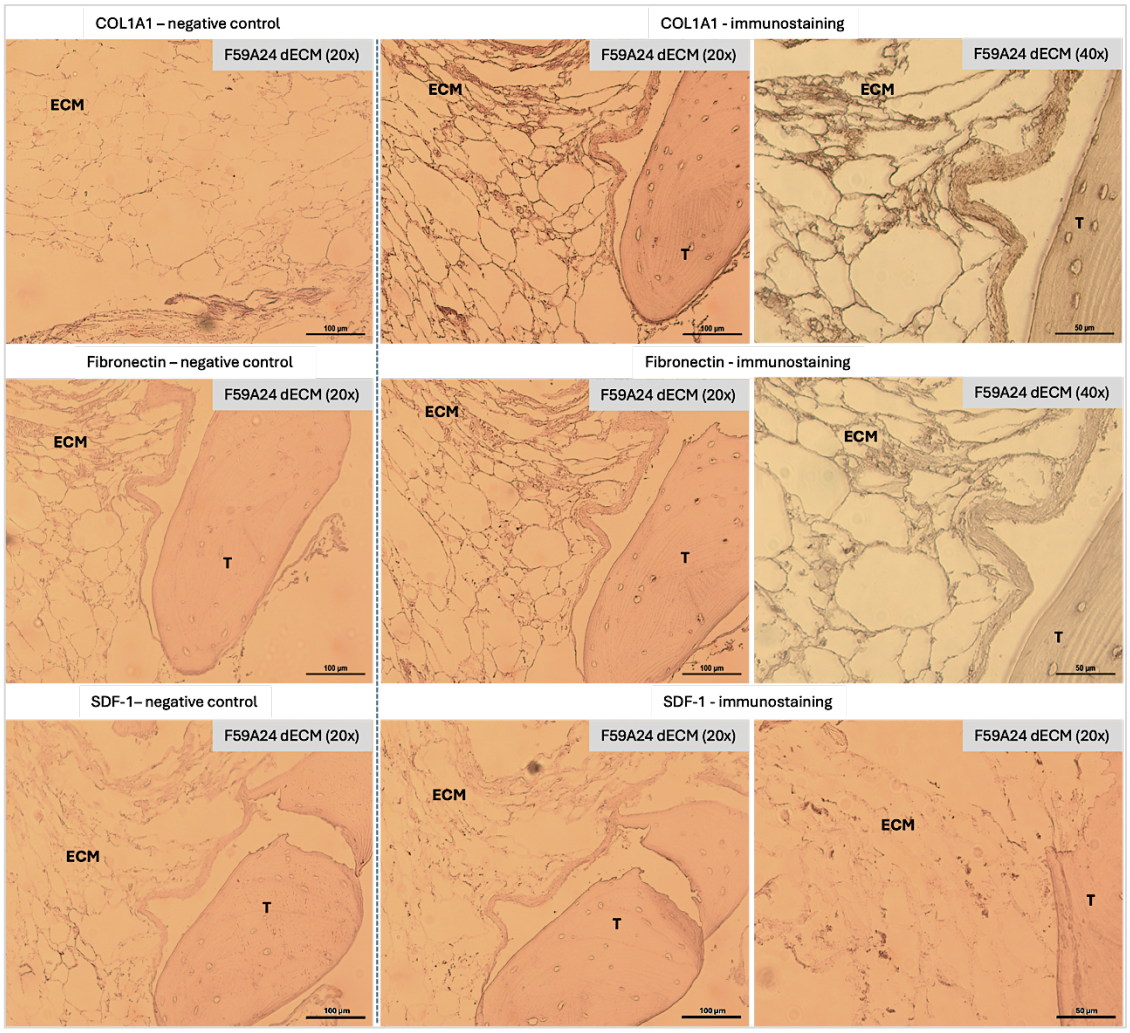

Figure 53: Representative immunohistochemical stainings of collagen type I (COL1A1), fibronectin (FN) and stromal cell–derived factor 1 (SDF-1), on human decellularized bone (femoral head/neck) extracellular matrix scaffolds (dECM). Positive staining for collagen type I (strong) and fibronectin (weak). Minimal staining/negativity for SDF-1. T = bone trabeculae; ECM = extracellular matrix. Histological samples imaged at 20x and 40x magnification on bright-field microscope (Olympus IX51 Inverted Microscope equipped with an attached digital camera).

Both collagen type I and fibronectin represent important, natural constitutive, ECM matrix elements.

Collagen type I is a main building block of bone, providing structural and functional (e.g., role in cell proliferation, differentiation and migration) support to cells within the BM [48,49,50].

Fibronectin is a key bone ECM component with an important role in: cell adhesion (e.g., mediated by specific binding sites for integrins) [39], allowing cells (e.g., MSCs, osteoblasts, osteoclasts, HSPC) to attach to bone ECM and to each other; ECM organization and stability (mediated by fibronectin polymerization), assuring that collagen fibers and other ECM components arrange correctly [40]; cell signaling, influencing the behavior of BM cells (e.g., cell proliferation, differentiation and migration), such as BM-MSCs (e.g., induction of BM-MSCs osteogenic differentiation by integrin α5β1-mediated activation of PI3K/AKT and Wnt/β-catenin signaling [42]) and HSCP (e.g., stimulation of myelopoiesis; HSPC migration, homing and retention [39]); and bone mineralization [41].

Conservation of those ECM components after decellularization corroborates the persistence of significant biological cues in the dECM platform under development, thus reinforcing its usefulness for studies in the context of BM-MSCs and HSPC biology.

After decellularization, the 3D structure and integrity of decellularized bone scaffolds was assessed by SEM, without previous decalcification. As represented in figure 54, below, 3D architecture showed to be preserved in all samples. However, as would be expected, bone destruction was observed at the cutting limits of bone pieces. At higher magnification power it is possible to detect the persistence of ECM fibers/fibrils (e.g., collagen) after decellularization. Image interpretation was performed with the aid of previously published data regarding SEM applications for bone imaging [37].

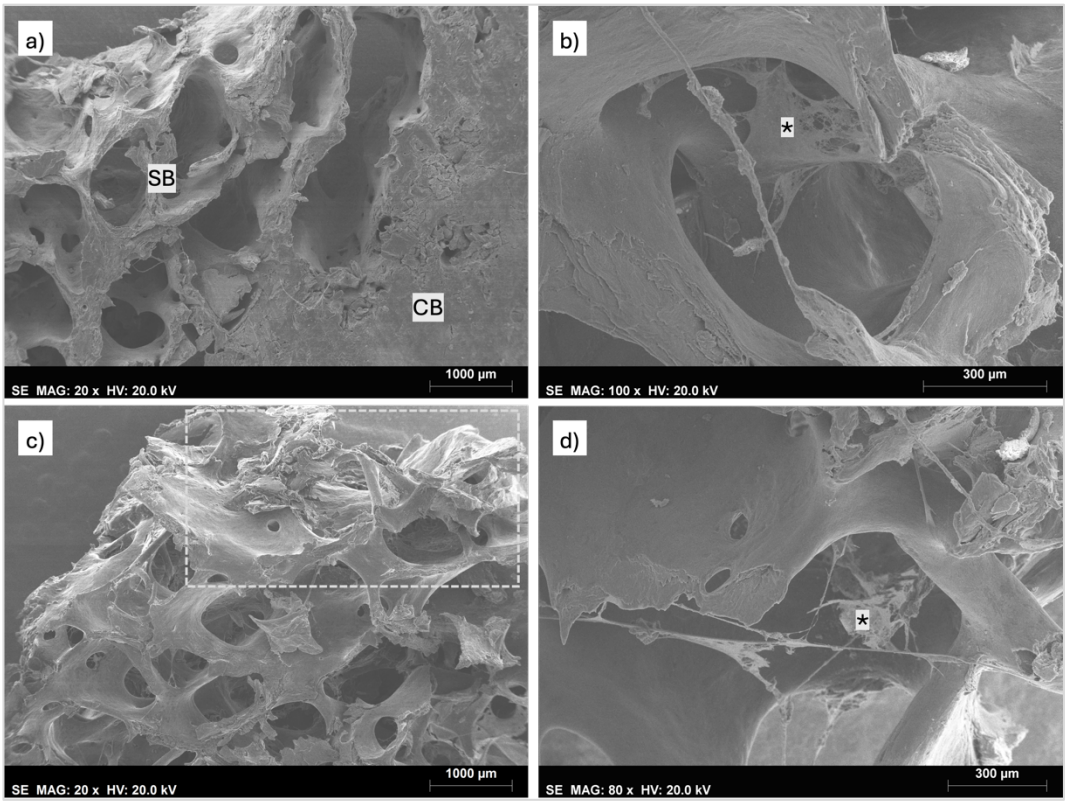

Figure 54: Representative SEM images of decellularized human bone (femoral head/neck) scaffolds – a) interface between compact bone (CB) and spongy bone (SB), showing preserved structural integrity; b) and d) decellularized bone trabecula with remaining ECM fibers/fibrils (*); c) bone structural disruption at the limits of bone cutting area (dashed box). Samples visualized on Hitachi scanning electron microscope (SEM), model S2400, with digital image acquisition by Bruker, software Quantax Esprit 1.9.

VI.3.2. Establishment of an *ex vivo* BM-MSCs 3D co-culture model on decellularized human femoral bone scaffolds

Ex vivo co-culture of control-derived BM-MSCs in decellularized bone extracellular matrix (dECM) scaffolds (5 mm, 10 mm and 15 mm of diameter) was performed for 17 days.

Cell viability assay (PrestoBlue™) was performed to assess cellular metabolic activity of scaffold-seeded cells at different timepoints, as a proxy of cell seeding and proliferation over time.

As depicted in Figure 55, below, an increase in cellular metabolic activity of scaffold plus BM-MSCs sets in comparison to controls (empty scaffold or medium only) was confirmed. However, it was not possible to conclude if scaffold size would influence the cell seeding and proliferative behaviour.

Regarding the decrease of fluorescence emission of 15 mm scaffold + BM-MSCs set at day 5, it was not possible to ascertain if it was due to biological issues or due to technical errors (e.g., inefficient cell seeding or attachment disruption due to shear stress induced by cell culture medium embedding or changes). For all setups, a plateau level was attained at day 10.

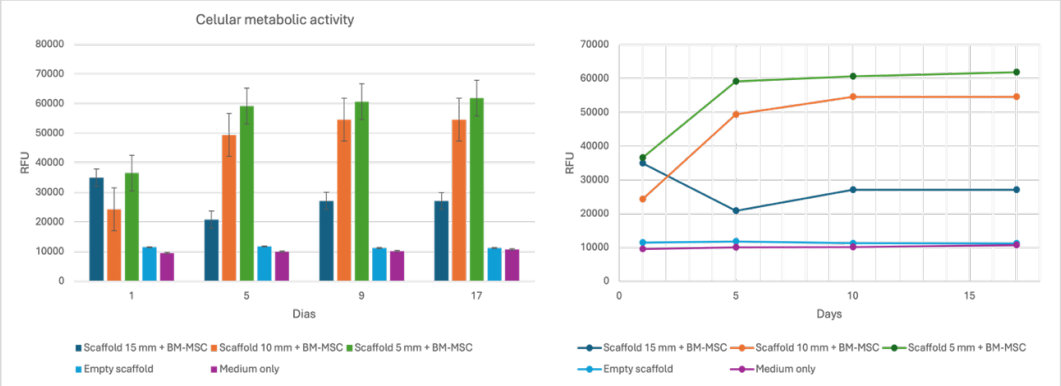

Figure 55: Cellular metabolic activity of control-derived BM-MSCs co-cultured in human bone (femoral head/neck) decellularized scaffolds of 5 mm, 10 mm or 15 mm of diameter, at different timepoints. Viability/metabolic assay performed with PrestoBlue™. Results expressed as mean relative fluorescence units (RFU) (±SE mean).

Histological head-to-head comparison of dECM scaffolds with control-derived BM-MSCs + dECM scaffolds sets after 17-day co-culture, represented in Figure 56, below, confirmed effective cell seeding and ECM deposition in co-culture sets. However, cell density and ECM deposition pattern in the seeded scaffolds were heterogeneous, with higher densities noticed in the upper half of the scaffold.

This heterogeneity was hypothesized to be related to either cell seeding methodology, since cells were seeded through the top surface of the scaffold (opposite to the basal surface, in contact with the bottom of the culture plate well), or to the conserved mineralized structure of the scaffold, which as previously mentioned could decrease porosity and limit cell permeation into the scaffold.

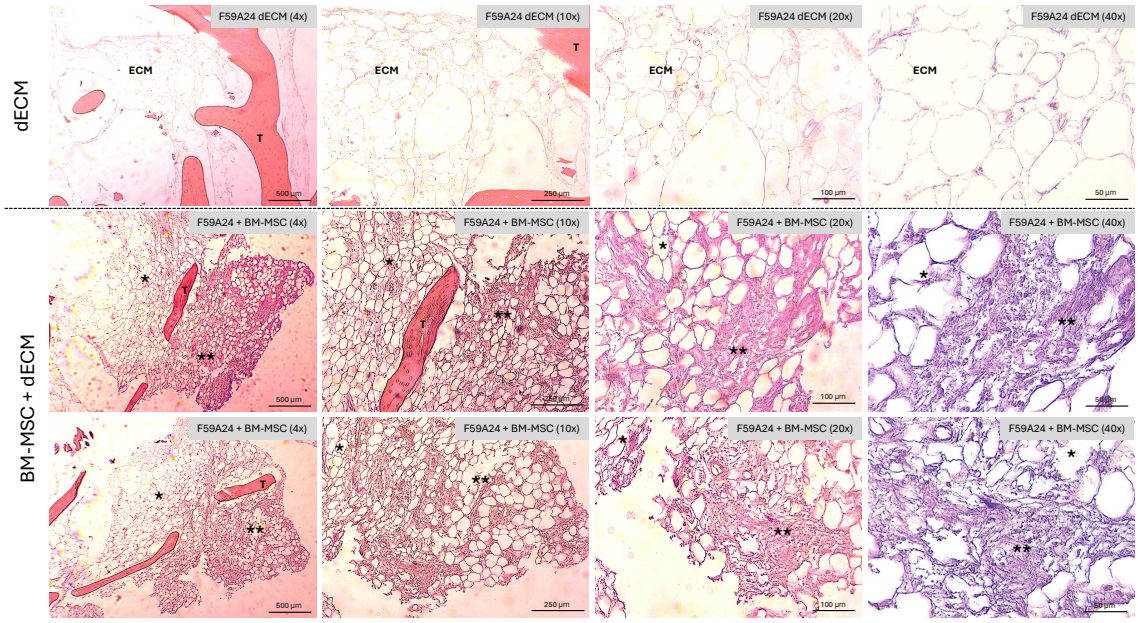

Figure 56: H&E stainings of decellularized human bone (femoral head/neck) scaffolds (upper row) in head-to-head comparison to BM-MSCs + dECM sets after 17-day co-culture. In contrast to dECM scaffolds, co-culture sets showed increased ECM deposition (pink-red color from eosin staining) and cellularity (dark-blue dots revealed by hematoxylin), in a heterogeneous pattern. T = bone trabeculae; * = ECM/cell lower-density areas; ** = ECM/cell higher-density areas. Histological samples imaged at 4x, 10x, 20x and 40x magnification on bright-field microscope (Olympus IX51 Inverted Microscope equipped with an attached digital camera).

ECM active production in control-derived BM-MSCs + dECM scaffolds co-culture sets was further confirmed by increased expression of collagen type I and fibronectin, as represented in Figure 57, below. Also represented is the increased expression of stromal cell-derived factor 1 (SDF-1) in the co-culture setting, denoting BM-MSCs activity.

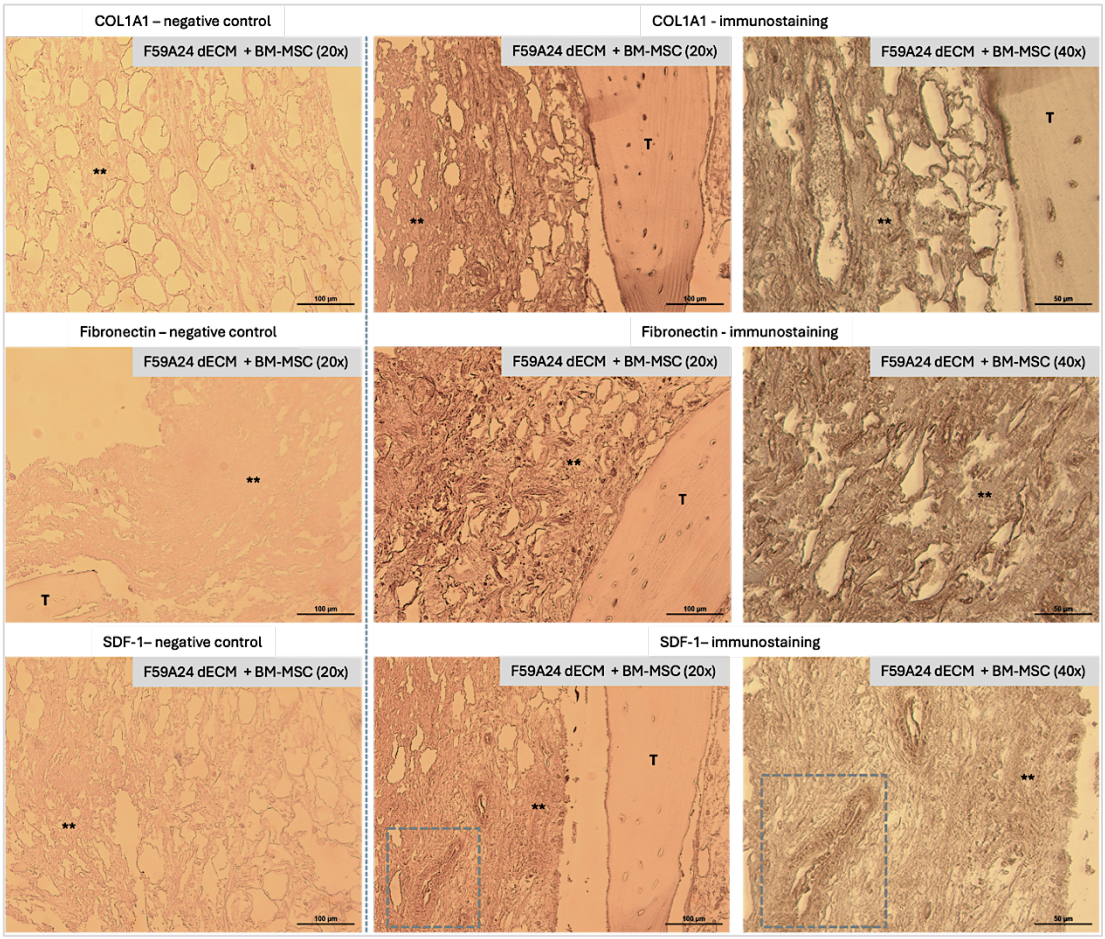

Figure 57: Representative immunohistochemical stainings of collagen type I (COL1A1), fibronectin (FN) and stromal cell–derived factor 1 (SDF-1), on BM-MSCs + dECM sets after 17-day co-culture. Positive staining for collagen type I (strong), fibronectin (strong) and SDF-1 (strong). ** = ECM/cell higher-density areas; dashed box = SDF-1 staining in blood vessel. T = bone trabeculae. Histological samples imaged at 20x and 40x magnification on bright-field microscope (Olympus IX51 Inverted Microscope equipped with an attached digital camera).

SDF-1 (also known as CXCL12, the ligand of CXCR4 receptor) is a chemokine present in several tissues, such as BM, where it is produced by stromal cells, osteoblasts and endothelial cells [46,47]. SDF-1 is a potent chemoattractant for hematopoietic cells, promoting the migration and engraftment of HSPC in specialized BM niches [43,44]. It is also an important regenerative molecule, whose release in the context of tissue injury creates a concentration gradient that attracts CXCR4 positive MSCs for tissue repairing through differentiation (e.g., osteoblast

differentiation in case of bone lesion), secretion of growth factors and immunomodulation [45].

The deposition of SDF-1 in control-derived BM-MSCs + dECM scaffolds sets observed in this experiment could be interpreted as a potential readout of the dECM platform capacity for HSPC support and expansion, which is planned to be tested in future works.

In accordance with the previous histological results, SEM imaging depicted cell seeding and active ECM deposition after 17-day co-culture of control-derived BM-MSCs in human bone scaffolds, as represented in Figure 58, below.

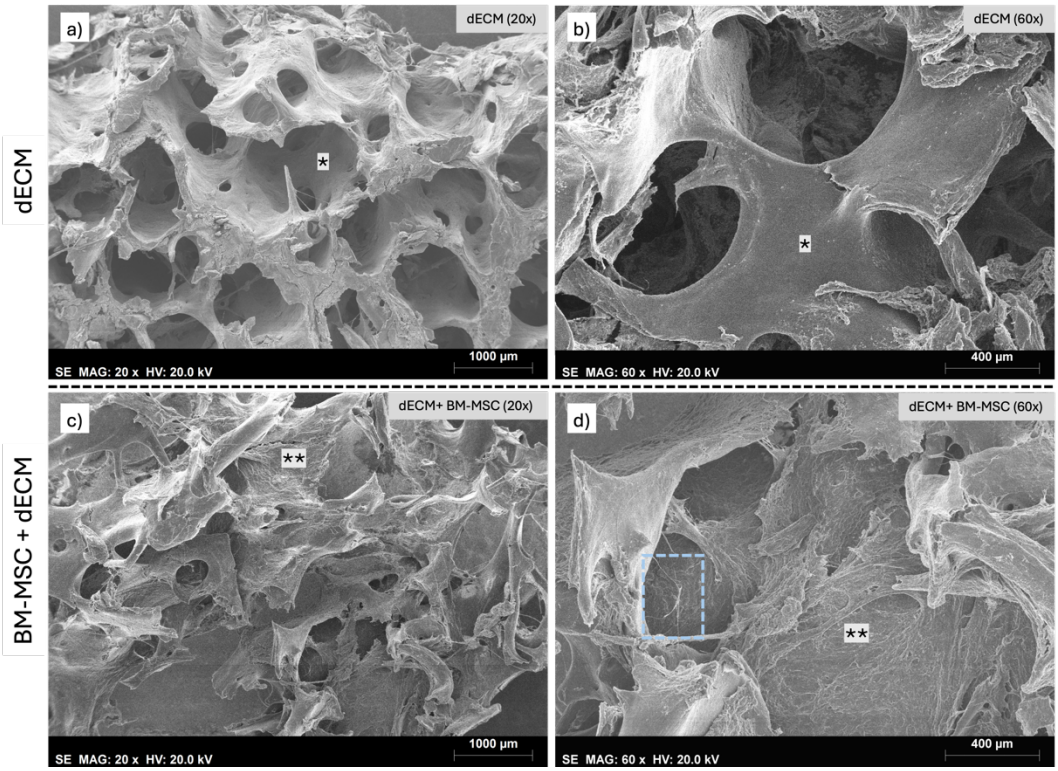

Figure 58: Representative SEM images of decellularized human bone (femoral head/neck) matrix (dECM) scaffold [a) and b)], compared to BM-MSCs + dECM scaffold set after 17-day co-culture [c) and d)]. Images c) and d) denoting rougher bone surface (**) in comparison to a) and b) (*), corresponding to active ECM deposition secondary to BM-MSCs activity. Mesenchymal stromal cell depicted in d) (dashed box). Samples visualized on Hitachi scanning electron microscope (SEM), model S2400, with digital image acquisition by Bruker, software Quantax Esprit 1.9.

VI.4. Conclusions

Considering the abovementioned results, it was concluded that the decellularization protocol was effective for human femoral bone samples, while preserving relevant biological properties for disease modeling and stem cell research, namely 3D structural integrity and ECM biochemical cues.

Co-culture of control-derived BM-MSCs in dECM scaffolds was feasible, and cell seeding and proliferation (assessed by proxy using a metabolic assay) as well as active ECM production were confirmed.

Upon the results, cell and ECM density heterogeneity in seeded dECM scaffolds should be further optimized to increase the efficiency of the model. A decalcification step before the decellularization protocol could be introduced in order to divide bone samples in identical parts (e.g., diameter; thickness) and increase porosity. In addition, a less harsh demineralization strategy (e.g. ultrasound decalcification with 0.5M, pH 7.4, EDTA solution, as published [38]) could be tested to reach an optimal balance between decreased bone hardness and increased porosity and preservation of the ultrastructural and biochemical properties of natural bone matrix.

As a final remark, with the goal of establishing a platform that better recreates the BM microenvironment, the experimental setup will be upgraded by the development of a bio-inspired prototype perfusion chamber system enclosing a dECM bone scaffold to support the expansion of either control-derived HSPC (in a first experimental stage) or of AA-derived HSPC in co-culture with functional BM-MSCs. The system is expected to allow a better mimicry of the *in vivo* BM niche towards different applications (e.g., disease study and modeling; generation of meaningful numbers of functional HSPC for regenerative medicine applications).

VI.5. References - Chapter VI

1. Bone. In: Mescher AL. eds. Junqueira's Basic Histology: Text and Atlas, 17th Edition. McGraw Hill; 2024. Assessed January 14, 2025.
2. Guezguez B, Campbell CJ, Boyd AL, et al. Regional localization within the bone marrow influences the functional capacity of human HSCs. Cell Stem Cell. 2013;13(2):175-189.
3. Lee-Thedieck C, Schertl P, Klein G. The extracellular matrix of hematopoietic stem cell niches. Adv Drug Deliv Rev. 2022 Feb;181:114069.
4. Jing D, Wobus M, Poitz DM, Bornhäuser M, Ehninger G, Ordemann R. Oxygen tension plays a critical role in the hematopoietic microenvironment in vitro. Haematologica. 2012 Mar;97(3):331-9.
5. Weijts B, Robin C. Capturing embryonic hematopoiesis in temporal and spatial dimensions. Exp Hematol. 2024;136:104257.
6. Congrains A, Bianco J, Rosa RG, Mancuso RI, Saad STO. 3D Scaffolds to Model the Hematopoietic Stem Cell Niche: Applications and Perspectives. Materials (Basel). 2021;14(3):569. Published 2021 Jan 26.
7. Kwon M, Kim BS, Yoon S, Oh SO, Lee D. Hematopoietic Stem Cells and Their Niche in Bone Marrow. Int J Mol Sci. 2024;25(13):6837. Published 2024 Jun 21.
8. Shen B, Tasdogan A, Ubellacker JM, et al. A mechanosensitive peri-arteriolar niche for osteogenesis and lymphopoiesis. Nature. 2021;591(7850):438-444.
9. Ventura, M.S.; Jahnen-dechent, W.; Labude, N.; Bovi, M.; Hieronymus, T.; Zenke, M.; Neurs, S. Cord blood-hematopoietic stem cell expansion in 3D fibrin scaffolds with stromal support. Biomaterials 2012, 33, 6987–6997.
10. Severn, C.E.; Hugo, M.; Eagle, M.J.; Rooney, P.; Mantalaris, A.; Toye, A.M. Polyurethane scaffolds seeded with CD34 + cells maintain early stem cells whilst also facilitating prolonged egress of haematopoietic progenitors. Sci. Rep. 2016, 6, 1–12.
11. Tomimori, Y.; Takagi, M.; Yoshida, T. The construction of an in vitro three-dimensional hematopoietic microenvironment for mouse bone marrow cells employing porous carriers. Cytotechnology 2000, 34, 121–130.
12. Bai, T.; Li, J.; Sinclair, A.; Imren, S.; Merriam, F.; Sun, F.; Delaney, C. Expansion of primitive human hematopoietic stem cells by culture in a zwitterionic hydrogel. Nat. Med. 2019, 25, 1566–1575.
13. Bourgine, P.E.; Klein, T.; Paczulla, A.M.; Shimizu, T.; Kunz, L.; Kokkaliaris, K.D. In vitro biomimetic engineering of a human hematopoietic niche with functional properties. Proc. Natl. Acad. Sci. USA 2018, 115, 5689–5693.
14. Huang, X.; Zhu, B.; Wang, X.; Xiao, R.; Wang, C. Three-dimensional co-culture of mesenchymal stromal cells and differentiated osteoblasts on human bio-derived bone scaffolds supports active multi-lineage hematopoiesis in vitro : Functional implication of the biomimetic HSC niche. Int. J. Mol. Med. 2016, 38, 1141–1151.
15. Abarrategi, A.; Mufti, G.; Bonnet, D.; Abarrategi, A.; Foster, K.; Hamilton, A.; Bonnet, D. Versatile humanized niche model enables study of normal and malignant human hematopoiesis Versatile humanized niche model enables study of normal and malignant human hematopoiesis. J. Clin. Investig. 2017, 127, 543–548.

16. Raic, A.; Rödling, L.; Kalbacher, H.; Lee-thedieck, C. Biomaterials Biomimetic macroporous PEG hydrogels as 3D scaffolds for the multiplication of human hematopoietic stem and progenitor cells. Biomaterials 2014, 35, 929–940.
17. Leisten, I.; Kramann, R.; Ventura, M.S.; Bovi, M.; Neuss, S.; Ziegler, P.; Schneider, R.K. 3D co-culture of hematopoietic stem and progenitor cells and mesenchymal stem cells in collagen scaffolds as a model of the hematopoietic niche. Biomaterials 2012, 33, 1736–1747.
18. Lai, W.Y.; Li, Y.Y.; Mak, S.K.; Ho, F.C.; Chow, S.T.; Chooi, W.H.; Chan, B.P. Reconstitution of bone-like matrix in osteogenically differentiated mesenchymal stem cell—Collagen constructs: A three-dimensional in vitro model to study hematopoietic stem cell niche. J. Tissue Eng. 2013, 4, 1–13.
19. Pievani, A.; Sacchetti, B.; Corsi, A.; Rambaldi, B.; Donsante, S.; Scagliotti, V.; Riminucci, M. Human umbilical cord blood-borne fibroblasts contain marrow niche precursors that form a bone / marrow organoid in vivo. Development 2017, 144, 1035–1044.
20. Hur, J.; Park, J.; Lee, S.E.; Yoon, C.-H.; Jang, J.H.; Yang, J.M.; Kim, H.-S. Human peripheral blood-born hematosphere as a niche for hematopoietic stem cell expansion. Cell Res. 2011, 45, 987–990.
21. Isern, J.; Martin-Antonio, B.; Ghazanfari, R.; Martin, A.M.; Lopez, J.A.; Toro, R.; Mendez-Ferre, S. Self-Renewing Human Bone Marrow Mesenspheres Promote Hematopoietic Stem Cell Expansion. Cell Rep. 2013, 3, 1714–1724.
22. Zhou, D.; Chen, L.; Ding, J.; Zhang, X.; Nie, Z.; Li, X. A 3D engineered scaffold for hematopoietic progenitor/stem cell co-culture in vitro. Sci. Rep. 2020, 10, 1–11.
23. Braham, M.V.J.; Ahlfeld, T.; Akkineni, A.R.; Minnema, M.C.; Dhert, W.J.A.; Robin, C.; Alblas, J. Endosteal and Perivascular Subniches in a 3D Bone Marrow Model for Multiple Myeloma. Tissue Eng. Part C Methods 2018, 24, 300–313.
24. Kräter, M.; Jacobi, A.; Otto, O.; Tietze, S.; Müller, K.; David, M.; Wobus, M. Bone marrow niche-mimetics modulate HSPC function via integrin signaling. Sci. Rep. 2017, 7, 1–15.
25. Bianco JER , Rosa RG , Congrains-Castillo A , et al. Characterization of a novel decellularized bone marrow scaffold as an inductive environment for hematopoietic stem cells. Biomater Sci. 2019;7(4):1516-1528.
26. Hashimoto, Y.; Funamoto, S.; Kimura, T.; Nam, K.; Fujisato, T.; Kishida, A. The effect of decellularized bone/bone marrow produced by high-hydrostatic pressurization on the osteogenic differentiation of mesenchymal stem cells. Biomaterials 2011, 32, 7060–7067.
27. Pereira AR, Rudert M, Herrmann M. Decellularized human bone as a 3D model to study skeletal progenitor cells in a natural environment. Methods Cell Biol. 2020;157:123-141.
28. Pereira AR, Lipphaus A, Ergin M, et al. Modeling of the Human Bone Environment: Mechanical Stimuli Guide Mesenchymal Stem Cell-Extracellular Matrix Interactions. Materials (Basel). 2021;14(16):4431. Published 2021 Aug 7.
29. Safdari M, Bibak B, Soltani H, Hashemi J. Recent advancements in decellularized matrix technology for bone tissue engineering. Differentiation. 2021;121:25-34.
30. Brouki Milan P, Masoumi F, Biazar E, Zare Jalise S, Mehrabi A. Exploiting the Potential of Decellularized Extracellular Matrix (ECM) in Tissue Engineering: A Review Study. Macromol Biosci. 2025;25(1):e2400322.

31. Hwang J, San BH, Turner NJ, et al. Molecular assessment of collagen denaturation in decellularized tissues using a collagen hybridizing peptide. Acta Biomater. 2017;53:268-278.
32. White LJ, Taylor AJ, Faulk DM, et al. The impact of detergents on the tissue decellularization process: A ToF-SIMS study. Acta Biomater. 2017;50:207-219.
33. Naresh KN, Lampert I, Hasserjian R, Lykidis D, Elderfield K, Horncastle D, Smith N, Murray-Brown W, Stamp GW. Optimal processing of bone marrow trephine biopsy: the Hammersmith Protocol. J Clin Pathol. 2006 Sep;59(9):903-11.
34. Lee SH, Erber WN, Porwit A, Tomonaga M, Peterson LC; International Council for Standardization In Hematology. ICSH guidelines for the standardization of bone marrow specimens and reports. Int J Lab Hematol. 2008 Oct;30(5):349-64.
35. Tang G, Liu Z, Liu Y, Yu J, Wang X, Tan Z, Ye X. Recent Trends in the Development of Bone Regenerative Biomaterials. Front Cell Dev Biol. 2021 May 7;9:665813.
36. Savi FM, Brierly GI, Baldwin J, Theodoropoulos C, Woodruff MA. Comparison of Different Decalcification Methods Using Rat Mandibles as a Model. J Histochem Cytochem. 2017 Dec;65(12):705-722.
37. Shah FA, Ruscsák K, Palmquist A. 50 years of scanning electron microscopy of bone-a comprehensive overview of the important discoveries made and insights gained into bone material properties in health, disease, and taphonomy. Bone Res. 2019 May 22;7:15.
38. Chow DH, Zheng L, Tian L, Ho KS, Qin L, Guo X. Application of ultrasound accelerates the decalcification process of bone matrix without affecting histological and immunohistochemical analysis. J Orthop Translat. 2018 Sep 5;17:112-120.
39. Wirth F, Lubosch A, Hamelmann S, Nakchbandi IA. Fibronectin and Its Receptors in Hematopoiesis. Cells. 2020 Dec 18;9(12):2717.
40. Sottile J, Hocking DC. Fibronectin polymerization regulates the composition and stability of extracellular matrix fibrils and cell-matrix adhesions. Mol Biol Cell. 2002 Oct;13(10):3546-59.
41. Neha E. H. Dinesh, Philippe M. Campeau, and Dieter P. Reinhardt. Fibronectin isoforms in skeletal development and associated disorders. American Journal of Physiology-Cell Physiology 2022 323:2, C536-C549.
42. Saidak Z, Le Henaff C, Azzi S, Marty C, Da Nascimento S, Sonnet P, Marie PJ. Wnt/β-catenin signaling mediates osteoblast differentiation triggered by peptide-induced α5β1 integrin priming in mesenchymal skeletal cells. J Biol Chem. 2015 Mar 13;290(11):6903-12.
43. Lapidot T, Dar A, Kollet O. How do stem cells find their way home? Blood. 2005 Sep 15;106(6):1901-10.
44. Singh P, Mohammad KS, Pelus LM. CXCR4 expression in the bone marrow microenvironment is required for hematopoietic stem and progenitor cell maintenance and early hematopoietic regeneration after myeloablation. Stem Cells. 2020 Jul;38(7):849-859.
45. Jin W, Liang X, Brooks A, Futrega K, Liu X, Doran MR, Simpson MJ, Roberts MS, Wang H. Modelling of the SDF-1/CXCR4 regulated in vivo homing of therapeutic mesenchymal stem/stromal cells in mice. PeerJ. 2018 Dec 6;6:e6072. doi: 10.7717/peerj.6072. PMID: 30564525; PMCID: PMC6286806.

46. Jung Y, Wang J, Schneider A, Sun YX, Koh-Paige AJ, Osman NI, McCauley LK, Taichman RS. Regulation of SDF-1 (CXCL12) production by osteoblasts; a possible mechanism for stem cell homing. Bone. 2006 Apr;38(4):497-508.
47. Yun HJ, Jo DY. Production of stromal cell-derived factor-1 (SDF-1)and expression of CXCR4 in human bone marrow endothelial cells. J Korean Med Sci. 2003 Oct;18(5):679-85.
48. Bentley SA, Alabaster O, Foidart JM. Collagen heterogeneity in normal human bone marrow. Br J Haematol. 1981 Jun;48(2):287-91.
49. Mizuno M, Fujisawa R, Kuboki Y. Type I collagen-induced osteoblastic differentiation of bone-marrow cells mediated by collagen-alpha2beta1 integrin interaction. J Cell Physiol. 2000 Aug;184(2):207-13.
50. Ghosh, K., Shome, D.K., Kulkarni, B. et al. Fibrosis and bone marrow: understanding causation and pathobiology. J Transl Med 21, 703 (2023).

VII. Final remarks and future directions

VII. Final remarks and future directions

The experiments performed in the context of this thesis project demonstrated that AA-derived BM-MSCs have distinct functional and molecular properties in comparison to control-derived BM-MSCs, thus influencing *in vitro* HSPC expansion.

In addition, despite no significant phenotypic and proliferative capacity differences between AA versus control-derived BM-MSCs were found, it was noticed that AA-derived BM-MSCs exhibited a tendency towards higher adipogenic differentiation in comparison to controls, which is consistent with previously published data and with the histological pattern of increased BM adipose tissue observed in trephine biopsies from AA patients.

From this point, a rational base is established for the study of AA-derived HSPC phenotypic, functional and molecular properties to evaluate - a) if, as demonstrated in control samples, AA-derived HSPC expansion differs according to feeder layer source (AA versus control-derived BM-MSCs); b) if AA-derived HSPC expansion could be optimized by co-culture with control-derived BM-MSCs feeder layer ± dECM 3D human bone scaffolds; c) whether drug modulation of AA-derived BM-MSCs´ cell signaling pathways, as assessed by the molecular studies performed, could reverse their less supportive effect on HSPC expansion.

Those goals are expected to allow not only the optimization of *ex vivo* culture settings towards the autologous expansion of AA-derived HSPC, but also to define strategies for *in vivo* modulation of AA-BM microenvironment, in a combined strategy to both improve immunomodulation and HSPC support (e.g., in adjunct to conventional treatments) and to recover a healthier niche for a more effective engraftment of HSPC (e.g., definition of the best conditioning regimens for HSPC autologous or allogeneic transplantation in AA).

To circumvent the structural and biochemical limitations of *in vitro* 2D culture systems, the natural human bone-derived dECM model that has been developed in this project showed to be feasible and thus will be applied to improve future experimental settings. Moreover, dynamic culture conditions (e.g., *ex vivo* perfusion chamber provided with a human bone dECM scaffold, under controlled oxygen tension and

biochemical composition) will be established, to better recreate the natural BM niche and thus attain more accurate and *in vivo* translatable results.

In what concerns molecular characterization, bulk mRNA-Seq was chosen as a first-glance strategy to effectively identify AA-associated molecular patterns, in a high-throughput manner. However, considering the advances in transcriptomics, single-cell mRNA sequencing will be a useful strategy in the future, being expected to better identify AA-derived BM-MSCs and HSPC specificities, namely, to find cell subpopulations associated either with disease establishment and severity or, on the contrary, with BM-MSCs-associated response against the immunological cytotoxic attack over HSPC that takes place in AA. Molecular study at the single-cell level resolution will thus be attempted, towards a better understanding of disease and, consequently, a better knowledge on how to develop novel therapeutic strategies for AA treatment.

In a future perspective, a co-culture device based on microfluidics as a bioengineered BM proxy for disease modeling and drug testing in the context of AA is also planned to be developed (in collaboration with INESC MN/i4HB), which is in line with the ultimate research goal of advancing personalized medicine and targeted therapies in aplastic anemia.

To conclude, it is important to remark the importance of strengthening the collaboration with the clinical units involved in the project, not only to increase the number of study samples (either disease or control-derived samples) available in the biobank, but also to share and discuss the experimental results, as well as to learn from the clinicians more about the *in vivo*, real-world, behaviour of disease (and of therapy responses and toxicities), which will provide us with relevant data to define research topics of interest and priorities.

VIII. Scientific outputs

VIII. Scientific outputs

Scientific outputs developed in the context of thesis project:

1.) Carvalho MS, Alves L, Bogalho I, Cabral JMS, da Silva CL. Impact of Donor Age on the Osteogenic Supportive Capacity of Mesenchymal Stromal Cell-Derived Extracellular Matrix. Front Cell Dev Biol. 2021 Oct 5;9:747521. doi: 10.3389/fcell.2021.747521. PMID: 34676216; PMCID: PMC8523799.

2.) Margarida Coucelo, Joana Azevedo, Isabel Bogalho, Ana Teresa Simões et al. OC 4 - NEXT GENERATION SEQUENCING APPROACH TO BONE MARROW FAILURE SYNDROMES – PORTUGUESE EXPERIENCE, EJC Paediatric Oncology, Volume 2, Supplement 1, 2023, 100035.

List of works under preparation for publication:

1.) I. Bogalho Martins; P. Kjöllerström, J. Sarmento Esteves, J. Santos, A, M. Coucelo, A. Teresa Simões, A. Catarina Oliveira, A. Fernandes-Platzgummer, D. Henrique, C.L. da Silva. Transcriptomic profiling of bone marrow-derived mesenchymal stromal cells from patients with acquired idiopathic aplastic anemia. [Experimental Hematology - https://www.exphem.org/]

2.) Ex Vivo Modeling of Aplastic Anemia Using an optimized 3D Decellularized Human Femoral Bone Platform (in collaboration with FCUL, iBB-SCERG (Focus Area C), iBB-BERG).

IX. References

1. Abarrategi, A.; Mufti, G.; Bonnet, D.; Abarrategi, A.; Foster, K.; Hamilton, A.; Bonnet, D. Versatile humanized niche model enables study of normal and malignant human hematopoiesis Versatile humanized niche model enables study of normal and malignant human hematopoiesis. J. Clin. Investig. 2017, 127, 543–548.
2. Aggarwal BB, Gupta SC, Kim JH. Historical perspectives on tumor necrosis factor and its superfamily: 25 years later, a golden journey. Blood. 2012 Jan 19;119(3):651-65.
3. Ahmad MK, Abdollah NA, Shafie NH, Yusof NM, Razak SRA. Dual-specificity phosphatase 6 (DUSP6): a review of its molecular characteristics and clinical relevance in cancer. Cancer Biol Med. 2018;15(1):14-28.
4. Alexander WS. Suppressors of cytokine signalling (SOCS) in the immune system. Nat Rev Immunol. 2002;2(6):410-416.
5. Ambrosi TH, Scialdone A, Graja A, et al. Adipocyte Accumulation in the Bone Marrow during Obesity and Aging Impairs Stem Cell-Based Hematopoietic and Bone Regeneration. Cell Stem Cell. 2017;20(6):771-784.e6. doi:10.1016/j.stem.2017.02.009
6. Ana M Biscaia Santos, Ana M Cristóvão Pinto, Ana R Pires, Joana G Antunes 2024. Immunohistochemistry protocol optimized at iMM-JLA. protocols.io. https://dx.doi.org/10.17504/protocols.io.j8nlkon2wv5r/v1
7. Andrade PZ, de Soure AM, Dos Santos F, Paiva A, Cabral JM, da Silva CL. Ex vivo expansion of cord blood haematopoietic stem/progenitor cells under physiological oxygen tensions: clear-cut effects on cell proliferation, differentiation and metabolism. J Tissue Eng Regen Med. 2013.
8. Andrade PZ, dos Santos F, Almeida-Porada G, da Silva CL, S Cabral JM. Systematic delineation of optimal cytokine concentrations to expand hematopoietic stem/progenitor cells in co-culture with mesenchymal stem cells. Mol Biosyst. 2010 Jul;6(7):1207-15.
9. Andrade, P.Z., et al., Stem cell bioengineering strategies to widen the therapeutic applications of haematopoietic stem/progenitor cells from umbilical cord blood. J Tissue Eng Regen Med, 2015. 9(9): p. 988-1003.
10. Angrisani, A., Di Fiore, A., De Smaele, E. et al. The emerging role of the KCTD proteins in cancer. Cell Commun Signal 19, 56 (2021).
11. Anthias C, Shaw BE, Bruce JG, et al. Role of Race/Ethnicity in Donor Decisions about Unrelated Hematopoietic Progenitor Cell Donation: Exploring Reasons for Higher Attrition among Racial/Ethnic Minorities. Biol Blood Marrow Transplant. 2020;26(3):593-599.
12. Atala, Anthony; Lanza, Robert; Mikos, Antonios G.; Nerem, Robert. Principles or Regenerative Medicine, 3rd edition, Chapters 14 and 15. Elsevier Inc. 2019.
13. Aubert G, Lansdorp PM. Telomeres and aging. Physiol Rev. 2008;88(2):557-579.
14. Babushok DV. A brief, but comprehensive, guide to clonal evolution in aplastic anemia. Hematology Am Soc Hematol Educ Program. 2018 Nov 30;2018(1):457-466.
15. Bacigalupo A, Socié G, Schrezenmeier H, et al. Bone marrow versus peripheral blood as the stem cell source for sibling transplants in acquired aplastic anemia: survival advantage for bone marrow in all age groups. Haematologica. 2012;97(8):1142-1148. doi:10.3324/haematol.2011.054841
16. Bacigalupo A, Socié G, Schrezenmeier H, Tichelli A, Locasciulli A, Fuehrer M, et al. Aplastic Anemia Working Party of the European Group for Blood and Marrow Transplantation (WPSAA-EBMT). Bone marrow versus peripheral blood as the stem

cell source for sibling transplants in acquired aplastic anemia: survival advantage for bone marrow in all age groups. Haematologica (2012) 97:1142–8.
17. Bacigalupo A. How I treat acquired aplastic anemia. Blood. 2017 Mar 16;129(11):1428-1436.
18. Bai, T.; Li, J.; Sinclair, A.; Imren, S.; Merriam, F.; Sun, F.; Delaney, C. Expansion of primitive human hematopoietic stem cells by culture in a zwitterionic hydrogel. Nat. Med. 2019, 25, 1566–1575.
19. Baker SJ, Ma'ayan A, Lieu YK, John P, Reddy MV, Chen EY, Duan Q, Snoeck HW, Reddy EP. B-myb is an essential regulator of hematopoietic stem cell and myeloid progenitor cell development. Proc Natl Acad Sci U S A. 2014 Feb 25;111(8):3122-7.
20. Balint B, Stamatovic D, Todorovic M, Elez M, Vojvodic D, Pavlovic M, Cucuz-Jokic M. Autologous transplant in the treatment of severe aplastic anemia - a case report. Transfus Apher Sci. 2011 Oct;45(2):137-41.
21. Barbara J. Bain, David M. Clark, Bridget S. Wilkins. Bone marrow pathology, Fifth edition, Chapter 9. Wiley-Blackwell, 2019.
22. Barbara NP, Wrana JL, Letarte M. Endoglin is an assessory protein that interacts with the signaling receptor complex of multiple members of the transforming growth factor-beta superfamily. J Biol Chem. 1999;274(2):584-594.
23. Baym M, Kryazhimskiy S, Lieberman TD, Chung H, Desai MM, Kishony R. Inexpensive multiplexed library preparation for megabase-sized genomes [published correction appears in PLoS One. 2015 Jun 18;10(6):e0131262. doi: 10.1371/journal.pone.0131262]. PLoS One. 2015;10(5):e0128036. Published 2015 May 22. doi:10.1371/journal.pone.0128036
24. Bentley SA, Alabaster O, Foidart JM. Collagen heterogeneity in normal human bone marrow. Br J Haematol. 1981 Jun;48(2):287-91.
25. Bianco, J.E.R., et al., Characterization of a novel decellularized bone marrow scaffold as an inductive environment for hematopoietic stem cells. Biomater Sci, 2019. 7(4): p. 1516-1528.
26. Birbrair A, Frenette PS. Niche heterogeneity in the bone marrow. Ann N Y Acad Sci. (2016) 1370:82–96.
27. Bone. In: Mescher AL. eds. Junqueira's Basic Histology: Text and Atlas, 17th Edition. McGraw Hill; 2024. Assessed January 14, 2025.
28. Boskovic S, Marín Juez R, Stamenkovic N, Radojkovic D, Stainier DY, Kojic S. The stress responsive gene ankrd1a is dynamically regulated during skeletal muscle development and upregulated following cardiac injury in border zone cardiomyocytes in adult zebrafish. Gene. 2021;792:145725.
29. Bourgine, P.E.; Klein, T.; Paczulla, A.M.; Shimizu, T.; Kunz, L.; Kokkaliaris, K.D. In vitro biomimetic engineering of a human hematopoietic niche with functional properties. Proc. Natl. Acad. Sci. USA 2018, 115, 5689–5693.
30. Bradshaw, D., Cashin, C.H., Kennedy, A.J. (1984). Anti-Inflammatory Effects of the Retinoids. In: Cunliffe, W.J., Miller, A.J. (eds) Retinoid Therapy. Springer, Dordrecht.
31. Braham, M.V.J.; Ahlfeld, T.; Akkineni, A.R.; Minnema, M.C.; Dhert, W.J.A.; Robin, C.; Alblas, J. Endosteal and Perivascular Subniches in a 3D Bone Marrow Model for Multiple Myeloma. Tissue Eng. Part C Methods 2018, 24, 300–313.
32. Branco A, Bucar S, Moura-Sampaio J, Lilaia C, Cabral JMS, Fernandes-Platzgummer A, Lobato da Silva C. Tailored Cytokine Optimization for ex vivo Culture Platforms

Targeting the Expansion of Human Hematopoietic Stem/Progenitor Cells. Front Bioeng Biotechnol. 2020 Sep 25;8:573282.
33. Branco A, Rayabaram J, Miranda CC, et al. Advances in ex vivo expansion of hematopoietic stem and progenitor cells for clinical applications. Front Bioeng Biotechnol. 2024;12:1380950.
34. Broglie L, Margolis D, Medin JA. Yin and Yang of mesenchymal stem cells and aplastic anemia. World J Stem Cells. 2017 Dec 26;9(12):219-226.
35. Brouki Milan P, Masoumi F, Biazar E, Zare Jalise S, Mehrabi A. Exploiting the Potential of Decellularized Extracellular Matrix (ECM) in Tissue Engineering: A Review Study. Macromol Biosci. 2025;25(1):e2400322.
36. Bucar S, Branco ADM, Mata MF, Milhano JC, Caramalho Í, Cabral JMS, Fernandes-Platzgummer A, da Silva CL. Influence of the mesenchymal stromal cell source on the hematopoietic supportive capacity of umbilical cord blood-derived CD34+-enriched cells. Stem Cell Res Ther. 2021 Jul 13;12(1):399.
37. Bueno C, Roldan M, Anguita E, et al. Bone marrow mesenchymal stem cells from patients with aplastic anemia maintain functional and immune properties and do not contribute to the pathogenesis of the disease. Haematologica. 2014;99(7):1168-1175.
38. Cabrita, G., Ferreira, BS, Lobato da Silva, C, Gonçalves, R, Almeida-Porada, G, Cabral, JMS, Hematopoietic stem cells: from the bone to the bioreactor. TRENDS in Biotechnology, 2003. 21(5): p. 233-240.
39. Carlson M (2019). org.Hs.eg.db: Genome wide annotation for Human. R package version 3.8.2.
40. Carmona-Luque M, Ballesteros-Ribelles A, Millán-López A, Blanco A, Nogueras S, Herrera C. The Effect of Cell Culture Passage on the Efficacy of Mesenchymal Stromal Cells as a Cell Therapy Treatment. J Clin Med. 2024 Apr 24;13(9):2480. doi: 10.3390/jcm13092480.
41. Carvalho MS, Alves L, Bogalho I, Cabral JMS, da Silva CL. Impact of Donor Age on the Osteogenic Supportive Capacity of Mesenchymal Stromal Cell-Derived Extracellular Matrix. Front Cell Dev Biol. 2021 Oct 5;9:747521.
42. Carvalho MS, Poundarik AA, Cabral JMS, da Silva CL, Vashishth D. Biomimetic matrices for rapidly forming mineralized bone tissue based on stem cell-mediated osteogenesis. Sci Rep 2018 8:14388 2018.
43. Cassim Bawa FN, Hu S, Gopoju R, et al. Adipocyte retinoic acid receptor α prevents obesity and steatohepatitis by regulating energy expenditure and lipogenesis. Obesity (Silver Spring). 2024;32(1):120-130.
44. Cawthorn WP, Scheller EL, Learman BS, Parlee SD, Simon BR, Mori H, et al. Bone marrow adipose tissue is an endocrine organ that contributes to increased circulating adiponectin during caloric restriction. Cell Metab. (2014) 20:368–75.
45. Chalise JP, Hashimoto S, Parajuli G, et al. Feedback regulation of Arid5a and Ppar-γ2 maintains adipose tissue homeostasis. Proc Natl Acad Sci U S A. 2019;116(30):15128-15133.
46. Chao YH, Lin CW, Pan HH, et al. Increased apoptosis and peripheral blood mononuclear cell suppression of bone marrow mesenchymal stem cells in severe aplastic anemia. Pediatr Blood Cancer. 2018;65(9):e27247.

47. Chao YH, Peng CT, Harn HJ, Chan CK, Wu KH. Poor potential of proliferation and differentiation in bone marrow mesenchymal stem cells derived from children with severe aplastic anemia. Ann Hematol. (2010) 89:715–23.
48. Chen J, Crawford R, Chen C, Xiao Y. The key regulatory roles of the PI3K/Akt signaling pathway in the functionalities of mesenchymal stem cells and applications in tissue regeneration. Tissue Eng Part B Rev. 2013;19(6):516-528. doi:10.1089/ten.TEB.2012.0672
49. Chen Q, Shou P, Zheng C, et al. Fate decision of mesenchymal stem cells: adipocytes or osteoblasts?. Cell Death Differ. 2016;23(7):1128-1139. doi:10.1038/cdd.2015.168
50. Chen YH, Yeh FL, Yeh SP, Ma HT, Hung SC, Hung MC, et al. Myocyte enhancer factor-2 interacting transcriptional repressor (MITR) is a switch that promotes osteogenesis and inhibits adipogenesis of mesenchymal stem cells by inactivating peroxisome proliferator-activated receptor gamma-2. J Biol Chem. (2011) 286:10671–80. Tripathy NK, Singh SP, Nityanand S. Enhanced adipogenicity of bone marrow mesenchymal stem cells in aplastic anemia. Stem Cells Int. (2014) 2014:276862.
51. Chongli Y, Ziaobo Z: Incidence survey of aplastic anemia in China. Chin Med Sci J 6:203, 1991.
52. Chow DH, Zheng L, Tian L, Ho KS, Qin L, Guo X. Application of ultrasound accelerates the decalcification process of bone matrix without affecting histological and immunohistochemical analysis. J Orthop Translat. 2018 Sep 5;17:112-120.
53. Clé DV, Santana-Lemos B, Tellechea MF, Prata KL, Orellana MD, Covas DT, Calado RT. Intravenous infusion of allogeneic mesenchymal stromal cells in refractory or relapsed aplastic anemia. Cytotherapy 2015; 17: 1696-1705.
54. Cleary MA, Narcisi R, Focke K, van der Linden R, Brama PA, van Osch GJ. Expression of CD105 on expanded mesenchymal stem cells does not predict their chondrogenic potential. Osteoarthritis Cartilage. 2016;24(5):868-872.
55. Congrains A, Bianco J, Rosa RG, Mancuso RI, Saad STO. 3D Scaffolds to Model the Hematopoietic Stem Cell Niche: Applications and Perspectives. Materials (Basel). 2021;14(3):569. Published 2021 Jan 26.
56. Crippa S, Santi L, Bosotti R, Porro G, Bernardo ME. Bone Marrow-Derived Mesenchymal Stromal Cells: A Novel Target to Optimize Hematopoietic Stem Cell Transplantation Protocols in Hematological Malignancies and Rare Genetic Disorders. J Clin Med. 2019 Dec 18;9(1):2.
57. Croft M, Duan W, Choi H, Eun SY, Madireddi S, Mehta A. TNF superfamily in inflammatory disease: translating basic insights. Trends Immunol. 2012;33(3):144-152. doi:10.1016/j.it.2011.10.004
58. Cuminetti V and Arranz L. Bone Marrow Adipocytes: The Enigmatic Components of the Hematopoietic Stem Cell Niche. J. Clin. Med. 2019, 8(5), 707.
59. da Silva CL, Gonçalves R, dos Santos F, Andrade PZ, Almeida-Porada G, Cabral JM. Dynamic cell-cell interactions between cord blood haematopoietic progenitors and the cellular niche are essential for the expansion of CD34+, CD34+CD38- and early lymphoid CD7+ cells. J Tissue Eng Regen Med. 2010;4(2):149-158.
60. Dallas NA, Samuel S, Xia L, et al. Endoglin (CD105): a marker of tumor vasculature and potential target for therapy. Clin Cancer Res. 2008;14(7):1931-1937.

61. de Almeida Fuzeta, M., et al., Addressing the Manufacturing Challenges of Cell-Based Therapies. Adv Biochem Eng Biotechnol, 2020. 171: p. 225-278.
62. De Felice L, Agostini F, Suriano C, Fraboni D, Gregorj C, Tirindelli MC, et al. Hematopoietic, mesenchymal, and immune cells are more enhanced in bone marrow than in peripheral blood from granulocyte colony-stimulating factor primed healthy donors. Biol Blood Marrow Transl. (2016) 22:1758–64.
63. Devlin MJ. Why does starvation make bones fat? Am J Hum Biol. (2011) 23:577–85.
64. DiMascio L, Voermans C, Uqoezwa M, et al. Identification of adiponectin as a novel hemopoietic stem cell growth factor. J Immunol. 2007;178(6):3511-3520.
65. Dobin A, Davis CA, Schlesinger F, et al. STAR: ultrafast universal RNA-seq aligner. Bioinformatics. 2013;29(1):15-21.doi:10.1093/bioinformatics/bts635 (https://github.com/alexdobin/STAR/releases/tag/2.7.11a)
66. Dominici M, Le Blanc K, Mueller I, et al. Minimal criteria for defining multipotent mesenchymal stromal cells. The International Society for Cellular Therapy position statement. Cytotherapy. 2006;8(4):315-317. doi:10.1080/14653240600855905
67. dos Santos F., Andrade P. Z., Boura J. S., Abecasis M. M., da Silva C. L., Cabral J. M. S. (2010). Ex vivo expansion of human mesenchymal stem cells: a more effective cell proliferation kinetics and metabolism under hypoxia. J. Cell. Physiol. 223 27–35.
68. Fan W, Li J, Wang Y, et al. CD105 promotes chondrogenesis of synovium-derived mesenchymal stem cells through Smad2 signaling. Biochem Biophys Res Commun. 2016;474(2):338-344. doi:10.1016/j.bbrc.2016.04.101
69. Fantuzzi G, Faggioni R. Leptin in the regulation of immunity, inflammation, and hematopoiesis. J Leukoc Biol. 2000;68(4):437-446. Pérez-Pérez A, Sánchez-Jiménez F, Vilariño-García T, Sánchez-Margalet V. Role of Leptin in Inflammation and Vice Versa. Int J Mol Sci. 2020 Aug 16;21(16):5887.
70. Fazeli PK, Horowitz MC, MacDougald OA, Scheller EL, Rodeheffer MS, Rosen CJ, et al. Marrow fat and bone–new perspectives. J Clin Endocrinol Metab. (2013) 98:935–45.
71. Fernandes-Platzgummer A, Andrade PZ, Cabral JMS, da Silva CL. Scalable Manufacturing of Human Hematopoietic Stem/Progenitor Cells Exploiting a Co-culture Platform with Mesenchymal Stromal Cells. Methods Mol Biol. 2021;2286:107-120.
72. Fingrut, Warren. The Need for Ethnically Diverse Stem Cell Donors. UBCMJ. 2015: 7.1 (44-47).
73. Friedman AD. C/EBPα in normal and malignant myelopoiesis. Int J Hematol. 2015;101(4):330-341. doi:10.1007/s12185-015-1764-6.
74. Fujimaki S, Harigae H, Sugawara T, Takasawa N, Sasaki T, Kaku M. Decreased expression of transcription factor GATA-2 in haematopoietic stem cells in patients with aplastic anaemia. Br J Haematol. (2001) 113:52–7.
75. Fureder W, Krauth MT, Sperr WR, Sonneck K, Simonitsch-Klupp I, Mullauer L, et al. Evaluation of angiogenesis and vascular endothelial growth factor expression in the bone marrow of patients with aplastic anemia. Am J Pathol. (2006) 168:123–30.
76. Furuhashi M, Saitoh S, Shimamoto K, Miura T. Fatty Acid-Binding Protein 4 (FABP4): Pathophysiological Insights and Potent Clinical Biomarker of Metabolic and Cardiovascular Diseases. Clin Med Insights Cardiol. 2015 Feb 2;8(Suppl 3):23-33.
77. Gal Ophir, Ninette Amariglio, Jasmine Jacob-Hirsch, Ran Elkon, Gideon Rechavi, Daniel M. Michaelson. Apolipoprotein E4 enhances brain inflammation by

modulation of the NF-κB signaling cascade, Neurobiology of Disease. Volume 20, Issue 3, 2005, Pages 709-718, ISSN 0969-9961.
78. Ganapathi KA, Townsley DM, Hsu AP, et al. GATA2 deficiency-associated bone marrow disorder differs from idiopathic aplastic anemia. Blood. 2015;125(1):56-70.
79. Gao M, Ge M, Huo J, et al. Leptin-mediated proinflammatory bone marrow environment in acquired aplastic anemia. Cytokine. 2022;152:155829. doi:10.1016/j.cyto.2022.155829
80. Gary L. Gilmore, Darlene K. DePasquale, John Lister, Richard K. Shadduck. Selection of CD34+ HSC from Pooled Cord Blood Samples Does Not Result in Co-Purification of Potential Alloreactive CD3+ T Cells. Blood, Volume 106, Issue 11, 2005, Page 5263, ISSN 0006-4971.
81. Gene [Internet]. Bethesda (MD): National Library of Medicine (US), National Center for Biotechnology Information; 2004 - [cited 2025 Jan 10]. Assession No. 28984, regulator of cell cycle (RGCC), Homo sapiens. Available from: https://www.ncbi.nlm.nih.gov/gene/28984
82. Genome sequence, primary assembly (GRCh38): https://ftp.ebi.ac.uk/pub/databases/gencode/Gencode_human/release_44/GRCh38.primary_assembly.genome.fa.gz.
83. Genome sequence, primary assembly (GRCh38): https://ftp.ebi.ac.uk/pub/databases/gencode/Gencode_human/release_44/GRCh38.primary_assembly.genome.fa.gz.
84. Gerber HP, Malik AK, Solar GP, Sherman D, Liang XH, Meng G, et al. VEGF regulates haematopoietic stem cell survival by an internal autocrine loop mechanism. Nature (2002) 417:954–8.
85. Gianelli U, Vener C, Raviele PR, Savi F, Somalvico F, Calori R, et al. VEGF expression correlates with microvessel density in Philadelphia chromosome- negative chronic myeloproliferative disorders. Am J Clin Pathol. (2007) 128:966–73.
86. Gil-Kulik P, Krzyżanowski A, Dudzińska E, Karwat J, Chomik P, Świstowska M, Kondracka A, Kwaśniewska A, Cioch M, Jojczuk M, Nogalski A, Kocki J. Potential Involvement of BIRC5 in Maintaining Pluripotency and Cell Differentiation of Human Stem Cells. Oxid Med Cell Longev. 2019 Jan 10;2019:8727925.
87. Gilmore GL, DePasquale DK, Lister J, Shadduck RK. Ex vivo expansion of human umbilical cord blood and peripheral blood CD34(+) hematopoietic stem cells. Exp Hematol. 2000;28(11):1297-1305.
88. Gonzaga VF, Wenceslau CV, Lisboa GS, Frare EO, Kerkis I. Mesenchymal Stem Cell Benefits Observed in Bone Marrow Failure and Acquired Aplastic Anemia. Stem Cells Int. 2017; 2017:8076529.
89. Ghosh, K., Shome, D.K., Kulkarni, B. et al. Fibrosis and bone marrow: understanding causation and pathobiology. J Transl Med 21, 703 (2023).
90. Greene ME, Pitts J, McCarville MA, et al. PPARgamma: observations in the hematopoietic system. Prostaglandins Other Lipid Mediat. 2000;62(1):45-73.
91. Groarke EM, Feng X, Aggarwal N, et al. Efficacy of JAK1/2 inhibition in murine immune bone marrow failure. Blood. 2023;141(1):72-89.
92. Guezguez B, Campbell CJ, Boyd AL, et al. Regional localization within the bone marrow influences the functional capacity of human HSCs. Cell Stem Cell. 2013;13(2):175-189.

93. Gulbagci NT, Li L, Ling B, et al. SHARP1/DEC2 inhibits adipogenic differentiation by regulating the activity of C/EBP. EMBO Rep. 2009;10(1):79-86.
94. Guo B, Huang X, Lee MR, Lee SA, Broxmeyer HE. Antagonism of PPAR-γ signaling expands human hematopoietic stem and progenitor cells by enhancing glycolysis. Nat Med. 2018 Mar;24(3):360-367.
95. Gupta V, Eapen M, Brazauskas R, et al. Impact of age on outcomes after bone marrow transplantation for acquired aplastic anemia using HLA-matched sibling donors. Haematologica. 2010;95(12):2119-2125.
96. Hamzic E, Whiting K, Gordon Smith E, Pettengell R. Characterization of bone marrow mesenchymal stromal cells in aplastic anaemia. Br J Haematol. (2015) 169:804–13.
97. Hashimoto, Y.; Funamoto, S.; Kimura, T.; Nam, K.; Fujisato, T.; Kishida, A. The effect of decellularized bone/bone marrow produced by high-hydrostatic pressurization on the osteogenic differentiation of mesenchymal stem cells. Biomaterials 2011, 32, 7060–7067.
98. Hettler F, Schreck C, Marquez SR, Engleitner T, Vilne B, Landspersky T, Weidner H, Hausinger R, Mishra R, Oellinger R, Rauner M, Naumann R, Peschel C, Bassermann F, Rad R, Istvanffy R, Oostendorp RAJ. Osteoprogenitor SFRP1 prevents exhaustion of hematopoietic stem cells via PP2A-PR72/130-mediated regulation of p300. Haematologica. 2023 Feb 1;108(2):490-501.
99. Hiyama E, Hiyama K. Telomere and telomerase in stem cells. Br J Cancer. 2007;96(7):1020-1024.
100. Holmberg LA, Seidel K, Leisenring W, Torok-Storb B. Aplastic anemia: analysis of stromal cell function in long-term marrow cultures. Blood (1994) 84:3685–90.
101. Hossain MJ, Xie S. Patient features and survival of pediatric aplastic anemia in the USA: a large institution experience. J Public Health (Oxf). 2019 Jun 1;41(2):329-337.
102. Hu X, Li J, Fu M, Zhao X, Wang W. The JAK/STAT signaling pathway: from bench to clinic. Signal Transduct Target Ther. 2021;6(1):402. Published 2021 Nov 26. doi:10.1038/s41392-021-00791-1
103. Huang, X.; Zhu, B.; Wang, X.; Xiao, R.; Wang, C. Three-dimensional co-culture of mesenchymal stromal cells and differentiated osteoblasts on human bio-derived bone scaffolds supports active multi-lineage hematopoiesis in vitro : Functional implication of the biomimetic HSC niche. Int. J. Mol. Med. 2016, 38, 1141–1151.
104. Hughes AM, Kuek V, Oommen J, Kotecha RS, Cheung LC. Murine bone-derived mesenchymal stem cells undergo molecular changes after a single passage in culture. Sci Rep. 2024 May 29;14(1):12396. doi: 10.1038/s41598-024-63009-8.
105. Hur, J.; Park, J.; Lee, S.E.; Yoon, C.-H.; Jang, J.H.; Yang, J.M.; Kim, H.-S. Human peripheral blood-born hematosphere as a niche for hematopoietic stem cell expansion. Cell Res. 2011, 45, 987–990.
106. Hwang J, San BH, Turner NJ, et al. Molecular assessment of collagen denaturation in decellularized tissues using a collagen hybridizing peptide. Acta Biomater. 2017;53:268-278.
107. Isern, J.; Martin-Antonio, B.; Ghazanfari, R.; Martin, A.M.; Lopez, J.A.; Toro, R.; Mendez-Ferre, S. Self-Renewing Human Bone Marrow Mesenspheres Promote Hematopoietic Stem Cell Expansion. Cell Rep. 2013, 3, 1714–1724.
108. Issaragrisil S: Epidemiology of aplastic anemia in Thailand. Thai Aplastic Anemia Study Group. Int J Hematol 70:137, 1999.

109. Jiang J, Li X, Zhang C, Wang J, Li J. Anti-cancer effects of Coix seed extract through KCTD9-mediated ubiquitination of TOP2A in lung adenocarcinoma. Cell Div. 2024;19(1):6. Published 2024 Feb 20.
110. Jin W, Liang X, Brooks A, Futrega K, Liu X, Doran MR, Simpson MJ, Roberts MS, Wang H. Modelling of the SDF-1/CXCR4 regulated in vivo homing of therapeutic mesenchymal stem/stromal cells in mice. PeerJ. 2018 Dec 6;6:e6072. doi: 10.7717/peerj.6072. PMID: 30564525; PMCID: PMC6286806.
111. Jing D, Wobus M, Poitz DM, Bornhäuser M, Ehninger G, Ordemann R. Oxygen tension plays a critical role in the hematopoietic microenvironment in vitro. Haematologica. 2012 Mar;97(3):331-9.
112. Jing S, Zhou H, Zou C, et al. Application of telomere biology and telomerase in mesenchymal stem cells. Nano TransMed, 2022, 1(2–4): e9130007.
113. Kagawa, Y., Low, Y.L., Pyun, J. et al. Fatty Acid-Binding Protein 4 is Essential for the Inflammatory and Metabolic Response of Microglia to Lipopolysaccharide. J Neuroimmune Pharmacol 18, 448–461 (2023).
114. Jung Y, Wang J, Schneider A, Sun YX, Koh-Paige AJ, Osman NI, McCauley LK, Taichman RS. Regulation of SDF-1 (CXCL12) production by osteoblasts; a possible mechanism for stem cell homing. Bone. 2006 Apr;38(4):497-508.
115. Kamata M, Okitsu Y, Fujiwara T, Kanehira M, Nakajima S, Takahashi T, et al. GATA2 regulates differentiation of bone marrow-derived mesenchymal stem cells. Haematologica (2014) 99:1686–96.
116. Kassambara, A., & Mundt, F. (2020). factoextra: Extract and Visualize the Results of Multivariate Data Analyses. R package version 1.0.7
117. Kaushansky K, Lichtman MA, Prchal JT, Levi MM, Press OW, Burns LJ, Caligiuri M. eds. Williams Hematology, 9e, Chapter 35 (Aplastic Anemia: Acquired and Inherited). New York, NY: McGraw-Hill.
118. Kevin Blighe, Sharmila Rana & Myles Lewis (2023). EnhancedVolcano: Publication-ready volcano plots with enhanced colouring and labeling. R package version 1.16.0. https://github.com/kevinblighe/EnhancedVolcano
119. Killick SB, Bown N, Cavenagh J, Dokal I, Foukaneli T, Hill A, Hillmen P, Ireland R, Kulasekararaj A, Mufti G, Snowden JA, Samarasinghe S, Wood A, Marsh JC; British Society for Standards in Haematology. Guidelines for the diagnosis and management of adult aplastic anaemia. Br J Haematol. 2016 Jan;172(2):187-207.
120. Kim DS, Jang IK, Lee MW, et al. Enhanced Immunosuppressive Properties of Human Mesenchymal Stem Cells Primed by Interferon-γ. EBioMedicine. 2018;28:261-273. doi:10.1016/j.ebiom.2018.01.002
121. Kim SY, Le Rademacher J, Antin JH, et al. Myelodysplastic syndrome evolving from aplastic anemia treated with immunosuppressive therapy: efficacy of hematopoietic stem cell transplantation. Haematologica. 2014;99(12):1868-1875.
122. Kornicka K., Marycz K., Tomaszewski K. A., Marędziak M., Śmieszek A. (2015). The effect of age on osteogenic and adipogenic differentiation potential of human adipose derived stromal stem cells (hASCs) and the impact of stress factors in the course of the differentiation process.
123. Kräter, M.; Jacobi, A.; Otto, O.; Tietze, S.; Müller, K.; David, M.; Wobus, M. Bone marrow niche-mimetics modulate HSPC function via integrin signaling. Sci. Rep. 2017, 7, 1–15.

124. Kreslavsky T, Vilagos B, Tagoh H, et al. Essential role for the transcription factor Bhlhe41 in regulating the development, self-renewal and BCR repertoire of B-1a cells. Nat Immunol. 2017;18(4):442-455.
125. Kuleshov, M. V., Jones, M. R., Rouillard, A. D., Fernandez, N. F., Duan, Q., Wang, Z., ... & Ma'ayan, A. (2016). Enrichr: a comprehensive gene set enrichment analysis web server 2016 update. Nucleic acids research, 44(W1), W90-W97
126. Kumar S, Geiger H. HSC Niche Biology and HSC Expansion Ex Vivo. Trends Mol Med. 2017 Sep;23(9):799-819. doi: 10.1016/j.molmed.2017.07.003.
127. Kumawat K, Gosens R. WNT-5A: signaling and functions in health and disease. Cell Mol Life Sci. 2016;73(3):567-587. doi:10.1007/s00018-015-2076-y
128. Kusuyama J, Bandow K, Ohnishi T, Hisadome M, Shima K, Semba I, Matsuguchi T. Osteopontin inhibits osteoblast responsiveness through the down-regulation of focal adhesion kinase mediated by the induction of low-molecular weight protein tyrosine phosphatase. Mol Biol Cell. 2017 May 15;28(10):1326-1336.
129. Kwon M, Kim BS, Yoon S, Oh SO, Lee D. Hematopoietic Stem Cells and Their Niche in Bone Marrow. Int J Mol Sci. 2024 Jun 21;25(13):6837.
130. Lai, W.Y.; Li, Y.Y.; Mak, S.K.; Ho, F.C.; Chow, S.T.; Chooi, W.H.; Chan, B.P. Reconstitution of bone-like matrix in osteogenically differentiated mesenchymal stem cell—Collagen constructs: A three-dimensional in vitro model to study hematopoietic stem cell niche. J. Tissue Eng. 2013, 4, 1–13.
131. Lapidot T, Dar A, Kollet O. How do stem cells find their way home? Blood. 2005 Sep 15;106(6):1901-10.
132. Lawrence M, Huber W, Pagès H, Aboyoun P, Carlson M, Gentleman R, Morgan M, Carey V (2013). “Software for Computing and Annotating Genomic Ranges.” PLoS Computational Biology, 9. doi:10.1371/journal.pcbi.1003118, http://www.ploscompbiol.org/article/info%3Adoi%2F10.1371%2Fjournal.pcbi.1003118
133. Lee H, Park BC, Soon Kang J, Cheon Y, Lee S, Jae Maeng P. MAM domain containing 2 is a potential breast cancer biomarker that exhibits tumour-suppressive activity. Cell Prolif. 2020;53(9):e12883.
134. Lee RH, Seo MJ, Pulin AA, Gregory CA, Ylostalo J, Prockop DJ. The CD34-like protein PODXL and alpha6-integrin (CD49f) identify early progenitor MSCs with increased clonogenicity and migration to infarcted heart in mice. Blood. 2009;113(4):816-826.
135. Lee SH, Erber WN, Porwit A, Tomonaga M, Peterson LC; International Council for Standardization In Hematology. ICSH guidelines for the standardization of bone marrow specimens and reports. Int J Lab Hematol. 2008 Oct;30(5):349-64.
136. Lee-Thedieck C, Schertl P, Klein G. The extracellular matrix of hematopoietic stem cell niches. Adv Drug Deliv Rev. 2022 Feb;181:114069.
137. Leisten, I.; Kramann, R.; Ventura, M.S.; Bovi, M.; Neuss, S.; Ziegler, P.; Schneider, R.K. 3D co-culture of hematopoietic stem and progenitor cells and mesenchymal stem cells in collagen scaffolds as a model of the hematopoietic niche. Biomaterials 2012, 33, 1736–1747.
138. Lento W, Congdon K, Voermans C, Kritzik M, Reya T. Wnt signaling in normal and malignant hematopoiesis. Cold Spring Harb Perspect Biol. 2013;5(2):a008011. Published 2013 Feb 1. doi:10.1101/cshperspect.a008011

139. Leung CG, Xu Y, Mularski B, Liu H, Gurbuxani S, Crispino JD. Requirements for survivin in terminal differentiation of erythroid cells and maintenance of hematopoietic stem and progenitor cells. J Exp Med. 2007;204(7):1603-1611.
140. Li J, Yang S, Lu S, Zhao H, Feng J, Li W, et al. Differential gene expression profile associated with the abnormality of bone marrow mesenchymal stem cells in aplastic anemia. PLoS ONE (2012) 7:e47764.
141. Li N, Song Y, Zhou J, Fang B. Arsenic trioxide improves hematopoiesis in refractory severe aplastic anemia. J Hematol Oncol. (2012) 5:61.
142. Li Q, Wu Y, Kang N. Marrow adipose tissue: its origin, function, and regulation in bone remodeling and regeneration. Stem Cells Int. (2018) 2018:7098456.
143. Li X, Li H, Shao MM, Miao J, Fu Y, Hu B. Downregulation of AHNAK2 inhibits cell cycle of lung adenocarcinoma cells by interacting with RUVBL1. Thorac Cancer. 2023;14(22):2093-2104. doi:10.1111/1759-7714.14989
144. Lin CM, Cooles FA, Isaacs JD. Basic Mechanisms of JAK Inhibition. Mediterr J Rheumatol. 2020;31(Suppl 1):100-104. Published 2020 Jun 11. doi:10.31138/mjr.31.1.100
145. Lin CS, Xin ZC, Dai J, Lue TF. Commonly used mesenchymal stem cell markers and tracking labels: Limitations and challenges. Histol Histopathol. 2013 Sep;28(9):1109-16.
146. Lin WD, Liao WL, Chen WC, Liu TY, Chen YC, Tsai FJ. Genome-wide association study identifies novel susceptible loci and evaluation of polygenic risk score for chronic obstructive pulmonary disease in a Taiwanese population. BMC Genomics. 2024;25(1):607. Published 2024 Jun 17.
147. Ling KW, Ottersbach K, van Hamburg JP, Oziemlak A, Tsai FY, Orkin SH, et al. GATA-2 plays two functionally distinct roles during the ontogeny of hematopoietic stem cells. J Exp Med. (2004) 200:871–82.
148. Liu T, Zhang L, Joo D, Sun SC. NF-κB signaling in inflammation. Signal Transduct Target Ther. 2017;2:17023-. doi:10.1038/sigtrans.2017.23
149. Liu W, Wang X. Research Advances on Suppressor of Cytokine Signaling 3 (SOCS3) in Animal Carbohydrate and Lipid Metabolism Processes. Pak J Biol Sci. 2022;25(12):1100-1108.
150. Liu Z, Zhang Y, Xiao H, et al. Cotransplantation of bone marrow-derived mesenchymal stem cells in haploidentical hematopoietic stem cell transplantation in patients with severe aplastic anemia: an interim summary for a multicenter phase II trial results [published correction appears in Bone Marrow Transplant. 2017 Jul;52(7):1080. doi: 10.1038/bmt.2017.85]. Bone Marrow Transplant. 2017;52(5):704-710.
151. Lojk J, Marc J. Roles of Non-Canonical Wnt Signalling Pathways in Bone Biology. Int J Mol Sci. 2021 Oct 7;22(19):10840.
152. Love MI, Huber W, Anders S (2014). “Moderated estimation of fold change and dispersion for RNA-seq data with DESeq2.” Genome Biology, 15, 550. doi:10.1186/s13059-014-0550-8
153. Lu G, Ota A, Ren S, et al. PPM1l encodes an inositol requiring-protein 1 (IRE1) specific phosphatase that regulates the functional outcome of the ER stress response. Mol Metab. 2013;2(4):405-416. Published 2013 Aug 3.
154. Luan C, Chen R, Chen B, Ding J, Ni M. Umbilical cord blood transplantation supplemented with the infusion of mesenchymal stem cell for an adolescent patient

with severe aplastic anemia: a case report and review of literature. Patient Prefer Adherence 2015; 9: 759-765.
155. Lund SA, Giachelli CM, Scatena M. The role of osteopontin in inflammatory processes. J Cell Commun Signal. 2009 Dec;3(3-4):311-22.
156. Luo R, Li L, Xiao F, Fu J. LncRNA FLG-AS1 Mitigates Diabetic Retinopathy by Regulating Retinal Epithelial Cell Inflammation, Oxidative Stress, and Apoptosis via miR-380-3p/SOCS6 Axis. Inflammation. 2022;45(5):1936-1949. doi:10.1007/s10753-022-01665-6
157. Lv Y, Qi J, Babon JJ, et al. The JAK-STAT pathway: from structural biology to cytokine engineering. Signal Transduct Target Ther. 2024;9(1):221. Published 2024 Aug 21. doi:10.1038/s41392-024-01934-w
158. Madsen MS, Siersbæk R, Boergesen M, Nielsen R, Mandrup S. Peroxisome proliferator-activated receptor γ and C/EBPα synergistically activate key metabolic adipocyte genes by assisted loading. Mol Cell Biol. 2014 Mar;34(6):939-54.
159. Maeda K, Kobayashi Y, Koide M, Uehara S, Okamoto M, Ishihara A, Kayama T, Saito M, Marumo K. The Regulation of Bone Metabolism and Disorders by Wnt Signaling. Int J Mol Sci. 2019 Nov 6;20(22):5525.
160. Margarida Coucelo, Joana Azevedo, Isabel Bogalho, Ana Teresa Simões et al. OC 4 - NEXT GENERATION SEQUENCING APPROACH TO BONE MARROW FAILURE SYNDROMES – PORTUGUESE EXPERIENCE, EJC Paediatric Oncology, Volume 2, Supplement 1, 2023, 100035.
161. Mary JY, Baumelou E, Guiguet M: Epidemiology of aplastic anemia in France: A prospective multicenter study. Blood 75:1646, 1990.
162. Mattiucci D, Maurizi G, Izzi V, et al. Bone marrow adipocytes support hematopoietic stem cell survival. J Cell Physiol. 2018;233(2):1500-1511. doi:10.1002/jcp.26037
163. McCahon E, Tang K, Rogers PC et al.: The impact of Asian descent on the incidence of acquired severe aplastic anaemia in children. Br J Haematol 121:170, 2003.
164. Medinger M, Drexler B, Lengerke C, Passweg J. Pathogenesis of Acquired Aplastic Anemia and the Role of the Bone Marrow Microenvironment. Front Oncol. 2018; 8:587.
165. Melnik BC. Acne Transcriptomics: Fundamentals of Acne Pathogenesis and Isotretinoin Treatment. Cells. 2023;12(22):2600. Published 2023 Nov 10.
166. Mendes SC, Robin C, Dzierzak E. Mesenchymal progenitor cells localize within hematopoietic sites throughout ontogeny. Development. 2005;132(5):1127-1136.
167. Michelozzi IM, Pievani A, Pagni F, Antolini L, Verna M, Corti P, et al. Human aplastic anaemia-derived mesenchymal stromal cells form functional haematopoietic stem cell niche in vivo. Br J Haematol. (2017) 179:669–73.
168. Miclau K, Hambright WS, Huard J, Stoddart MJ, Bahney CS. Cellular expansion of MSCs: Shifting the regenerative potential. Aging Cell. 2023 Jan;22(1):e13759.
169. Mirfakhraie R, Ardakani MT, Hajifathali A, et al. Highlighting the interaction between immunomodulatory properties of mesenchymal stem cells and signaling pathways contribute to Graft Versus Host Disease management. Transpl Immunol. 2022;71:101524.
170. Mizuno M, Fujisawa R, Kuboki Y. Type I collagen-induced osteoblastic differentiation of bone-marrow cells mediated by collagen-alpha2beta1 integrin interaction. J Cell Physiol. 2000 Aug;184(2):207-13.

171. Moorer MC, Riddle RC. Regulation of Osteoblast Metabolism by Wnt Signaling. Endocrinol Metab (Seoul). 2018 Sep;33(3):318-330.
172. Morgan M, Pagès H, Obenchain V, Hayden N (2024). Rsamtools: Binary alignment (BAM), FASTA, variant call (BCF), and tabix file import. R package version 2.20.0, https://bioconductor.org/packages/Rsamtools
173. Morris EV, Edwards CM. Bone marrow adipose tissue: a new player in cancer metastasis to bone. Front Endocrinol. (Lausanne) (2016) 7:90.
174. Narcisi R, Cleary MA, Brama PA, et al. Long-term expansion, enhanced chondrogenic potential, and suppression of endochondral ossification of adult human MSCs via WNT signaling modulation. Stem Cell Reports. 2015;4(3):459-472.
175. Naresh KN, Lampert I, Hasserjian R, Lykidis D, Elderfield K, Horncastle D, Smith N, Murray-Brown W, Stamp GW. Optimal processing of bone marrow trephine biopsy: the Hammersmith Protocol. J Clin Pathol. 2006 Sep;59(9):903-11.
176. Naveiras O, Nardi V, Wenzel PL, Hauschka PV, Fahey F, Daley GQ. Bone-marrow adipocytes as negative regulators of the haematopoietic microenvironment. Nature. 2009;460(7252):259-263. doi:10.1038/nature08099
177. Neha E. H. Dinesh, Philippe M. Campeau, and Dieter P. Reinhardt. Fibronectin isoforms in skeletal development and associated disorders. American Journal of Physiology-Cell Physiology 2022 323:2, C536-C549.
178. Neo SH, Her Z, Othman R, et al. Expansion of human bone marrow-derived mesenchymal stromal cells with enhanced immunomodulatory properties. Stem Cell Res Ther. 2023;14(1):259. Published 2023 Sep 19. doi:10.1186/s13287-023-03481-7
179. Nyati KK, Agarwal RG, Sharma P, Kishimoto T. Arid5a Regulation and the Roles of Arid5a in the Inflammatory Response and Disease. Front Immunol. 2019;10:2790. Published 2019 Dec 5.
180. Oo SM, Oo HK, Takayama H, et al. Selenoprotein P-mediated reductive stress impairs cold-induced thermogenesis in brown fat. Cell Rep. 2022;38(13):110566.
181. Osorio EY, Gugala Z, Patterson GT, et al. Inflammatory stimuli alter bone marrow composition and compromise bone health in the malnourished host. Front Immunol. 2022;13:846246. Published 2022 Aug 2. doi:10.3389/fimmu.2022.846246
182. Ou G, Tian Z, Su M, Yu M, Gong J, Chen Y. Identification of gemcitabine resistance-related AHNAK2 gene associated with prognosis and immune infiltration in pancreatic cancer. Heliyon. 2024;10(13):e33687. Published 2024 Jun 27. doi:10.1016/j.heliyon.2024.e33687
183. Pang Y, Xiao HW, Zhang H, Liu ZH, Li L, Gao Y, Li HB, Jiang ZJ, Tan H, Lin JR, Du X, Weng JY, Nie DN, Lin DJ, Zhang XZ, Liu QF, Xu DR, Chen HJ, Ge XH, Wang XY, Xiao Y. Allogeneic Bone Marrow-Derived Mesenchymal Stromal Cells Expanded In Vitro for Treatment of Aplastic Anemia: A Multicenter Phase II Trial. Stem Cells Transl Med 2017; 6: 1569-1575.
184. Park M, Park CJ, Jang S, Kim DY, Lee JH, Lee JH, Lee KH, Hwang K, Lee YH. Reduced expression of osteonectin and increased natural killer cells may contribute to the pathophysiology of aplastic anemia. Appl Immunohistochem Mol Morphol. 2015 Feb;23(2):139-45.
185. Park YH, Yun JI, Han NR, Park HJ, Ahn JY, Kim C, Choi JH, Lee E, Lim JM, Lee ST. Mass production of early-stage bone-marrow-derived mesenchymal stem cells of rat using gelatin-coated matrix. Biomed Res Int. 2013;2013:347618.

186. Pereira AR, Lipphaus A, Ergin M, et al. Modeling of the Human Bone Environment: Mechanical Stimuli Guide Mesenchymal Stem Cell-Extracellular Matrix Interactions. Materials (Basel). 2021;14(16):4431. Published 2021 Aug 7.
187. Pereira AR, Rudert M, Herrmann M. Decellularized human bone as a 3D model to study skeletal progenitor cells in a natural environment. Methods Cell Biol. 2020;157:123-141.
188. Peter V. N. Bodine, Weiguang Zhao, Yogendra P. Kharode, Frederick J. Bex, Andre-Jean Lambert, Mary Beth Goad, Tripti Gaur, Gary S. Stein, Jane B. Lian, Barry S. Komm, The Wnt Antagonist Secreted Frizzled-Related Protein-1 Is a Negative Regulator of Trabecular Bone Formation in Adult Mice, Molecular Endocrinology, Volume 18, Issue 5, 1 May 2004, Pages 1222–1237.
189. Peters IJA, de Pater E, Zhang W. The role of GATA2 in adult hematopoiesis and cell fate determination. Front Cell Dev Biol. 2023 Nov 14;11:1250827.
190. Pham, L. H., Vu, N. B., Van Pham, P. The subpopulation of CD105 negative mesenchymal stem cells show strong immunomodulation capacity compared to CD105 positive mesenchymal stem cells. 2019. Biomedical Research and Therapy, 6(4), 3131-3140.
191. Picelli S, Faridani OR, Björklund AK, Winberg G, Sagasser S, Sandberg R. Full-length RNA-seq from single cells using Smart-seq2. Nat Protoc. 2014;9(1):171-181. doi:10.1038/nprot.2014.006
192. Pievani, A.; Sacchetti, B.; Corsi, A.; Rambaldi, B.; Donsante, S.; Scagliotti, V.; Riminucci, M. Human umbilical cord blood-borne fibroblasts contain marrow niche precursors that form a bone / marrow organoid in vivo. Development 2017, 144, 1035–1044.
193. Ping Z, Chen S, Hermans SJF, et al. Activation of NF-κB driven inflammatory programs in mesenchymal elements attenuates hematopoiesis in low-risk myelodysplastic syndromes. Leukemia. 2019;33(2):536-541. doi:10.1038/s41375-018-0267-x
194. Podleśny-Drabiniok, A., Novikova, G., Liu, Y. et al. BHLHE40/41 regulate microglia and peripheral macrophage responses associated with Alzheimer's disease and other disorders of lipid-rich tissues. Nat Commun 15, 2058 (2024).
195. R Core Team (2021) R: A Language and Environment for Statistical Computing. R Foundation for Statistical Computing, Vienna. https://www.R-project.org
196. Rah B, Rather RA, Bhat GR, et al. JAK/STAT Signaling: Molecular Targets, Therapeutic Opportunities, and Limitations of Targeted Inhibitions in Solid Malignancies. Front Pharmacol. 2022;13:821344. Published 2022 Mar 24. doi:10.3389/fphar.2022.821344
197. Raic, A.; Rödling, L.; Kalbacher, H.; Lee-thedieck, C. Biomaterials Biomimetic macroporous PEG hydrogels as 3D scaffolds for the multiplication of human hematopoietic stem and progenitor cells. Biomaterials 2014, 35, 929–940.
198. Raju GSR, Pavitra E, Bandaru SS, et al. HOTAIR: a potential metastatic, drug-resistant and prognostic regulator of breast cancer. Mol Cancer. 2023;22(1):65. Published 2023 Mar 30.
199. Raudvere, U., Kolberg, L., Kuzmin, I., Arak, T., Adler, P., Peterson, H., & Vilo, J. (2019). g:Profiler: a web server for functional enrichment analysis and conversions of gene lists (2019 update). Nucleic Acids Research, 47(W1), W191-W198

200. Ren X, Ma L, Wang N, et al. Antioxidant Gene Signature Impacts the Immune Infiltration and Predicts the Prognosis of Kidney Renal Clear Cell Carcinoma. Front Genet. 2021;12:721252. Published 2021 Aug 19.
201. Riether C, Schürch CM, Ochsenbein AF. Regulation of hematopoietic and leukemic stem cells by the immune system. Cell Death Differ. (2015) 22:187– 98.
202. Roberto Avellino, Ruud Delwel; Expression and regulation of C/EBPα in normal myelopoiesis and in malignant transformation. Blood 2017; 129 (15): 2083–2091.
203. Roberts JL, Liu G, Paglia DN, et al. Deletion of Wnt5a in osteoclasts results in bone loss through decreased bone formation. Ann N Y Acad Sci. 2020;1463(1):45-59.
204. Robinson, K., Prins, J. & Venkatesh, B. Clinical review: Adiponectin biology and its role in inflammation and critical illness. Crit Care 15, 221 (2011).
205. Rodrigues NP, Janzen V, Forkert R, Dombkowski DM, Boyd AS, Orkin SH, et al. Haploinsufficiency of GATA-2 perturbs adult hematopoietic stem-cell homeostasis. Blood (2005) 106:477–84.
206. Rosa M et al. Successful Bone Marrow Recovery After an Immunoablative Regimen with Autologous Cord Blood Transplant in a Child with Idiopathic Severe Aplastic Anemia: A Case Report. Transplant Proc. 2020 Mar;52(2):653-656.
207. Rosen ED, Hsu CH, Wang X, Sakai S, Freeman MW, Gonzalez FJ, Spiegelman BM. C/EBPalpha induces adipogenesis through PPARgamma: a unified pathway. Genes Dev. 2002 Jan 1;16(1):22-6.
208. Safdari M, Bibak B, Soltani H, Hashemi J. Recent advancements in decellularized matrix technology for bone tissue engineering. Differentiation. 2021;121:25-34.
209. Saidak Z, Le Henaff C, Azzi S, Marty C, Da Nascimento S, Sonnet P, Marie PJ. Wnt/β-catenin signaling mediates osteoblast differentiation triggered by peptide-induced α5β1 integrin priming in mesenchymal skeletal cells. J Biol Chem. 2015 Mar 13;290(11):6903-12.
210. Sandhya R. Panch, James Szymanski, Bipin N. Savani, David F. Stroncek. Sources of Hematopoietic Stem and Progenitor Cells and Methods to Optimize Yields for Clinical Cell Therapy. Biology of Blood and Marrow Transplantation. Volume 23, Issue 8, 2017, Pages 1241-1249, ISSN 1083-8791.
211. Sauer, S., Pavel, P., Schmitt, A. et al. Low-dose peripheral blood stem cell graft after high-dose chemotherapy - an evaluation of hematopoietic reconstitution. BMC Cancer 20, 353 (2020).
212. Savage SA, Bertuch AA. The genetics and clinical manifestations of telomere biology disorders. Genet Med. 2010;12(12):753-764.
213. Savi FM, Brierly GI, Baldwin J, Theodoropoulos C, Woodruff MA. Comparison of Different Decalcification Methods Using Rat Mandibles as a Model. J Histochem Cytochem. 2017 Dec;65(12):705-722.
214. Saxena P, Srivastava J, Rai B, et al. Elevated senescence in the bone marrow mesenchymal stem cells of acquired aplastic anemia patients: A possible implication of DNA damage responses and telomere attrition. Biochim Biophys Acta Mol Basis Dis. 2024;1870(3):167025.
215. Scheinberg P, Cooper JN, Sloand EM, Wu CO, Calado RT, Young NS. Association of telomere length of peripheral blood leukocytes with hematopoietic relapse, malignant transformation, and survival in severe aplastic anemia [published correction appears in JAMA. 2010 Nov 3;304(17):1901]. JAMA. 2010;304(12):1358-1364.

216. Scheinberg P. Aplastic anemia: therapeutic updates in immunosuppression and transplantation. Hematology Am Soc Hematol Educ Program. 2012; 2012:292-300.
217. Schrezenmeier H, Passweg JR, Marsh JC, Bacigalupo A, Bredeson CN, Bullorsky E, et al. Worse outcome and more chronic GVHD with peripheral blood progenitor cells than bone marrow in HLA-matched sibling donor transplants for young patients with severe acquired aplastic anemia. Blood (2007) 110:1397–400.
218. Schrezenmeier H, Passweg JR, Marsh JC, et al. Worse outcome and more chronic GVHD with
219. Schrier SL, Mentzer WC, Rosmarin AG. Aplastic anemia: Pathogenesis, clinical manifestations, and diagnosis. www.uptodate.com (Literature review current through: May 2019. Topic last updated: Oct 03, 2017).
220. Schrier SL, Mentzer WC, Rosmarin AG. Treatment of aplastic anemia in adults. www.uptodate.com (Literature review current through: May 2019. Topic last updated: Jul 06, 2018).
221. Sebo ZL, Rendina-Ruedy E, Ables GP, et al. Bone Marrow Adiposity: Basic and Clinical Implications. Endocr Rev. 2019;40(5):1187-1206. doi:10.1210/er.2018-00138
222. Serakinci N, Graakjaer J, Kolvraa S. Telomere stability and telomerase in mesenchymal stem cells. Biochimie. 2008;90(1):33-40. doi:10.1016/j.biochi.2007.09.005
223. Severn, C.E.; Hugo, M.; Eagle, M.J.; Rooney, P.; Mantalaris, A.; Toye, A.M. Polyurethane scaffolds seeded with CD34 + cells maintain early stem cells whilst also facilitating prolonged egress of haematopoietic progenitors. Sci. Rep. 2016, 6, 1–12.
224. Shah FA, Ruscsák K, Palmquist A. 50 years of scanning electron microscopy of bone-a comprehensive overview of the important discoveries made and insights gained into bone material properties in health, disease, and taphonomy. Bone Res. 2019 May 22;7:15.
225. Shaik, S., Martin, E.C., Hayes, D.J., Gimble, J, V. Devireddyal, R. Transcriptomic Profiling of Adipose Derived Stem Cells Undergoing Osteogenesis by RNA-Seq. Sci Rep 9, 11800 (2019).
226. Sharma V, Rawat S, Gupta S, Tamta S, Sharma R, Seth T, Mohanty S. Human Acquired Aplastic Anemia Patients' Bone-Marrow-Derived Mesenchymal Stem Cells Are Not Influenced by Hematopoietic Compartment and Maintain Stemness and Immune Properties. Anemia. 2021 Apr 29;2021:6678067.
227. Shay JW. Role of Telomeres and Telomerase in Aging and Cancer. Cancer Discov. 2016 Jun;6(6):584-93.
228. Shen B, Tasdogan A, Ubellacker JM, et al. A mechanosensitive peri-arteriolar niche for osteogenesis and lymphopoiesis. Nature. 2021;591(7850):438-444.
229. Shi YN, Zhu N, Liu C, et al. Wnt5a and its signaling pathway in angiogenesis. Clin Chim Acta. 2017;471:263-269.
230. Singh P, Mohammad KS, Pelus LM. CXCR4 expression in the bone marrow microenvironment is required for hematopoietic stem and progenitor cell maintenance and early hematopoietic regeneration after myeloablation. Stem Cells. 2020 Jul;38(7):849-859.
231. Shipounova IN, Petrova TV, Svinareva DA, Momotuk KS, Mikhailova EA, Drize NI. Alterations in hematopoietic microenvironment in patients with aplastic anemia. Clin Transl Sci. (2009) 2:67–74.

232. Simões, I.N., et al., Acellular Urethra Bioscaffold: Decellularization of Whole Urethras for Tissue Engineering Applications. Sci Rep, 2017. 7: p. 41934.
233. Singh R, Kim YH, Lee SJ, Eom HS, Choi BK. 4-1BB immunotherapy: advances and hurdles. Exp Mol Med. 2024;56(1):32-39.
234. Sloand EM, Read EJ, Scheinberg P, Tang Y, More K, Leitman SF, Maciejewski J, Young NS. Mobilization, collection, and immunomagnetic selection of peripheral blood CD34 cells in recovered aplastic anemia patients. Transfusion. 2007 Jul;47(7):1250-3.
235. Socié G, Henry-Amar M, Bacigalupo A, et al. European Bone Marrow Transplantation-Severe Aplastic Anaemia Working Party. Malignant tumors occurring after treatment of aplastic anemia. N Engl J Med. 1993;329(16):1152-1157.
236. Song Y, Li N, Liu Y, Fang B. Improved outcome of adults with aplastic anaemia treated with arsenic trioxide plus ciclosporin. Br J Haematol. (2013) 160:266–9.
237. Sottile J, Hocking DC. Fibronectin polymerization regulates the composition and stability of extracellular matrix fibrils and cell-matrix adhesions. Mol Biol Cell. 2002 Oct;13(10):3546-59.
238. Staal FJ, Clevers HC. WNT signalling and haematopoiesis: a WNT-WNT situation. Nat Rev Immunol. 2005;5(1):21-30. doi:10.1038/nri1529
239. Stelzer, G., Rosen, N., Plaschkes, I., Zimmerman, S., Twik, M., Fishilevich, S., ... & Lancet, D. (2016). The GeneCards Suite: From Gene Data Mining to Disease Genome Sequence Analyses. Current Protocols in Bioinformatics, 54(1), 1.30.1-1.30.33
240. Stucker S, Chen J, Watt FE, Kusumbe AP. Bone Angiogenesis and Vascular Niche Remodeling in Stress, Aging, and Diseases. Front Cell Dev Biol. 2020;8:602269. Published 2020 Nov 26. doi:10.3389/fcell.2020.602269
241. Su, H., Na, N., Zhang, X. et al. The biological function and significance of CD74 in immune diseases. Inflamm. Res. 66, 209–216 (2017).
242. Suh HC, Gooya J, Renn K, Friedman AD, Johnson PF, Keller JR. C/EBPalpha determines hematopoietic cell fate in multipotential progenitor cells by inhibiting erythroid differentiation and inducing myeloid differentiation. Blood. 2006 Jun 1;107(11):4308-16.
243. Takada I, Kouzmenko AP, Kato S. Wnt and PPARgamma signaling in osteoblastogenesis and adipogenesis. Nat Rev Rheumatol. 2009;5(8):442-447. doi:10.1038/nrrheum.2009.137
244. Tang G, Liu Z, Liu Y, Yu J, Wang X, Tan Z, Ye X. Recent Trends in the Development of Bone Regenerative Biomaterials. Front Cell Dev Biol. 2021 May 7;9:665813.
245. Tang NN, Xu RB, Jiang B, et al. AHNAK2 Regulates NF-κB/MMP-9 Signaling to Promote Pancreatic Cancer Progression. Biochem Genet. Published online June 12, 2024. doi:10.1007/s10528-024-10844-z
246. Tomimori, Y.; Takagi, M.; Yoshida, T. The construction of an in vitro three-dimensional hematopoietic microenvironment for mouse bone marrow cells employing porous carriers. Cytotechnology 2000, 34, 121–130.
247. Tong Q, Tsai J, Hotamisligil GS. GATA transcription factors and fat cell formation. Drug News Perspect. (2003) 16:585–8.
248. Tonglin H, Yanna Z, Xiaoling Y, Ruilan G, Liming Y. Single-Cell RNA-Seq of Bone Marrow Cells in Aplastic Anemia. Front Genet. 2022 Jan 3;12:745483.

249. Torlakovic EE, Brynes RK, Hyjek E, et al. ICSH guidelines for the standardization of bone marrow immunohistochemistry. Int J Lab Hematol. 2015;37(4):431-449.
250. Trinh T, Ropa J, Aljoufi A, et al. Leptin receptor, a surface marker for a subset of highly engrafting long-term functional hematopoietic stem cells. Leukemia. 2021;35(7):2064-2075.
251. Tripathy NK, Singh SP, Nityanand S. Enhanced adipogenicity of bone marrow mesenchymal stem cells in aplastic anemia. Stem Cells Int. 2014;2014:276862.
252. Tsai FY, Keller G, Kuo FC, Weiss M, Chen J, Rosenblatt M, et al. An early haematopoietic defect in mice lacking the transcription factor GATA-2. Nature (1994) 371:221–6.
253. Tzec-Interián JA, González-Padilla D, Góngora-Castillo EB. Bioinformatics perspectives on transcriptomics: a comprehensive review of bulk and single-cell RNA sequencing analyses. Quantitative Biology. 2025;e78.
254. Val CH, de Oliveira MC, Lacerda DR, et al. SOCS2 modulates adipose tissue inflammation and expansion in mice. J Nutr Biochem. 2020;76:108304.
255. van der Eerden B, van Wijnen A. Meeting report of the 2016 bone marrow adiposity meeting. Adipocyte (2017) 6:304–13.
256. Vanhollebeke B, Pays E. The function of apolipoproteins L. Cell Mol Life Sci. 2006;63(17):1937-1944.
257. Vasanthan J, Gurusamy N, Rajasingh S, Sigamani V, Kirankumar S, Thomas EL, Rajasingh J. Role of Human Mesenchymal Stem Cells in Regenerative Therapy. Cells. 2020 Dec 31;10(1):54.
258. Ventura, M.S.; Jahnen-dechent, W.; Labude, N.; Bovi, M.; Hieronymus, T.; Zenke, M.; Neurs, S. Cord blood-hematopoietic stem cell expansion in 3D fibrin scaffolds with stromal support. Biomaterials 2012, 33, 6987–6997.
259. Wagner EM. Monitoring gene expression: quantitative real-time rt-PCR. Methods Mol Biol. 2013;1027:19-45.
260. Wan S, Xie J, Liang Y, Yu X. Pathological roles of bone marrow adipocyte-derived monocyte chemotactic protein-1 in type 2 diabetic mice. Cell Death Discov. 2023;9(1):412. Published 2023 Nov 13. doi:10.1038/s41420-023-01708-3
261. Wang H, Leng Y, Gong Y. Bone Marrow Fat and Hematopoiesis. Front Endocrinol (Lausanne). 2018; 9:694. Published 2018 Nov 28.
262. Wang HY, Ding TL, Xie Y, Xu XP, Yu L, Chen T. Osteogenic and adipogenic differentiation of bone marrow-derived mesenchymal stem cells in patients with aplastic anemia. Zhonghua Nei Ke Za Zhi (2009) 48:39–43.
263. Wang XA, Li JP, Wu KH, Yang SF, Chao YH. Mesenchymal Stem Cells in Acquired Aplastic Anemia: The Spectrum from Basic to Clinical Utility. Int J Mol Sci. 2023 Feb 24;24(5):4464.
264. Wang Y, McReynolds LJ, Dagnall C, Katki HA, Spellman SR, Wang T, Hicks B, Freedman ND, Jones K, Lee SJ, Savage SA, Gadalla SM. Pre-transplant short telomeres are associated with high mortality risk after unrelated donor haematopoietic cell transplant for severe aplastic anaemia. Br J Haematol. 2020 Jan;188(2):309-316.
265. Wang Y, Zhang L, Chen H, Yang J, Cui Y, Wang H. Coronary artery disease-associated immune gene RBP1 and its pan-cancer analysis. Front Cardiovasc Med. 2023 Mar 9;10:1091950.

266. Warnes, G. R., Bolker, B., Bonebakker, L., Gentleman, R., Liaw, W. H. A., Lumley, T., Maechler, M., Magnusson, A., Moeller, S., Schwartz, M., & Venables, B. 1 (2023). gplots: Various R Programming Tools for Plotting Data. R package version 3.1.3. https://CRAN.R-project.org/package=gplots
267. Weijts B, Robin C. Capturing embryonic hematopoiesis in temporal and spatial dimensions. Exp Hematol. 2024;136:104257.
268. White LJ, Taylor AJ, Faulk DM, et al. The impact of detergents on the tissue decellularization process: A ToF-SIMS study. Acta Biomater. 2017;50:207-219.
269. Wickham H (2016). ggplot2: Elegant Graphics for Data Analysis. Springer-Verlag New York. ISBN 978-3-319-24277-4, https://ggplot2.tidyverse.org
270. Wirth F, Lubosch A, Hamelmann S, Nakchbandi IA. Fibronectin and Its Receptors in Hematopoiesis. Cells. 2020 Dec 18;9(12):2717.
271. Wong HY, Schwarz H. CD137 / CD137 ligand signalling regulates the immune balance: A potential target for novel immunotherapy of autoimmune diseases. J Autoimmun. 2020;112:102499. doi:10.1016/j.jaut.2020.102499
272. Wu J, Wang Y, Jiang Z. TNFSF9 Is a Prognostic Biomarker and Correlated with Immune Infiltrates in Pancreatic Cancer. J Gastrointest Cancer. 2021;52(1):150-159. doi:10.1007/s12029-020-00371-6
273. Wu J, Wang Y. Role of TNFSF9 bidirectional signal transduction in antitumor immunotherapy. Eur J Pharmacol. 2022;928:175097. doi:10.1016/j.ejphar.2022.175097
274. Wu L, Mo W, Zhang Y, Deng H, Li Y, Zhou R, et al. Impairment of hematopoietic stem cell niches in patients with aplastic anemia. Int J Hematol. (2015) 102:645–53.
275. Wu L, Mo W, Zhang Y, et al. Vascular and perivascular niches, but not the osteoblastic niche, are numerically restored following allogeneic hematopoietic stem cell transplantation in patients with aplastic anemia. Int J Hematol. 2017;106(1):71-81. doi:10.1007/s12185-017-2217-1
276. Wu L, Mo W, Zhang Y, Zhou M, Li Y, Zhou R, et al. Vascular and perivascular niches, but not the osteoblastic niche, are numerically restored following allogeneic hematopoietic stem cell transplantation in patients with aplastic anemia. Int J Hematol. (2017) 106:71–81.
277. Wu T, Hu E, Xu S, Chen M, Guo P, Dai Z, Feng T, Zhou L, Tang W, Zhan L, Fu x, Liu S, Bo X, Yu G (2021). “clusterProfiler 4.0: A universal enrichment tool for interpreting omics data.” The Innovation, 2(3), 100141. doi:10.1016/j.xinn.2021.100141.
278. Wu X, Jiang J, Gu Z, Zhang J, Chen Y, Liu X. Mesenchymal stromal cell therapies: immunomodulatory properties and clinical progress. Stem Cell Res Ther. 2020;11(1):345. Published 2020 Aug 8.
279. Xie, Z., Yu, W., Ye, G. et al. Single-cell RNA sequencing analysis of human bone-marrow-derived mesenchymal stem cells and functional subpopulation identification. Exp Mol Med 54, 483–492 (2022).
280. Xu C, Feng C, Huang P, et al. TNFα and IFNγ rapidly activate PI3K-AKT signaling to drive glycolysis that confers mesenchymal stem cells enhanced anti-inflammatory property. Stem Cell Res Ther. 2022;13(1):491. Published 2022 Oct 4. doi:10.1186/s13287-022-03178-3
281. Xu M, Wen J, Xu Q, et al. AHNAK2 Promotes the Progression of Differentiated Thyroid Cancer through PI3K/AKT Signaling Pathway. Curr Cancer Drug Targets. 2024;24(2):220-229. doi:10.2174/1568009622666220908092506

282. Xu Y, Takahashi Y, Wang Y, Hama A, Nishio N, Muramatsu H, et al. Downregulation of GATA-2 and overexpression of adipogenic gene- PPARgamma in mesenchymal stem cells from patients with aplastic anemia. Exp Hematol. (2009) 37:1393–9.
283. Xue C, Yao Q, Gu X, et al. Evolving cognition of the JAK-STAT signaling pathway: autoimmune disorders and cancer. Signal Transduct Target Ther. 2023;8(1):204. Published 2023 May 19. doi:10.1038/s41392-023-01468-7
284. Yao W, Cheng Z, Shahnazari M, Dai W, Johnson ML, Lane NE. Overexpression of secreted frizzled-related protein 1 inhibits bone formation and attenuates parathyroid hormone bone anabolic effects. J Bone Miner Res. 2010 Feb;25(2):190-9.
285. Yao, H., Ren, D., Wang, Y. et al. KCTD9 inhibits the Wnt/β-catenin pathway by decreasing the level of β-catenin in colorectal cancer. Cell Death Dis 13, 761 (2022).
286. Ye R, Liu D, Guan H, et al. AHNAK2 promotes thyroid carcinoma progression by activating the NF-κB pathway. Life Sci. 2021;286:120032. doi:10.1016/j.lfs.2021.120032
287. Yin X, Yang J, Liu Y, et al. Altered expression of leptin and leptin receptor in the development of immune-mediated aplastic anemia in mice. Exp Ther Med. 2019;18(2):1047-1056. doi:10.3892/etm.2019.7660
288. Yong AS, Goh AS, Rahman M et al.: Epidemiology of aplastic anemia in the state of Sabah, Malaysia. Med J Malaysia 53:59, 1998.
289. Yoshizato T, Dumitriu B, Hosokawa K, et al. Somatic Mutations and Clonal Hematopoiesis in Aplastic Anemia. N Engl J Med. 2015;373(1):35-47. doi:10.1056/NEJMoa1414799
290. Young NS, Maciejewski J: Mechanisms of disease: The pathophysiology of acquired aplastic anemia. N Engl J Med 336:1365, 1997.
291. Young NS. Aplastic anaemia. Lancet. 1995 Jul 22;346(8969):228-32.
292. Yu G, Wang L, Han Y, He Q (2012). “clusterProfiler: an R package for comparing biological themes among gene clusters.” OMICS: A Journal of Integrative Biology, 16(5), 284-287. doi:10.1089/omi.2011.0118
293. Yuan Z, Li Q, Luo S, et al. PPARγ and Wnt Signaling in Adipogenic and Osteogenic Differentiation of Mesenchymal Stem Cells. Curr Stem Cell Res Ther. 2016;11(3):216-225. doi:10.2174/1574888x10666150519093429
294. Yun HJ, Jo DY. Production of stromal cell-derived factor-1 (SDF-1)and expression of CXCR4 in human bone marrow endothelial cells. J Korean Med Sci. 2003 Oct;18(5):679-85.
295. Zeng W, Chen G, Kajigaya S, et al. Gene expression profiling in CD34 cells to identify differences between aplastic anemia patients and healthy volunteers. Blood. 2004;103(1):325-332. doi:10.1182/blood-2003-02-0490
296. Zeng W, Chen G, Kajigaya S, Nunez O, Charrow A, Billings EM, et al. Gene expression profiling in CD34 cells to identify differences between aplastic anemia patients and healthy volunteers. Blood (2004) 103:325–32.
297. Zhang N, Dai YL, Huang LF, Liu WL. Zhongguo Shi Yan Xue Ye Xue Za Zhi. [Therapeutic effect of lithium chloride combined with cyclosporine A on mouse model with aplastic anemia]. 2012;20(3):654-657
298. Zhang S, Cai Z, Li H. AHNAKs roles in physiology and malignant tumors. Front Oncol. 2023;13:1258951. Published 2023 Nov 14. doi:10.3389/fonc.2023.1258951

299.Zhang X, Wang P, Chen T, et al. Kctd9 Deficiency Impairs Natural Killer Cell Development and Effector Function. Front Immunol. 2019;10:744. Published 2019 Apr 10.
300.Zhao J, Wang C, Song Y, Fang B. Arsenic trioxide and microRNA-204 display contrary effects on regulating adipogenic and osteogenic differentiation of mesenchymal stem cells in aplastic anemia. Acta Biochim Biophys Sin (2014) 46:885–93.
301.Zhou Q, Huang L, Liu Y, et al. Single-cell RNA sequencing depicts metabolic changes in children with aplastic anemia. Front Oncol. 2023;13:1075408. Published 2023 Mar 29. doi:10.3389/fonc.2023.1075408
302.Zhou Q, Huang L, Liu Y, Huang J, Wen L, Yang J, Liang J, Chen Y, Chen C. Single-cell RNA sequencing depicts metabolic changes in children with aplastic anemia. Front Oncol. 2023 Mar 29;13:1075408.
303.Zhou, D.; Chen, L.; Ding, J.; Zhang, X.; Nie, Z.; Li, X. A 3D engineered scaffold for hematopoietic progenitor/stem cell co-culture in vitro. Sci. Rep. 2020, 10, 1–11.
304.Zhu C, Lian Y, Wang C, Wu P, Li X, Gao Y, Fan S, Ai L, Fang L, Pan H, Cheng T, Shi J, Zhu P. Single-cell transcriptomics dissects hematopoietic cell destruction and T-cell engagement in aplastic anemia. Blood. 2021 Jul 8;138(1):23-33.
305.Zhu H, Hu X, Feng S, Li Y, Zhang Y, Qiu S, Chen R, Ye Y, Gu L, Jian Z, Xu X, Xiong X. APOL4, a Novel Immune-Related Prognostic Biomarker for Glioma. J Clin Med. 2022 Sep 29;11(19):5765.
306.Zhu YS, Mo TT, Jiang C, Zhang JN. Osteonectin bidirectionally regulates osteoblast mineralization. J Orthop Surg Res. 2023 Oct 8;18(1):761.
307.Zhu, A., Ibrahim, J. G., & Love, M. I. (2019). Heavy-tailed prior distributions for sequence count data: removing the noise and preserving large differences. Bioinformatics, 35(12), 2084-2092
308.Zhuang H, Zhang X, Zhu C, et al. Molecular Mechanisms of PPAR-γ Governing MSCs Osteogenic and Adipogenic Differentiation. Curr Stem Cell Res Ther. 2016;11(3):255-264. doi:10.2174/1574888x10666150531173309
309.Zoch ML, Clemens TL, Riddle RC. New insights into the biology of osteocalcin. Bone. 2016 Jan;82:42-9.

X. Appendix

X.i. Appendix A

Table A.1: FastQC Basic Statistics

Table A.1: FastQC Basic Statistics				
Samples	**Sample ID**	**Total sequences**	**Sequences flagged as poor quality**	**%GC**
AA	AM15	20515252	0	45%
	AM10	22500591	0	44%
	AM08	29601887	0	45%
	AM87	26923608	0	45%
Controls	CF18	21732004	0	46%
	CM11	54740823	0	45%
	CF10	40550205	0	45%
	CM78	32144362	0	45%

Table A.2: Summary of mapping statistics

Table A.2: Mapping statistics (Human reference genome GRCh38).						
Samples	Sample ID	Number of input reads	Uniquely mapped reads %	Average of input read length	Average mapped length	Mismatch rate per base %
AA	AM08	29601887	90.82%	98	98,18	0.16%
	AM10	22500591	91.70%	98	98,11	0.17%
	AM15	20515252	88,93%	98	98,04	0,17%
	AM87	26923608	89.75%	98	97,72	0.16%
Controls	CF18	21732004	88.10%	99	98,12	0,17%
	CF10	40550205	90.94%	98	98,05	0,17%
	CM11	54740823	90,28%	98	98,16	0,16%
	CM78	32144362	89,20%	99	98,25	0,17%

X.ii. Appendix B

B.1. - FACSCalibur™ flow cytometer (BD Biosciences) – representative images of flow cytometry analysis of BM-MSCs samples using FCS Express™7 (De Novo Software by Dotmatics).

a) F18 (control-derived BM-MSCs)

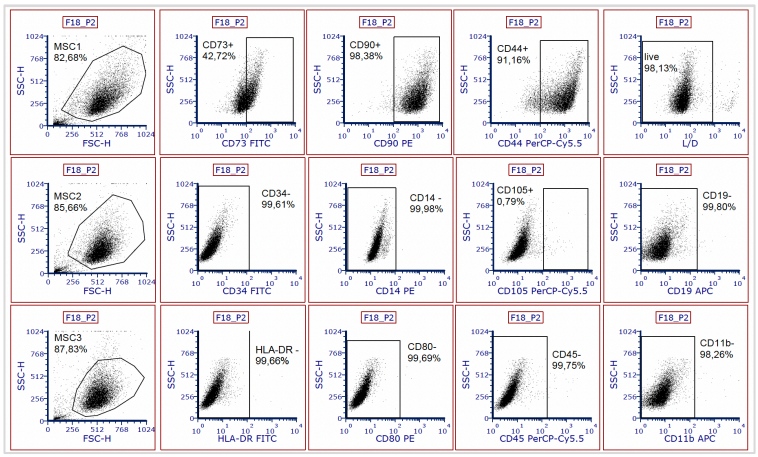

b) M15 (AA-derived BM-MSCs)

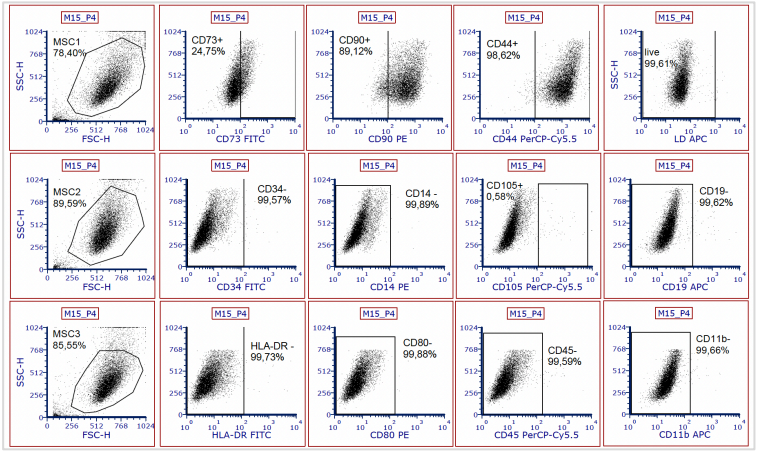

B.2. - FACSCanto™ II (BD Biosciences) – representative images of flow cytometry analysis of BM-MSCs samples using FCS Express™7 (De Novo Software by Dotmatics).

a) M11 (control-derived MSCs)

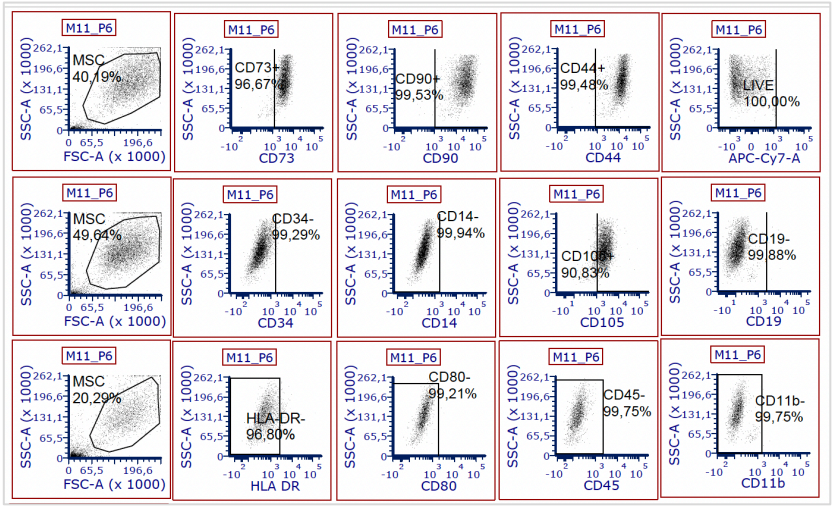

b) M10 (AA-derived BM-MSCs)

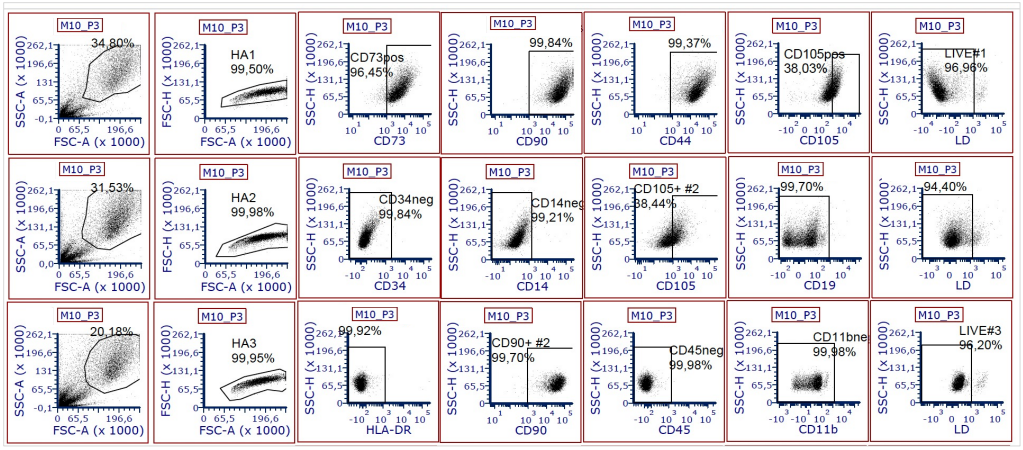

B.3. - AA-derived and control-derived BM-MSCs immunophenotypic profile – Mean fluorescence intensity (MFI) of cell surface positive markers for MSCs identification (CD73, CD90, CD44, CD105) (±SE mean); MFI coefficient of variation (CV) (±SE mean). Data acquisition performed with FACSCalibur™ (BD Biosciences) flow cytometer. P = cell passage number.

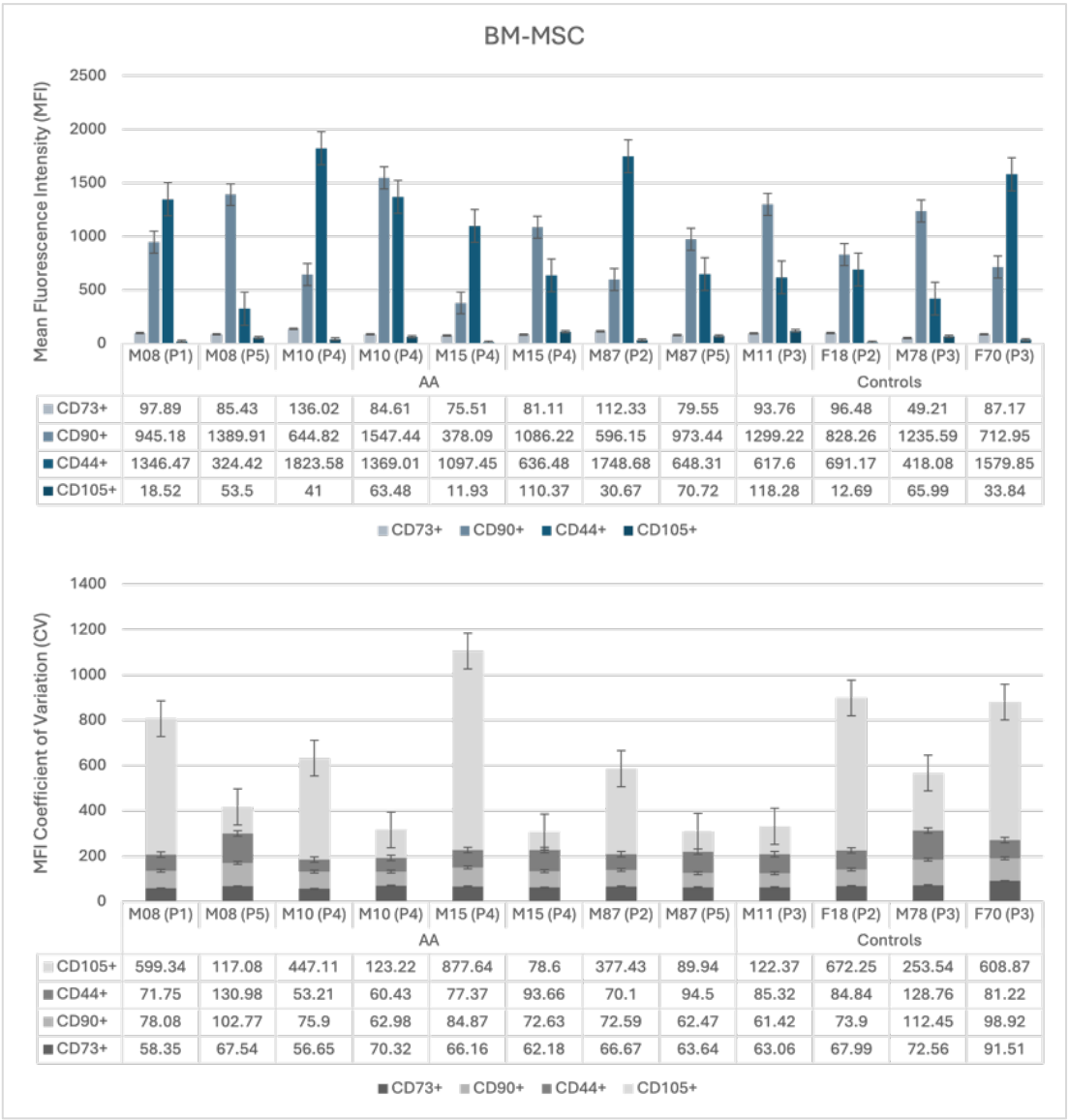

	M08 (P1)	M08 (P5)	M10 (P4)	M10 (P4)	M15 (P4)	M15 (P4)	M87 (P2)	M87 (P5)	M11 (P3)	F18 (P2)	M78 (P3)	F70 (P3)
	AA								Controls			
CD73+	97.89	85.43	136.02	84.61	75.51	81.11	112.33	79.55	93.76	96.48	49.21	87.17
CD90+	945.18	1389.91	644.82	1547.44	378.09	1086.22	596.15	973.44	1299.22	828.26	1235.59	712.95
CD44+	1346.47	324.42	1823.58	1369.01	1097.45	636.48	1748.68	648.31	617.6	691.17	418.08	1579.85
CD105+	18.52	53.5	41	63.48	11.93	110.37	30.67	70.72	118.28	12.69	65.99	33.84

	M08 (P1)	M08 (P5)	M10 (P4)	M10 (P4)	M15 (P4)	M15 (P4)	M87 (P2)	M87 (P5)	M11 (P3)	F18 (P2)	M78 (P3)	F70 (P3)
	AA								Controls			
CD105+	599.34	117.08	447.11	123.22	877.64	78.6	377.43	89.94	122.37	672.25	253.54	608.87
CD44+	71.75	130.98	53.21	60.43	77.37	93.66	70.1	94.5	85.32	84.84	128.76	81.22
CD90+	78.08	102.77	75.9	62.98	84.87	72.63	72.59	62.47	61.42	73.9	112.45	98.92
CD73+	58.35	67.54	56.65	70.32	66.16	62.18	66.67	63.64	63.06	67.99	72.56	91.51

B.4. - AA-derived and control-derived BM-MSCs immunophenotypic profile – Mean fluorescence intensity (MFI) of cell surface positive markers for MSCs identification (CD73, CD90, CD44, CD105) (±SE mean); MFI coefficient of variation (CV) (±SE mean). Data acquisition performed with FACSCanto™ II (BD Biosciences) flow cytometer. P = cell passage number.

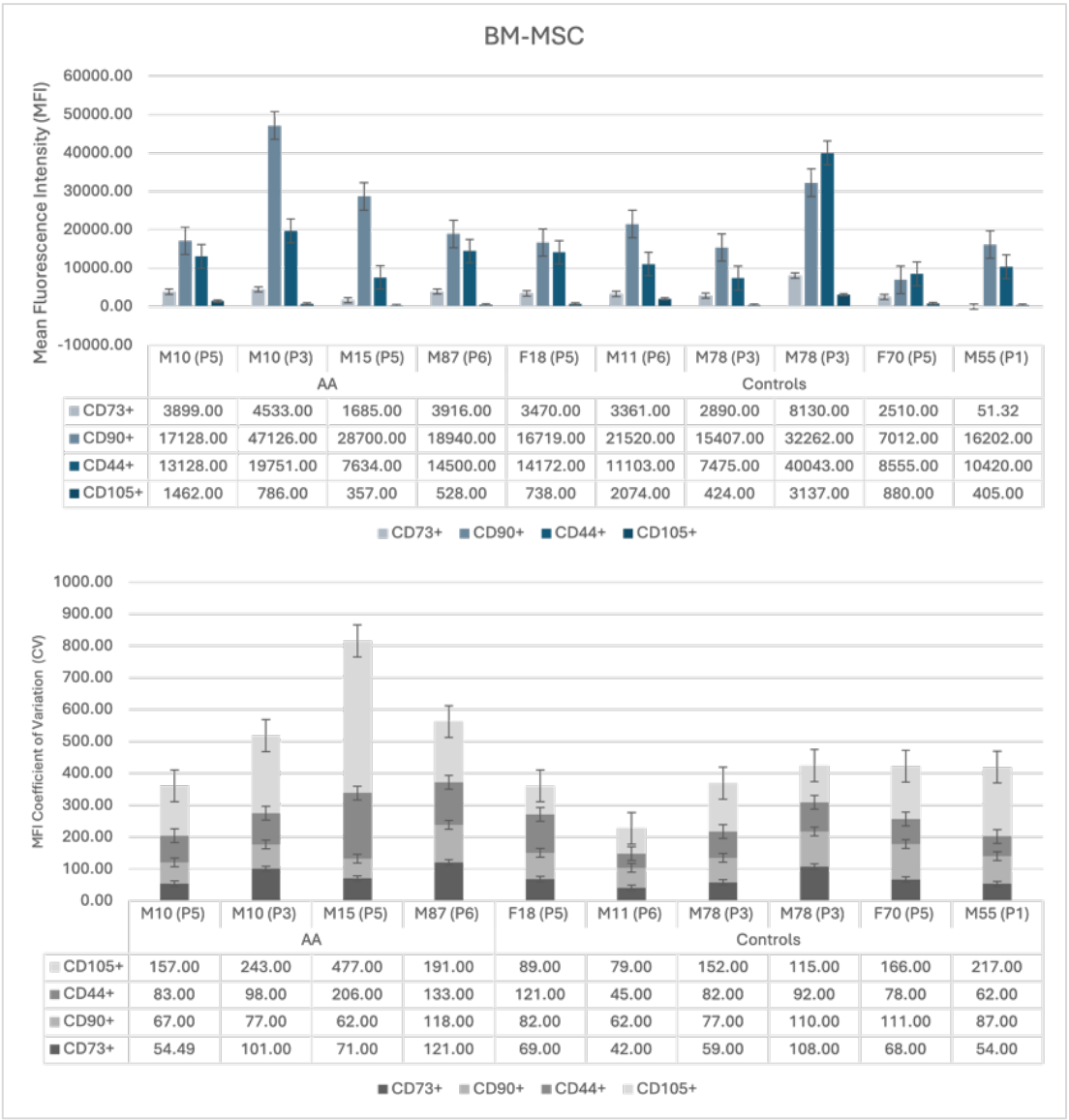

	M10 (P5)	M10 (P3)	M15 (P5)	M87 (P6)	F18 (P5)	M11 (P6)	M78 (P3)	M78 (P3)	F70 (P5)	M55 (P1)
	AA				Controls					
CD73+	3899.00	4533.00	1685.00	3916.00	3470.00	3361.00	2890.00	8130.00	2510.00	51.32
CD90+	17128.00	47126.00	28700.00	18940.00	16719.00	21520.00	15407.00	32262.00	7012.00	16202.00
CD44+	13128.00	19751.00	7634.00	14500.00	14172.00	11103.00	7475.00	40043.00	8555.00	10420.00
CD105+	1462.00	786.00	357.00	528.00	738.00	2074.00	424.00	3137.00	880.00	405.00

	M10 (P5)	M10 (P3)	M15 (P5)	M87 (P6)	F18 (P5)	M11 (P6)	M78 (P3)	M78 (P3)	F70 (P5)	M55 (P1)
	AA				Controls					
CD105+	157.00	243.00	477.00	191.00	89.00	79.00	152.00	115.00	166.00	217.00
CD44+	83.00	98.00	206.00	133.00	121.00	45.00	82.00	92.00	78.00	62.00
CD90+	67.00	77.00	62.00	118.00	82.00	62.00	77.00	110.00	111.00	87.00
CD73+	54.49	101.00	71.00	121.00	69.00	42.00	59.00	108.00	68.00	54.00

B.5. - FACSCanto™ II (BD Biosciences) – representative images of flow cytometry analysis of HSPC using FCS Express™7 (De Novo Software by Dotmatics).

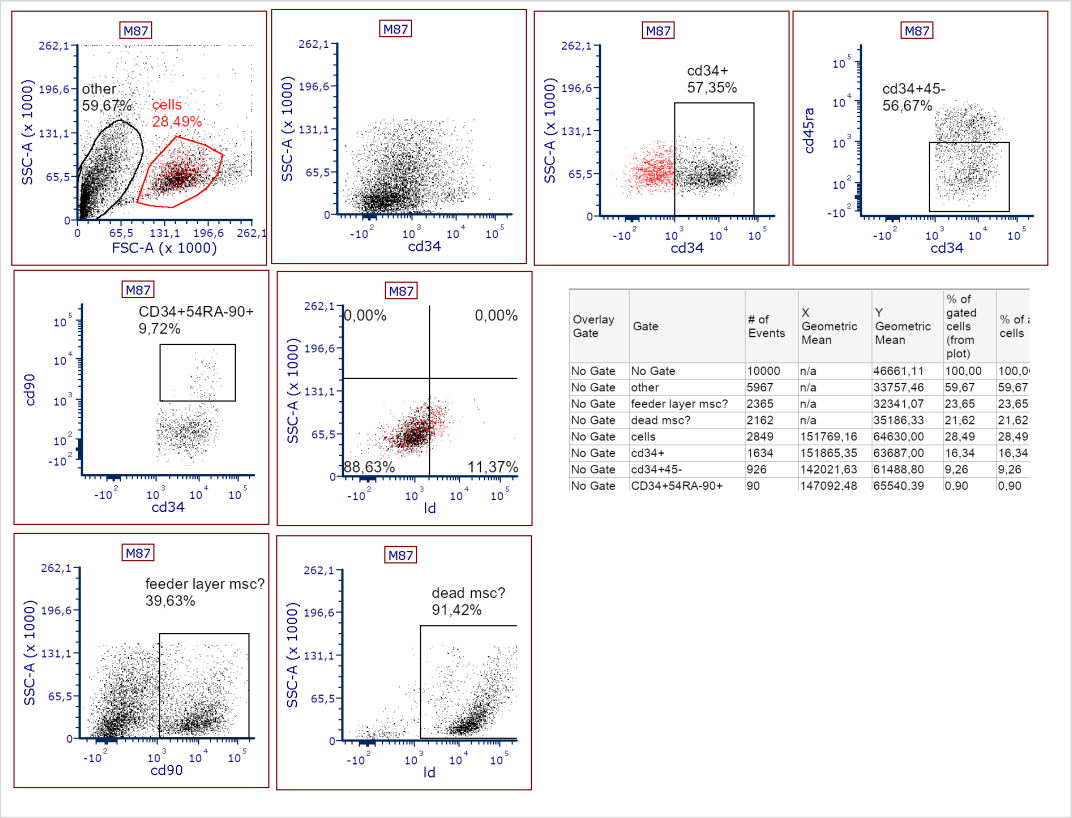

Overlay Gate	Gate	# of Events	X Geometric Mean	Y Geometric Mean	% of gated cells (from plot)	% of cells
No Gate	No Gate	10000	n/a	46661,11	100,00	100,0
No Gate	other	5967	n/a	33757,46	59,67	59,67
No Gate	feeder layer msc?	2365	n/a	32341,07	23,65	23,65
No Gate	dead msc?	2162	n/a	35186,33	21,62	21,62
No Gate	cells	2849	151769,16	64630,00	28,49	28,49
No Gate	cd34+	1634	151865,35	63687,00	16,34	16,34
No Gate	cd34+45-	926	142021,63	61488,80	9,26	9,26
No Gate	CD34+54RA-90+	90	147092,48	65540,39	0,90	0,90

X.iii. Appendix C

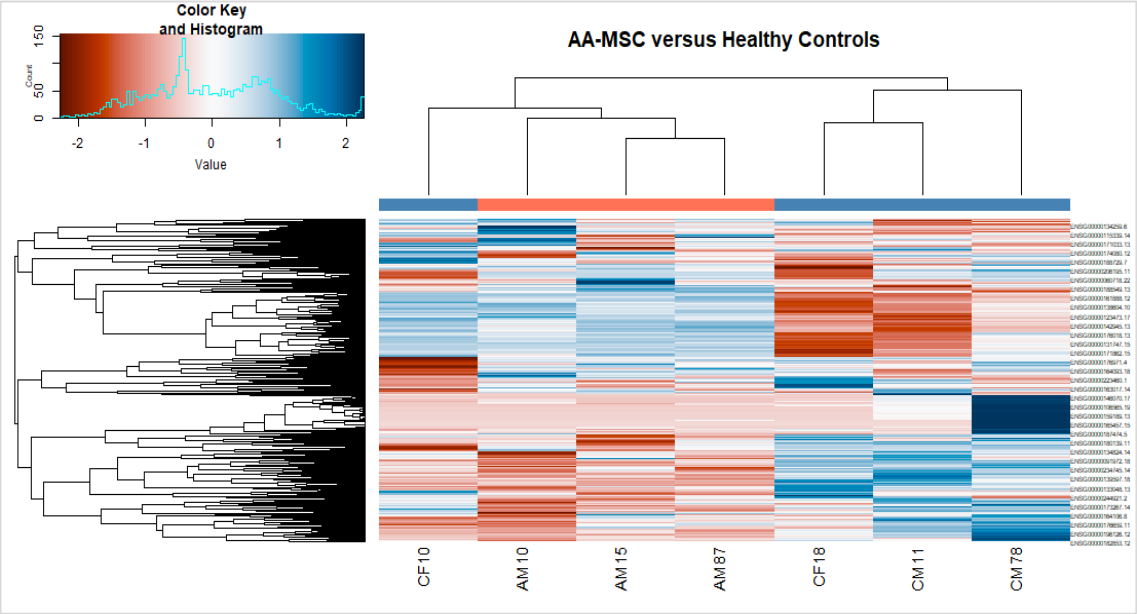

Figure C.1: Heatmap and dendrogram designed from scaled (z-score) VST-transformed counts matrix of the 500 most variable genes. Clustering of samples by gene expression. Sample AM08 removed.

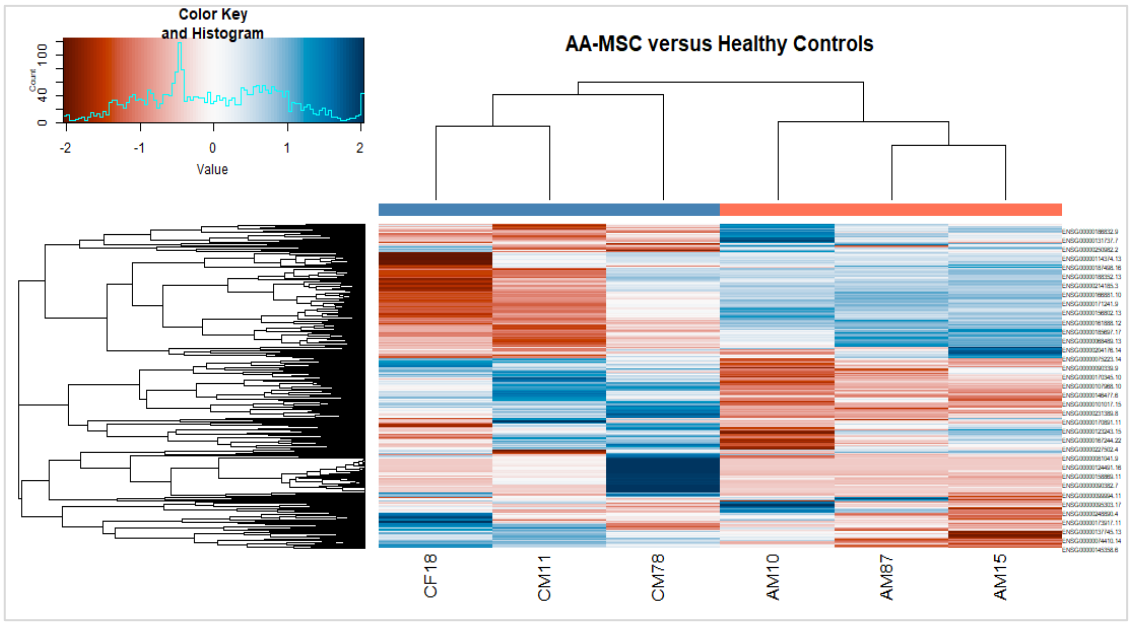

Figure C.2: Heatmap and dendrogram designed from scaled (z-score) VST-transformed counts matrix of the 500 most variable genes. Clustering of samples by gene expression. Sample AM08 removed. Samples AM08 and CF10 removed.

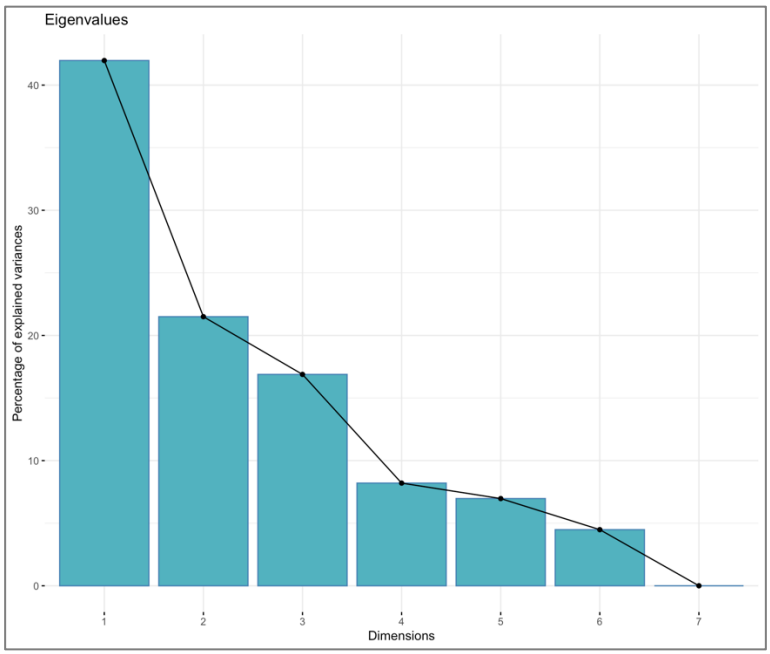

Figure C.3: Eigenvalues showing the relative amount of variation explained by the different Principal Components.

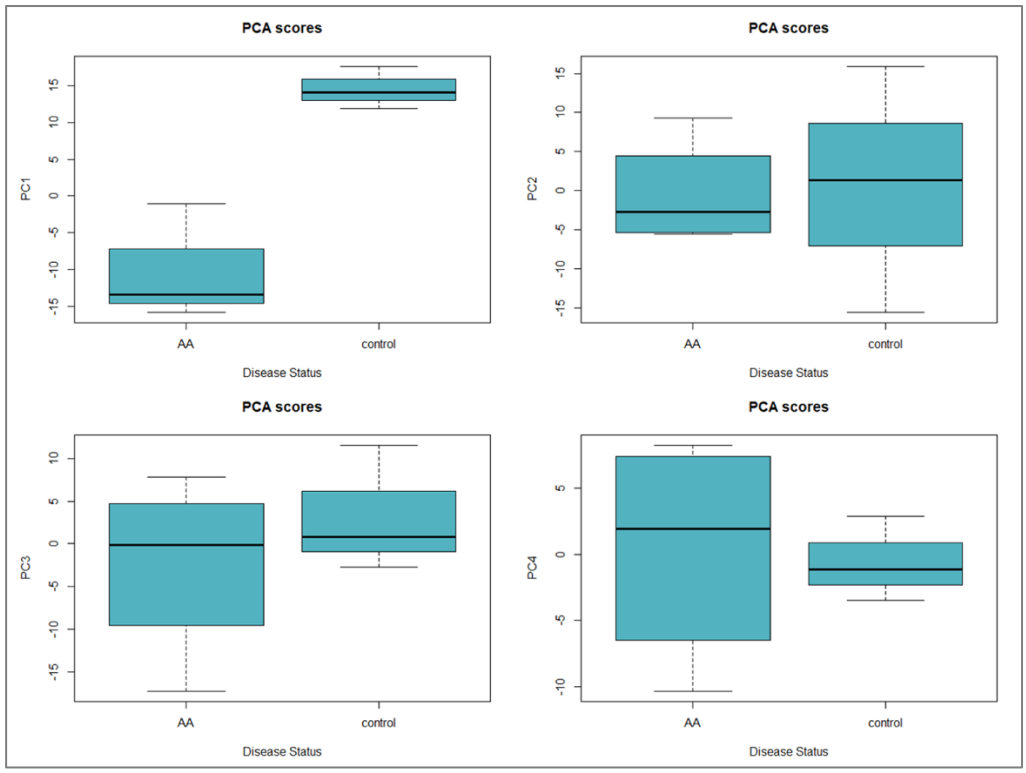

Figure C.4: Boxplots representing PCA scores for PC1, PC2, PC3 and PC4.

X.iv. Appendix D

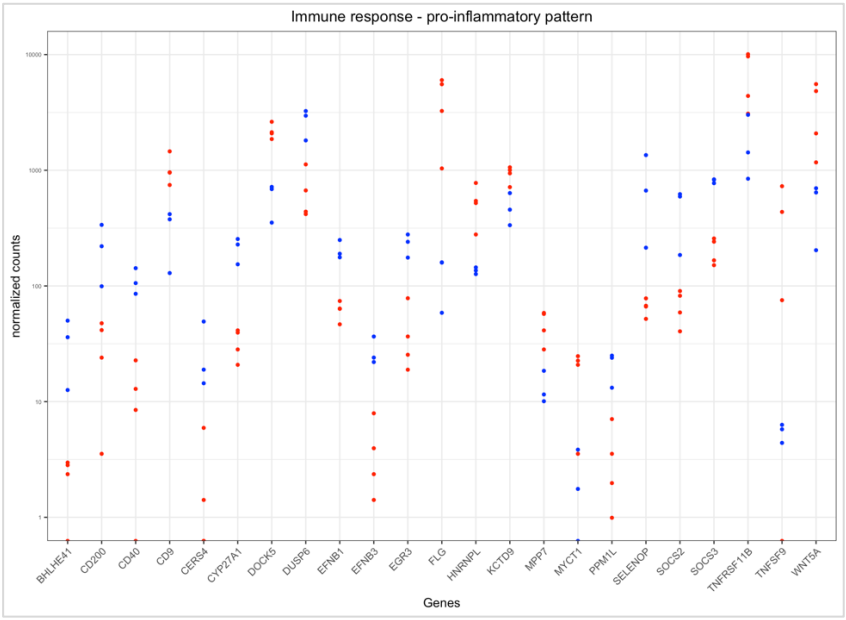

Figure D.1: Strip chart of differently expressed genes (AA versus controls) by biological function - immune response-related genes: AA-derived BM-MSCs showing up-regulation of pro-inflammatory genes and down-regulation of anti-inflammatory genes in comparison to controls.

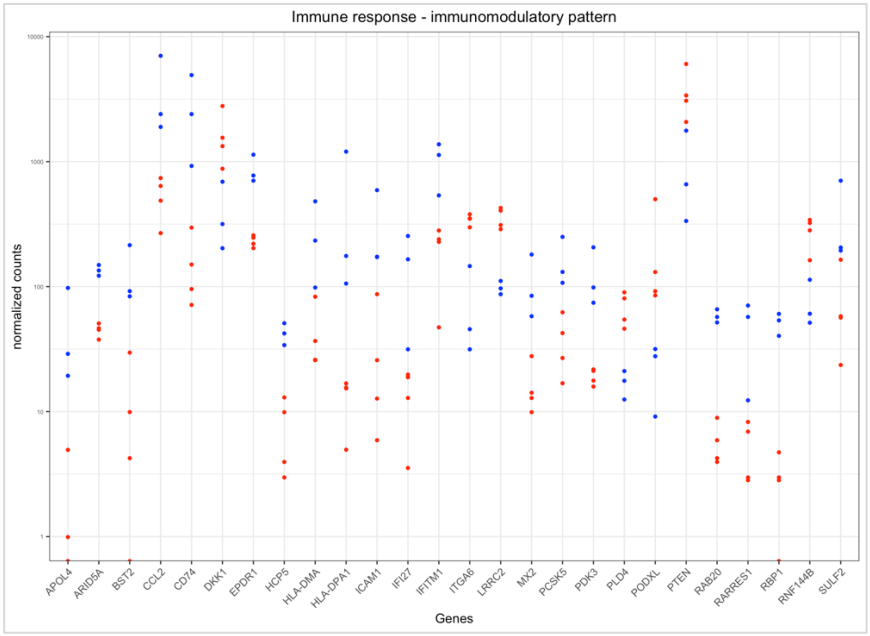

Figure D.2: Strip chart of differently expressed genes (AA versus controls) by biological function - immune response-related genes: AA-derived BM-MSCs showing down-regulation of pro-inflammatory genes and up-regulation of anti-inflammatory genes in comparison to controls.

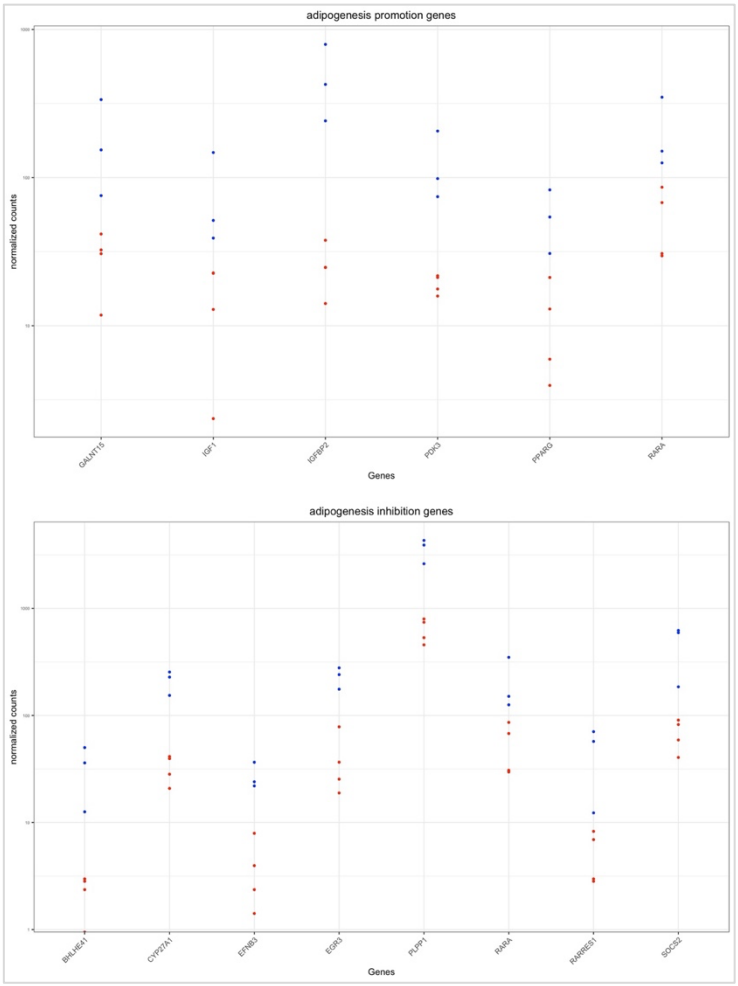

Figure D.3: Strip chart of differently expressed genes (AA versus controls) by biological function - adipogenesis-related genes: AA-derived BM-MSCs showing down-regulation of both adipogenesis promotion and adipogenesis inhibition genes, in comparison to controls.

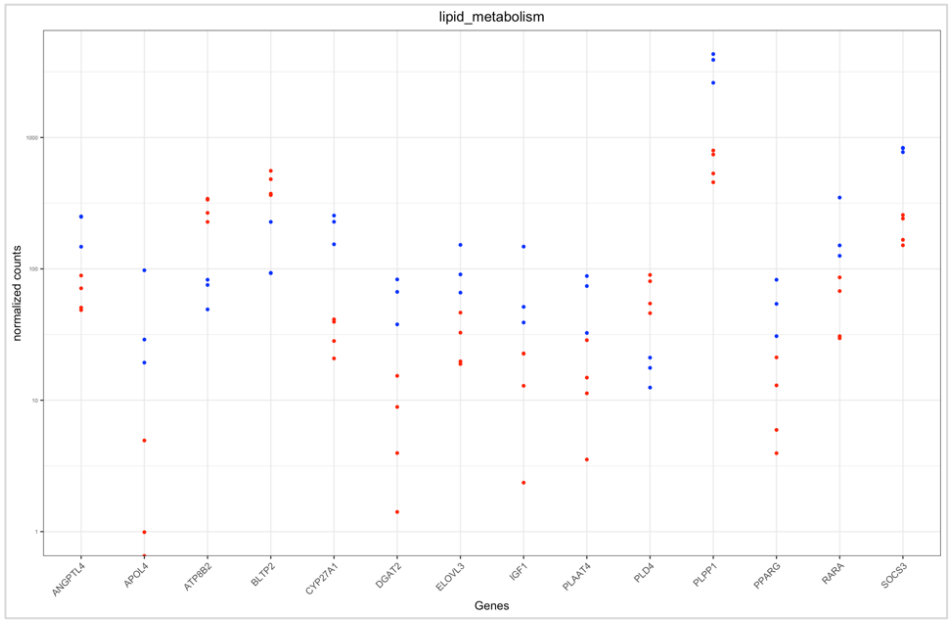

Figure D.4: Strip chart of differently expressed genes (AA versus controls) by biological function - lipid metabolism-related genes.

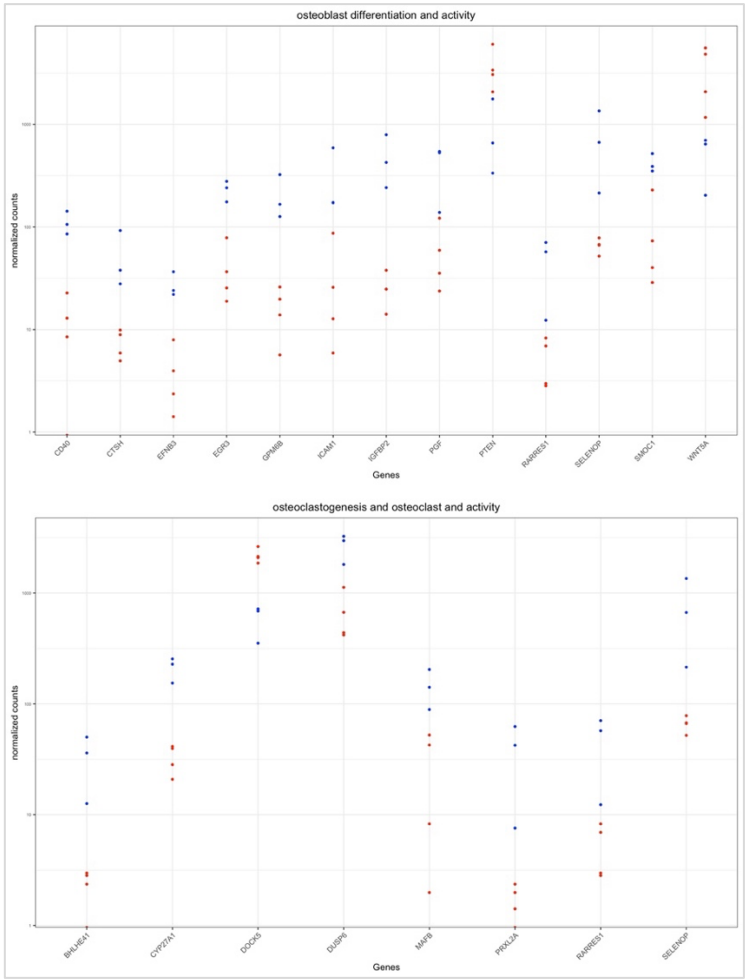

Figure D.5: Strip chart of differently expressed genes (AA versus controls) by biological function - osteoblast and osteoclast differentiation and activity-related genes.

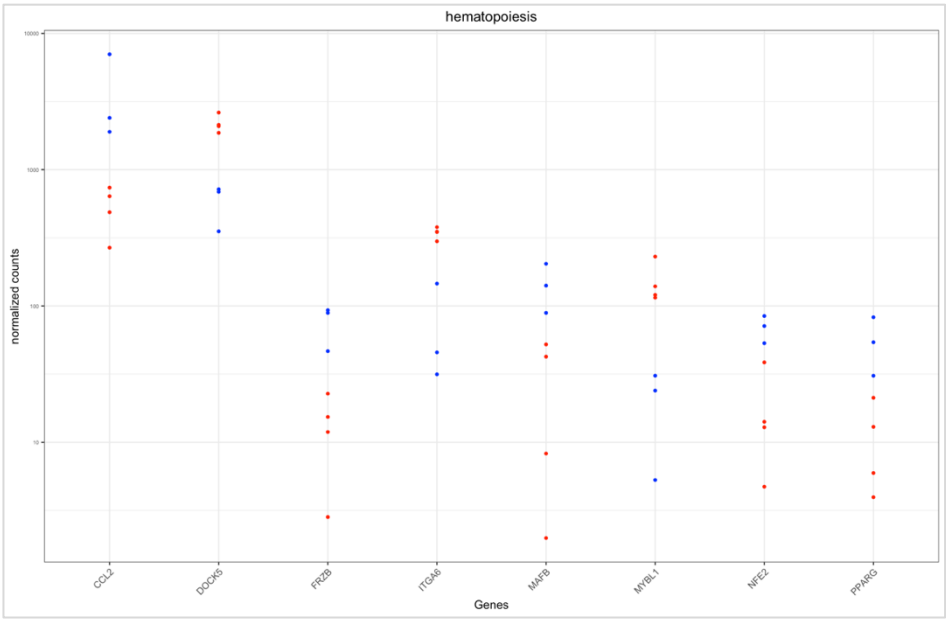

Figure D.6: Strip chart of differently expressed genes (AA versus controls) by biological function - hematopoietic support-related genes.

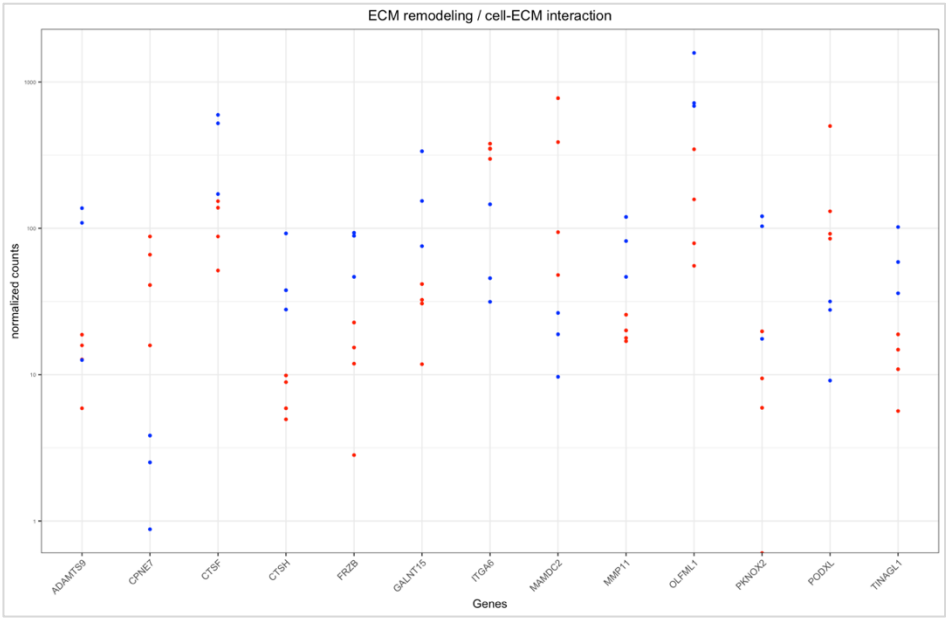

Figure D.7: Strip chart of differently expressed genes (AA versus controls) by biological function - ECM remodeling and cell-ECM interactions.

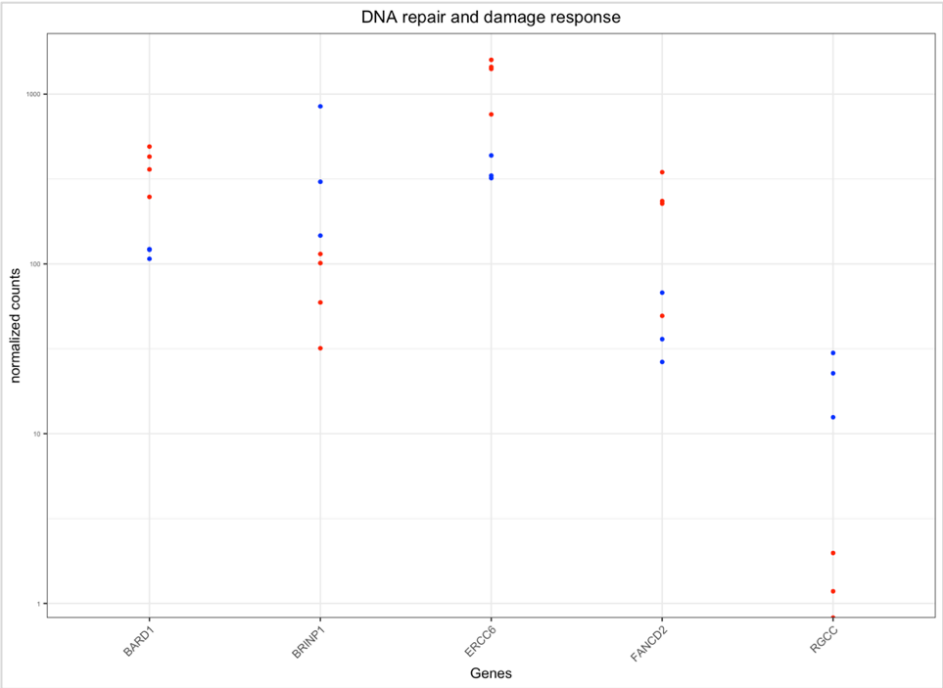

Figure D.8: Strip chart of differently expressed genes (AA versus controls) by biological function - DNA repair and DNA damage response.

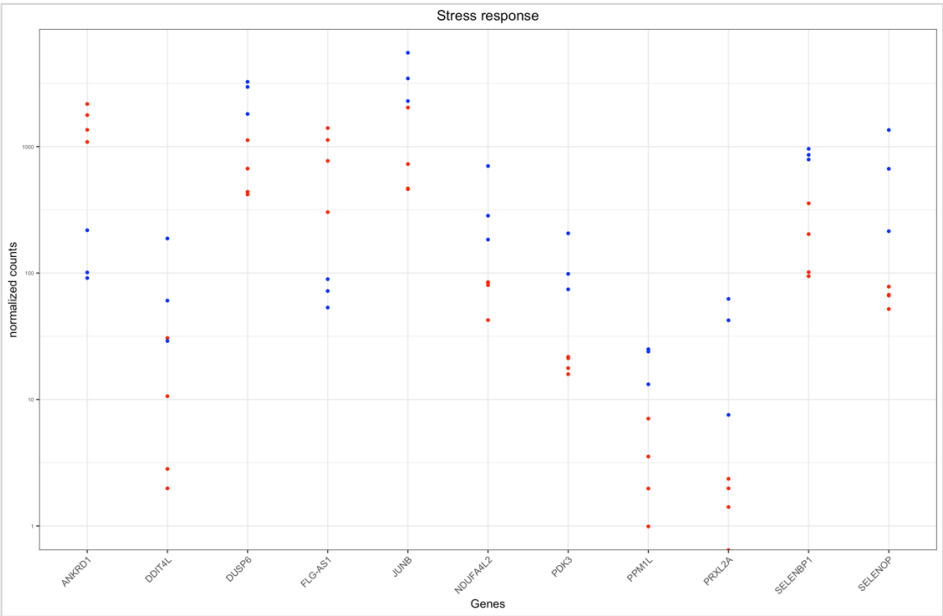

Figure D.9: Strip chart of differently expressed genes (AA versus controls) by biological function - Stress response.

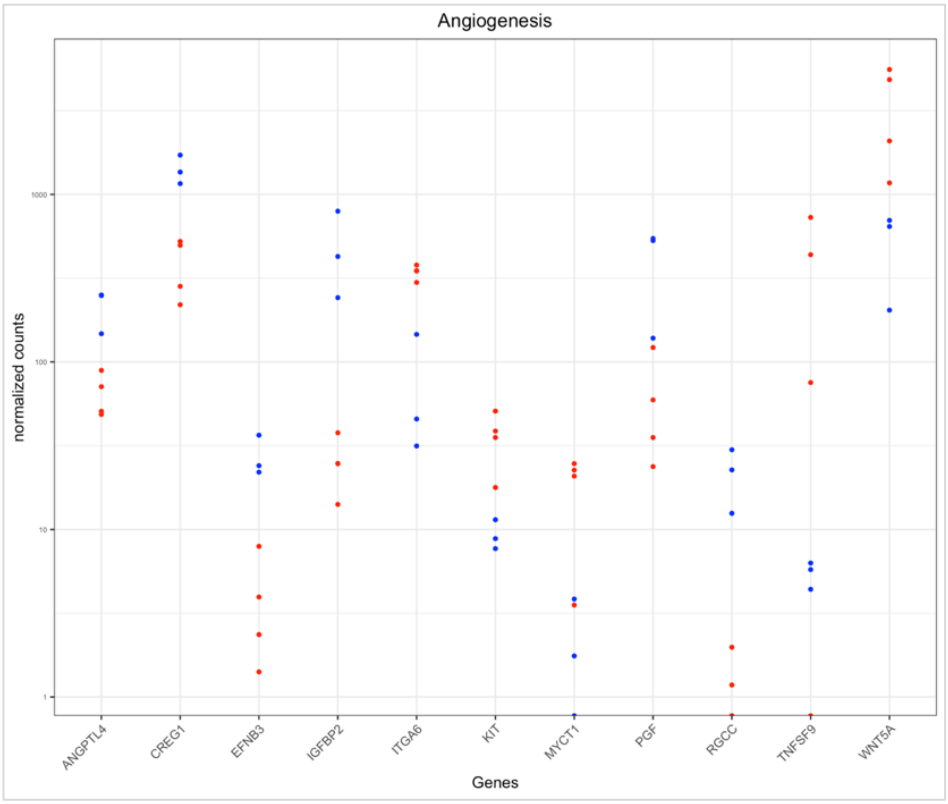

Figure D.10: Strip chart of differently expressed genes (AA versus controls) by biological function - Angiogenesis.

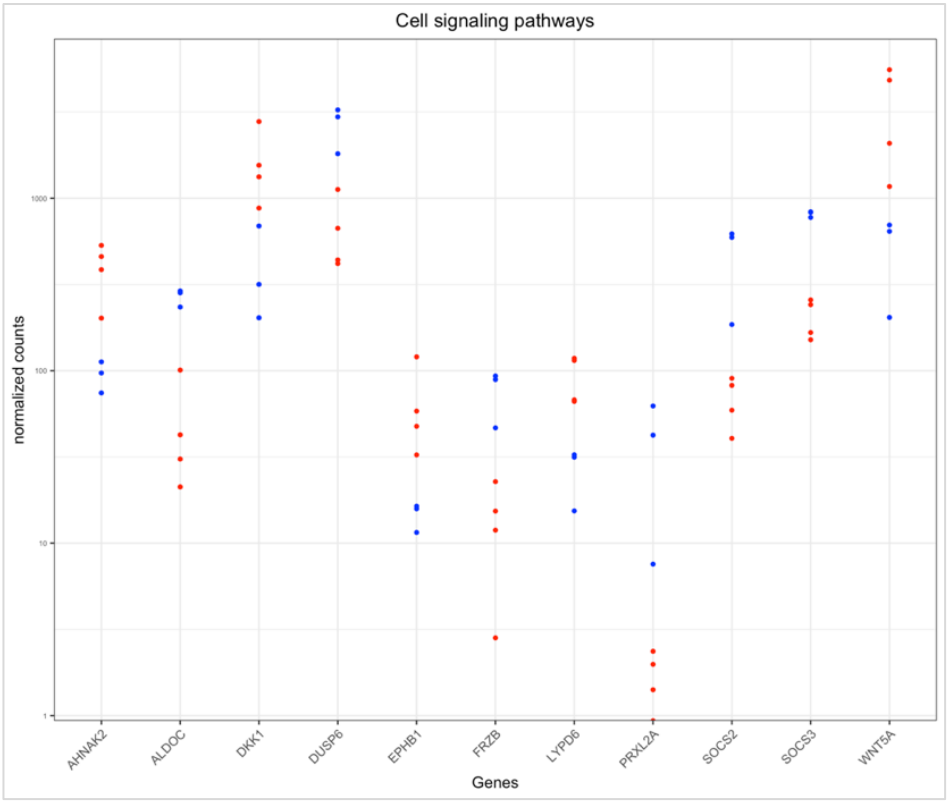

Figure D.11: Heatmap of differently expressed genes (AA versus controls) by biological function - Cell signaling.

X.v. Appendix E

Table E.1: L2FC and padj for differently expressed genes (AA versus controls) by biological function - immune response-related genes: pro-inflammatory pattern.

Gene symbol	log2Fold Change	padj
TNFSF9	4.21892886	0.021928883
WNT5A	2.477853627	0.000235227
MYCT1	2.365737868	0.029305147
HNRNPL	1.83582578	9.30E-06
DOCK5	1.793512051	2.30E-07
DKK1	1.769633118	0.002632571
MPP7	1.542811799	0.005261244
CD9	1.524443099	0.002637562
KCTD9	0.798098394	0.022872327
EFNB1	-1.620957832	9.30E-07
SOCS3	-1.924864374	8.66E-11
PPM1L	-2.17735351	0.015180068
EGR3	-2.340538776	3.17E-05
CD200	-2.573797058	0.001091256
CYP27A1	-2.611213003	6.48E-11
SOCS2	-2.620806387	1.09E-06
SELENOP	-3.339835479	1.32E-08
RBP1	-4.113121298	7.80E-08

Table E.2: L2FC and padj for differently expressed genes (AA versus controls) by biological function - immune response-related genes: immunomodulatory pattern.

Gene symbol	log2 Fold Change	padj
FLG	4.854254393	3.15E-15
PODXL	2.83718376	0.00044028
PLD4	1.823677745	0.00027295
RNF144B	1.731316405	0.00017949
PTEN	1.646898584	0.01086371
TNFRSF11B	1.63264282	0.00884692
ARID5A	-1.501025734	2.57E-06
JUNB	-1.694260989	0.00944809
EPDR1	-1.840651455	1.35E-10
DUSP6	-1.844621708	0.00010941
SULF2	-1.85731842	0.01487028
PCSK5	-1.880548998	0.0016283
IFITM1	-2.081966897	0.0012492
HCP5	-2.271243716	0.00099454
HLA-DMA	-2.379322359	0.00066366
EFNB3	-2.381425953	0.00322696
MX2	-2.508418079	7.67E-05
PDK3	-2.57969599	1.00E-06
GPR183 (EBI2)	-2.604357196	0.0137661
CCL2 (MCP-1)	-2.636950446	5.60E-06
RARRES1 (TIG1)	-2.764628971	0.00158121
ICAM1	-2.834963155	0.00189187
CD40	-3.015803953	0.00017101
BST2	-3.113512972	0.00166406
IFI27	-3.157594638	0.00011659
RAB20	-3.172872773	1.88E-08
CERS4	-3.226529538	0.00905934
BHLHE41 (DEC2/SHARP1)	-3.668617222	0.00032345
CD74	-3.988273966	1.55E-09
APOL4	-4.508226818	0.00016452
HLA-DPA1	-5.008771364	3.97E-09

Table E.3: L2FC and padj for differently expressed genes (AA versus controls) by biological function - adipogenesis-related genes.

Gene symbol	log2 Fold Change	padj
Adipogenesis promotion		
RARA	-1.6618734	0.00688921
IGF1	-1.9212446	0.01794838
PPARG	-1.9959591	0.00742104
GALNT15	-2.4471397	0.00023523
IGFBP2	-4.1493214	1.57E-15
Adipogenesis inhibition		
RARA	-1.6618734	0.00688921
EGR3	-2.3405388	3.17E-05
EFNB3	-2.381426	0.00322696
CYP27A1	-2.611213	6.48E-11
SOCS2	-2.6208064	1.09E-06
RARRES1 (TIG1)	-2.764629	0.00158121
BHLHE41 (DEC2/SHARP1)	-3.6686172	0.00032345

Table E.4: L2FC and padj for differently expressed genes (AA versus controls) by biological function - lipid metabolism-related genes.

Gene symbol	log2 Fold Change	padj
BLTP2	1.50262802	0.00111442
PLD4	1.82367775	0.00027295
ATP8B2	1.98927231	1.80E-09
ELOVL3	-1.5379413	0.00600931
ANGPTL4	-1.6028079	9.32E-05
RARA	-1.6618734	0.00688921
PLAAT4	-1.6973963	0.02133021
IGF1	-1.9212446	0.01794838
SOCS3	-1.9248644	8.66E-11
PPARG	-1.9959591	0.00742104
PLPP1	-2.4347655	1.45E-13
CYP27A1	-2.611213	6.48E-11
DGAT2	-2.7976261	0.00018009
APOL4	-4.5082268	0.00016452

Table E.5: L2FC and padj for differently expressed genes (AA versus controls) by biological function - osteoblast and osteoclast differentiation and activity-related genes.

Gene symbol	log2 Fold Change	padj
Osteoblast differentiation and activity		
PTEN	1.646898584	0.010863713
SMOC1	-1.781574381	0.014445916
EGR3	-2.340538776	3.17E-05
EFNB3	-2.381425953	0.003226962
PGF	-2.461994837	0.000632299
ICAM1	-2.834963155	0.001891875
SELENOP	-3.339835479	1.32E-08
GPM6B	-3.493860751	9.20E-10
IGFBP2	-4.149321449	1.57E-15
Osteoclast differentiation and activity		
WNT5A	2.477853627	0.000235227
DOCK5	1.793512051	2.30E-07
MAFB	-1.837604208	0.035690368
DUSP6	-1.844621708	0.000109413
CYP27A1	-2.611213003	6.48E-11
RARRES1	-2.764628971	0.001581209
SELENOP	-3.339835479	1.32E-08
BHLHE41	-3.668617222	0.000323455
PRXL2A	-4.282714957	0.000313103

Table E.6: L2FC and padj for differently expressed genes (AA versus controls) by biological function - hematopoietic support-related genes.

Gene symbol	log2 Fold Change	padj
ITGA6	1.98828782	0.00048047
MYBL1	2.73911489	1.76E-05
NFE2	-1.5334518	0.02760218
MAFB	-1.8376042	0.03569037
PPARG	-1.9959591	0.00742104
FRZB (SFRP3)	-2.2460044	0.00071179
CCL2 (MCP-1)	-2.6369504	5.60E-06

Table E.7: L2FC and padj for differently expressed genes (AA versus controls) by biological function - ECM remodeling and cell-ECM interactions.

Gene symbol	log2 Fold Change	padj
ITGA6	1.988287823	0.00048047
PODXL	2.83718376	0.00044028
MAMDC2	3.829928546	3.16E-05
CPNE7	4.087386752	5.91E-06
CTSF	-1.728142681	0.00392201
MMP11	-1.835385593	0.00053798
TINAGL1	-2.088543562	0.0012492
FRZB (SFRP3)	-2.246004361	0.00071179
ADAMTS9	-2.263655254	0.00817428
OLFML1	-2.3502057	0.00079147
GALNT15	-2.447139672	0.00023523
CTSH	-2.555574902	0.00040775
PKNOX2	-2.644640745	0.01182407

Table E.8: L2FC and padj for differently expressed genes (AA versus controls) by biological function - DNA repair and DNA damage response.

Gene symbol	log2 Fold Change	padj
BARD1	1.603617078	3.03E-06
ERCC6	1.740807049	1.16E-06
FANCD2	1.964547304	0.004806992
BRINP1	-2.179638284	0.002223902
RGCC	-4.176665305	0.00132973

Table E.9: L2FC and padj for differently expressed genes (AA versus controls) by biological function - Stress response.

Gene symbol	log2 Fold Change	padj
ANKRD1	3.472624018	6.38E-16
FLG-AS1	3.532297602	3.75E-11
JUNB	-1.694260989	0.00944809
DUSP6	-1.844621708	0.00010941
SELENBP1	-2.000183681	0.00022838
PPM1L	-2.17735351	0.01518007
NDUFA4L2	-2.221615874	9.31E-05
DDIT4L	-2.366359767	0.01960197
PDK3	-2.57969599	1.00E-06
SELENOP	-3.339835479	1.32E-08
PRXL2A	-4.282714957	0.0003131

Table E.10: L2FC and padj for differently expressed genes (AA versus controls) by biological function - Angiogenesis.

Gene symbol	log2 Fold Change	padj
TNFSF9 (4-1BBL/CD137L)	4.21892886	0.02192888
WNT5A	2.477853627	0.00023523
MYCT1	2.365737868	0.02930515
ITGA6	1.988287823	0.00048047
KIT	1.618768215	0.00983716
ANGPTL4	-1.602807883	9.32E-05
CREG1	-1.750677491	3.76E-05
EFNB3	-2.381425953	0.00322696
PGF	-2.461994837	0.0006323
IGFBP2	-4.149321449	1.57E-15
RGCC	-4.176665305	0.00132973

Table E.11: L2FC and padj for differently expressed genes (AA versus controls) by biological function - Cell signaling.

Gene symbol	log2 Fold Change	padj
Wnt		
LYPD6	1.611843134	0.001436787
DKK1	1.769633118	0.002632571
AHNAK2	1.921244007	8.43E-06
WNT5A	2.477853627	0.000235227
FRZB (SFRP3)	-2.246004361	0.000711794
ALDOC	-2.246447133	0.000103704
MAPK/PI3K/Akt		
EPHB1	1.885509318	0.00270059
AHNAK2	1.921244007	8.43E-06
DUSP6	-1.844621708	0.000109413
PRXL2A	-4.282714957	0.000313103
NF-kB		
AHNAK2	1.921244007	8.43E-06
JAK-STAT		
SOCS3	-1.924864374	8.66E-11
SOCS2	-2.620806387	1.09E-06

X.vi. Appendix F

Table F.1: List of genes of interest but not differently expressed between AA and controls.

Genes of Interest - No significant differences between AA vs. controls		
Angiogenesis	**Inherited AA**	**Somatic Mutations and Clonal Hematopoiesis in acquired AA**
RUNX1	TERC	DNMT3A
VEGFA	TERT	ASXL1
bFGF/FGF2	DKC1	BCOR
HGF	TINF2	BCORL1
ANGPT1	FANCA	
PDGFA	FANCB	
PDGFB	GATA2	
TGFB1	SRP72	
MSC anti-inflammatory cytokines		**MSC pro-inflammatory cytokines**
IL-10		IL-6
PGE2		IL-8
IDO		IL-1b
HLA-G5		**Adipokines**
TGFB1		ADIPOQ (adiponectin)
Osteogenesis		RETN (resistin)
SPARC (osteonectin)		NAMPT (visfastin)
BGLAP (osteocalcin)		APLN (apelin)
SPP1 (osetopontin)		LEP (leptin)
FN1 (fibronectin)		LEPR (leptin receptor)

X.vii. Appendix G

Table G.1. - Pro-inflammatory pattern genes	
CD9	Brosseau C, Colas L, Magnan A, Brouard S. CD9 Tetraspanin: A New Pathway for the Regulation of Inflammation? Front Immunol. 2018 Oct 9;9:2316.
MPP7	Cheng X, Sun D, Li H, Zhang J, Luo Q, Jin X, Chen Y, Yuan Q, Wang B. MPP7 is a potential prognostic marker and is associated with cancer metabolism and immune infiltration in clear cell renal cell carcinoma: a bioinformatics analysis based on the TCGA database. Transl Androl Urol. 2023 Apr 28;12(4):642-658.
DOCK5	Watanabe M, Terasawa M, Miyano K, Yanagihara T, Uruno T, Sanematsu F, Nishikimi A, Côté JF, Sumimoto H, Fukui Y. DOCK2 and DOCK5 act additively in neutrophils to regulate chemotaxis, superoxide production, and extracellular trap formation. J Immunol. 2014 Dec 1;193(11):5660-7.
HNRNPL	Sudhakaran M, Doseff AI. Role of Heterogeneous Nuclear Ribonucleoproteins in the Cancer-Immune Landscape. Int J Mol Sci. 2023 Mar 7;24(6):5086.
MYCT1	Xu J, Sun Y, Fu W, Fu S. MYCT1 in cancer development: Gene structure, regulation, and biological implications for diagnosis and treatment. Biomed Pharmacother. 2023 Sep;165:115208.
WNT5A	Huang Y, Xue Q, Chang J, Wang X, Miao C. Wnt5a: A promising therapeutic target for inflammation, especially rheumatoid arthritis. Cytokine. 2023 Dec;172:156381.
TNFSF9	Wong HY, Schwarz H. CD137 / CD137 ligand signalling regulates the immune balance: A potential target for novel immunotherapy of autoimmune diseases. J Autoimmun. 2020 Aug;112:102499.
KCTD9	Yao H, Ren D, Wang Y, Wu L, Wu Y, Wang W, Li Q, Liu L. KCTD9 inhibits the Wnt/β-catenin pathway by decreasing the level of β-catenin in colorectal cancer. Cell Death Dis. 2022 Sep 2;13(9):761.
EFNB1	Mori T, Maeda N, Inoue K, Sekimoto R, Tsushima Y, Matsuda K, Yamaoka M, Suganami T, Nishizawa H, Ogawa Y, Funahashi T, Shimomura I. A novel role for adipose ephrin-B1 in inflammatory response. PLoS One. 2013 Oct 1;8(10):e76199.
SOCS3	Santos MRG, Queiroz-Junior CM, Madeira MFM, Machado FS. Suppressors of cytokine signaling (SOCS) proteins in inflammatory bone disorders. Bone. 2020 Nov;140:115538.
PPM1L	Wang B, Zhou Q, Bi Y, Zhou W, Zeng Q, Liu Z, Liu X, Zhan Z. Phosphatase PPM1L Prevents Excessive Inflammatory Responses and Cardiac Dysfunction after Myocardial Infarction by Inhibiting IKKβ Activation. J Immunol. 2019 Sep 1;203(5):1338-1347.
EGR3	Li S, Miao T, Sebastian M, Bhullar P, Ghaffari E, Liu M, Symonds AL, Wang P. The transcription factors Egr2 and Egr3 are essential for the control of inflammation and antigen-induced proliferation of B and T cells. Immunity. 2012 Oct 19;37(4):685-96.
CD200	Varnum MM, Kiyota T, Ingraham KL, Ikezu S, Ikezu T. The anti-inflammatory glycoprotein, CD200, restores neurogenesis and enhances amyloid phagocytosis in a mouse model of Alzheimer's disease. Neurobiol Aging. 2015 Nov;36(11):2995-3007.
CYP27A1	Hendrikx T, Jeurissen ML, Bieghs V, Walenbergh SM, van Gorp PJ, Verheyen F, Houben T, Guichot YD, Gijbels MJ, Leitersdorf E, Hofker MH, Lütjohann D, Shiri-Sverdlov R. Hematopoietic overexpression of Cyp27a1 reduces hepatic inflammation independently of 27-hydroxycholesterol levels in Ldlr(-/-) mice. J Hepatol. 2015 Feb;62(2):430-6.
SOCS2	Sobah ML, Liongue C, Ward AC. SOCS Proteins in Immunity, Inflammatory Diseases, and Immune-Related Cancer. Front Med (Lausanne). 2021 Sep 16;8:727987.
SELENOP	Mal'tseva VN, Goltyaev MV, Turovsky EA, Varlamova EG. Immunomodulatory and Anti-Inflammatory Properties of Selenium-Containing Agents: Their Role in the

	Regulation of Defense Mechanisms against COVID-19. Int J Mol Sci. 2022 Feb 21;23(4):2360.
DKK1	Jaschke NP, Pählig S, Sinha A, Adolph TE, Colunga ML, Hofmann M, Wang A, Thiele S, Schwärzler J, Kleymann A, Gentzel M, Tilg H, Wielockx B, Hofbauer LC, Rauner M, Göbel A, Rachner TD. Dickkopf1 fuels inflammatory cytokine responses. Commun Biol. 2022 Dec 20;5(1):1391.
RBP1	Dolin HH, Franco JH, Chen X, Pan ZK. Retinoic Acid-Induced Regulation of Inflammatory Pathways Is a Potential Sepsis Treatment. Infect Immun. 2023 Apr 18;91(4):e0045722. doi: 10.1128/iai.00457-22.

Table G.2. – Immunomodulatory pattern genes	
PTEN	Li XF, Chen X, Bao J, Xu L, Zhang L, Huang C, Meng XM, Li J. PTEN negatively regulates the expression of pro-inflammatory cytokines and chemokines of fibroblast-like synoviocytes in adjuvant-induced arthritis. Artif Cells Nanomed Biotechnol. 2019 Dec;47(1):3687-3696.
RNF144B	Li G, Zhang J, Zhao Z, Wang J, Li J, Xu W, Cui Z, Sun P, Yuan H, Wang T, Li K, Bai X, Ma X, Li P, Fu Y, Cao Y, Bao H, Li D, Liu Z, Zhu N, Tang L, Lu Z. RNF144B negatively regulates antiviral immunity by targeting MDA5 for autophagic degradation. EMBO Rep. 2024 Oct;25(10):4594-4624.
PLD4	Gavin AL, Huang D, Huber C, Mårtensson A, Tardif V, Skog PD, Blane TR, Thinnes TC, Osborn K, Chong HS, Kargaran F, Kimm P, Zeitjian A, Sielski RL, Briggs M, Schulz SR, Zarpellon A, Cravatt B, Pang ES, Teijaro J, de la Torre JC, O'Keeffe M, Hochrein H, Damme M, Teyton L, Lawson BR, Nemazee D. PLD3 and PLD4 are single-stranded acid exonucleases that regulate endosomal nucleic-acid sensing. Nat Immunol. 2018 Sep;19(9):942-953.
PODXL	Amo L, Díez-García J, Tamayo-Orbegozo E, Maruri N, Larrucea S. Podocalyxin Expressed in Antigen Presenting Cells Promotes Interaction With T Cells and Alters Centrosome Translocation to the Contact Site. Front Immunol. 2022 May 31;13:835527.
EPDR1	Qian X, Cai J, Zhang Y, Shen S, Wang M, Liu S, Meng X, Zhang J, Ye Z, Qiu S, Zhong X, Gao P. EPDR1 promotes PD-L1 expression and tumor immune evasion by inhibiting TRIM21-dependent ubiquitylation of IkappaB kinase-β. EMBO J. 2024 Oct;43(19):4248-4273.
SULF2	Siegel RJ, Singh AK, Panipinto PM, Shaikh FS, Vinh J, Han SU, Kenney HM, Schwarz EM, Crowson CS, Khuder SA, Khuder BS, Fox DA, Ahmed S. Extracellular sulfatase-2 is overexpressed in rheumatoid arthritis and mediates the TNF-α-induced inflammatory activation of synovial fibroblasts. Cell Mol Immunol. 2022 Oct;19(10):1185-1195.
PCSK5	Ito H, Nozaki K, Sakimura K, Abe M, Yamawaki S, Aizawa H. Activation of proprotein convertase in the mouse habenula causes depressive-like behaviors through remodeling of extracellular matrix. Neuropsychopharmacology. 2021 Jan;46(2):442-454.
IFITM1	Yánez DC, Ross S, Crompton T. The IFITM protein family in adaptive immunity. Immunology. 2020 Apr;159(4):365-372.
HCP5	Kulski JK. Long Noncoding RNA HCP5, a Hybrid HLA Class I Endogenous Retroviral Gene: Structure, Expression, and Disease Associations. Cells. 2019 May 20;8(5):480.
GPR183 (EBI2)	Misselwitz B, Wyss A, Raselli T, Cerovic V, Sailer AW, Krupka N, Ruiz F, Pot C, Pabst O. The oxysterol receptor GPR183 in inflammatory bowel diseases. Br J Pharmacol. 2021 Aug;178(16):3140-3156.
CCL2 (~MCP-1)	Gschwandtner M, Derler R, Midwood KS. More Than Just Attractive: How CCL2 Influences Myeloid Cell Behavior Beyond Chemotaxis. Front Immunol. 2019 Dec 13;10:2759.
IFI27	Zhao X, Zhang L, Wang J, Zhang M, Song Z, Ni B, You Y. Identification of key biomarkers and immune infiltration in systemic lupus erythematosus by integrated bioinformatics analysis. J Transl Med. 2021 Jan 19;19(1):35.

HLA-DPA1	Chen Z, Chen R, Ou Y, Lu J, Jiang Q, Liu G, Wang L, Liu Y, Zhou Z, Yang B, Zuo L. Construction of an HLA Classifier for Early Diagnosis, Prognosis, and Recognition of Immunosuppression in Sepsis by Multiple Transcriptome Datasets. Front Physiol. 2022 May 24;13:870657.
APOL4	Paz-Barba M, Muñoz Garcia A, de Winter TJJ, de Graaf N, van Agen M, van der Sar E, Lambregtse F, Daleman L, van der Slik A, Zaldumbide A, de Koning EJP, Carlotti F. Apolipoprotein L genes are novel mediators of inflammation in beta cells. Diabetologia. 2024 Jan;67(1):124-136.
ARID5A	Nyati KK, Zaman MM, Sharma P, Kishimoto T. Arid5a, an RNA-Binding Protein in Immune Regulation: RNA Stability, Inflammation, and Autoimmunity. Trends Immunol. 2020 Mar;41(3):255-268.
JUNB	Ren FJ, Cai XY, Yao Y, Fang GY. JunB: a paradigm for Jun family in immune response and cancer. Front Cell Infect Microbiol. 2023 Sep 4;13:1222265.
HLA-DMA	Alvaro-Benito M, Morrison E, Wieczorek M, Sticht J, Freund C. Human leukocyte Antigen-DM polymorphisms in autoimmune diseases. Open Biol. 2016 Aug;6(8):160165.
*MX2**	Meng XW, Cheng ZL, Lu ZY, Tan YN, Jia XY, Zhang M. MX2: Identification and systematic mechanistic analysis of a novel immune-related biomarker for systemic lupus erythematosus. Front Immunol. 2022 Aug 18;13:978851.
PDK3	Li C, Liu C, Zhang J, Lu Y, Jiang B, Xiong H, Li C. Pyruvate dehydrogenase kinase regulates macrophage polarization in metabolic and inflammatory diseases. Front Immunol. 2023 Dec 18;14:1296687.
RARRES1 (~TIG1)	Möller-Hackbarth K, Dabaghie D, Charrin E, Zambrano S, Genové G, Li X, Wernerson A, Lal M, Patrakka J. Retinoic acid receptor responder1 promotes development of glomerular diseases via the Nuclear Factor-κB signaling pathway. Kidney Int. 2021 Oct;100(4):809-823.
*ICAM1***	Bui TM, Wiesolek HL, Sumagin R. ICAM-1: A master regulator of cellular responses in inflammation, injury resolution, and tumorigenesis. J Leukoc Biol. 2020 Sep;108(3):787-799.
BST2	Tiwari R, de la Torre JC, McGavern DB, Nayak D. Beyond Tethering the Viral Particles: Immunomodulatory Functions of Tetherin (BST-2). DNA Cell Biol. 2019 Nov;38(11):1170-1177.
*RAB20**	Prashar A, Schnettger L, Bernard EM, Gutierrez MG. Rab GTPases in Immunity and Inflammation. Front Cell Infect Microbiol. 2017 Sep 29;7:435.
*CD74***	Su H, Na N, Zhang X, Zhao Y. The biological function and significance of CD74 in immune diseases. Inflamm Res. 2017 Mar;66(3):209-216.
TNFRSF11B	Saidenberg Kermanac'h N, Bessis N, Cohen-Solal M, De Vernejoul MC, Boissier MC. Osteoprotegerin and inflammation. Eur Cytokine Netw. 2002 Apr-Jun;13(2):144-53. PMID: 12101070.
FLG	Liljedahl ER, Gliga A, de Paula HK, Engfeldt M, Julander A, Lidén C, Lindh C, Broberg K. Inflammation-related proteins in blood after dermal exposure to some common chemicals depend on the skin barrier gene filaggrin - a human experimental study. Environ Toxicol Pharmacol. 2024 Jan;105:104346.
DUSP6	Zhang Z, Chen Y, Zheng L, Du J, Wei S, Zhu X, Xiong JW. A DUSP6 inhibitor suppresses inflammatory cardiac remodeling and improves heart function after myocardial infarction. Dis Model Mech. 2023 May 1;16(5):dmm049662.
*EFNB3**	Darling TK, Lamb TJ. Emerging Roles for Eph Receptors and Ephrin Ligands in Immunity. Front Immunol. 2019 Jul 4;10:1473.
*CD40***	Senhaji N, Kojok K, Darif Y, Fadainia C, Zaid Y. The Contribution of CD40/CD40L Axis in Inflammatory Bowel Disease: An Update. Front Immunol. 2015 Oct 16;6:529.
CERS4	Alexandropoulou I, Grammatikopoulou MG, Gkouskou KK, Pritsa AA, Vassilakou T, Rigopoulou E, Lindqvist HM, Bogdanos DP. Ceramides in Autoimmune Rheumatic Diseases: Existing Evidence and Therapeutic Considerations for Diet as an Anticeramide Treatment. Nutrients. 2023 Jan 2;15(1):229.

BHLHE41 (~DEC2/SHARP1)	Bret C, Desmots-Loyer F, Moreaux J, Fest T. BHLHE41, a transcriptional repressor involved in physiological processes and tumor development. Cell Oncol (Dordr). 2024 Sep 10.

Table G.3. – Adipogenesis inhibition genes	
RARA	Green AC, Kocovski P, Jovic T, Walia MK, Chandraratna RAS, Martin TJ, Baker EK, Purton LE. Retinoic acid receptor signalling directly regulates osteoblast and adipocyte differentiation from mesenchymal progenitor cells. Exp Cell Res. 2017 Jan 1;350(1):284-297.
SOCS2	Val CH, de Oliveira MC, Lacerda DR, Barroso A, Batista NV, Menezes-Garcia Z, de Assis DRR, Cramer AT, Brant F, Teixeira MM, Glória Souza D, Ferreira AM, Machado FS. SOCS2 modulates adipose tissue inflammation and expansion in mice. J Nutr Biochem. 2020 Feb;76:108304.
EGR3	Wan X, Wang L, Khan MA, Peng L, Zhang K, Sun X, Yi X, Wang Z, Chen K. Shift work promotes adipogenesis via cortisol-dependent downregulation of EGR3-HDAC6 pathway. Cell Death Discov. 2024 Mar 11;10(1):129.
EFNB3	Arthur A, Gronthos S. Eph-Ephrin Signaling Mediates Cross-Talk Within the Bone Microenvironment. Front Cell Dev Biol. 2021 Feb 9;9:598612.
CYP27A1	Li J, Daly E, Campioli E, Wabitsch M, Papadopoulos V. De novo synthesis of steroids and oxysterols in adipocytes. J Biol Chem. 2014 Jan 10;289(2):747-64.
RARRES1 (~TIG1)	Maimouni S, Issa N, Cheng S, Ouaari C, Cheema A, Kumar D, Byers S. Tumor suppressor RARRES1- A novel regulator of fatty acid metabolism in epithelial cells. PLoS One. 2018 Dec 17;13(12):e0208756.
BHLHE41 (~DEC2/SHARP1)	Gulbagci NT, Li L, Ling B, Gopinadhan S, Walsh M, Rossner M, Nave KA, Taneja R. SHARP1/DEC2 inhibits adipogenic differentiation by regulating the activity of C/EBP. EMBO Rep. 2009 Jan;10(1):79-86.
MMP11	Andarawewa KL, Rio M-C. New insights into MMP function in adipogenesis. The Cancer Degradome: In: Proteases and Cancer Biology, Edwards D, Hoyer-Hansen G, Blasi F, Sloane BF (Eds.). New York: Springer; 2008 p. 361–372.

Table G.4. – Adipogenesis promotion genes	
IGFBP2	Wang Y, Liu Y, Fan Z, Liu D, Wang F, Zhou Y. IGFBP2 enhances adipogenic differentiation potentials of mesenchymal stem cells from Wharton's jelly of the umbilical cord via JNK and Akt signaling pathways. PLoS One. 2017 Aug 31;12(8):e0184182.
PPARG	Zhuang H, Zhang X, Zhu C, Tang X, Yu F, Shang GW, Cai X. Molecular Mechanisms of PPAR-γ Governing MSCs Osteogenic and Adipogenic Differentiation. Curr Stem Cell Res Ther. 2016;11(3):255-64.
IGF1	Hu L, Yang G, Hägg D, Sun G, Ahn JM, Jiang N, Ricupero CL, Wu J, Rodhe CH, Ascherman JA, Chen L, Mao JJ. IGF1 Promotes Adipogenesis by a Lineage Bias of Endogenous Adipose Stem/Progenitor Cells. Stem Cells. 2015 Aug;33(8):2483-95.
GALNT15	Takahashi A, Koike R, Watanabe S, Kuribayashi K, Wabitsch M, Miyamoto M, Komuro A, Seki M, Nashimoto M, Shimizu-Ibuka A, Yamashita K, Iwata T. Polypeptide N-acetylgalactosaminyltransferase-15 regulates adipogenesis in human SGBS cells. Sci Rep. 2024 Aug 29;14(1):20049.
RARA	Cao J, Ma Y, Yao W, Zhang X, Wu D. Retinoids Regulate Adipogenesis Involving the TGFβ/SMAD and Wnt/β-Catenin Pathways in Human Bone Marrow Mesenchymal Stem Cells. Int J Mol Sci. 2017 Apr 15;18(4):842.

Table G.5. – Lipid metabolism genes	
BLTP2	Neuman SD, Levine TP, Bashirullah A. A novel superfamily of bridge-like lipid transfer proteins. Trends Cell Biol. 2022 Nov;32(11):962-974.
PLD4	Singh S, Dransfeld U, Ambaw Y, Lopez-Scarim J, Farese RV Jr, Walther TC. PLD3 and PLD4 synthesize S,S-BMP, a key phospholipid enabling lipid degradation in lysosomes. bioRxiv [Preprint]. 2024 Mar 21:2024.03.21.586175.

ATP8B2	Takatsu H, Nishimura N, Kosugi Y, Ogawa H, Nakayama K, Colin E, Platzer K, Abou Jamra R, Redler S, Prouteau C, Ziegler A, Shin HW. De Novo Missense Variations of ATP8B2 Impair Its Phosphatidylcholine Flippase Activity. Mol Cell Biol. 2024;44(11):473-488.
ELOVL3	Westerberg R, Månsson JE, Golozoubova V, Shabalina IG, Backlund EC, Tvrdik P, Retterstøl K, Capecchi MR, Jacobsson A. ELOVL3 is an important component for early onset of lipid recruitment in brown adipose tissue. J Biol Chem. 2006 Feb 24;281(8):4958-68.
ANGPTL4	Kersten S. Role and mechanism of the action of angiopoietin-like protein ANGPTL4 in plasma lipid metabolism. J Lipid Res. 2021;62:100150.
RARA	Bonet ML, Ribot J, Palou A. Lipid metabolism in mammalian tissues and its control by retinoic acid. Biochim Biophys Acta. 2012 Jan;1821(1):177-89.
PLAAT4 (~RARRES3)	Zhao JY, Yuan XK, Luo RZ, Wang LX, Gu W, Yamane D, Feng H. Phospholipase A and acyltransferase 4/retinoic acid receptor responder 3 at the intersection of tumor suppression and pathogen restriction. Front Immunol. 2023 Mar 31;14:1107239.
IGF1	Zhang D, Wei Y, Huang Q, Chen Y, Zeng K, Yang W, Chen J, Chen J. Important Hormones Regulating Lipid Metabolism. Molecules. 2022 Oct 19;27(20):7052.
SOCS3	Sachithanandan N, Fam BC, Fynch S, Dzamko N, Watt MJ, Wormald S, Honeyman J, Galic S, Proietto J, Andrikopoulos S, Hevener AL, Kay TW, Steinberg GR. Liver-specific suppressor of cytokine signaling-3 deletion in mice enhances hepatic insulin sensitivity and lipogenesis resulting in fatty liver and obesity. Hepatology. 2010 Nov;52(5):1632-42.
PPARG	Hernandez-Quiles M, Broekema MF, Kalkhoven E. PPARgamma in Metabolism, Immunity, and Cancer: Unified and Diverse Mechanisms of Action. Front Endocrinol (Lausanne). 2021 Feb 26;12:624112.
PLPP1	GeneCards: The Human Gene Database. 1 https://www.genecards.org/cgi-bin/carddisp.pl?gene=PLPP1 Accessed January 24, 2025.
DGAT2	Chitraju C, Walther TC, Farese RV Jr. The triglyceride synthesis enzymes DGAT1 and DGAT2 have distinct and overlapping functions in adipocytes. J Lipid Res. 2019 Jun;60(6):1112-1120.
*APOL4**	Duchateau PN, Movsesyan I, Yamashita S, Sakai N, Hirano K, Schoenhaus SA, O'Connor-Kearns PM, Spencer SJ, Jaffe RB, Redberg RF, Ishida BY, Matsuzawa Y, Kane JP, Malloy MJ. Plasma apolipoprotein L concentrations correlate with plasma triglycerides and cholesterol levels in normolipidemic, hyperlipidemic, and diabetic subjects. J Lipid Res. 2000 Aug;41(8):1231-6.
*CYP27A1***	Brlek P, Bulić L, Glavaš Weinberger D, Bošnjak J, Pavlović T, Tomić S, Krivdić Dupan Z, Borić I, Primorac D. Successful Treatment of a Rare Cholesterol Homeostasis Disorder Due to CYP27A1 Gene Mutation with Chenodeoxycholic Acid Therapy. Biomedicines. 2023 May 12;11(5):1430.

Table G.6. – Osteoblast differentiation and activity genes	
SMOC1	Choi YA, Lim J, Kim KM, Acharya B, Cho JY, Bae YC, Shin HI, Kim SY, Park EK. Secretome analysis of human BMSCs and identification of SMOC1 as an important ECM protein in osteoblast differentiation. J Proteome Res. 2010 Jun 4;9(6):2946-56.
EFNB3	Martin TJ, Allan EH, Ho PW, Gooi JH, Quinn JM, Gillespie MT, Krasnoperov V, Sims NA. Communication between ephrinB2 and EphB4 within the osteoblast lineage. Adv Exp Med Biol. 2010;658:51-60.
PGF	McCoy RJ, Widaa A, Watters KM, Wuerstle M, Stallings RL, Duffy GP, O'Brien FJ. Orchestrating osteogenic differentiation of mesenchymal stem cells--identification of placental growth factor as a mechanosensitive gene with a pro-osteogenic role. Stem Cells. 2013 Nov;31(11):2420-31.
ICAM1	Kong L, Yang X. Study of Intercellular Adhesion Molecule-1 (ICAM-1) in Bone Homeostasis. Curr Drug Targets. 2020;21(4):328-337.

SELENOP	Sharma AR, Sharma G, Lee YH, Chakraborty C, Lee SS, Seo EM. Sodium Selenite Promotes Osteoblast Differentiation via The WNT/ß-Catenin Signaling Pathway. Cell J. 2022 Jun;24(6):309-315.
GPM6B	Drabek K, van de Peppel J, Eijken M, van Leeuwen JP. GPM6B regulates osteoblast function and induction of mineralization by controlling cytoskeleton and matrix vesicle release. J Bone Miner Res. 2011 Sep;26(9):2045-51.
IGFBP2	i G, Wai C, DeMambro V, Rosen CJ, Clemmons DR. IGFBP-2 directly stimulates osteoblast differentiation. J Bone Miner Res. 2014 Nov;29(11):2427-38.
EGR3	Leclerc N, Noh T, Cogan J, Samarawickrama DB, Smith E, Frenkel B. Opposing effects of glucocorticoids and Wnt signaling on Krox20 and mineral deposition in osteoblast cultures. J Cell Biochem. 2008 Apr 15;103(6):1938-51.
PTEN	Dong J, Xu X, Zhang Q, Yuan Z, Tan B. Critical implication of the PTEN/PI3K/AKT pathway during BMP2-induced heterotopic ossification. Mol Med Rep. 2021 Apr;23(4):254.

Table G.7. – Osteoclast differentiation and activity genes	
MAFB	Kim K, Kim JH, Lee J, Jin HM, Kook H, Kim KK, Lee SY, Kim N. MafB negatively regulates RANKL-mediated osteoclast differentiation. Blood. 2007 Apr 15;109(8):3253-9.
DUSP6	Zhang B, Yuan P, Xu G, Chen Z, Li Z, Ye H, Wang J, Shi P, Sun X. DUSP6 expression is associated with osteoporosis through the regulation of osteoclast differentiation via ERK2/Smad2 signaling. Cell Death Dis. 2021 Sep 2;12(9):825.
RARRES1 (~TIG1)	Henning P, Conaway HH, Lerner UH. Retinoid receptors in bone and their role in bone remodeling. Front Endocrinol (Lausanne). 2015 Mar 11;6:31.
PRXL2A	Xu Y, Morse LR, da Silva RA, Odgren PR, Sasaki H, Stashenko P, Battaglino RA. PAMM: a redox regulatory protein that modulates osteoclast differentiation. Antioxid Redox Signal. 2010 Jul 1;13(1):27-37.
CYP27A1	Fang Z, Cheng G, He M, Lin Y. CYP27A1 deficiency promoted osteoclast differentiation. PeerJ. 2023 Mar 3;11:e15041.
SELENOP	Yang T, Lee SY, Park KC, Park SH, Chung J, Lee S. The Effects of Selenium on Bone Health: From Element to Therapeutics. Molecules. 2022 Jan 8;27(2):392.
BHLHE41 (~DEC2/SHARP1)	Zhang Y, Li X, Lang J, Li W, Huang D, Sun W, Yang L, Li W, Wang Y, Zhang L. Basic-helix-loop-helix family member e41 suppresses osteoclastogenesis and abnormal bone resorption disease via NFATc1. iScience. 2024 Feb 1;27(3):109059.
WNT5A	Kobayashi Y, Uehara S, Udagawa N, Takahashi N. Regulation of bone metabolism by Wnt signals. J Biochem. 2016 Apr;159(4):387-92.
DOCK5	Vives V, Laurin M, Cres G, Larrousse P, Morichaud Z, Noel D, Côté JF, Blangy A. The Rac1 exchange factor Dock5 is essential for bone resorption by osteoclasts. J Bone Miner Res. 2011 May;26(5):1099-110.

Table G.8. – Hematopoietic support-related genes	
ITGA6	Notta F, Doulatov S, Laurenti E, Poeppl A, Jurisica I, Dick JE. Isolation of single human hematopoietic stem cells capable of long-term multilineage engraftment. Science. 2011 Jul 8;333(6039):218-21.
MYBL1	Clarke ML, Lemma RB, Walton DS, Volpe G, Noyvert B, Gabrielsen OS, Frampton J. MYB insufficiency disrupts proteostasis in hematopoietic stem cells, leading to age-related neoplasia.
NFE2	Di Tullio A, Passaro D, Rouault-Pierre K, Purewal S, Bonnet D. Nuclear Factor Erythroid 2 Regulates Human HSC Self-Renewal and T Cell Differentiation by Preventing NOTCH1 Activation. Stem Cell Reports. 2017 Jul 11;9(1):5-11.
MAFB	Sarrazin S, Mossadegh-Keller N, Fukao T, Aziz A, Mourcin F, Vanhille L, Kelly Modis L, Kastner P, Chan S, Duprez E, Otto C, Sieweke MH. MafB restricts M-CSF-dependent myeloid commitment divisions of hematopoietic stem cells. Cell. 2009 Jul 23;138(2):300-13.

PPARG	Guo B, Huang X, Lee MR, Lee SA, Broxmeyer HE. Antagonism of PPAR-γ signaling expands human hematopoietic stem and progenitor cells by enhancing glycolysis. Nat Med. 2018 Mar;24(3):360-367.
FRZB (~SFRP3)	Lento W, Congdon K, Voermans C, Kritzik M, Reya T. Wnt signaling in normal and malignant hematopoiesis. Cold Spring Harb Perspect Biol. 2013 Feb 1;5(2):a008011.
CCL2 (~MCP-1)	Yamazaki S, Mabuchi Y, Kimura T, Suto EG, Hisamatsu D, Naraoka Y, Kondo A, Azuma Y, Kikuchi R, Nishikii H, Morishita S, Araki M, Komatsu N, Akazawa C. Activated mesenchymal stem/stromal cells promote myeloid cell differentiation via CCL2/CCR2 signaling. Stem Cell Reports. 2024 Mar 12;19(3):414-425.

Table G.9. – ECM remodeling and cell-ECM interactions genes	
CTSF	Vidak E, Javoršek U, Vizovišek M, Turk B. Cysteine Cathepsins and their Extracellular Roles: Shaping the Microenvironment. Cells. 2019 Mar 20;8(3):264.
MMP11	Almalki SG, Agrawal DK. Effects of matrix metalloproteinases on the fate of mesenchymal stem cells. Stem Cell Res Ther. 2016 Sep 9;7(1):129.
TINAGL1	Tian WQ, Chen SY, Chuan FN, Zhao WR, Zhou B. Down-regulated TINAGL1 in fibroblasts impairs wound healing in diabetes. FASEB J. 2022 Mar;36(3):e22235.
ADAMTS9	U.S. National Library of Medicine. ADAMTS9 ADAM metallopeptidase with thrombospondin type 1 motif 9 [Homo sapiens (human)]. National Center for Biotechnology Information. https://www.ncbi.nlm.nih.gov/gene/56999. Accessed January 25, 2025.
GALNT15	Liu HZ, Song XQ, Zhang H. Sugar-coated bullets: Unveiling the enigmatic mystery 'sweet arsenal' in osteoarthritis. Heliyon. 2024 Mar 11;10(6):e27624.
CTSH	Vidak E, Javoršek U, Vizovišek M, Turk B. Cysteine Cathepsins and their Extracellular Roles: Shaping the Microenvironment. Cells. 2019 Mar 20;8(3):264.
PKNOX2	Chen L, Li H, Liu X, Zhang N, Wang K, Shi A, Gao H, Akdis D, Saguner AM, Xu X, Osto E, Van de Veen W, Li G, Bayés-Genís A, Duru F, Song J, Li X, Hu S. PBX/Knotted 1 homeobox-2 (PKNOX2) is a novel regulator of myocardial fibrosis. Signal Transduct Target Ther. 2024 Apr 22;9(1):94.
OLFML1	Murakami K, Kikugawa S, Kobayashi Y, Uehara S, Suzuki T, Kato H, Udagawa N, Nakamura Y. Olfactomedin-like protein OLFML1 inhibits Hippo signaling and mineralization in osteoblasts. Biochem Biophys Res Commun. 2018 Oct 28;505(2):419-425.
FRZB (~SFRP3)	Thysen S, Cailotto F, Lories R. Osteogenesis induced by frizzled-related protein (FRZB) is linked to the netrin-like domain. Lab Invest. 2016 May;96(5):570-80.
ITGA6	Mao L, Wang L, Xu J, Zou J. The role of integrin family in bone metabolism and tumor bone metastasis. Cell Death Discov. 2023 Apr 10;9(1):119.
PODXL	Lee RH, Seo MJ, Pulin AA, Gregory CA, Ylostalo J, Prockop DJ. The CD34-like protein PODXL and alpha6-integrin (CD49f) identify early progenitor MSCs with increased clonogenicity and migration to infarcted heart in mice. Blood. 2009 Jan 22;113(4):816-26.
MAMDC2	Lee H, Park BC, Soon Kang J, Cheon Y, Lee S, Jae Maeng P. MAM domain containing 2 is a potential breast cancer biomarker that exhibits tumour-suppressive activity. Cell Prolif. 2020 Sep;53(9):e12883.
CPNE7	Lee D, Park KS, Yoon GJ, Lee HJ, Lee JY, Park YS, Park JC, Lee G, Chung CP, Park YJ. Identification of cell-penetrating osteogenic peptide from copine-7 protein and its delivery system for enhanced bone formation. J Biomed Mater Res A. 2019 Nov;107(11):2392-2402.

Table G.10. – DNA repair and damage response genes	
BRINP1	Magni M, Buscemi G, Zannini L. Cell cycle and apoptosis regulator 2 at the interface between DNA damage response and cell physiology. Mutat Res Rev Mutat Res. 2018 Apr-Jun;776:1-9.
RGCC	Gene [Internet]. Bethesda (MD): National Library of Medicine (US), National Center for Biotechnology Information; 2004 - [cited 2025 Jan 10]. Assession No. 28984, regulator of cell cycle (RGCC), Homo sapiens. Available from: https://www.ncbi.nlm.nih.gov/gene/28984
BARD1	Tarsounas M, Sung P. The antitumorigenic roles of BRCA1-BARD1 in DNA repair and replication. Nat Rev Mol Cell Biol. 2020 May;21(5):284-299.
FANCD2	Lemonidis K, Arkinson C, Rennie ML, Walden H. Mechanism, specificity, and function of FANCD2-FANCI ubiquitination and deubiquitination. FEBS J. 2022 Aug;289(16):4811-4829.
ERCC6	Wang S, Min Z, Ji Q, Geng L, Su Y, Liu Z, Hu H, Wang L, Zhang W, Suzuiki K, Huang Y, Zhang P, Tang TS, Qu J, Yu Y, Liu GH, Qiao J. Rescue of premature aging defects in Cockayne syndrome stem cells by CRISPR/Cas9-mediated gene correction. Protein Cell. 2020 Jan;11(1):1-22.

Table G.11. – Stress response genes	
ANKRD1	Boskovic S, Marín Juez R, Stamenkovic N, Radojkovic D, Stainier DY, Kojic S. The stress responsive gene ankrd1a is dynamically regulated during skeletal muscle development and upregulated following cardiac injury in border zone cardiomyocytes in adult zebrafish. Gene. 2021 Aug 5;792:145725.
FLG-AS1	Luo R, Li L, Xiao F, Fu J. LncRNA FLG-AS1 Mitigates Diabetic Retinopathy by Regulating Retinal Epithelial Cell Inflammation, Oxidative Stress, and Apoptosis via miR-380-3p/SOCS6 Axis. Inflammation. 2022 Oct;45(5):1936-1949.
JUNB	Ren FJ, Cai XY, Yao Y, Fang GY. JunB: a paradigm for Jun family in immune response and cancer. Front Cell Infect Microbiol. 2023 Sep 4;13:1222265.
DUSP6	Ahmad MK, Abdollah NA, Shafie NH, Yusof NM, Razak SRA. Dual-specificity phosphatase 6 (DUSP6): a review of its molecular characteristics and clinical relevance in cancer. Cancer Biol Med. 2018 Feb;15(1):14-28.
PPM1L	Lu G, Ota A, Ren S, Franklin S, Rau CD, Ping P, Lane TF, Zhou ZH, Reue K, Lusis AJ, Vondriska T, Wang Y. PPM1l encodes an inositol requiring-protein 1 (IRE1) specific phosphatase that regulates the functional outcome of the ER stress response. Mol Metab. 2013 Aug 3;2(4):405-16.
NDUFA4L2	Meng L, Yang X, Xie X, Wang M. Mitochondrial NDUFA4L2 protein promotes the vitality of lung cancer cells by repressing oxidative stress. Thorac Cancer. 2019 Apr;10(4):676-685.
DDIT4L	Michalski C, Cheung C, Oh JH, Ackermann E, Popescu CR, Archambault AS, Prusinkiewicz MA, Da Silva R, Majdoubi A, Viñeta Paramo M, Xu RY, Reicherz F, Patterson AE, Golding L, Sharma AA, Lim CJ, Orban PC, Klein Geltink RI, Lavoie PM. DDIT4L regulates mitochondrial and innate immune activities in early life. JCI Insight. 2024 Feb 6;9(5):e172312.
SELENBP1	Song Y, Kurose A, Li R, Takeda T, Onomura Y, Koga T, Mutoh J, Ishida T, Tanaka Y, Ishii Y. Ablation of Selenbp1 Alters Lipid Metabolism via the Pparα Pathway in Mouse Kidney. Int J Mol Sci. 2021 May 19;22(10):5334.
SELENOP	Oo SM, Oo HK, Takayama H, Ishii KA, Takeshita Y, Goto H, Nakano Y, Kohno S, Takahashi C, Nakamura H, Saito Y, Matsushita M, Okamatsu-Ogura Y, Saito M, Takamura T. Selenoprotein P-mediated reductive stress impairs cold-induced thermogenesis in brown fat. Cell Rep. 2022 Mar 29;38(13):110566.
PRXL2A	Ren X, Ma L, Wang N, Zhou R, Wu J, Xie X, Zhang H, Liu D, Ma X, Dang C, Kang H, Zhou Z. Antioxidant Gene Signature Impacts the Immune Infiltration and Predicts the Prognosis of Kidney Renal Clear Cell Carcinoma. Front Genet. 2021 Aug 19;12:721252.
PDK3	Wang X, Shen X, Yan Y, Li H. Pyruvate dehydrogenase kinases (PDKs): an overview toward clinical applications. Biosci Rep. 2021 Apr 30;41(4):BSR20204402.

Table G.12. – Angiogenesis-related genes	
ANGPTL4	Chaube B, Citrin KM, Sahraei M, Singh AK, de Urturi DS, Ding W, Pierce RW, Raaisa R, Cardone R, Kibbey R, Fernández-Hernando C, Suárez Y. Suppression of angiopoietin-like 4 reprograms endothelial cell metabolism and inhibits angiogenesis. Nat Commun. 2023 Dec 12;14(1):8251.
CREG1	Yan C, Fang P, Zhang H, Tao J, Tian X, Li Y, Zhang J, Sun M, Li S, Wang H, Han Y. CREG1 promotes angiogenesis and neovascularization. Front Biosci (Landmark Ed). 2014 Jun 1;19(7):1151-61.
PGF	Accornero F, Molkentin JD. Placental growth factor as a protective paracrine effector in the heart. Trends Cardiovasc Med. 2011 Nov;21(8):220-4.
RGCC	Cui XB, Guo X, Chen SY. Response gene to complement 32 deficiency causes impaired placental angiogenesis in mice. Cardiovasc Res. 2013 Sep 1;99(4):632-9.
EFNB3	Royet A, Broutier L, Coissieux MM et al. Ephrin-B3 supports glioblastoma growth by inhibiting apoptosis induced by the dependence receptor EphA4. Oncotarget. 2017 Apr 4;8(14):23750-23759.
IGFBP2	Slater T, Haywood NJ, Matthews C, Cheema H, Wheatcroft SB. Insulin-like growth factor binding proteins and angiogenesis: from cancer to cardiovascular disease. Cytokine Growth Factor Rev. 2019 Apr;46:28-35.
KIT	Salajegheh, A. (2016). C-KIT: Tyrosine Kinase Receptors with Potential to Initiate Angiogenesis. In: Angiogenesis in Health, Disease and Malignancy. Springer, Cham.
ITGA6	Khademi R, Malekzadeh H, Bahrami S, Saki N, Khademi R, Villa-Diaz LG. Regulation and Functions of α6-Integrin (CD49f) in Cancer Biology. Cancers (Basel). 2023 Jul 2;15(13):3466.
MYCT1	Kabir AU et al. Dual role of endothelial Myct1 in tumor angiogenesis and tumor immunity. Sci Transl Med. 2021 Mar 3;13(583):eabb6731.
WNT5A	Shi YN, Zhu N, Liu C, Wu HT, Gui Y, Liao DF, Qin L. Wnt5a and its signaling pathway in angiogenesis. Clin Chim Acta. 2017 Aug;471:263-269.
TNFSF9 (~4-1BBL)	Wu J, Wang Y, Yang Y, Liu F, Chen J, Jiang Z, Jiang Z. TNFSF9 promotes metastasis of pancreatic cancer through Wnt/Snail signaling and M2 polarization of macrophages. Aging (Albany NY). 2021 Sep 13;13(17):21571-21586. | Hwang I, Kim JW, Ylaya K, Chung EJ, Kitano H, Perry C, Hanaoka J, Fukuoka J, Chung JY, Hewitt SM. Tumor-associated macrophage, angiogenesis and lymphangiogenesis markers predict prognosis of non-small cell lung cancer patients. J Transl Med. 2020 Nov 23;18(1):443.

Table G.13. – Cell signaling-related genes	
PRXL2A	He H, Guo F, Li Y, Saaoud F, Kimmis BD, Sandhu J, Fan M, Maulik D, Lessner S, Papasian CJ, Fan D, Jiang Z, Fu M. Adiporedoxin suppresses endothelial activation via inhibiting MAPK and NF-κB signaling. Sci Rep. 2016 Dec 12;6:38975.
SOCS3	Hu X, Li J, Fu M, Zhao X, Wang W. The JAK/STAT signaling pathway: from bench to clinic. Signal Transduct Target Ther. 2021 Nov 26;6(1):402.
SOCS2	Lv Y, Qi J, Babon JJ, Cao L, Fan G, Lang J, Zhang J, Mi P, Kobe B, Wang F. The JAK-STAT pathway: from structural biology to cytokine engineering. Signal Transduct Target Ther. 2024 Aug 21;9(1):221. doi: 10.1038/s41392-024-01934-w. Erratum in: Signal Transduct Target Ther. 2024 Oct 17;9(1):290.
DUSP6	Ecker V, Brandmeier L, Stumpf M, Giansanti P, Moreira AV, Pfeuffer L, Fens MHAM, Lu J, Kuster B, Engleitner T, Heidegger S, Rad R, Ringshausen I, Zenz T, Wendtner CM, Müschen M, Jellusova J, Ruland J, Buchner M. Negative feedback regulation of MAPK signaling is an important driver of chronic lymphocytic leukemia progression. Cell Rep. 2023 Oct 31;42(10):113017.
FRZB	Kawano Y, Kypta R. Secreted antagonists of the Wnt signalling pathway. J Cell Sci. 2003 Jul 1;116(Pt 13):2627-34.

ALDOC	Caspi M, Perry G, Skalka N, Meisel S, Firsow A, Amit M, Rosin-Arbesfeld R. Aldolase positively regulates of the canonical Wnt signaling pathway. Mol Cancer. 2014 Jul 4;13:164.
AHNAK2	Zhang S, Cai Z, Li H. AHNAKs roles in physiology and malignant tumors. Front Oncol. 2023 Nov 14;13:1258951.
WNT5A	Kumawat K, Gosens R. WNT-5A: signaling and functions in health and disease. Cell Mol Life Sci. 2016 Feb;73(3):567-87.
DKK1	Jiang H, Zhang Z, Yu Y, Chu HY, Yu S, Yao S, Zhang G, Zhang BT. Drug Discovery of DKK1 Inhibitors. Front Pharmacol. 2022 Mar 9;13:847387.
LYPD6	Özhan G et al. Lypd6 enhances Wnt/β-catenin signaling by promoting Lrp6 phosphorylation in raft plasma membrane domains. Dev Cell. 2013 Aug 26;26(4):331-45.
EPHB1	Vindis C, Cerretti DP, Daniel TO, Huynh-Do U. EphB1 recruits c-Src and p52Shc to activate MAPK/ERK and promote chemotaxis. J Cell Biol. 2003 Aug 18;162(4):661-71.